AD-A082 332 GENERAL ELECTRIC CO PHILADELPHIA PA SPACE DIV F/G 4/1
DESIGN STUDY OF A LASER RADAR SYSTEM FOR SPACELIGHT APPLICATION--ETC(U)
DEC 79 W F BREHM, J L BUCKLEY F19628-78-C-0204
UNCLASSIFIED AFGL-TR-79-0264 NL

1 of 3
AD
A082332

UNCLASSIFIED

SECURITY CLASSIFICATION OF THIS PAGE (When Data Entered)

19

REPORT DOCUMENTATION PAGE

READ INSTRUCTIONS BEFORE COMPLETING FORM

1. REPORT NUMBER 18 AFGL-TR-79-0264	2. GOVT ACCESSION NO.	3. RECIPIENT'S CATALOG NUMBER 9
4. TITLE (and Subtitle) 6 DESIGN STUDY OF A LASER RADAR SYSTEM FOR SPACEFLIGHT APPLICATION.		5. TYPE OF REPORT & PERIOD COVERED Final Report, 7 Sep 78 - 7 Dec 79 6. PERFORMING ORG. REPORT NUMBER
7. AUTHOR(s) 10 W. F. Brehm J. L. Buckley		8. CONTRACT OR GRANT NUMBER(s) 15 F19628-78-C-0264
9. PERFORMING ORGANIZATION NAME AND ADDRESS General Electric Space Division Valley Forge Space Center, P.O. Box 8555 Philadelphia, PA 19101		10. PROGRAM ELEMENT, PROJECT, TASK AREA & WORK UNIT NUMBERS 62101F 16 6690~~04AA~~ 17 04
11. CONTROLLING OFFICE NAME AND ADDRESS Air Force Geophysics Laboratory Hanscom AFB, Massachusetts 01731 Monitor / Donald E. Bedo / LKO		12. REPORT DATE 11 December 1979 13. NUMBER OF PAGES 264
14. MONITORING AGENCY NAME & ADDRESS (if different from Controlling Office) 12 249		15. SECURITY CLASS. (of this report) Unclassified 15a. DECLASSIFICATION/DOWNGRADING SCHEDULE

16. DISTRIBUTION STATEMENT (of this Report)

Approved for public release; distribution unlimited.

17. DISTRIBUTION STATEMENT (of the abstract entered in Block 20, if different from Report)

18. SUPPLEMENTARY NOTES

19. KEY WORDS (Continue on reverse side if necessary and identify by block number)

Laser Radar	Space Shuttle Payload
Lidar	Optical Radar
Atmospheric Density	Differential Absorption
Raleigh/Mie Scattering	Raman Scattering

lambda to the 4th power

20. ABSTRACT (Continue on reverse side if necessary and identify by block number)

This report provides the analyses of several laser measurement techniques for the determination of the density of the neutral atmosphere from space. Several operational concepts of a laser radar system for spaceflight applications were investigated, including also, a proof-of-concept balloon-based experiment. The recommended baseline density measurement technique uses two wavelengths and the wavelength dependence of Rayleigh scattering ($1/\lambda^4$) and Mie scattering ($\sim 1/\lambda$) to separate the neutral atmosphere returns from those of aerosols and particulates.

DD FORM 1473 1 JAN 73 EDITION OF 1 NOV 65 IS OBSOLETE

Unclassified

about 1/lamoda

405025 Gm

SECURITY CLASSIFICATION OF THIS PAGE (When Data Entered)

PREFACE

This document is the final report for the Design Study of a Laser Radar System for Spaceflight Application, which was performed by the General Electric Company's Space Division for the Air Force Geophysics Laboratory (AFGL) Hanscom AFB. This study was performed under contract F19628-78-C-0204 for Dr. Donald E. Bedo, Contract Manager, LKO (Telephone (617) 861-3313).

The following individuals at GE contributed to this study effort:

W. F. Brehm	Systems Engineering and Phase 2 Principal Investigator
Dr. J. L. Buckley	Phase 1 Principal Investigator and Phase 2 Consultant
Dr. M. J. Linevsky	Phase 1 Rayleigh/MIE and O_2 DIAL Analyses
H. W. Halsey	LIDAR System Consultant
Dr. F. N. Alyea	Computer Simulation Program
Dr. G. W. Bethke	Phase 1 Vibrational/Rotational RAMAN Analysis

This page intentionally left blank.

AFGL LIDAR FINAL REPORT

SECTION 1

INTRODUCTION

SECTION 1

INTRODUCTION

This report completes the technical effort by the General Electric Space Division for the Air Force Geophysics Laboratory relative to the Design Study of a Laser Radar System for Spaceflight Application. The primary objective of this study is to investigate conceptually the requirements for, and formulate a realistic design for, a laser radar system which is compatible with flight operation aboard the Space Shuttle System or other AF satellite, including also, a proof-of-concept balloon-based experiment. The primary scientific purpose of the spaceflight experiment is the determination, on a near real-time basis, of the atmospheric density at all altitudes of interest, i.e., 40 km to the ground, while at the same time retaining as a goal a minimum of hardware complexity.

The primary objective of this study has been accomplished, in that an operational concept of a laser radar system for spaceflight applications has been developed. The baseline concept uses the fundamental and frequency-tripled neodymium wavelengths in combination with the difference in wavelength dependence of Rayleigh scattering ($1/\lambda^4$) and Mie scattering ($\sim 1/\lambda$) to separate the neutral atmosphere returns from those of aerosols and particulates. A summary of this design study which led to the selection of the baseline lidar system design concept is provided in Section 2 of this report.

INTRODUCTION (CONTINUED)

Section 3 provides a description of the study objectives with Section 4 providing the approach to ensure that these objectives can be met with a viable instrument design concept.

Shuttle/Spacelab experiment performance results are provided in Section 5 for both the Rayleigh/Mie and Differential Absorption Lidar (DIAL) analysis techniques studied for the determination of atmospheric density.

Section 6 provides the balloon experiment performance results based on the Rayleigh/Mie analysis.

Experiment hardware descriptions are provided in Section 7 for the implementation of an operational atmospheric density measurement concept within the Atmospheric Lidar Multi-User Instrument System (ALMIS), the Standard Test Rack (STR) Lidar Experiment, as an adjunct to the WINDSAT Lidar Experiment, and as a proof-of-concept (feasibility demonstration) Balloon-Based Lidar Experiment.

This report is published in a facing page format in which a summarizing or pictorial presentation is provided on the righthand page, while the facing lefthand page contains a detailed narrative of the points summarized and/or illustrated on the facing page. This format is found most useful to facilitate the use of this material in technical and management presentations.

SECTION 2

SUMMARY

ANALYSIS SUMMARY OF DENSITY MEASUREMENT TECHNIQUES

The accompanying chart provides a summary of the results of our investigation relative to several density measurement techniques which include the Raman scattering, doppler broadened Rayleigh, Rayleigh/Mie separation, and O_2-DIAL techniques. Each technique is discussed in the following paragraphs.

Raman scattering was found to produce signal levels that are impractically small. Appendix A of this report discusses this problem and shows that the combination of current laser powers with the range from the lower atmosphere to the Shuttle limits the amount of available photons to make a meaningful measurement.

The doppler broadened Rayleigh technique was found to be technologically impractical. The complexities of laser control, particularly when merged with the seven kilometer per second velocity of the Shuttle and its attendant doppler shift became a developmental problem that was deemed not to be near-term practical.

Rayleigh/Mie separation was found to be the most practical technique, particularly for higher altitudes and clear weather. The extension to one percent accuracy was found doubtful, however, but 2 to 5% is certainly achievable.

The oxygen (O_2) DIAL technique operating in the saddle between two lines was found to be very feasible at low altitudes; in fact, the signal-to-noise ratios are expected to improve as haze and cloudy weather conditions are encountered because signal return is dependent on scattering from these aerosols.

A tentative recommendation then, is to continue to explore both the DIAL and the Rayleigh/Mie measurements in order to get a combined approach to the problem that can meet the baseline requirements.

GENERAL ELECTRIC

space division

ANALYSIS SUMMARY OF DENSITY MEASUREMENT TECHNIQUES

- RAMAN SCATTER: SIGNAL LEVELS IMPRACTICALLY SMALL
- DOPPLER BROADENED RAYLEIGH: TECHNOLOGY IMPRACTICALLY COMPLEX
- RAYLEIGH/MIE SEPARATION: FEASIBLE FOR HIGHER ALTITUDES IN CLEAR WEATHER; EXTENSION TO 1% ACCURACY DOUBTFUL
- O_2 - DIAL: FEASIBLE AT LOWER ALTITUDES IN CLEAR WEATHER, SIGNALS MAY IMPROVE WITH HAZE; FEASIBLE EXTENSION TO 1% ACCURACY

RECOMMENDATION: USE BOTH RAYLEIGH/MIE AND O_2 DIAL TO GIVE BEST ALTITUDE AND ACCURACY COVERAGE

RAYLEIGH/MIE SEPARATION

CONCLUSIONS

The conclusions shown on the accompanying chart indicate that this technique is an attractive means for the determination of atmospheric density from Shuttle. Although certain restrictions are indicated, e.g., night operation in order to avoid daylight backscatter interference impacting the measurement accuracy, the original goal of 15% accuracy from Shuttle is feasible with the potential of reaching 5% and even a 1% limit.

These conclusions are drawn from the performance analysis data shown in Section 5 of this report.

GENERAL ELECTRIC

space division

RAYLEIGH / MIE SEPARATION CONCLUSIONS

A TECHNICALLY REALISTIC LIDAR OPERATING AT 1060 Nm AND 353 Nm CAN PROVIDE DENSITY MEASUREMENTS WITH 15% ACCURACY FROM SHUTTLE

- o AT NIGHT
- o IN CLEAR SKIES
- o ABOVE BOUNDARY LAYER (5 Km)
- o UP TO ~ 50 Km
- o FOR 100 SHOTS (70Km HORIZONTAL RANGE)
- o WITH 1 Km VERTICAL RESOLUTION

5% ACCURACY APPEARS ACHIEVABLE ABOVE 10 Km PROVIDING THAT

- o AEROSOL BACKSCATTER RATIOS ARE WELL CHARACTERIZED, OR
- o AEROSOL LEVELS ARE LOWER THAN LOWTRAN 3B MODEL

1% ACCURACY APPEARS TO BE A FINAL LIMIT, AND ONLY ACHIEVABLE OVER RESTRICTED RANGES OF CONDITIONS.

O_2 - DIAL CONCLUSIONS

The conclusions shown on this chart are drawn from the performance analysis data shown in Section 5 of this report. The results, in particular, indicate that this technique is an attractive approach to obtain atmospheric density in the lower altitude regions. Similar restrictions are shown to those indicated for the Rayleigh/Mie technique, e.g., night operation to prevent daylight backscatter interference on the measurement accuracy.

O_2 - DIAL CONCLUSIONS

O_2 - DIAL WORKING IN THE SADDLE BETWEEN TWO STRONG ABSORPTION LINES APPEARS FEASIBLE AS A TECHNIQUE TO MEASURE DENSITY REMOTELY TO 15% WITH POTENTIAL FOR HIGHER ACCURACIES

- o AT NIGHT
- o MULTIPLE SHOTS
- o LOWTRAN 3B ATMOSPHERE
- o GROUND TO ABOUT 12 Km ON CLEAR DAYS

O_2 - DIAL WORKING DIRECTLY ON ABSORPTION LINES APPEARS TO REQUIRE IMPRACTICALLY FINE LASER STABILITY AND CONTROL

SUMMARY OF DENSITY MEASUREMENT TECHNIQUES

This chart provides a summary of the Rayleigh/Mie and the O_2-DIAL density measurement techniques. Noted within this summary is the conclusion that these two techniques are in essence complementary to each other, i.e., each providing greater accuracies in two different altitude regions, e.g., the Rayleigh/Mie technique at altitudes above 6 km, and the O_2-DIAL technique at altitudes below 15 km. In either case both techniques require night only operation and multiple shot averaging to meet the accuracy goals.

GENERAL ELECTRIC

space division

SUMMARY OF DENSITY MEASUREMENT TECHNIQUES

1) INCOHERENT RAYLEIGH / MIE USING Nd AND Nd x3 WILL MEET INITIAL OBJECTIVES
   - a) NIGHT ONLY
   - b) CLEAR SKY
   - c) $Z \geq 6Km$
   - d) EXTENSION TO BETTER ACCURACY LIMITED
2) O_2 - DIAL WORKING IN "SADDLE" REGION WILL MEET OBJECTIVES
   - a) NIGHT ONLY
   - b) $Z \leq 15Km$
   - c) POSSIBLE EXTENSION TO BETTER (1%) ACCURACY
3) COMBINATION OF TWO TECHNIQUES WILL MEET OVERALL OBJECTIVES
   - a) NIGHT ONLY
   - b) MULTI-SHOT AVERAGING
   - c) NOMINAL ATMOSPHERE AND HAZE

EYE SAFETY CONCLUSIONS

The basis for eye safety considerations is the American National Standard for the Safe Use of Lasers (ANSI-Z136.1-1976). This document details the maximum permissible exposure (MPE) allowed for the human eye as a function of laser duration and wavelength. A suggested set of criteria for use in eye safety considerations for Shuttle experiments include the following items:

- For Day - The day adapted eye with a pupil diameter of 2.5 mm
- For Night - A 10-inch diameter telescope over land and 50 mm binoculars over sea
- Atmospheric scintillation effects give hot spots which are 10 times the mean energy density
- Multimode laser beam inhomogeneities are 3 times the mean energy density
- Gaussian laser beam peak energy density is 2 times the mean energy density
- Atmospheric Transmission is 50%

These criteria were selected as conservative, reasonable values and are not intended as the final word on eye safety requirements. They are used in the analysis to show that published eye safe energy densities on the ground and in near ground air space can be met with the Lidar systems under consideration. Actual operational eye safety criteria will require a stringent examination of parameters, operating procedures and safeguards in order to achieve a standard of safety which is acceptable.

The damage mechanisms encountered in humans and the wavelength regions involved are shown in the tabulation below. In addition, below 300 nm, the absorption in the ozone layer will provide additional protection from radiation damage.

WAVELENGTH RANGE	DAMAGE MECHANISMS
$<$315 nm	CORNEAL & SKIN
315-400 nm	CORNEAL & SKIN & SMALL RETINAL
400-1500 nm	RETINAL TO VARYING DEGREES
10.6 μm	CORNEAL & SKIN

GENERAL ELECTRIC

space division

EYE SAFETY CONCLUSIONS

- NEED VARIABLE LASER BEAM WIDTH TO OBTAIN MAXIMUM EYESAFE ENERGY DENSITY/NARROWEST BEAM DIVERGENCE TO GIVE
  - –MAXIMUM SCIENCE RETURN
  - –DIFFERENT EYE SAFETY CRITERIA FOR DAY/NIGHT AND LAND/SEA
- EXPERIMENTS WHICH MAY BE DONE AT Nd x 3 (353 NM) PROVIDE MINIMUM PHYSIOLOGICAL AND POLITICAL IMPACT
  - –PHYSIOLOGICAL – MINIMUM EYE SAFETY HAZARD
  - –POLITICAL – NOT READILY VISIBLE TO EYE
- 10-INCH TELESCOPE MAY BE TOO BIG. SOME EVIDENCE POINTS TO 6-INCH MAXIMUM DIMENSIONS OF SCINTILLATION INDUCED HOT SPOTS WITH MUCH LARGER DISTANCES BETWEEN SPOTS SO THAT 10- AND 16-INCH TELESCOPES MAY POSE THE SAME THREAT TO EYE SAFETY AS THE 6-INCH TELESCOPE.

SHUTTLE LIDAR CAN BE DESIGNED TO MEET ALL KNOWN EYE SAFETY STANDARDS

LIDAR CONFIGURATION CONCEPT

A possible Lidar configuration for the Space Shuttle is shown in the accompanying chart. It is compatible with a Standard Test Rack which is a payload carrier developed at General Electric, designed to be flown and directly interfacing with the Orbiter. Components shown are compatible in size to a one meter optical telescope and a single Nd:YAG laser system. Support electronics, power distribution units and data systems may be included as optional packages within the modular panels of the STR.

GENERAL ELECTRIC

space division

LIDAR CONFIGURATION CONCEPT

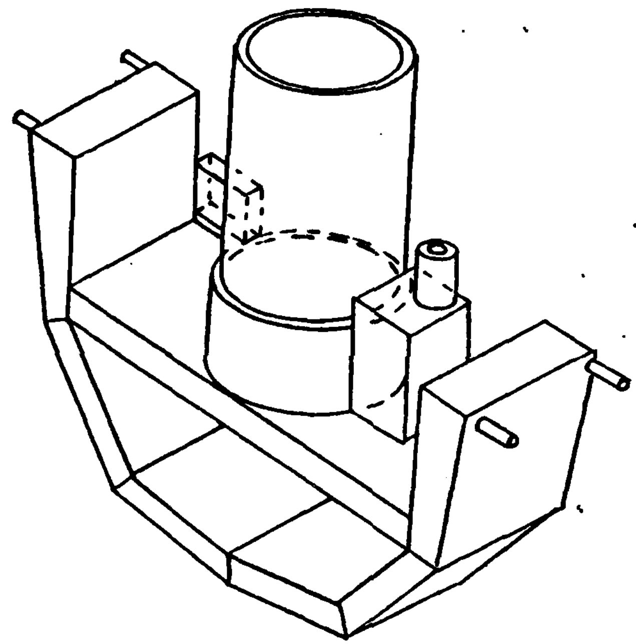

- o COMPATIBLE WITH SHUTTLE / STANDARD TEST RACK
- o 1 METER DIAMETER TELESCOPE
- o Nd:YAG LASER SYSTEM
- o TWO-WAVELENGTH DETECTOR

BALLOON-BASED LIDAR SUMMARY

Functionally, the requirements for this experiment are similar to the Shuttle/Spacelab experiment hardware descriptions given earlier except that it is balloon-based and, therefore, can be scaled down in size and power without compromising measurement accuracy goals. Not only are balloon-based experiments attractive from an overall cost point of view, since many support services by government agencies are provided at minimal cost to the experimenter, and the experiment in itself can be made cheaper; but also, the basic experiment package is usually a much simpler item when compared to a flight qualified hardware item.

The balloon-based LIDAR experiment can readily use off-the-shelf components for all required hardware elements, i.e., the laser, telescope receiver, detectors, power supply, supporting electronics, and battery package. The only areas requiring some design analysis are the thermal control and structural (gondola and optical bench) elements, which are necessary for providing thermal alignment stability for critical optical components and mechanical interfaces for component mounting/packaging, respectively.

An operational advantage of the balloon experiment over the Shuttle-based experiment is the capability to operate during daylight hours, if necessary, and still provide the desired measurement accuracy for density determination.

GENERAL ELECTRIC

BALLOON-BASED LIDAR SUMMARY

space division

- USES Nd:YAG LASER AT TWO WAVELENGTHS, 1060 NM AND 353 NM, AND RAYLEIGH/MIE SEPARATION TECHNIQUE FOR MOLECULAR DENSITY DETERMINATION.
- CAN OPERATE DAY OR NIGHT FROM GROUND TO 40 KM - NIGHT OPERATION PREFERRED TO MINIMIZE BACKGROUND INTERFERENCE AND AVERAGE POWER REQUIREMENTS.
- CAN MEET 10% MEASUREMENT ACCURACY GOALS AT ALTITUDES ABOVE 5 KM WITH EYE-SAFE, LOW POWER, LIDAR SYSTEM.
- CAN USE LOW-COST OFF-THE-SHELF HARDWARE.
- CAN OPERATE DOWNWARD LOOKING, TO SIMULATE OPERATIONAL LIDAR EXPERIMENT, WITH OPTIONS FOR BOTH HORIZONTAL AND UPWARD LOOKS AT ALTITUDES ABOVE 18 KM (FOR AIRCRAFT AVOIDANCE), IF DESIRED.

AN ATTRACTIVE APPROACH FOR
PROOF-OF-CONCEPT DEMONSTRATION

SECTION 3

OBJECTIVES

PRECEDING PAGE BLANK-NOT FILMED

STUDY OBJECTIVE

Two factors of current technology make the application of Lidar in space real. First, laser technology is maturing, particularly in the area of hardened lasers and rugged systems that can operate in the adverse environment of a space mission. Second, the Space Shuttle coming on-line provides a system to carry lasers into space. Large power and weight requirements can be met and relatively inexpensive missions can be undertaken to evaluate the potential operational use of systems. We have applied these two technology factors in the current study. Our objective is to couple lasers and the Shuttle into a study that will tackle one of the key problems of remote sensing: the density of the neutral atmosphere.

Our study objective has been to define the scientific basis of a system that will allow us to measure density from Shuttle. We have emphasized near term solutions and practical theoretical analysis. Our objective is to define a system that can be useful on a near term mission on Shuttle.

GENERAL ELECTRIC

STUDY OBJECTIVE

space division

DEFINE A LASER RADAR (LIDAR) INSTRUMENT SYSTEM TO MEASURE ATMOSPHERIC DENSITY FROM THE CLOUD TOPS TO 30 Km BY REMOTE OBSERVATION FROM THE SPACE SHUTTLE ORBITER.

- o SCIENTIFIC ANALYSIS
- o DESIGN IMPLEMENTATION CONCEPTS

STUDY SCOPE

The figure describes the major elements of our study. This report covers Tasks 1 and 2 with an initial look at the engineering definition of Task 3. Our emphasis has been on Task 2, defining a density measurement technique that will in fact provide useful data. Significant engineering work on the application of LIDAR experiments to Shuttle has been going on concurrently with the NASA-LaRC Lidar Phase B Study. For further references, see Atmospheric Lidar Multi-User Instrument System Definition Study final report (October 1979) by General Electric for NASA Langley Research Center (Contract NAS 1-15476).

STUDY SCOPE

AFGL/GE — MID-TERM

TASK 1 REQUIREMENTS ANALYSIS → WORKING SESSION → TASK 2 CONCEPT DEVELOPMENT → PRE-SENTATION → TASK 3 ENGINEERING DEFINITION → FINAL REPORT

TASK 1 REQUIREMENTS ANALYSIS

- STATEMENT OF WORK
- SHUTTLE INTERFACES
- SAFETY REQUIREMENTS
- AIRFORCE OBJECTIVES
- EXISTING TECHNOLOGIES
- PRELIMINARY PRIORITIES
- FIRST ORDER ANALYSES

TASK 2 CONCEPT DEVELOPMENT

-SENSING TECHNIQUE
  AEROSOL/PARTICLE DISCRIMINATION
  EFFECTS OF CLOUDS
  ALTITUDE RESOLUTION-1KM GOAL
  ACCURACY ANALYSIS-15% GOAL
  SIGNAL-TO-NOISE RATIO
  CALIBRATION APPROACH
  ATMOSPHERIC OPTICS
  BACKGROUND MEASUREMENTS

-LASER SYSTEM
  TYPE/WAVELENGTHS
  STABILITY,RELIABILITY,LIFETIME
  POWER,SIZE,COOLING
  REPETITION RATE
  DIVERGENCE/SAFETY

-RECEIVER
  APERTURE SIZE
  IMAGE QUALITY
  RELAY OPTICS
  SPECTRAL FILTERS

-DETECTORS
  TYPE
  SIGNAL LEVELS
  NOISE/LINEARITY
  ELECTRONICS

TASK 3 ENGINEERING DEFINITION

-SYSTEM ENGINEERING
- MECHANICAL
  CONFIGURATION,SIZE,WEIGHT
  THERMAL/STRUCTURAL
  ALIGNMENT/STABILITY
- ELECTRICAL
  FUNCTION,POWER
  COMMAND & CONTROL
  DATA & TELEMETRY
  POWER SYSTEM
- OPERATIONAL/ENVIRONMENTAL
  MISSION PROFILES
  HUMAN INTERACTION
  CLEANLINESS
  EMC/ISOLATION/SHIELDING
  SUPPORT EQUIPMENT
- SAFETY
  LASER OPERATION

-LASER ENGINEERING
  HARDWARE LAYOUT
  THERMAL DESIGN
  STABILITY/LIFETIME
  PROBLEM AREAS

-RECEIVER ENGINEERING
  CONFIGURATION
  TOLERANCES

-DETECTOR ENGINEERING
  PACKAGING
  OPERATION
  ELECTRONICS

STUDY EMPHASIS

The goals of this study were clearly defined in the Statement of Work. Through discussions and analysis we have developed certain areas of emphasis in order to guide our study. Density to ±10% accuracy is a goal that we think is pessimistic. We don't want to stop with a system that is fundamentally limited to 10% accuracy, so we emphasize techniques in our analysis that will allow us to proceed to the 1% range. While the operational goal is global coverage, we've been emphasizing night only operation from the Eastern Test Range for the Shuttle orbit, nominal orbits that will be achieved in near term. Night-only operation is selected to demonstrate the near-term technique without the noise generated by scattered sunlight. While the goal is to measure neutral density from the cloud tops up to 30 kilometers, we are emphasizing the region between the ground and 20 kilometers hoping to reach 30 if possible. We must be compatible with the Shuttle, but we are particularly concerned in our engineering aspects about flying as an independent payload on the Shuttle, not as part of a Spacelab mission. The Spacelab compatibility has been studied in some detail for NASA Langley in the previously referenced study. Eye Safety is a goal and a requirement. We cannot fly lasers that will cause a hazard to observers on the ground. To meet the eye-safety requirements our first emphasis is to operate if possible in non-visible wavelengths, where corneal damage, as opposed to retinal damage, is the key factor and where tolerance to photons is much higher. Similarly, non-visible wavelengths provide political advantages. Laser lifetime has long been a problem with remote instrumentation and missions. We are aiming to provide untended operation involvement and with minimum operational interfaces with the Shuttle or with other payloads. In all, these emphases defined a practical approach to the real problem of the study.

GENERAL ELECTRIC

space division

STUDY EMPHASIS

GOAL	EMPHASIS
DENSITY TO $\pm$10% ACCURACY	EXTENSION OF TECHNIQUE TO $\pm$ 1%
GLOBAL COVERAGE	NIGHT-ONLY FROM NOMINAL ETR SHUTTLE ORBITS
CLOUD TOPS TO 30 Km	GROUND TO 20 Km
SHUTTLE COMPATIBLE	NON-SPACELAB ACCOMMODATION
EYE SAFETY	NON-VISIBLE WAVELENGTHS
LASER LIFETIME	7 DAY SORTIE MISSION
ORBITAL OPERATION	MINIMUM MANNED INTERACTION; NO PHYSICAL ADJUSTMENT IN ORBIT

FLIGHT ACCOMMODATIONS

As we develop a system configuration to fly on Shuttle we're looking at a flight independent of Spacelab. The Spacelab accommodations have been described in detail in the NASA/Lidar Study. The key driver is to use only nominal Orbiter interfaces and resources. We want to be an easy payload to fly without major integration costs and without major impact in terms of auxillary power, extensive man interfaces or complex data interfaces. Power and total energy appear to be matters that will require careful consideration in the optimization of this system.

FLIGHT ACCOMMODATIONS

- SHUTTLE ENVIRONMENT
- NOT SPACELAB MISSION
- HANDS-OFF OPERATION
- NOMINAL ORBITER INTERFACES
- NOMINAL ORBITER RESOURCES

SECTION 4

APPROACH

PRECEDING PAGE BLANK-NOT FILMED

APPROACH

Our approach to this study is two-fold: first, to consider and evaluate several density measurement techniques which will provide the desired accuracy and, second, to develop potential experiment configurations which can be used for implementation of the desired technique(s). As a result, the following portions of this section are divided in two parts with the first portion providing our approach towards satisfying scientific requirements, and the second portion providing our approach towards satisfying systems engineering requirements, stressing in either case, an approach which will provide a viable operational experiment concept for spaceflight application.

SCIENCE APPROACH

MEASUREMENT TECHNIQUES CONSIDERED

Our analysis considered four possible measurement techniques for the determination of neutral density from a spaceborne Lidar system. The first technique, Rayleigh/Mie separation, depends on the dramatic λ^{-4} change in scattering cross-section of the neutral gas molecules to separate their signature from the λ^{-1} dependence of aerosols. In principle, we operate in the red to near-infrared region with a laser beam which is scattered heavily by typical aerosols. From the long wavelength scattering we determine the aerosol contribution and extrapolate that contribution to the ultraviolet or near-ultraviolet where the scattering from the neutral gases has gone up by a factor of λ^{-4}. With a second laser beam in the near-ultraviolet, we get a signal that is determined predominantly by Rayleigh scattering, and subsequently correct for the Mie scattering fraction based on the infra-red measurements. We emphasize this technique heavily because the tools for implementing it are at hand with a Neodymium laser operating at 1060 nm and tripled to 353 nm.

Differential absorption by O_2 is a very promising method in theory. Light is transmitted at two closely spaced wavelengths on and off an absorption line of oxygen. Return signals are ratioed and a direct measurement is made of the oxygen density. Since oxygen and nitrogen are well mixed, this gives us the density of the atmosphere. Theorectical calculations were made on this process and are discussed in detail. A general conclusion is that the technology to implement this technique in space is not ready for near-term implementation.

Raman scattering of laser radiation has been explored for a long time as a means of remote sensing. When a laser photon hits a molecule and is scattered through the Raman process, energy is taken from the photon and the light that is scattered comes out distinctly shifted into the red. This process gives a clear and unique, measurement of the molecular concentration and would, in principal, measure neutral density to well within the precision required. However, cross sections for Raman scattering are so small that we find with practical lasers and receivers in orbit there are just not enough photons to operate.

A final technique that we looked at quickly is the separation of back scattered light into two components by looking at the bandwidth of the return beam. Laser radiation scattered from particles will come back at essentially the wavelength of the transmitter. The particles are moving slowly and add no doppler scattering. Molecules, where the random velocity is approximately the speed of sound, scatter and broaden the laser line. In principle, we could isolate the strong central peak in the return and characterize it as an aerosol return, then look in the wings of the return signal and measure the contribution from molecules. This process provides a good signature but has very severe instrumental difficulties because of the narrow frequencies involved.

GENERAL ELECTRIC

space division

MEASUREMENT TECHNIQUES CONSIDERED

MEASUREMENT TECHNIQUE	STUDY EMPHASIS
• RAYLEIGH / MIE SEPARATION - TWO WAVELENGTHS	PRIMARY ANALYSIS
• O_2 DIFFERENTIAL ABSORPTION LIDAR (DIAL)	PRIMARY ANALYSIS
• N_2 RAMAN SCATTERING - VIBRATION AND ROTATION	CURSORY ANALYSIS (SEE APPENDIX A)
• DOPPLER BROADENED RAYLEIGH SCATTER	QUALITATIVELY ELIMINATED

ANALYSIS TOOLS USED

We addressed the four preceeding techniques with a variety of analytical tools. First we started with existing analysis work that has been going on at GE for a number of years and with published information in the literature. Hand analyses were applied in a number of cases to formulate the experiment and to determine the sensitivity to various error sources. The entire Raman signal analysis was done analytically. Finally, computer simulations were applied to the two main techniques we emphasized. Using GE programs to simulate the Lidar from orbit with a nominal earth atmosphere and typical aerosol contents, we were able to derive signals and signal-to-noise ratios as a function of range for the two techniques. The computer program remains up and running and is being used to continue more in-depth study of the promising areas.

GENERAL ELECTRIC

space division

ANALYSIS TOOLS USED

- EXISTING ANALYSES
  - PREVIOUS GE WORK
  - PUBLISHED DATA
  - BACKGROUND LEVELS
  - EYE SAFETY
- HAND ANALYSES
  - EXPERIMENT FORMULATIONS
  - ERROR SENSITIVITY
  - RAMAN SIGNAL LEVELS
- COMPUTER SIMULATIONS
  - RAYLEIGH / MIE SIGNAL LEVELS
  - O_2 DIAL SIGNAL, SNR, ERROR SENSITIVITY

EYE SAFETY

The nomograph shown was developed to correlate laser energy and beam divergence with maximum permissible exposure to observers as a function of laser wavelength. The relationship between laser energy and energy density on the ground is based on a very low 200 kilometer orbit.

Energy density calculations, based only on laser energy, beam divergence angle and range, were modified by the additional multiplication factors shown in the chart on the left. These factors are considered reasonable values for each of the identified parameters. First, scintillation effects in the atmosphere may provide hot spots on the ground up to 10 times the nominal energy density. Similarly, beam inhomogeneities in the laser may generate bright spots up to 3 times the nominal beam output. Finally, we used an atmospheric transmission of 50% representing a relatively average day. The maximum permissible exposure is clearly defined in ANSI Z136.1. The challenge with the space application of lidar is to define the conditions of the observer. Consequently, we've examined naked eye exposure, both for a day and night adapted eye. We've also considered viewers with binoculars, 6" telescopes, 10" telescopes, and 16" telescopes (which would most likely be only available in controlled observatories). From this nomograph we can lay any envisioned concept against the requirements to define beam divergence vs. the energy of the laser transmitter. Conclusions are drawn in the instrument definition phase of this study in Task 3.

EYE SAFETY

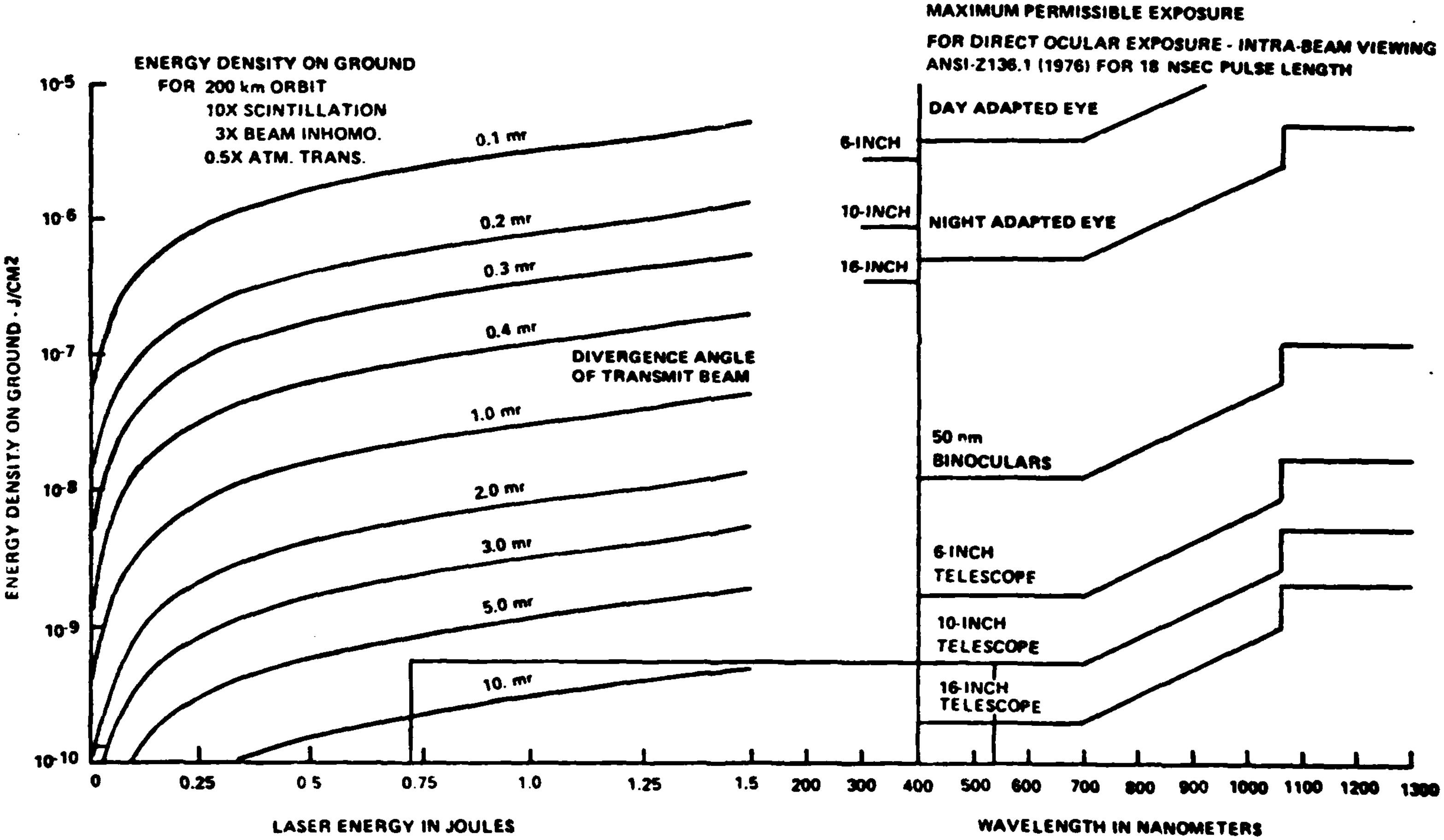
ENERGY DENSITY ON GROUND
FOR 200 km ORBIT
10X SCINTILLATION
3X BEAM INHOMO.
0.5X ATM. TRANS.
0.1 mr
0.2 mr
0.3 mr
0.4 mr
DIVERGENCE ANGLE
OF TRANSMIT BEAM
1.0 mr
2.0 mr
3.0 mr
5.0 mr
10. mr
ENERGY DENSITY ON GROUND - J/CM2
LASER ENERGY IN JOULES
MAXIMUM PERMISSIBLE EXPOSURE
FOR DIRECT OCULAR EXPOSURE - INTRA-BEAM VIEWING
ANSI-Z136.1 (1976) FOR 18 NSEC PULSE LENGTH
DAY ADAPTED EYE
6-INCH
10-INCH
NIGHT ADAPTED EYE
16-INCH
50 mm
BINOCULARS
6-INCH
TELESCOPE
10-INCH
TELESCOPE
16-INCH
TELESCOPE
WAVELENGTH IN NANOMETERS

INSTRUMENT CONCEPTS

In order to scale our analyses to something reasonable we defined a general instrument concept for the spaceborne Lidar. The parameters we've chosen are clearly feasible for near-term Shuttle flights. We baselined a Nd:YAG laser putting out 2 Joules per pulse, 10 pulses per second at 1060 nm. This laser is realistic in present hardened technology and is suitable for near-term missions. We assumed doublers with 30% conversion to the green (530 nm), and triplers with 10% conversion into the near ultra-violet (353 nm).

We've taken the Nd:YAG laser as a pump to develop a laser pumped dye system for the O_2 DIAL technique.

The receiver has been baselined at 1 meter diameter in a general Cassegrain configuration. This provides a compact and inexpensive telescope which will fit easily in a number of Shuttle payload configurations. Optical quality and co-alignment at 2 milliradians are such that the telescope can be built in a passive configuration using readily available assembly techniques.

For detection, the main challenge is operating at the 1060 nm fundamental of the laser. A recently announced Varian photomultiplier tube provides 2% quantum efficiency there. The tube must be cryogenically cooled at all times. At the 700 nm, 530 nm and 353 nm wavelengths, photomultipliers will be used with approximately 15%, 20% and 30% quantum efficiency, respectively. We've assumed high transmittance filters around the laser light with relatively broad transmittances. The filter situation becomes much more severe if we operate in daylight with a strong scattered sunlight background. This nominal instrument is used in the Shuttle experiment analyses for scaling the signal-to-noise ratios and for designing a system configuration.

INSTRUMENT CONCEPTS

LASER: Nd: YAG — 2 JOULE / PULSE — 10 PULSE / SECOND

ACCESSORIES:
- DOUBLER — 30% CONVERSION TO 530 NM
- TRIPLER — 10% CONVERSION TO 353 NM
- DYE SYSTEM FOR 0_2 DIAL

TELESCOPE: 1 METER DIAMETER — CASSEGRAIN CONFIGURATION

IMAGE QUALITY: 2 MR BLUR ALLOWABLE

COALIGNMENT: 2 MR PEAK ERROR

DETECTORS:
1060 NM - VARIAN PMT (COOLED) 2% QE
700, 530, 353 VARIAN PMT 15%, 20%, 30% QE

FILTERS:
HIGH TRANSMITTANCE
RELATIVELY BROAD FOR NIGHT OPERATION

LASER APPROACHES

The two lasers approaches that we envision for the density measurement techniques, Rayleigh/Mie and O_2 DIAL, are shown in the chart. For the Rayleigh/Mie separation technique the system is essentially ready to go. We have discussed it with a number of laser manufacturers and believe that we are not faced with technological development to implement this system. For the O_2 DIAL technique, the laser system has one major developmental question, the control of the linewidth and frequency for the on-line portion of the system. The criticality of this control is analyzed later.

GENERAL ELECTRIC

space division

LASER APPROACHES

RAYLEIGH/MIE TECHNIQUE

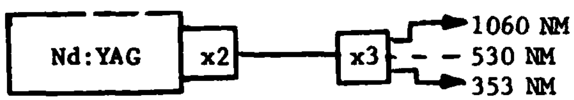

- TECHNOLOGY READY
- NOT COST DRIVER
- 10^7 PULSES TOTAL
- 1060 NM DETECTOR REQUIRED
- USE 1060 NM & 353 NM TO REDUCE EYE-SAFETY CONCERNS *

O_2 DIAL TECHNIQUE

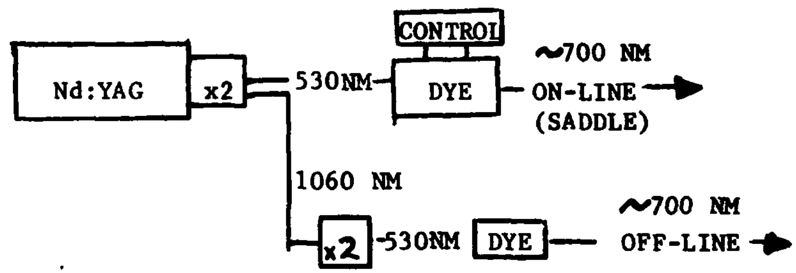

- MODULE-LEVEL TECHNOLOGY IN HAND
- ON-LINE CONTROL LOOP MAY BE COMPLEX
- COST NOT PROHIBITIVE
- 10^7 PULSES TOTAL; DYE QUANTITIES TBD
- DETECTORS AT 700 NM STANDARD
- 700 NM HAS REDUCED EYE SAFETY CONCERN*

* MINIMUM PSYCHOLOGICAL IMPACT

LASER OPTIONS FOR COMBINED RAYLEIGH/MIE PLUS O_2 DIAL

Two concepts were developed to implement the combined Rayleigh/Mie and O_2 DIAL laser systems. The first concept uses a single Nd:YAG laser with an optical switchyard to activate a number of modules to provide the four required laser outputs. While all technology exists, the complexity of interaction may make this an expensive approach. The second option considered two independent systems, and is attractive by optimizing each system for the job to be done. It requires two lasers and two sets of support electronics; using two lasers may require power levels in excess of what is conveniently provided on Shuttle. Clearly there is a lot of optimization to be done depending on the exact solution to the scientific analyses. The technology in the laser area is growing rapidly and we feel confident that the chosen techniques can in fact be implemented.

GENERAL ELECTRIC

LASER OPTIONS FOR COMBINED RAYLEIGH / MIE PLUS O_2 - DIAL

space division

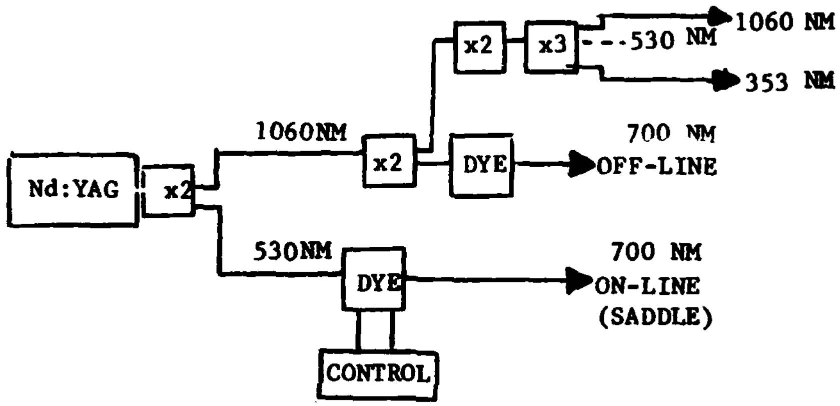

SINGLE Nd:YAG LASER CONCEPT

- o COMPLEX OPTICAL "SWITCH YARD"
- o MANY POTENTIAL MODULE ARRANGEMENTS
- o ALL SUB-MODULE TECHNOLOGY EXISTS
- o EFFICIENCY OPTIMIZATION REQUIRED

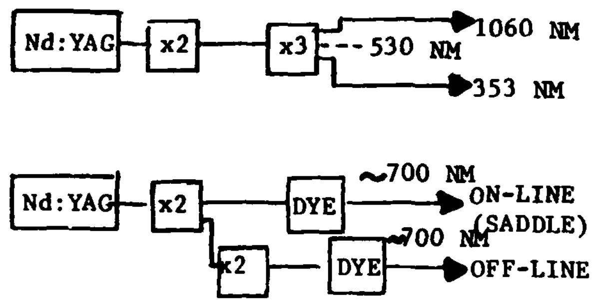

DUAL Nd:YAG LASER CONCEPT

- o TWO LASERS PROVIDE
  - HIGHER REDUNDANCY
  - SIMPLER MODULES
  - HIGHER COST

  TRADES REQUIRED
- o POWER AVAILABILITY MAY BE A BIG FACTOR HERE

OPTIMIZATION OF TECHNOLOGY VERSUS RESOURCES IS THE CHALLENGE HERE

SYSTEMS ENGINEERING APPROACH

PRECEDING PAGE BLANK-NOT FILMED

SYSTEMS ENGINEERING APPROACH

The chart on the accompanying page identifies those areas, relative to the design of the instrument, requiring tradeoffs which are bounded by the required design characteristics for meeting science requirements, and the design constraints which are imposed by Shuttle accommodations and flight environments. Instrument characteristics meeting the science requirements are developed early in the program based on the evaluation of performance analyses similar to those shown in Sections 5 and 6, and are usually bounded by state-of-the-art technology. Shuttle accommodations and flight environments are limited by the capability inherently designed into the Shuttle, the particular payload configuration flown, and associated launch/landing trajectory/in-flight orbit characteristics. The design tradeoffs, therefore, are used for the development of a preferred instrument hardware configuration which not only meets the criteria satisfying the science requirements, but also ensures compatibility with Shuttle accommodations and flight environments.

Physical parameters such as size and weight affect both Shuttle flight charges and instrument costs. Power influences the size of the thermal control system and power supply subsystems. Critical optical component alignment requirements impact the degree of complexity required by the structural support and thermal control subsystems. The point is that many parameters are influenced by one another and, therefore, the design tradeoffs must encompass the full scope of parameters, and their variations, in order to develop a feasible and cost effective preferred instrument design concept.

GENERAL ELECTRIC

space division

SYSTEMS ENGINEERING APPROACH

INSTRUMENT CHARACTERISTICS TO MEET SCIENCE REQUIREMENTS

- LASER / TRANSMITTER SYSTEM
- RECEIVER SYSTEM
- DETECTORS

DESIGN TRADEOFFS

- SIZE
- WEIGHT
- POWER
- STRUCTURAL
- THERMAL
- ALIGNMENT STABILITY
- C&DH
- ATTITUDE
- SAFETY

SHUTTLE ACCOMMODATIONS AND FLIGHT ENVIRONMENTS

- CREW/C&W I/F
- PALLET / STR
- SUPPORT S/S
  - POWER
  - THERMAL
  - C&DH
- ENVIRONMENTS
  - THERMAL
  - g's
  - VIBRATION
  - CONTAMINATION
- ATTITUDE

PREFERRED CONCEPT (FEASIBLE AND COST EFFECTIVE)

DESIGN PHILOSOPHY

This chart provides the design philosophy used relative to defining the characteristics of the preferred instrument concept. Our approach here is that a cost effective and low risk design concept be pursued which meets the study objectives without lengthy and costly test programs and integration procedures which are normally associated with flight qualified hardware programs. By making use of existing technology and standardized hardware components, and stressing a simplistic design approach, we can ensure the evolution of an operational instrument concept with minimum perturbations expected during the development program.

GENERAL ELECTRIC

space division

DESIGN PHILOSOPHY

- AVOID COMPLEXITY AND MAINTAIN ADEQUATE MARGINS
- MAXIMIZE USE OF EXISTING TECHNOLOGY
- MAXIMIZE USE OF FLIGHT QUALIFIED COMPONENTS (NASA STD HWD)
- MINIMIZE DEPENDANCE ON SHUTTLE ACCOMMODATIONS
- COMPLY WITH NASA SAFETY POLICIES AND PROCEDURES FOR SHUTTLE PAYLOADS.

SECTION 5

SHUTTLE/SPACELAB EXPERIMENT PERFORMANCE

PRECEDING PAGE BLANK-NOT FILMED

SHUTTLE/SPACELAB EXPERIMENT PERFORMANCE

This section is divided into the following three major parts:

1) Computer Simulation Program - this subsection presents the key elements used in the computer simulations for the analysis of the Rayleigh/Mie and O_2-DIAL density measurements techniques.

2) Rayleigh/Mie Analysis - this subsection presents the equations and results obtained to evaluate the expected performance of this technique from the Space Shuttle.

3) O_2-DIAL Analysis - this subsection presents equations and expected accuracy results as they pertain to this measurement technique.

COMPUTER SIMULATION PROGRAM

COMPUTER SIMULATION PROGRAM

This section describes the key elements of the computer simulation program which were used to analyze the Rayleigh/Mie and O_2 DIAL density measurement techniques. Described herein are the basic transfer equations, the models for properties of aerosols and atmospheres, and the basic numerical techniques used to come up with the simulation results.

ATMOSPHERIC RADIATIVE TRANSFER

To analyze the Lidar equation we use a basic radiative transfer solution. The change in intensity in the beam passing through an incremental range dx is equal to a source in the volume at that range interval minus the loss from the beam in transversing to that altitude. We've treated the problem in one dimension, assuming that the atmosphere is homogeneous in the horizontal plane. For the loss functions we use only single scattering because the atmosphere is optically thin. We do not consider self emission from the atmosphere in the range of wavelengths and times that we're addressing. Any self emission, scattered sunlight, etc. must be added analytically after the computer solution is found. The downward ray intensity is found directly from the loss of energy integrated from the Shuttle to the altitude of interest, and can be expressed in terms of a transmission function. The absorption coefficient α_T is the total absorption loss from the beam from all causes: aerosol absorption, aerosol scattering, molecular absorption, and molecular scattering. The source in the volume element is equal to the energy in the downward directed beam times the backscatter coefficient at that altitude. The backscatter coefficient is a sum of backscattering from molecules and aerosols. The return signal generated in a given range bin is the integral of that source function over that range bin attenuated by the absorption between the top of that range bin and the Shuttle altitude.

ATMOSPHERIC RADIATION TRANSFER

- RADIATIVE TRANSFER EQUATION

CHANGE IN INTENTSITY		SOURCE		SINK
$\frac{dI}{dx}$	=	ε	-	$I\alpha_T$

- DOWNWARD RAY ($\varepsilon = 0$)

$$I(X) = I_o\, e^{-\int_o^x \alpha_T dx} = I_o\, T(X)$$

- SOURCE IN A VOLUME ELEMENT

$$\varepsilon = I(X)\, \alpha_B\, (X)$$

$$\Delta I(X_1, X_2) = \int_{X_1}^{X_2} \varepsilon\, e^{-\int_{X_2}^{x} \alpha_T dx}\, dX^1$$

- RECEIVED SIGNAL

$$I_R = \Delta I(X_1, X_2)\, T(X_2)$$

RADIATIVE PROPERTY MODELS

The extinction of the beam is the sum of the molecular absorption, molecular scattering, aerosol absorption, and aerosol scattering coefficients. Principal features of these coefficients are portrayed graphically in the following pages. To calculate absorption profiles for O_2 we must recognize that they are a function of pressure, temperature and wavelength. We use standard values for line strengths, Boltzman distributions appropriate to the temperature at the altitude of interest, and Voigt profiles that include the appropriate pressure broadening terms for each altitude.

Absorption by aerosols in a complex function of number density and wavelength, and strongly dependent on type of aerosol as is shown in the following pages. Particularly crucial is the source of the aerosol; continental vs. maritime, and urban vs. rural. In our calculations we used the generally accepted standard aerosol description incorporated in LOWTRAN 3B. For scattering functions we use the well understood Rayleigh scattering properties of molecules.

RADIATIVE PROPERTY MODELS

- EXTINCTION

MOLECULAR AEROSOL

$$\alpha_T = \underbrace{\alpha_{MA} + \alpha_{MS}}_{\text{MOLECULAR}} + \underbrace{\alpha_{AA} + \alpha_{AS}}_{\text{AEROSOL}}$$

- ABSORPTION
  - O_2 LINE ABSORPTION - $f(T,P,\lambda)$

    LINE STRENGTH
    BOLTZMANN DISTRIBUTION
    VOIGT PROFILE
  - AEROSOL ABSORPTION - $f(n,\lambda)$

    LOWTRAN 3b

- SCATTERING
  - MOLECULAR (RAYLEIGH) - $f(T,P,\lambda)$

    LOWTRAN 3b
  - AEROSOL - $f(n,\lambda)$

    LOWTRAN 3b

ATTENUATION COEFFICIENTS FOR AEROSOL TRANSMITTANCE (ABSORPTION AND TOTAL EXTINCTION)

This figure* which is included here for reference purposes only, provides absorption and total extinction data for aerosols over a broad range of wavelengths. The chart is normalized to a 1 km path length in a standard sea level atmosphere. The curves should be shifted in the direction of equivalent path lengths according to the scaling factor shown on the right side, in order to determine the corresponding transmittance values for other than 1 km equivalent path lengths.

The symbols C6, C7A, and C7 are the designations used in the LOWTRAN model to identify the molecular scattering, aerosol absorption, and aerosol extinction coefficients, respectively. The values shown for the aerosols are based on measurements of continental aerosols under moderate visibility conditions, i.e., 23 km. These curves were subsequently updated in the LOWTRAN 3B model to account for differences between maritime, urban, rural and average continental aerosol models within the first few kilometers of the atmosphere. The following four charts provide further definition on these aerosol models.

* Taken from: Selby, J.E.A., and McClatchey, R.A. (1975) Atmospheric Transmittance from 0.25 to 28.5 μM: Computer Code LOWTRAN 3, AFCRL-TR-75-0255.

GENERAL ELECTRIC

ATTENUATION COEFFICIENTS FOR AEROSOL TRANSMITTANCE (ABSORPTION AND TOTAL EXTINCTION)

space division

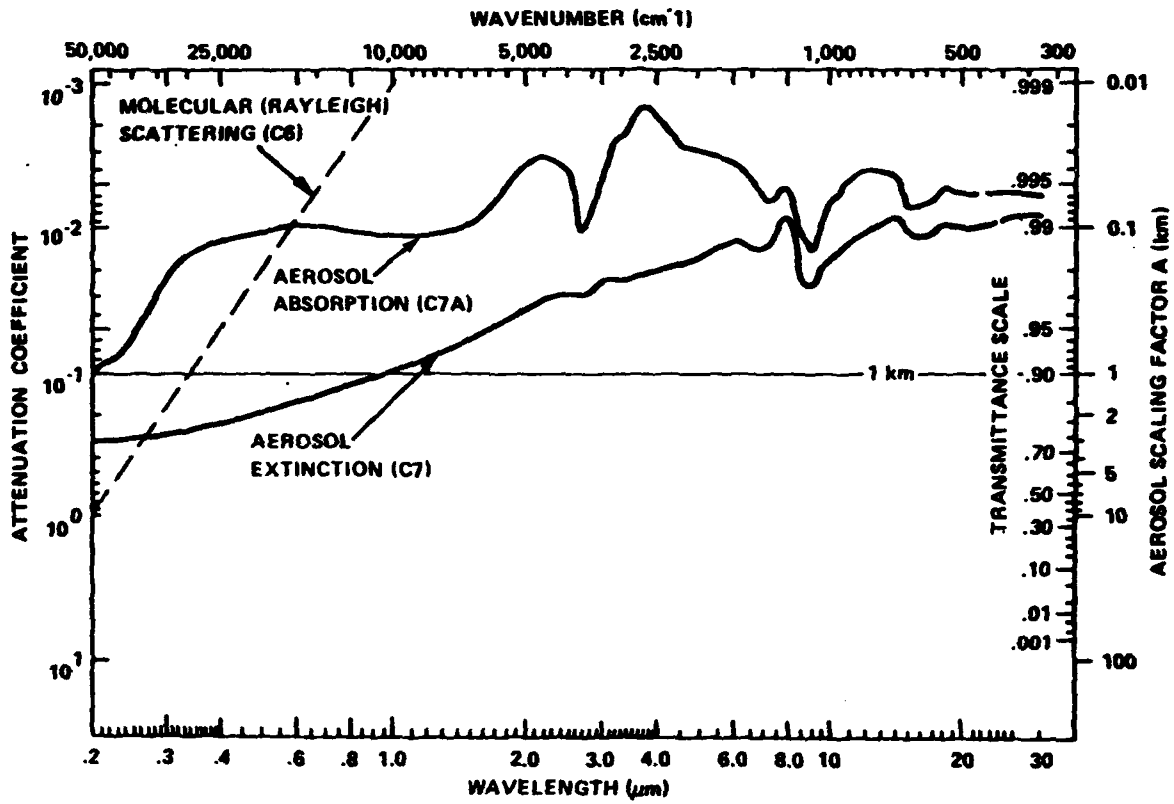

SIZE DISTRIBUTIONS FOR LOWTRAN 3B AEROSOL MODELS

This figure* identifies the distribution of aerosols that go into making up the properties of the LOWTRAN 3B model. Both Rural and Maritime aerosol models are portrayed; however, our analyses dealt strictly with the Rural Model which is intended to replace the LOWTRAN 3 Aerosol Model, a preliminary version of the Rural Model. For comparison purposes, the earlier LOWTRAN 3 Aerosol Model is included in the figure for the Rural Model and is labeled Modified Haze C.

The reference source* for this data indicates that the Urban Model in LOWTRAN 3B is assumed to have the same size distribution as shown for the Rural Model. Also, that the Tropospheric Model, which was developed primarily for use above the boundary layer, has the same size distribution as the small particle component of the Rural and Urban Models, i.e., the $n_1(r)$ curve in the Rural Model figure.

Two component curves are shown to provide for aerosol mixture varaitions, e.g., the Rural Model is assumed to be a mixture of 70 per cent water soluble aerosols, $n_1(r)$, and 30 per cent dust-like aerosols, $n_2(r)$.

* Taken from: Selby,J.E.A., Shettle, E.P., and McClatchey, R.A. (1976), Atmospheric Transmittance from 0.25 to 28.5 μm: Supplement LOWTRAN 3B, AFGL-TR-76-0258.

GENERAL ELECTRIC

SIZE DISTRIBUTIONS FOR
LOWTRAN 3B AEROSOL MODELS

space division

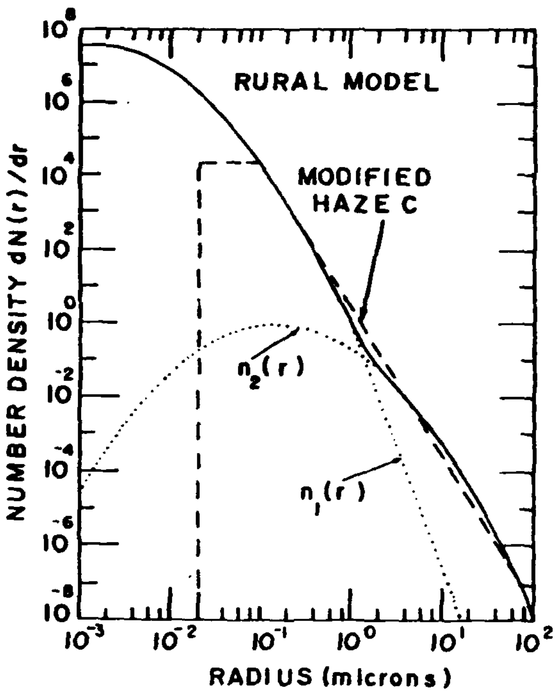

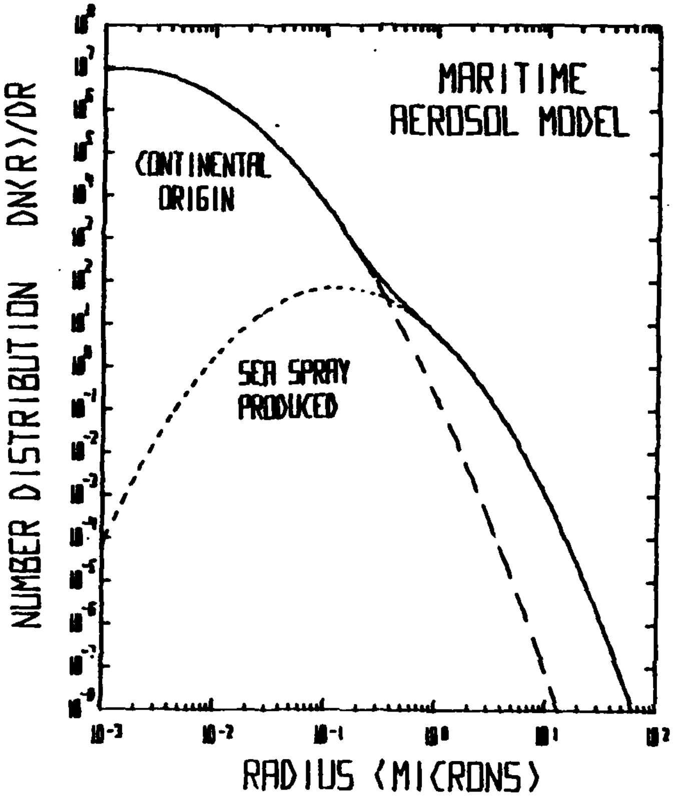

AEROSOL MODELS COMPARISON

The change in extinction coefficient vs. wavelength for aerosols clearly depends on the type of aerosol, whether it is rural, urban, or maritime. Of particular interest in this figure* is the general slope of extinction coefficient vs. wavelength in the region between one micron and 0.3 microns, which varies approximately one over wavelength. On the other hand, in this region, the slope for scattering from molecules in the Rayleigh model varies as one over wavelength to the 4th power. These differences in slopes are the basis of the Rayleight/Mie technique to determine the aerosol contributions to the density measurements. Also, note particularly the close convergence of the slopes for many of the aerosol models shown in this figure.

* The reference source is on page 68.

GENERAL ELECTRIC

AEROSOL MODELS COMPARISON

space division

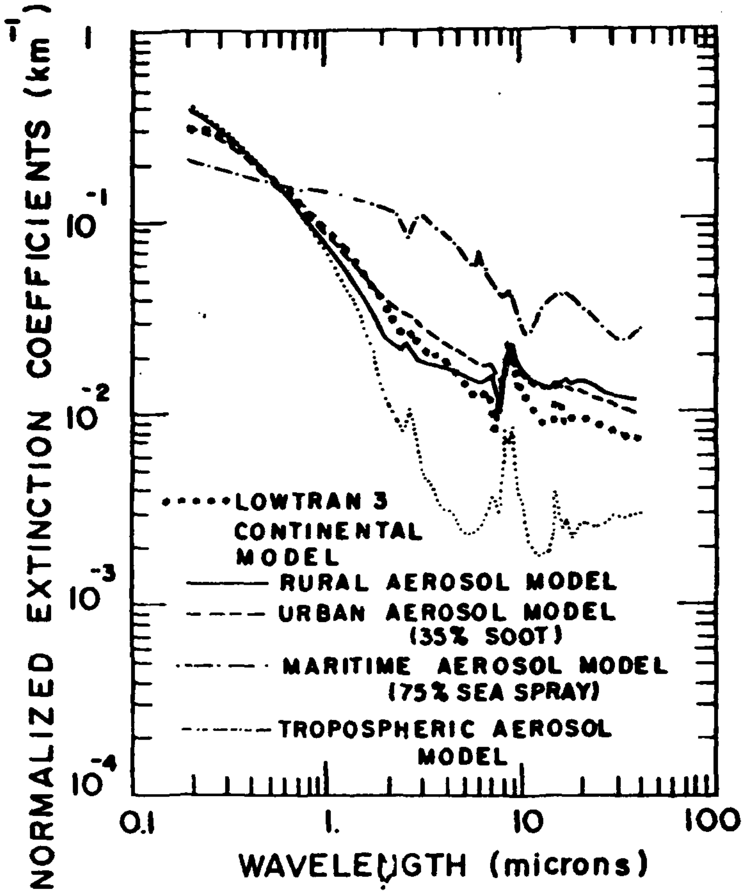

SCATTERING AND ABSORPTION CONTRIBUTIONS TO RURAL AEROSOL MODEL EXTINCTION COEFFICIENT

The Rural Aerosol Model* shows clearly that absorption from aerosols is not a prime factor in the analysis, particularly below the strong molecular peaks in the mid infrared. In the visible, scattering is the dominant effect of these aerosols, such that we can project their absorption characteristics with some confidence.

The Rural Model is intended to represent the aerosol conditions one finds in continental areas which are not directly influenced by urban and/or industrial aerosol sources. This continental, rural aerosol background is partly the product of reactions between various gases in the atmosphere and partly due to dust particles picked up from the surface. The particle concentration is largely dependent on the history of the airmass carrying the aerosol particles. In stagnating airmasses, e.g., under wintertype temperature inversions, the concentrations may increase to values causing the surface layer visibilities to drop to a few kilometers.

* Taken from: Shettle, E.P., and Fenn, R.W. (1976) Models of the Atmospheric Aerosols and their Optical Properties in AGARD Conference Proceedings No. 183, Optical Propagation in the Atmosphere, presented at the Electromagnetic Wave Propagation Panel Symposium, Lyngby, Denmark, 27-31 October 1975. (Available from NTIS, Acc. No. N76-29817).

GENERAL ELECTRIC

SCATTERING AND ABSORPTION CONTRIBUTIONS TO RURAL MODEL EXTINCTION COEFFICIENT

space division

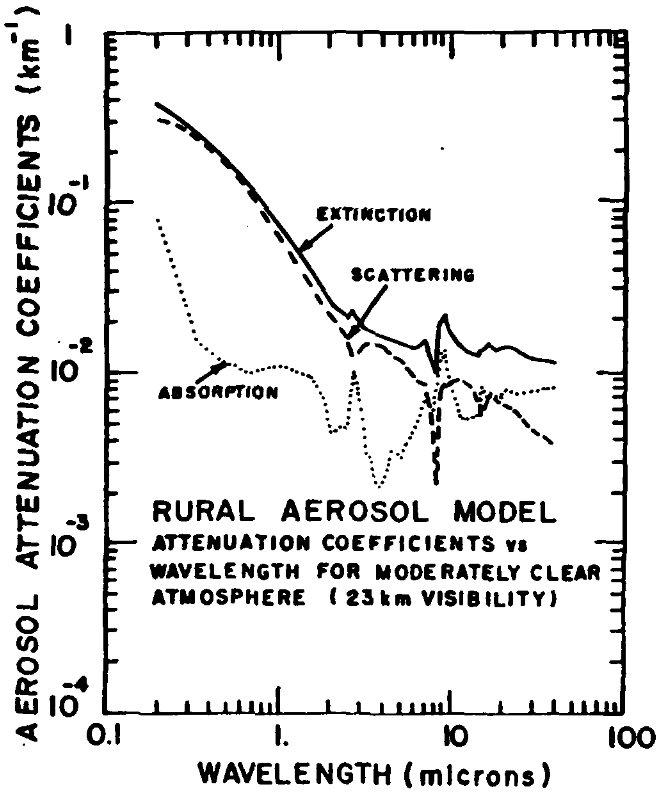

SCATTERING AND ABSORPTION CONTRIBUTIONS TO URBAN AEROSOL MODEL EXTINCTION COEFFICIENT

Urban aerosols* which might be observed in regions near population or industrial centers are characterized by significant absorption throughout the visible and infrared region. The Urban Model is a modification of the Rural Model with the addition of aerosols from man-made products, hydrocarbons and the like, generated from industry and transportation. LIDAR techniques have been used to address pollution problems in urban areas; however, our present study is more interested in the large scale density variations, and hence we find the Urban Aerosol Model inappropriate.

*The reference source is on page 72.

GENERAL ELECTRIC

URBAN AEROSOL MODEL

space division

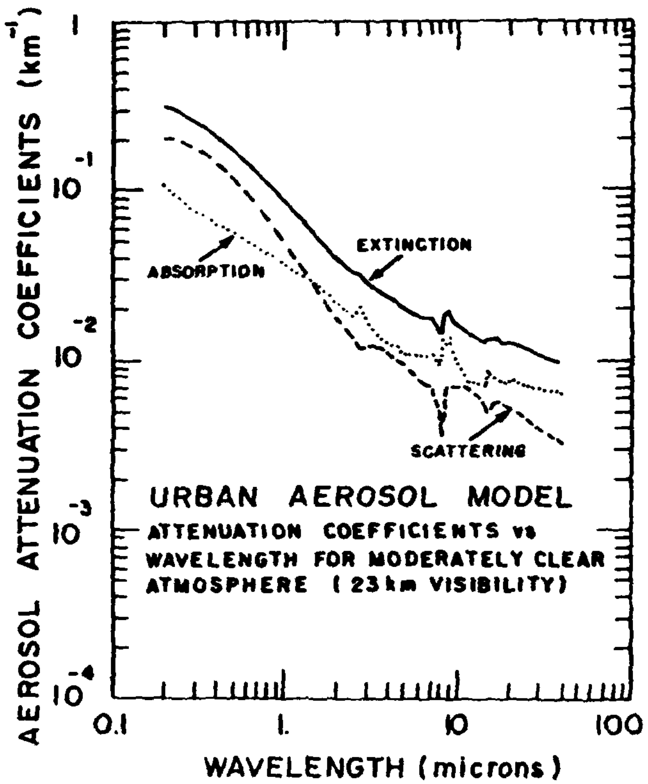

NORMALIZED SCATTERING PHASE FUNCTION OF AEROSOL AND AIR BASED ON THE MODEL

A critical factor in our analysis is the backscatter coefficient of the aerosols. This figure shows a calculated scattering phase function for aerosols and air based on the LOWTRAN model. Particular concern is near the scattering angle of 180° where there is a strong backscatter peak in the aerosols. The magnitude of this peak is highly dependent on the size distribution and origin of the aerosols, including a sizable wavelength dependence as shown by the corresponding variation in backscatter peak values. The uncertainty in the ratio of the backscatter peak for aerosols to the backscatter peak for molecules is a significant error term in our analyses.

The model used to develop the aerosol curves shown in this figure is based on a "clear" atmosphere, i.e., visibility of 23 km at ground level, and the Modified Haze C size distribution shown on page 69, with the exception of a large particle cutoff (vertical line) made at a radius of 10 microns. Further information can be obtained in Section 2.3 of the reference source identified below.

* Taken from: McClatchey, R.A., Fenn, R.W., Selby, J.E.A.,Volz, F.E., and Garing, J.S. (1971), Optical Properties of the Atmosphere (Revised), AFCRL-71-0279.

GENERAL ELECTRIC

NORMALIZED SCATTERING PHASE FUNCTION OF AEROSOL AND AIR BASED ON THE MODEL

space division

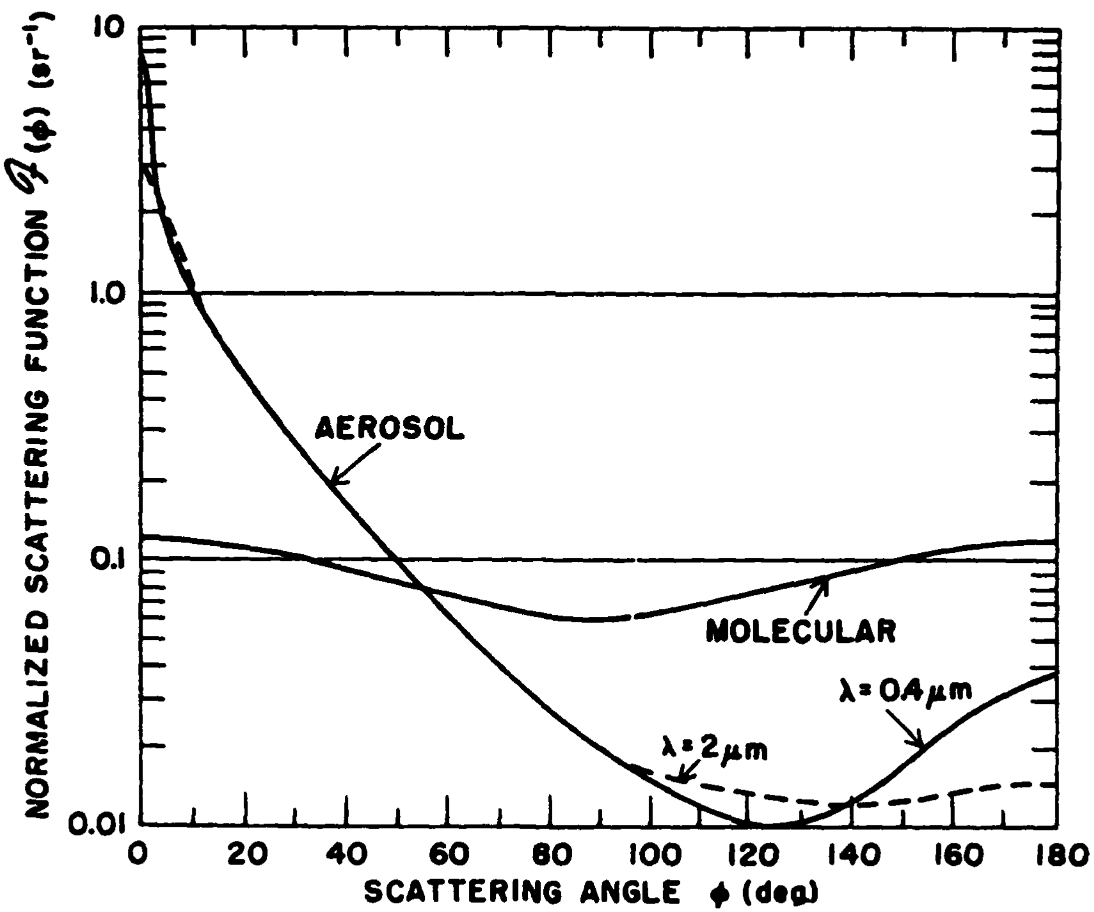

SCATTERING ANGLE PHASE FUNCTION FOR 1.06μ

This figure* highlights even more dramatically the variation in backscatter coefficient that can be seen among the various types of aerosols.

* The reference source is on page 72.

GENERAL ELECTRIC

space division

SCATTERING ANGLE PHASE FUNCTION FOR 1.06 MICRONS

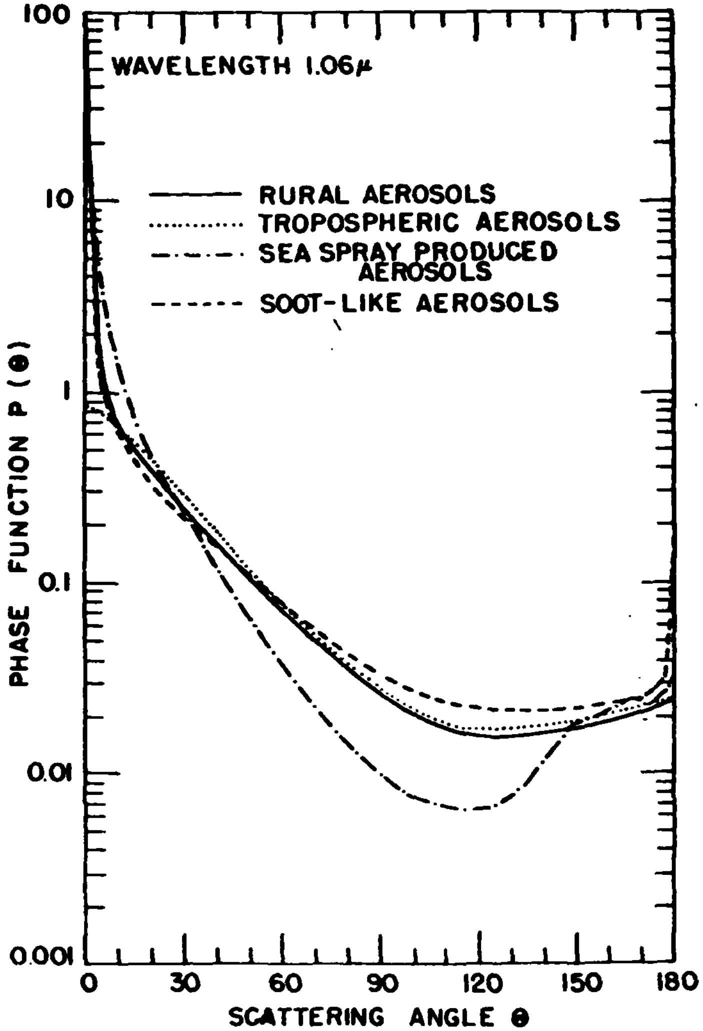

SCATTERING ANGLE PHASE FUNCTION FOR 10.6 μ

This figure* identifies the aerosol properties for operation at 10.59 micrometers. These data are included for reference purposes only. Our model is capable of handling backscattering from the CO_2 laser at 10.6 microns, should it be desired in some future analysis. However, we are not considering operating with a CO_2 laser at this time.

* The reference source is on page 72.

GENERAL ELECTRIC

SCATTERING ANGLE PHASE FUNCTION FOR 10.6 MICRONS

space division

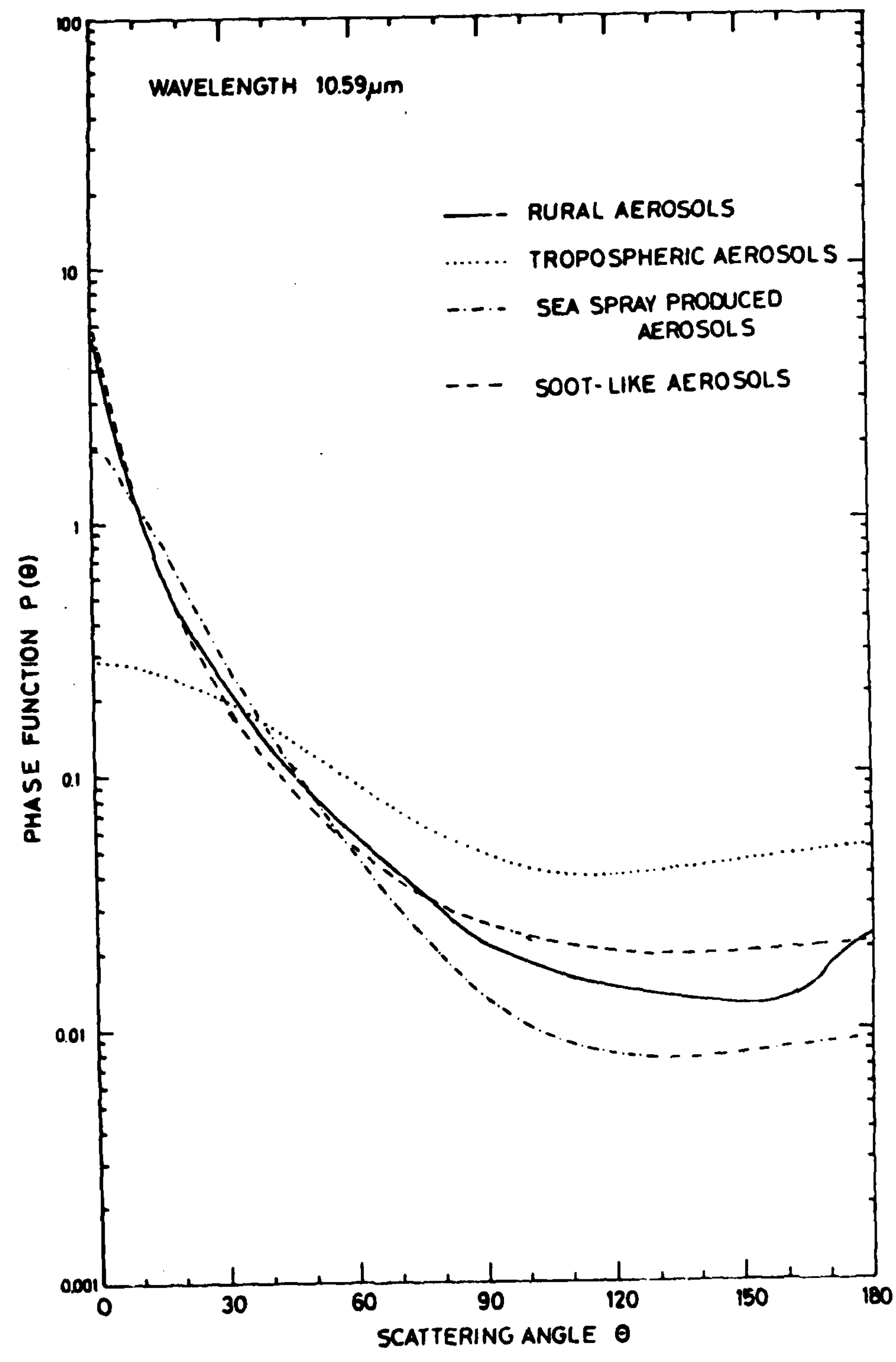

ATMOSPHERIC AEROSOL MODELS

This figure* provides the vertical distribution of the attenuation coefficients for various aerosol models which have been developed for the boundary layer, the upper troposphere, the stratosphere, and the upper atmosphere. A good description of these models, and some examples of scaling to other wavelengths can be found in the reference source for this figure from which the following summary has been extracted.

(a) For the Boundary Layer (below 2 km), 10 models have been defined which describe the aerosols in rural, urban, and maritime environments for several surface meteorological ranges between 2 and 50 km.

(b) For the upper troposphere there are two models which represent spring and summer conditions versus fall and winter conditions.

(c) In the stratosphere (up to 30 km), models are presented for background, moderate, high, and extreme volcanic conditions for each of the two seasonal models.

(d) For the upper atmosphere (above 30 km), two models are presented. One of these corresponds to the most likely background conditions, and the other represents the high aerosol concentrations often observed at these altitudes (in thin layers).

Also shown for comparison are the Rayleigh profile, and ELTERMAN's 1968 model.

Atmospheric Aerosol Models used in our analysis are as follows:

(a) Temperature/Pressure
- Mid-latitude summer

(b) Aerosol Concentration
- Standard Rural
- Visibility

  Variable
  23 KM

* The reference source is on page 72.

ATMOSPHERIC AEROSOL MODELS

GENERAL ELECTRIC

space division

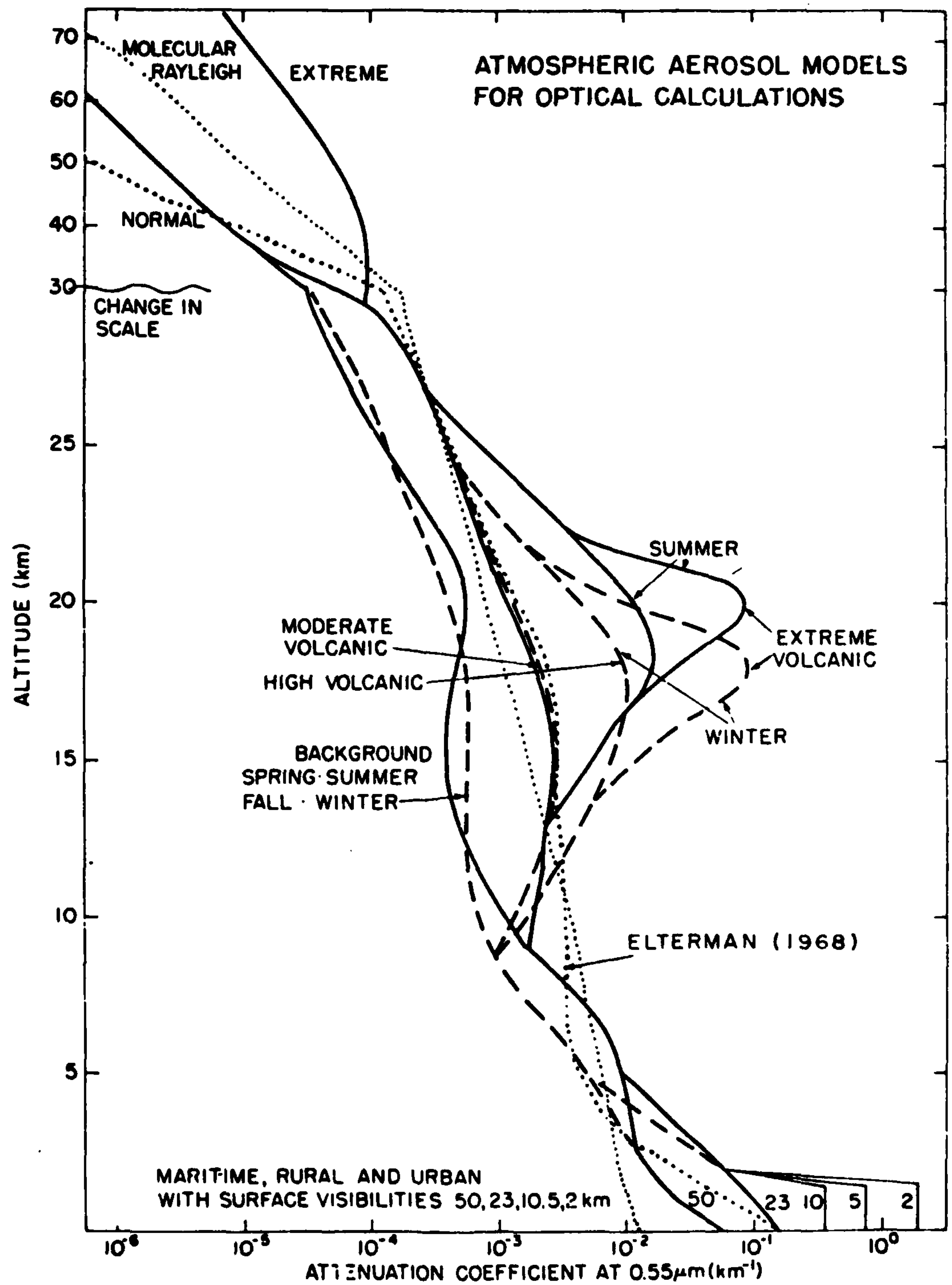

NUMERICAL TECHNIQUES USED IN OUR ANALYSIS

The numerical techniques summarized below were used for the design of the laser radar systems considered in this study and are based on the scattering models implemented in the LOWTRAN 3B computer program. Atmospheric transmission is computed by integration of the atmospheric extinction coefficient along the laser beam. Absorption and scattering coefficients are derived from the tabular atmospheric properties provided by LOWTRAN. Interpolation is performed linearly in temperature and logarithmically in pressure and species concentration. The integration assumes that the extinction coefficient can be fit by a quadratic in pressure and that the pressure decays exponentially with altitude over an integration step. The step sizes used for the calculations are 1 km at low altitudes and 2 km for altitudes above 35 km. The top of the atmosphere is assumed to be 86 km.

For the O_2 DIAL calculations the details of the absorption line profile are required. These were obtained by assuming Voight line shapes with a spectral resolution of 0.001 cm^{-1} at the line center. The resolution was doubled at every other wavenumber point and the line wings were cut off at 10 cm^{-1}. The laser beam was convolved with the absorption line by integration using Simpson's rule.

- ALTITUDE RESOLUTION
  - EXPONENTIAL INTEGRATION
  - 1 - 2 KM BITES
  - 65 POINTS IN 86 KM
- WAVENUMBER RESOLUTION
  - LINE CENTER 0.001 CM^{-1}
  - SPACING DOUBLES EVERY OTHER POINT (SIMPSON'S RULE)
  - LIMIT 2 ABSORPTION LINES
- CONVOLUTION WITH LASER PULSE
  - SIMPSON'S RULE
  - LINEAR AT EDGE OF PULSE

RAYLEIGH/MIE ANALYSIS

LIDAR EQUATION

The general LIDAR equation describes the interrelations among transmitted power, atmospheric properties, and detected signal.

This equation was modeled to calculate the Rayleigh/Mie return signals for all the cases considered, using a nominal LIDAR with

Transmitted Power:	1J/pulse at 1060 nm
	0.1J/pulse at 353 nm
Receiver Area:	1 m^2
Collection efficiency:	0.06 counts/photon

The model makes several assumptions that should be kept in mind:

a) Single scattering is assumed. Since typical model atmospheres are optically thin ($T \sim 0.5 - 0.8$), this is not a serious approximation

b) No clouds are assumed

c) The receiver FOV views the total transmitted beam. This is realistic for the ranges considered

d) No atmospheric emission or scattered sunlight are included. These must be addressed manually in the error analyses.

e) The atmosphere is assumed to be horizontally uniform when multiple shots are averaged. To some extent, this assumption is the exact problem we are trying to measure, so care has been taken not to average over large horizontal ranges.

The following pages outline the application of the LIDAR equation to the measurement of atmospheric density by the Rayleigh/Mie separation technique.

GENERAL ELECTRIC

space division

LIDAR EQUATION

$$P = \frac{J \lambda A H \beta_{180} \Delta R}{h c R^2} \, \mathrm{Exp}\left[-2\int_0^R (\alpha + \sigma\rho)\, dR\right]$$

J = TRANSMITTED ENERGY J/PULSE

P = RETURN COUNTS/PULSE

λ = WAVELENGTH

H = SYSTEM EFFICIENCY

β_{180} = 180° BACKSCATTER COEFFICIENT Km^{-1} $STER^{-1}$

α = EXTINCTION COEFFICIENT EXCLUDING ABSORBING GAS

σ = ABSORPTION COEFFICIENT OF GAS

ρ = GAS DENSITY

h = PLANKS CONSTANT

R = RANGE TO SCATTERING CELL

ΔR = RANGE CELL LENGTH

A = RECEIVER AREA

ANALYSIS OF RAYLEIGH/MIE SEPARATION

The technique for the determination of molecular density using Rayleigh/Mie separation is shown in this model.

1060 Signal: The LIDAR system measures the return signal as a function of range and/or altitude. This signal is dominated by aerosol scattering.

1060 Rayleigh Fraction: Using the standard LOWTRAN 3B model, an estimate is made of the fraction of the 1060 signal caused by Rayleigh (molecular) scatter. (Uncertainty in this estimate is carried as an error term in the error analysis). Subtracting this fraction leaves the clear measure of aerosol content in the atmosphere, designated 1060 aerosol.

Wavelength Variation: The extrapolation of the effects of aerosols, as measured at 1060 nm, to 353 nm is critical to the analysis. Nominal haze and aerosol models are used to make this extrapolation, but carry uncertainties in extrapolation as a parameter in the error analysis.

353 Signal: The LIDAR signal measured at 353 nm is dominated by Rayleigh scattering from the atmosphere, particularly for altitudes above the 5 km limit of the ground haze layer. The 1060 measurement allows us to subtract the aerosol contribution at 353 nm.

353 Rayleigh Fraction: We have derived a best estiamte of the Rayleigh contribution to return signal at 353 nm. Using a haze model for final correction of target-to-Shuttle attentuation, and well-established Rayleigh scattering cross-section for O_2 and N_2, we finally derive molecular density.

This treatment is adequate to define the feasibility of the basic experimental approach. A high priority extension of this analysis is the inclusion of a more refined data set (meteorological maps, cloud cover, target area, and iterative analysis) into the experiment model, along with appropriate analysis algorithms, to approach the maximum contribution that an operational LIDAR could make to the density problem.

GENERAL ELECTRIC

ANALYSIS OF RAYLEIGH / MIE SEPARATION USING Nd (1060) AND Nd x3 (353Nm)

space division

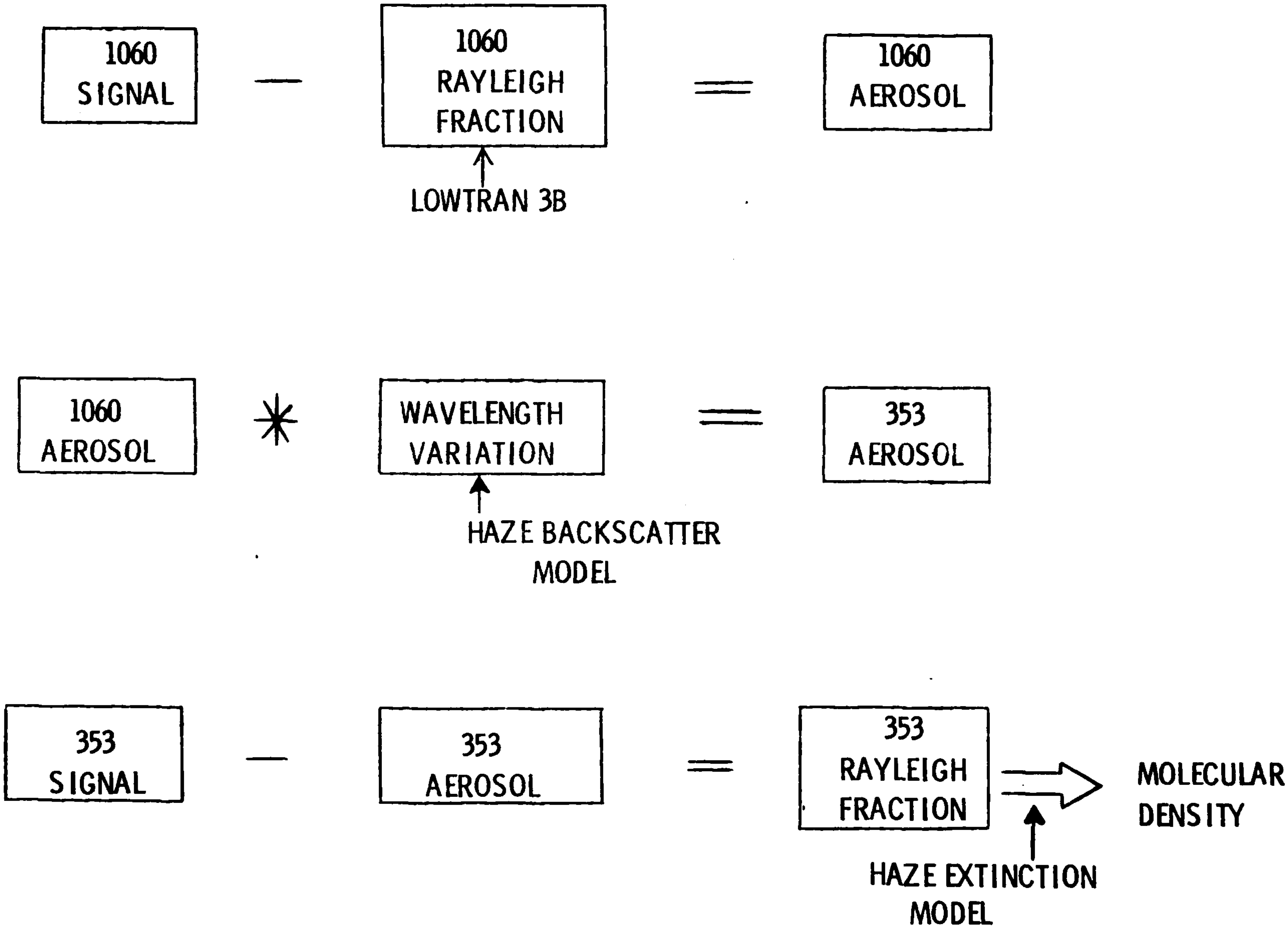

PHOTON RETURNS AT 15 KM USING LOWTRAN 3B ATMOSPHERE

This figure illustrates the potential strength of the Rayleigh/Mie approach. At 15 km the return signal at 1060 nm is dominated by Mie (aerosol) scattering. Rayleigh (molecular) scattering contributes only 25% of the total return. Thus, with even a rough knowledge of molecular concentration (density), we can measure aerosols very accurately.

At 353 nm, the aerosol effects are strongly overshadowed by molecular scattering, and contribute only 10% of the total signal. This contribution is corrected for by the 1060 nm aerosol measurement to give accurate density values.

A value of .04 was used for the normalized aerosol backscatter phase function ØA. This value is used in the following series of figures for the Rayleigh/Mie analysis of the Shuttle/Spacelab experiment.

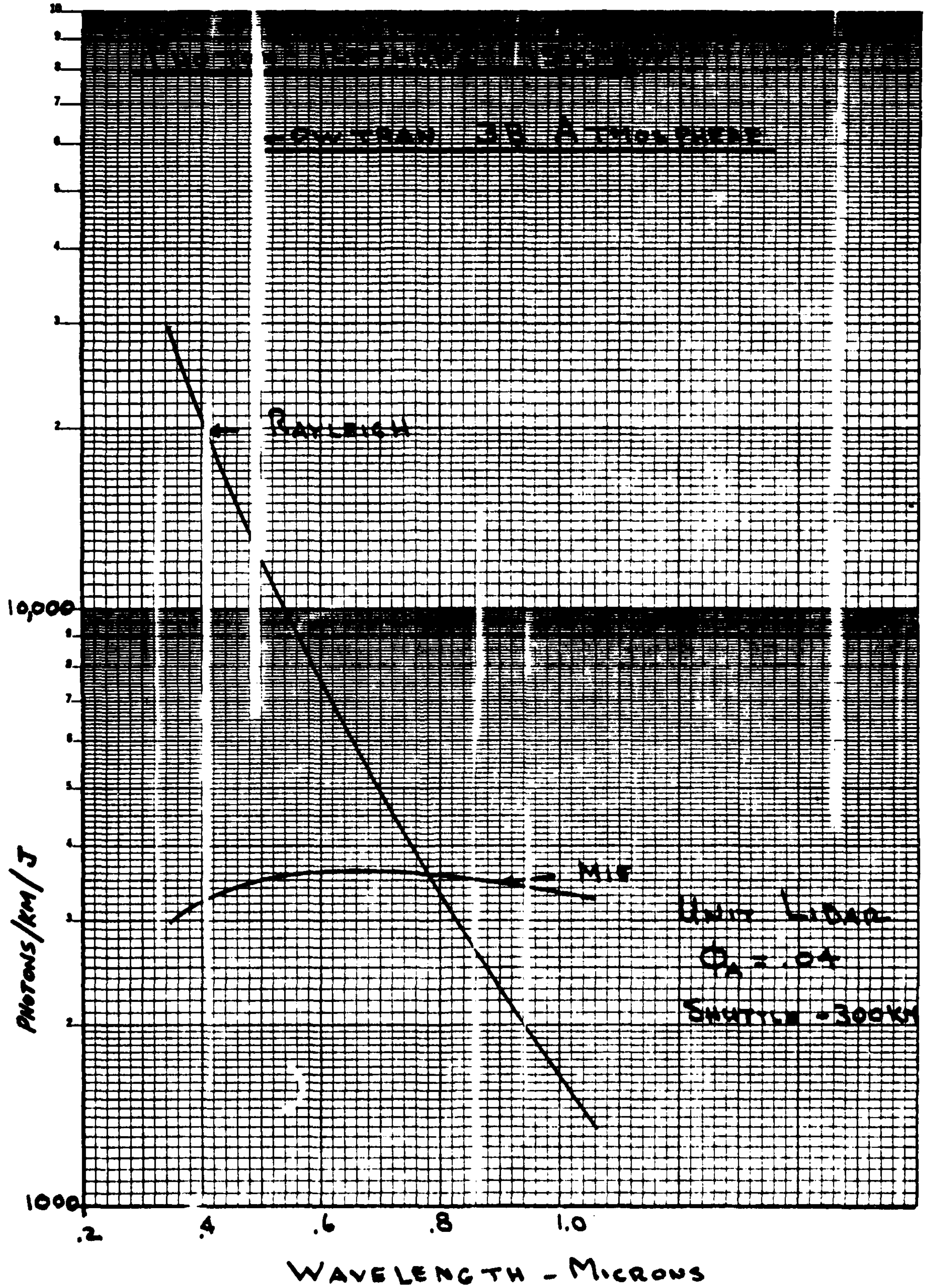

LOWTRAN 3B ATMOSPHERE
RAYLEIGH
MIE
UNIT LIDAR
Φ_A = .04
SHUTTLE - 300 KM
PHOTONS/KM/J
10,000
1000
.2
.4
.6
.8
1.0
WAVELENGTH - MICRONS

AEROSOL VOLUME BACKSCATTER COEFFICIENT

The largest uncertainty in the preceding figure is the wavelength dependence of the Mie scattering function. This figure illustrates the wavelength variation of the Mie back-scattering coefficient for several typical cases.

Both low and high altitude hazes have $1/\lambda$ backscatter variations between 1060 nm and 353 nm. Clouds, however, have a complex variation dependent on cloud type (i.e. particle size distribution, ice/water, etc.) Only the haze problem is addressed in our analysis.

GENERAL ELECTRIC

space division

AEROSOL VOLUME BACKSCATTER COEFFICIENT

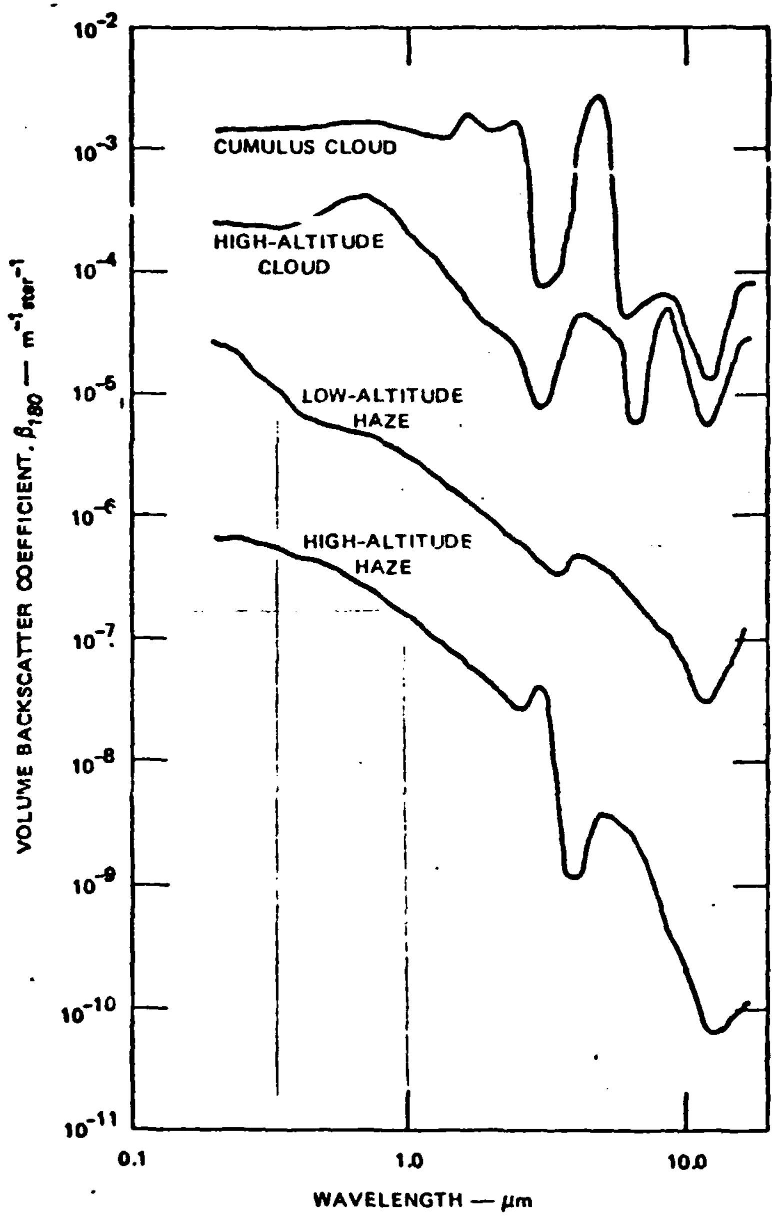

AEROSOL EXTINCTION COEFFICIENTS

The Lidar equation presented previously includes an exponential loss term to describe the two-way signal attenuation resulting from total extinction (absorption and scattering) by aerosols and molecules over the optical path. This figure shows the wavelength variation of total extinction coefficients for haze and Rayleigh scatter employed in our computer simulation. The coefficients are peak values (i.e. Rayleigh scatter at sea level) and are scaled proportional to particle density in the model.

GENERAL ELECTRIC

AEROSOL EXTINCTION COEFFICIENTS

space division

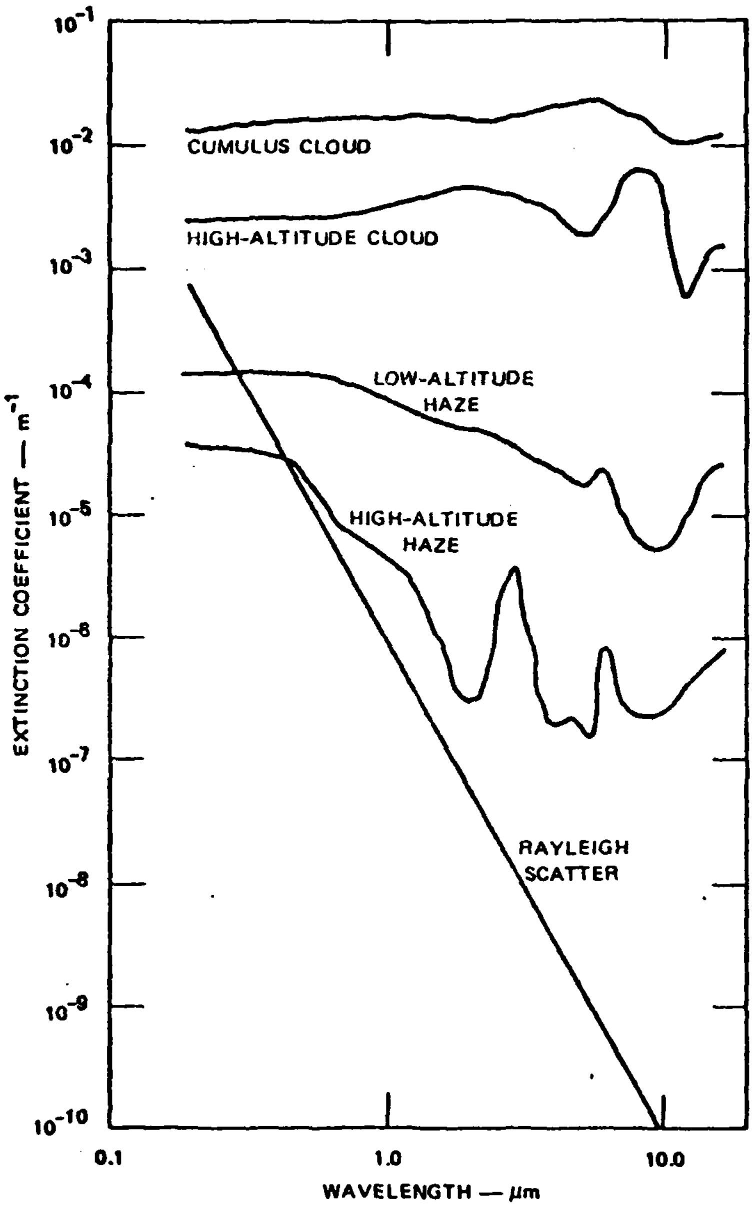

EXPECTED LIDAR RETURNS FOR STANDARD LOWTRAN 3B ATMOSPHERE (λ = 353 NM)

When all the atmosphere and aerosol parameters are combined with a Shuttle-borne Lidar system, the computer model predicts the 353 nm signal levels shown in the accompanying figure.

The "Total" return is the actual count that would be recorded in telemetry. The contributions from "Aerosol" and "Molecule" are defined by the ratio of aerosol and Rayleigh backscatterig coefficients at each altitude.
The curves displays several interesting features:

A) Total signals per shot are not exceedingly high. It is clear that multiple shot averaging will be required to achieve desired accuracies.

B) Above 20 km, aerosols contribute less than 10% of the total signal at 353 nm. Therefore, even fairly rough aerosol measurements at 1060 nm would be sufficient to achieve 10% density measurements above 20 km, if enough counts can be measured to provide a statistically significant signal.

C) The stratospheric aerosol layer in the 7-20 km region shows up clearly in the simulation. The range of variability of this layer was shown earlier in the figure on page 83. Uncertainties in the properties of these aerosols is a significant potential error term in the measurement.

D) The boundary layer aerosols near the ground create the most dramatic feature in the simulation, as the aerosol return overwhelms the molecular return below 5 km. Also in this region, total extinction effects absorb and scatter up to 85% of the return signal. The combination of increased aerosol return and significant total extinction severely limit the achieveable accuracies below 5 km.

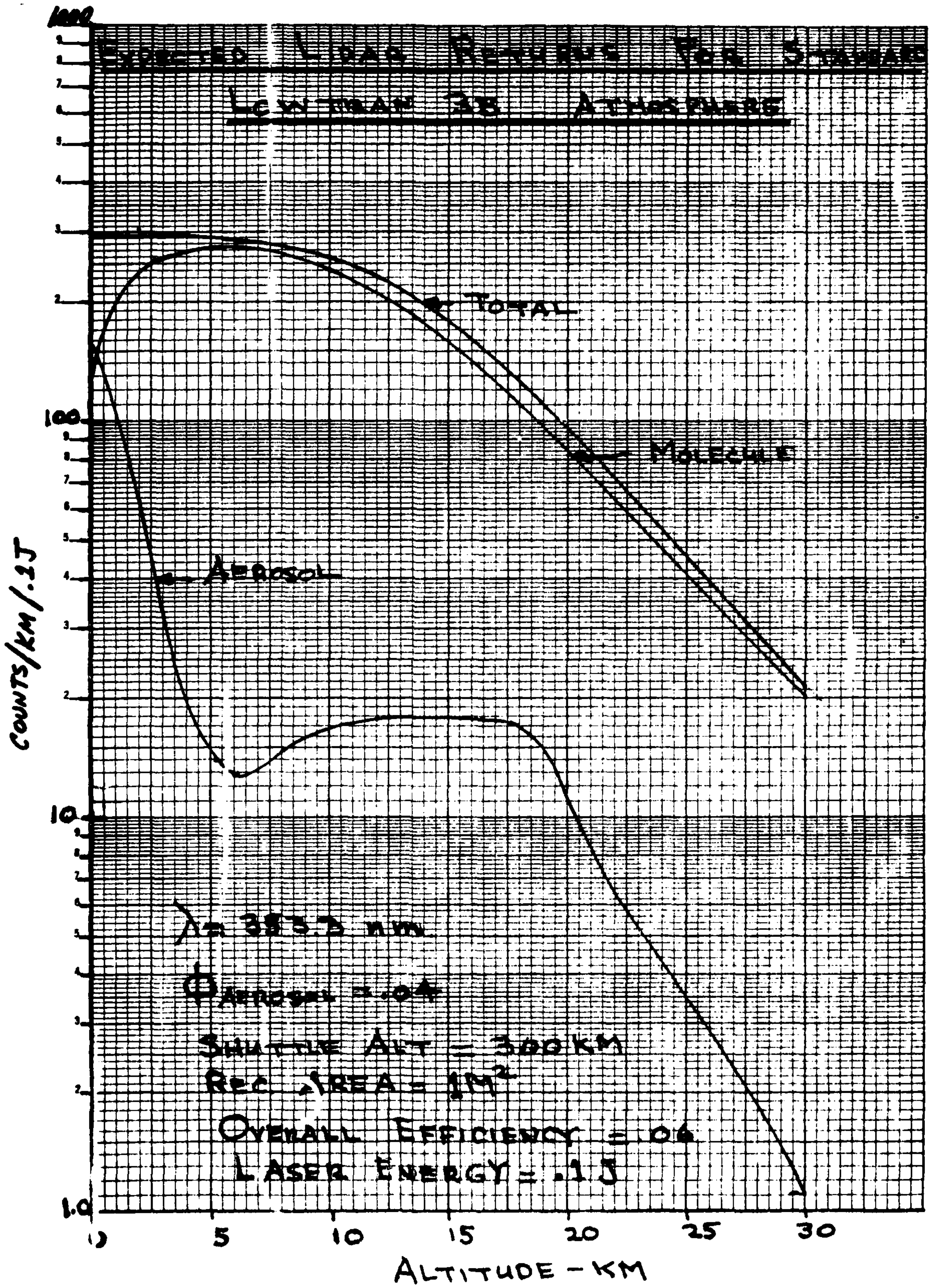
EXPECTED LIDAR RETURNS FOR STANDARD
LOWTRAN 3B ATMOSPHERE
TOTAL
MOLECULE
AEROSOL
λ = 353.3 nm
Φ AEROSOL = .04
SHUTTLE ALT = 300 KM
REC AREA = 1M²
OVERALL EFFICIENCY = .06
LASER ENERGY = .1 J
COUNTS/KM/.1J
ALTITUDE - KM
1000
100
10
1.0
0
5
10
15
20
25
30

EXPECTED LIDAR RETURNS FOR STANDARD LOWTRAN 3B ATMOSPHERE (λ = 1060 NM)

The 1060 signal provides a good measurement of aerosols over the entire altitude range. Signal levels are useable, and aerosols contribute the majority of the signal that is observed. The influence of the ground layer is again significant, even in a clear model with 23 km visibility at the ground. Both aerosol scattering and total extinction effects increase sharply below 5 km, varying by factors of two or more over a single 1 km range bin. This will make useable data extremely difficult to extract reliably from the actual Lidar return.

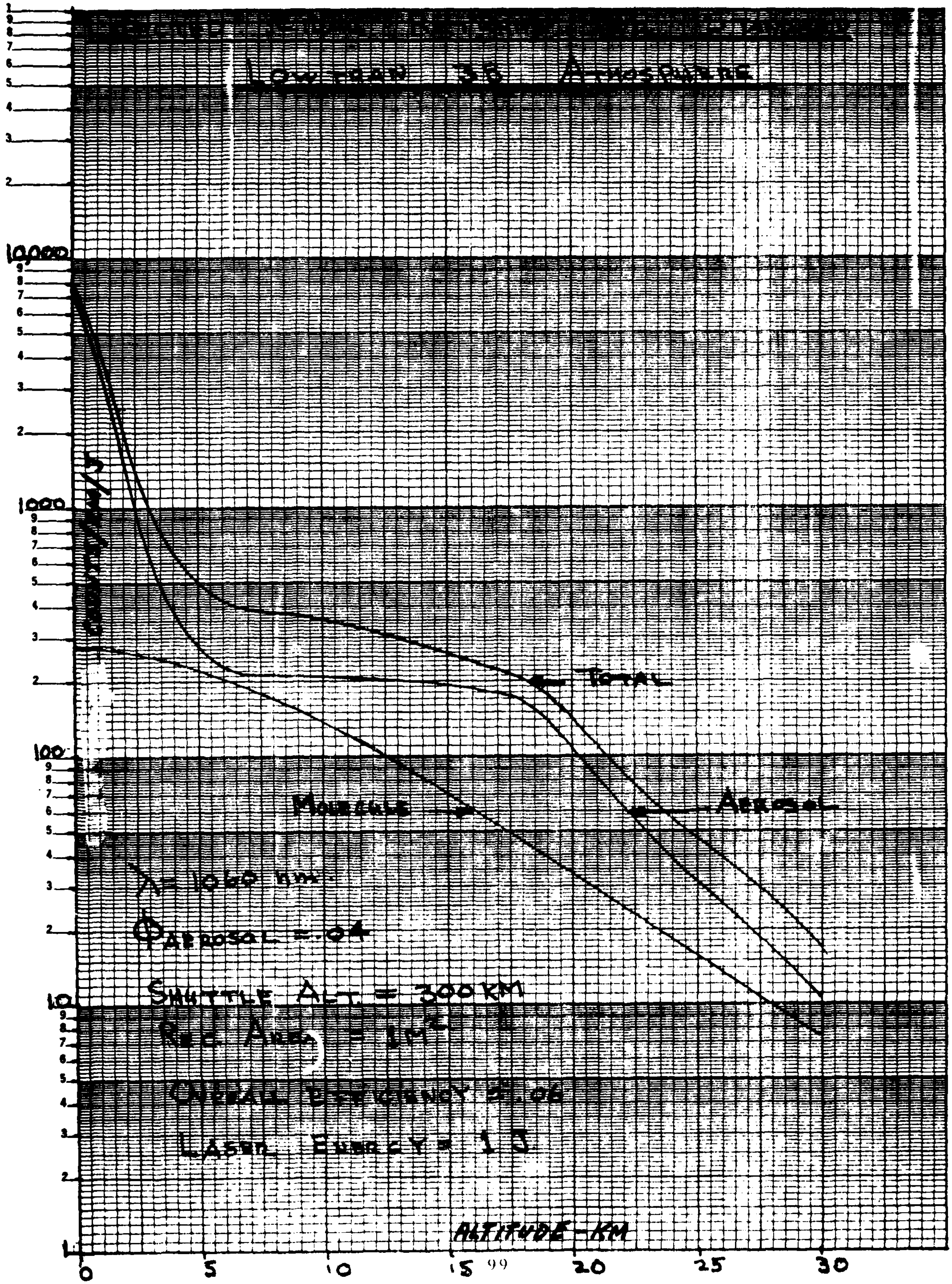
LOWTRAN 3B ATMOSPHERES
COUNTS/SHOT
TOTAL
AEROSOL
MOLECULE
λ = 1060 nm
Φ AEROSOL = .04
SHUTTLE ALT = 300 KM
REC. AREA = 1 M²
OVERALL EFFICIENCY = .06
LASER ENERGY = 1 J
ALTITUDE - KM
10,000
1000
100
10
1
0
5
10
15
20
25
30

ERROR ANALYSIS - 1060/353 RAYLEIGH/MIE SEPARATION

To estimate the accuracies we can expect in density measurements from Shuttle, we adapted the error analysis of Remsberg and Gordley (Applied Optics, 17, 4, 1978, p. 624). The Lidar equation defines the detected signal P (counts per joule per km range bin):

C	=	Appropriately dimensioned constant function
J	=	Transmitted energy in joules per pulse
λ	=	Wavelength
H	=	System efficiency (optical efficiency times quantum efficiency)
A	=	Receiver area
R	=	Range from Shuttle to target bin
β_{Ray}	=	Rayleigh backscatter coefficient, cross-section times density, at each altitude and wavelength.
β_A	=	Aerosol backscatter coefficient, cross-section times concentration, at each altitude and wavelength.
α	=	Total extinction coefficient per km, aerosol absorption and scatter, at each altitude and wavelength.

The pages immediately following the accompanying chart provide an explanation for each of the error terms shown in the error equation.

GENERAL ELECTRIC

ERROR ANALYSIS

1060 / 353 RAYLEIGH / MIE SEPARATION

space division

$$P = C(\mathcal{S},\lambda,H,A,R)\left(\beta_{RAY}+\beta_A\right) \mathrm{EXP}\left(-2\int_0^R \alpha \, dR\right)$$

$$\left(\frac{\delta\beta_{RAY}}{\beta_{RAY}}\right)^2 = \left(1+\frac{\beta_A}{\beta_{RAY}}\right)^2_{353}\left[\left(\frac{\delta P}{P}\right)^2_{353} + \left(2\overline{R\alpha}\,\frac{\delta\alpha}{\alpha}\right)^2_{353}\right]$$

DENSITY ERROR

~ 0.1 FOR LOWTRAN 3B

SHOT NOISE AT 353 NM

AVERAGE EXTINCTION

UNCERTAINTY IN EXTINCTION ~ 0.1

$$+\left(\frac{\beta_A}{\beta_{RAY}}\right)^2_{353}\left[\left(\frac{\delta P}{P_A}\right)^2_{1060} + \left(\frac{\delta R_{ATIO}}{R_{ATIO}}\right)^2_{1060/353} + \left(\frac{\beta_{RAY}}{\beta_A}\cdot\frac{\delta\beta_{RAY}}{\beta_{RAY}}\right)^2_{1060}\right]$$

~ 0.1 FOR LOW TRAN 3B

SHOT NOISE AT 1060 NM

UNCERTAINTY IN BACKSCATTER RATIO FROM 1060 TO 353 NM

~ 0.5 FOR LOW TRAN 3B

DIFFERENCE BETWEEN REAL ATMOSPHERE AND ASSUMED ATMOSPHERE ~ 0.1

NIGHT OPERATION - NO BACKGROUND
NO DETECTOR NOISE
NO MOLECULAR ABSORPTION

AD-A082 332 GENERAL ELECTRIC CO PHILADELPHIA PA SPACE DIV F/G 4/1
DESIGN STUDY OF A LASER RADAR SYSTEM FOR SPACELIGHT APPLICATION--ETC(U)
DEC 79 W F BREHM, J L BUCKLEY F19628-78-C-0204

UNCLASSIFIED AFGL-TR-79-0264 NL

2 of 3
AD
A082 332

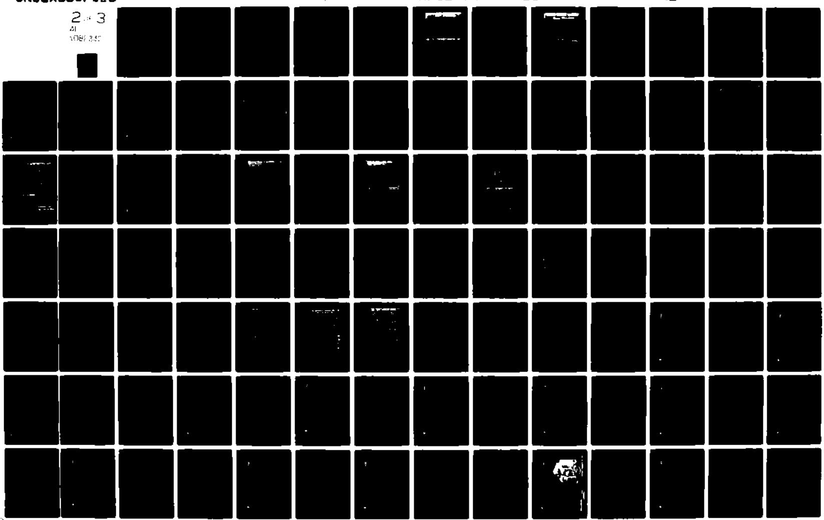

EXPLANATION OF ERROR TERMS

The Lidar equation is differentiated with respect to each measurement variable to find the various contributions to density error, $\dfrac{\delta\beta_{Ray}}{\beta_{Ray}}$. For clarity, the error equation displays the squared values of each term:

$\left(\dfrac{\delta\beta_{Ray}}{\beta_{Ray}}\right)^2$ is the density error from the measurement, following a linearized, first-order data reduction approach as described earlier for the figure on page 89.

$\left(1 + \dfrac{\beta_A}{\beta_{Ray}}\right)^2_{353}$ is calculated at each altitude for the model atmosphere. The curve data on page 97 show that β_A/β_{Ray} is around 0.1 for 353 nm (above 5 km), and is therefore a nearly negligible factor. Between 5 km and the ground β_A/β_{Ray} grows to about 1.2, making this error term increase from $(1.1)^2 \sim 1.2$ to $(2.2)^2 \sim 5$.

$\left(\frac{\delta_P}{P}\right)^2_{353}$ is shot-noise in the 353 nm signal. For averaging N multiple shots this term becomes $\frac{1}{N}\left(\frac{\delta_P}{P}\right)^2$. Assuming Poisson statistics, $\delta P = \sqrt{P}$, and the term becomes $\frac{1}{N}\left(\frac{1}{\sqrt{P}}\right)^2$. The curve data on page 97 shows P in the general range of 20-200 per shot, and shot noise will be a major error term in most cases.

$\left(2R\bar{\alpha}\frac{\delta\alpha}{\alpha}\right)^2_{353}$ is the term that addresses the uncertainty in extinction on the two way pass from Shuttle to sample volume and return. $R\bar{\alpha}$ is calculated to each altitude for the model, and is typically less than 0.1 for altitudes above 15 km. The uncertainty in α at 353 is primarily the uncertainty in Rayleigh scatter caused by lack of knowledge of density itself. We assumed ($\delta\alpha/\alpha$) to be 0.1. The term $(2R\bar{\alpha}\frac{\delta\alpha}{\alpha})^2$ is then of order $(2 \times 0.1 \times 0.1)^2$, or about $(2\%)^2$*. It is therefore not a major error term at the 10% level, but becomes a botton limit to the best achieveable accuracy at the 1% level.

* At altitudes above 15 km. At 5 km this term is on the order of about $(8\%)^2$.

(CONTINUED)

EXPLANATION OF ERROR TERMS (CONTINUED)

$\left(\frac{\beta_A}{\beta_{Ray}}\right)^2_{353}$ enters again as a multiplier for all of the 1060 nm factors, because errors in aerosol measurements at 1060 nm must be weighted by the relative effect of aerosols at 353. Since this factor is around 0.1 (see above), all 1060 nm errors are strongly reduced in impact.

$\left(\frac{\delta_P}{P_A}\right)^2_{1060}$ is shot noise at 1060, and is scaled to N shot as discussed above.

$\left(\frac{\delta_{Ratio}}{Ratio}\right)^2_{1060/353}$ is the uncertainty we have in ratioing the 1060 nm aerosol signal to the 353 nm measurement. This ratio is dependent on aerosol type, but may be reduced by target location knowledge (urban, maritime, etc.), ground truth data, or internal experiment iteration. To account for these possibilities, we have carried δ Ratio/Ratio as a parameter in our error analyses using 0%, 50%, and 100% as characteristic levels. This term has a major effect on the accuracy of the experiment.

$$\left(\frac{\beta_{Ray}}{\beta_A} \cdot \frac{\delta\beta_{Ray}}{\beta_{Ray}}\right)^2_{1060}$$

reflects the uncertainty in subtracting the Rayleigh contribution from the total 1060 nm return to give an aerosol measurement. β_{RAY}/β_A is typically around 0.5 at 1060 nm, as seen in the figure on page 99.

$\delta\beta_{Ray}/\beta_{Ray}$ is taken as 0.1 to reflect an apriori uncertainty in density of 10%. This product is then a 5% term, but is multiplied by $(\beta_A/\beta_{Ray})_{353} \sim 0.1$ (see above) to give a negligible 0.5% contribution in the relatively clear atmosphere of the LOWTRAN 3B model.

In overview, shot noise at 353 nm $(\delta P/P)_{353}$, and the uncertainty in backscatter ratio are the two terms that dominate experiment errors at the 10% level for altitudes above 15 km. As lower altitudes are approached, the term containing the optical thickness and uncertainty in extinction coefficient will become the major contributor to experiment errors at the 10% level.

EXPECTED ERROR IN TWO COLOR DENSITY MEASUREMENTS

(SINGLE SHOT)

The expected density uncertainties from a single-shot Rayleigh/Mie measurement from Shuttle are shown in the accompanying figure. Shot noise at 353 nm is the dominant source of error at high altitudes. At mid-altitudes, shot noise and ratio uncertainties are approximately equal contributors. Below 5 km, the increase in aerosol scattering cause rapid increases in several error terms, with

$$\left(1 + \frac{\beta_A}{\beta_{Ray}}\right)^2_{353} \times \left(2R\bar{\alpha}\ \frac{\delta\alpha}{\alpha}\right)^2_{353} \quad \text{growing from}$$

$\sim(2\%)^2$ or lower up to $(50\%)^2$ near the ground. Similarly

$$\left(\frac{\beta_A}{\beta_{Ray}}\right)_{353} \times \left(\frac{\delta\,\text{ratio}}{\text{Ratio}}\right)^2 \quad \text{grows to } 1^2 \times (0,\ 50\%,\ 100\%)^2$$

near the ground. These two effects appear to provide fundamental experiment limitations at low altitudes.

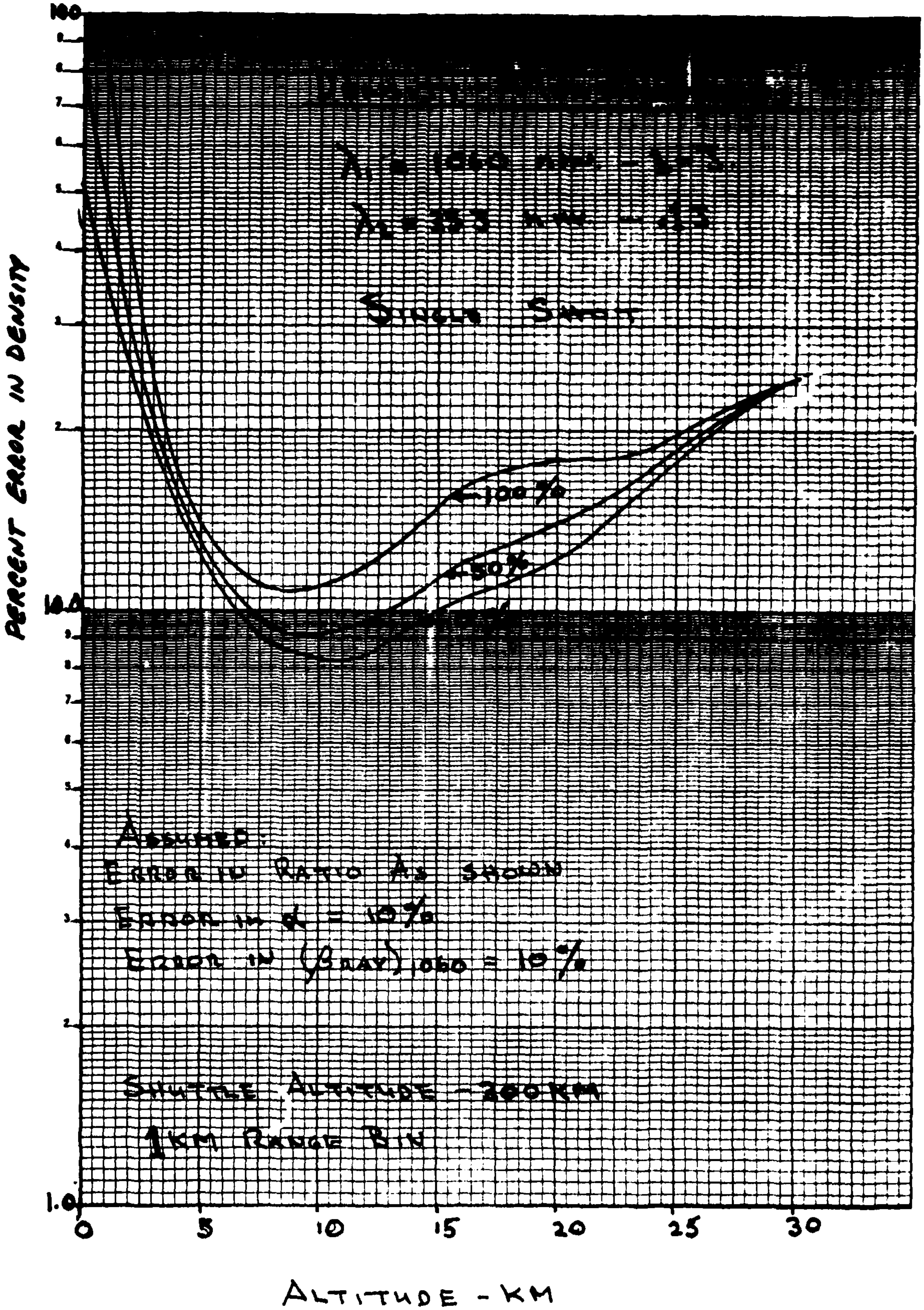

λ_1 = 1060 nm - BHS
λ_2 = 353 nm - 45
SINGLE SHOT
100%
50%
ASSUMED:
ERROR IN RATIO AS SHOWN
ERROR IN α = 10%
ERROR IN $(\beta_{RAY})_{1060}$ = 10%
SHUTTLE ALTITUDE - 200KM
1KM RANGE BIN
PERCENT ERROR IN DENSITY
ALTITUDE - KM

EXPECTED ERROR IN TWO COLOR DENSITY MEASUREMENTS
(100 SHOTS)

When 100 shots are averaged, the performance of the Lidar increases significantly. With a reasonable understanding of aerosol scattering ratio, ($\delta \text{Ratio}/\text{Ratio}$) $\sim$ 50%, we can achieve better than 10% density accuracy from 5 km to above 30 km.

With our baseline laser firing at 10 pulses per second, 100 shots takes 10 seconds. Typical orbit velocity is 7km/sec, so we must average over a 70 km ground trace.

Our linearized error analysis is not really comprehensive enough to address residual errors in the 2% to 5% range. However, we are confident that a more extensive iterative analysis would be able to demonstrate 1-2% errors over most of the upper altitude range for $(\delta \text{Ratio}/\text{Ratio})^2$ small.

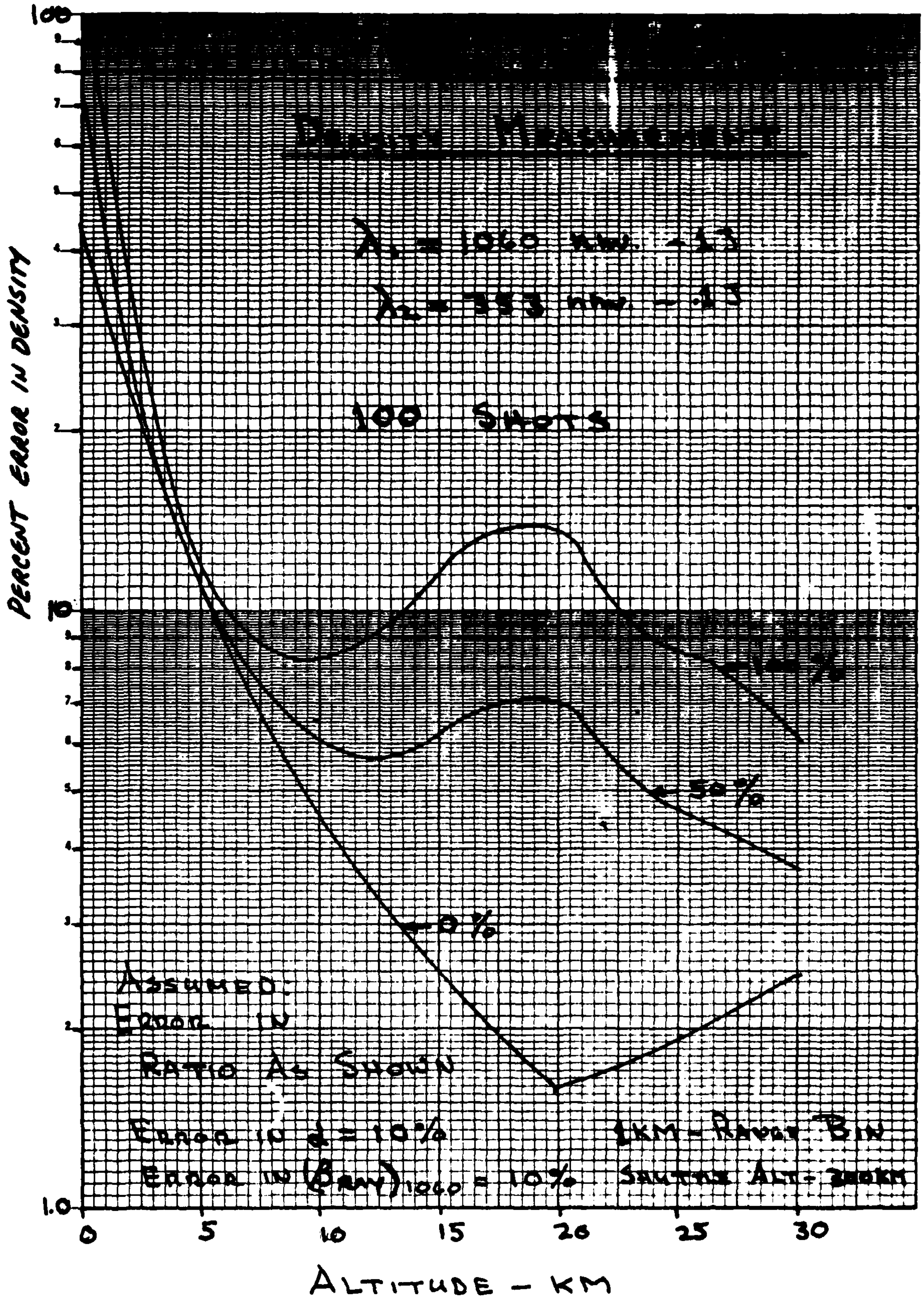

100 SHOTS
PERCENT ERROR IN DENSITY
ALTITUDE – KM
100
10
1.0
0
5
10
15
20
25
30
50%
0%
ASSUMED ERROR IN RATIO AS SHOWN
ERROR IN α = 10%
1KM – RANGE BIN

O_2 - DIAL ANALYSIS

PRECEDING PAGE BLANK-NOT FILMED

DIFFERENTIAL ABSORPTION LIDAR

(DIAL)

The remaining portion of this section contains the analysis pertaining to the Differential Absorption LIDAR (DIAL) density measurement technique. This technique was documented by Remsberg and Gordley in Applied Optics Vol. 17, No. 4/15 February 1978. The equations which were used in our analysis and shown on pages 115 and 131 were extracted from this reference source.

Differential Absorption Lidar (DIAL) is a powerful technique which can be implemented on Shuttle payloads for the remote determination of density at specific range cells. This technique has also been broadly applied in ground based systems for the detection of trace species and pollutants in the atmosphere. Its potential for density measurement was analyzed in this study by treating oxygen (O_2) as the sample species, and the assumption that oxygen is well mixed with nitrogen, in order to determine total density.

For range resolved measurements, signal returns from scattering cells at various ranges are processed for a wavelength on an absorption line and a wavelength off the absorption line, as shown by the figure on the accompanying page, which defines the major parameters in the two-wavelength DIAL geometry.

The differential absorption technique relies, in part, on differences in photons returned from two adjacent range cells at the wavelength of minimum absorption λ_{OFF} for the species to be measured. Variations in the return photons in λ_{OFF} are due principally to the range dependence of the LIDAR return. The error for off-line returns for a given range cell is then calculated by Poisson statistics.

GENERAL ELECTRIC

space division

DIFFERENTIAL ABSORPTION LIDAR
DIAL

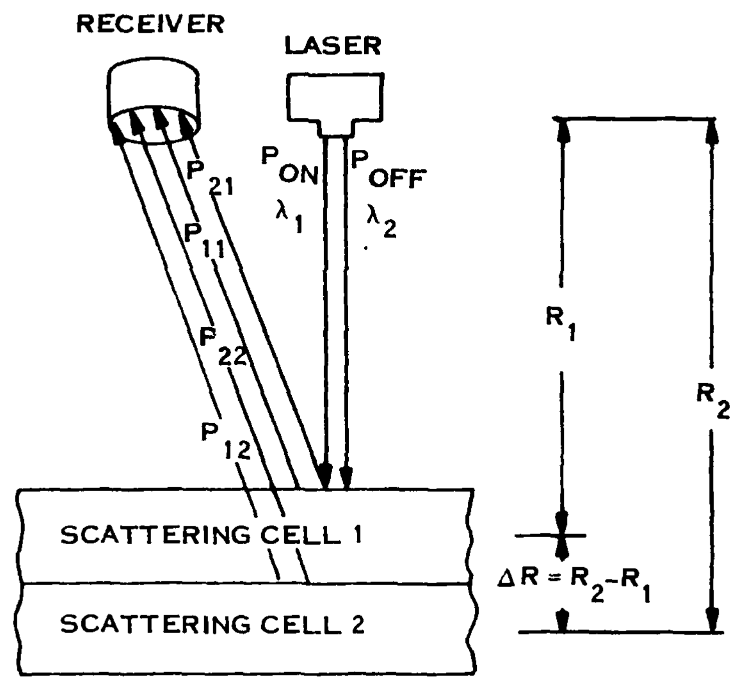

RANGE-RESOLVED MEASUREMENT OF ATMOSPHERIC SPECIES DENSITY BY TWO-WAVELENGTH DIAL

RANGE RESOLVED DIAL

The DIAL equation shown on the accompanying page gives the species density (ρ) in terms of species differential absorption ($\Delta\sigma$) ratio of adjacent cell return signals (P_{ij}) and cell backscattering (β_{ij}) and extinction (α_{i}) coefficients for each wavelength.

The equation demonstrates the potential power of the DIAL technique. For example:

- Instrumental efficiencies and calibration are not sources of uncertainty, because only ratios of signals (P_{ij}) enter. Absolute signal levels are not required with high accuracy.

- Intervening atmosphere is not a factor, as it was for the Rayleigh/Mie analyses. DIAL only assumes a reasonably well mixed atmosphere over the same volume of one kilometer.

- Finally, if the "on-line" and "off-line" wavelengths are close enough ($\lambda_1 \approx \lambda_2$) that broadband atmospheric properties (scatter and absorption) can be taken as constant for both wavelengths, the DIAL equation reduces to a very clean and direct ratio of observed signal levels, shown at the bottom of the chart, and is independent of atmosphere models.

GENERAL ELECTRIC

space division

RANGE RESOLVED DIAL

$$\rho = \frac{1}{2\Delta\sigma\,\Delta R}\left[\mathrm{LN}\left(\frac{P_{22}\,P_{11}}{P_{12}\,P_{21}}\right) + \mathrm{LN}\left(\frac{\beta_{12}\,\beta_{21}}{\beta_{11}\,\beta_{22}}\right) - 2\int_{R_1}^{R_2}(\alpha_1-\alpha_2)\,dr\right]$$

P_{ij} = RETURN FOR WAVELENGTH i AND SCATTERING CELL j

β_{ij} = BACKSCATTER COEFFICIENT FOR WAVELENGTH i AND CELL j

α_i = AVERAGE BROADBAND EXTINCTION COEFFICIENT FOR WAVELENGTH i

i = 1 REPRESENTS ON-LINE

i = 2 = REPRESENTS OFF-LINE

ΔR = RANGE BETWEEN SCATTERING CELL CENTERS

$\Delta\sigma$ = DIFFERENCE IN SPECIES ABSORPTION ON-LINE MINUS OFF-LINE

ρ = AVERAGE SPECIES DENSITY OVER CELL

$$\rho = \frac{1}{2\Delta\sigma\,\Delta R}\,\mathrm{LN}\left(\frac{P_{22}\,P_{11}}{P_{12}\,P_{21}}\right) \quad \text{IF } \lambda_1 \approx \lambda_2$$

OXYGEN A-BAND

The Oxygen A-Band is the most promising absorption band for DIAL density measurements for the following reasons.

- The A-band falls in a spectral region ($\lambda < 1000$ nm) that allows photon detection (photomultipliers) with sensitivity and response time adequate for LIDAR detection.
- Oxygen is well mixed globally in the atmosphere, as opposed to other potential trace species.
- Tunable dye laser technology is advanced enough in the visible to consider near-term O_2 DIAL systems in space.
- The A-band line strengths and widths are measured and well understood.
- As a forbidden magnetic dipole transition, the A-band has absorption coefficients small enough to allow (hopefully) probing of the total atmosphere (unfortunately, our analysis shows this is a problem).

Our computer program incorporates the strengths and widths of the A-band lines, and calculates the Voight profiles for the specific lines at the nominal temperature and pressure at each altitude.

GENERAL ELECTRIC

OXYGEN A-BAND

space division

$$b\,^1\Sigma_g^+ \longleftarrow X\,^3\Sigma_g^-$$

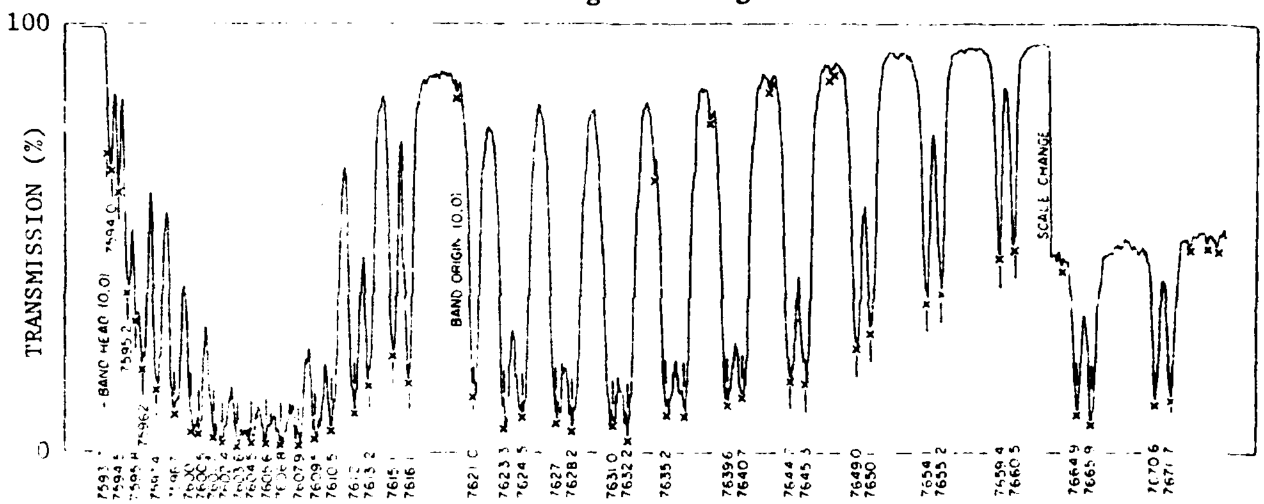

- MAGNETIC DIPOLE TRANSITION WITH DOUBLET-LIKE STRUCTURE
- (0, 0) VIBRATION BAND USED
- R-BRANCH AND P-BRANCH PAIRS
- VOIGHT PROFILES WITH STRENGTHS AND WIDTHS FROM BURCH AND GRYUNAK (1969)

TWO PASS OPTICAL THICKNESS FOR OXYGEN

The absorption lines of O_2 in the A-band are so strong and narrow that they are totally absorbent to LIDAR measurements. Korb* has suggested that the saddle region between line pairs might provide a more suitable sample required for density/pressure measurements from Shuttle.

To check our computer model, we evaluated the transmittance function between two lines, as suggested by Korb ($J'' = 14$ and 15) in the 0-0 vibration band. The figure on the accompanying page shows the two-pass optical thickness between these two lines for sample heights of 5 km and 0 km (ground). Korb's curve data and GE's calculations are shown for comparison. The data show a flat saddle region that is quite opaque at the ground (transmission = $e^{-6.5} = 1.5 \times 10^{-3}$) and still opaque at 5 km ($t = e^{-2} = 0.14$). The DIAL concept uses this saddle region to reduce the demands on laser frequency control by providing a smooth region of uniform O_2 absorption properties. The following charts provide a detailed description of the DIAL signal analyses.

* C. L. Korb, "A Laser Technique for the Remote Measurement of Pressure in the Troposphere," Proc. 8th International Laser Radar Conference, Drexel Univ., Philadelphia, PA, June 1977.

TWO PASS OPTICAL THICKNESS FOR OXYGEN

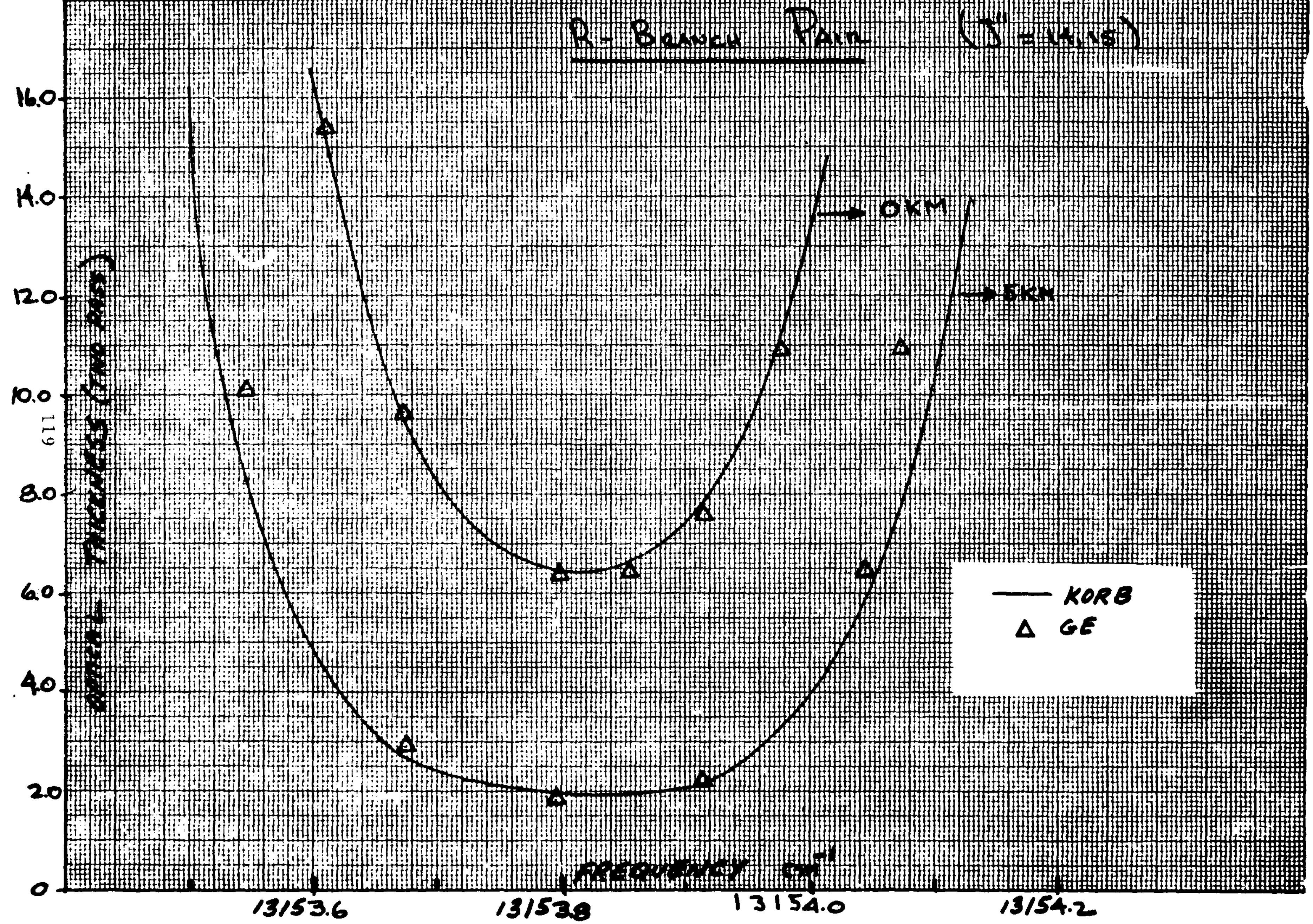

EXPECTED RETURNS AT SURFACE (P BRANCH PAIR)

This figure shows expected returns from a sea level range bin for a weaker O_2 line pair ($J'' = 12,13$) in the P branch in order to assess its potential for low altitude density measurements. The expected returns are provided as a function of frequency relative to the mid-point position between the two absorption lines. While the line centers are black, potentially usable returns are possible in the saddle region.

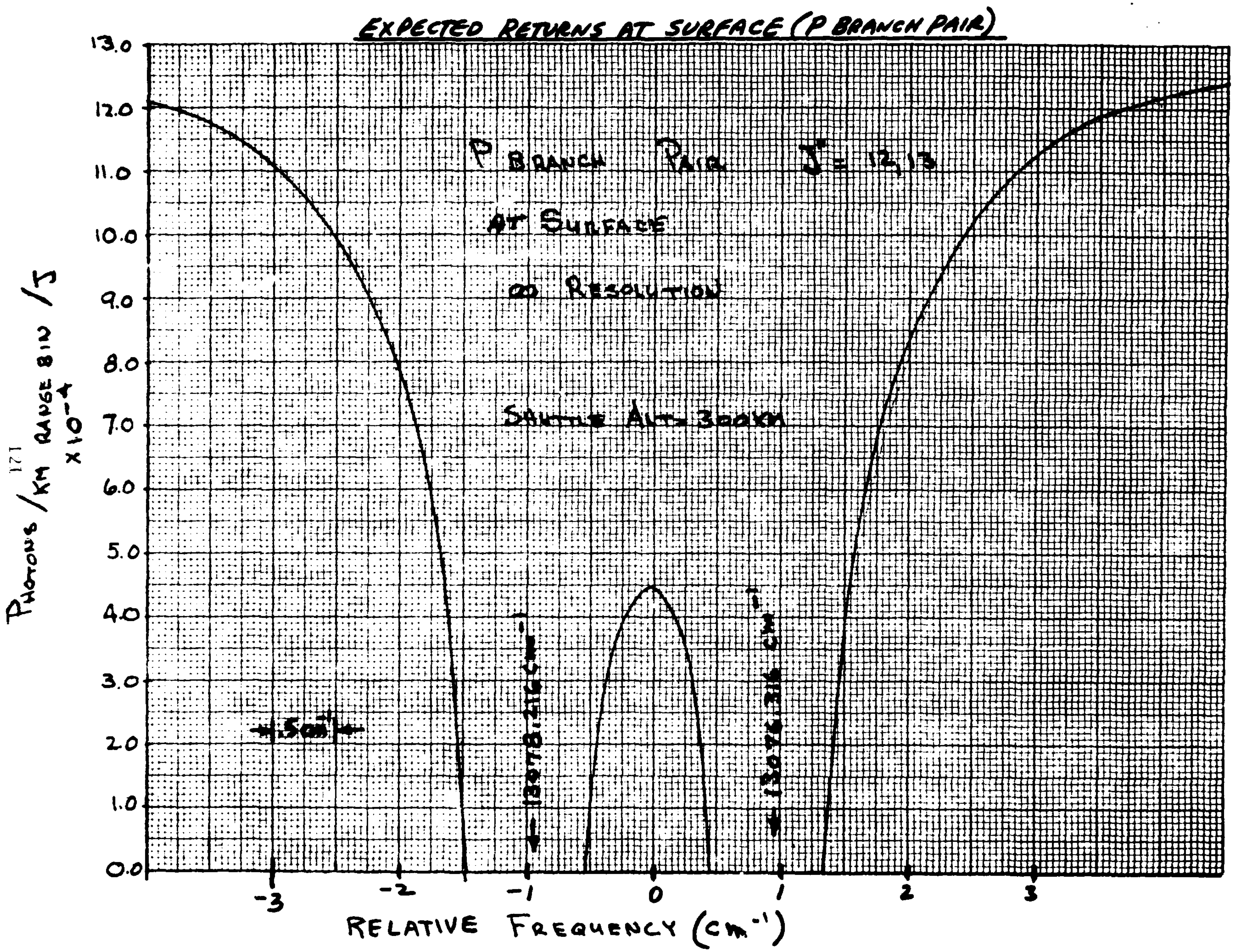
EXPECTED RETURNS AT SURFACE (P BRANCH PAIR)
P BRANCH PAIR J" = 12,13
AT SURFACE
∞ RESOLUTION
SHUTTLE ALT = 300KM
13078.216 cm⁻¹
13076.316 cm⁻¹
.5 cm⁻¹
13.0
12.0
11.0
10.0
9.0
8.0
7.0
6.0
5.0
4.0
3.0
2.0
1.0
0.0
-3
-2
-1
0
1
2
3
RELATIVE FREQUENCY (cm⁻¹)
PHOTONS /KM RANGE BIN /J
X10⁻⁴

EXPECTED RETURNS AT 6 KM (R BRANCH PAIR)

This figure shows the dramatic impact of the absorption data, provided in the preceding chart, on the LIDAR return from a 6 km altitude range bin for the O_2 (J" - 14,15) pair using the LOWTRAN 3B atmospheric model. Expected returns are provided as a function of frequency relative to the 13153.420 cm^{-1} line. The following comments are of particular importance to the DIAL concept:

- The center of the two lines (13153.420 cm^{-1} and 13154.169 cm^{-1}) are totally black, yielding no LIDAR return at all.

- The saddle region between the two lines yields a potentially usable return; however, the response wave is narrow and very steep and, therefore, lacks a more desirous "flat-top" which would be less sensitive to frequency variations.

EXPECTED RETURNS AT 6 KM (R BRANCH PAIR)

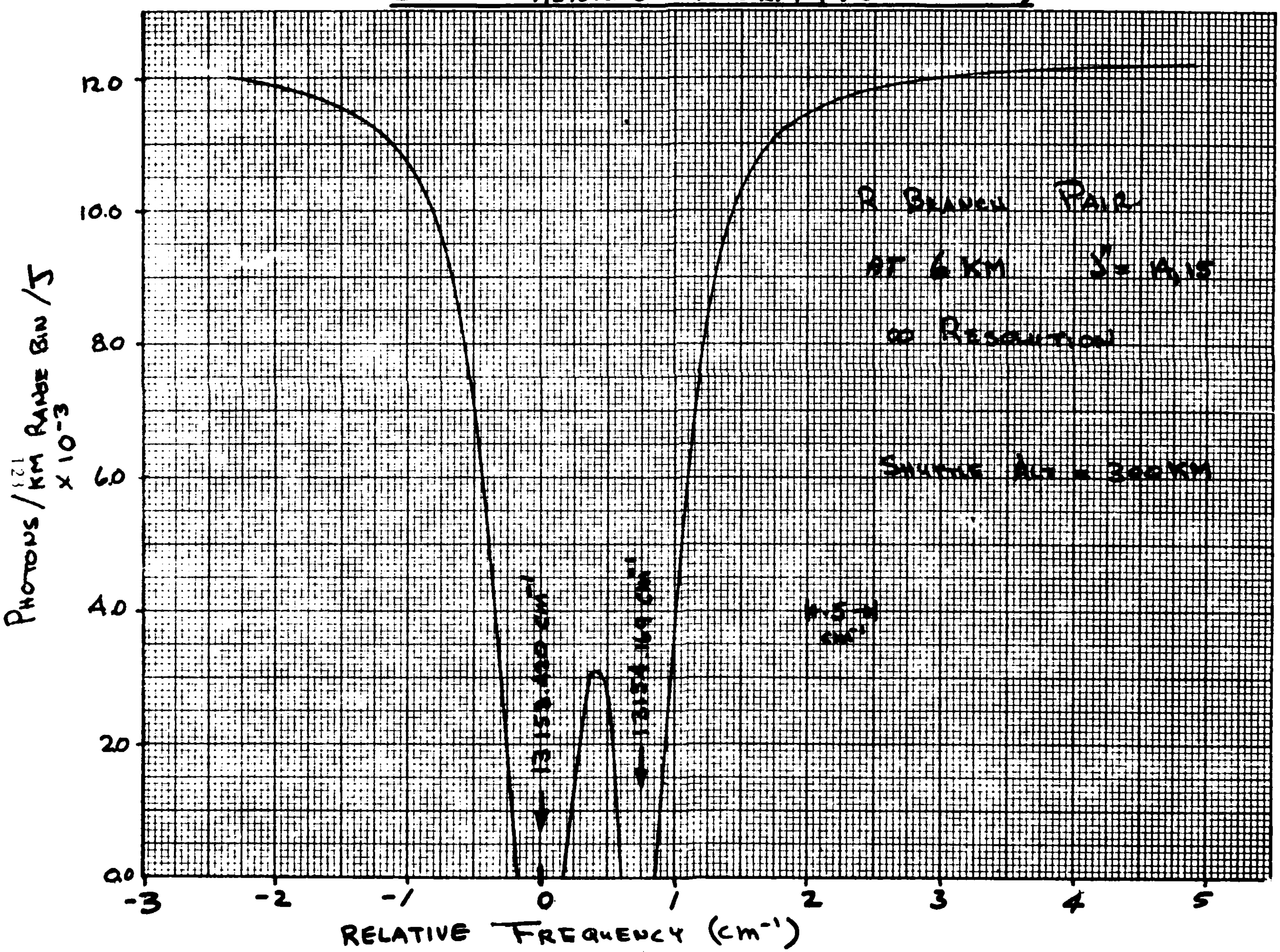

EXPECTED RETURNS AT 30 KM (P BRANCH PAIR)

This figure shows expected returns from a 30 km altitude range bin for a single O_2 line in the P Branch (J" - 12). (This is one of the pair of lines analyzed in the preceding figure.) Expected returns are provided as a function of the frequency relative to the center of the line. The following comments are apparent from the curve data shown:

- The center of the line is totally absorbed, yielding no LIDAR return.
- The line has a much narrower width than at ground level (see page 121) but is clearly in the square-root region of the curve-of-growth because of the total amount of atmospheric oxygen available for absorption, even above 30 km.
- Gross photon counts are low because of reduced aerosols for scattering at 30 km.

EXPECTED RETURNS AT 30KM (P BRANCH SINGLE LINE)

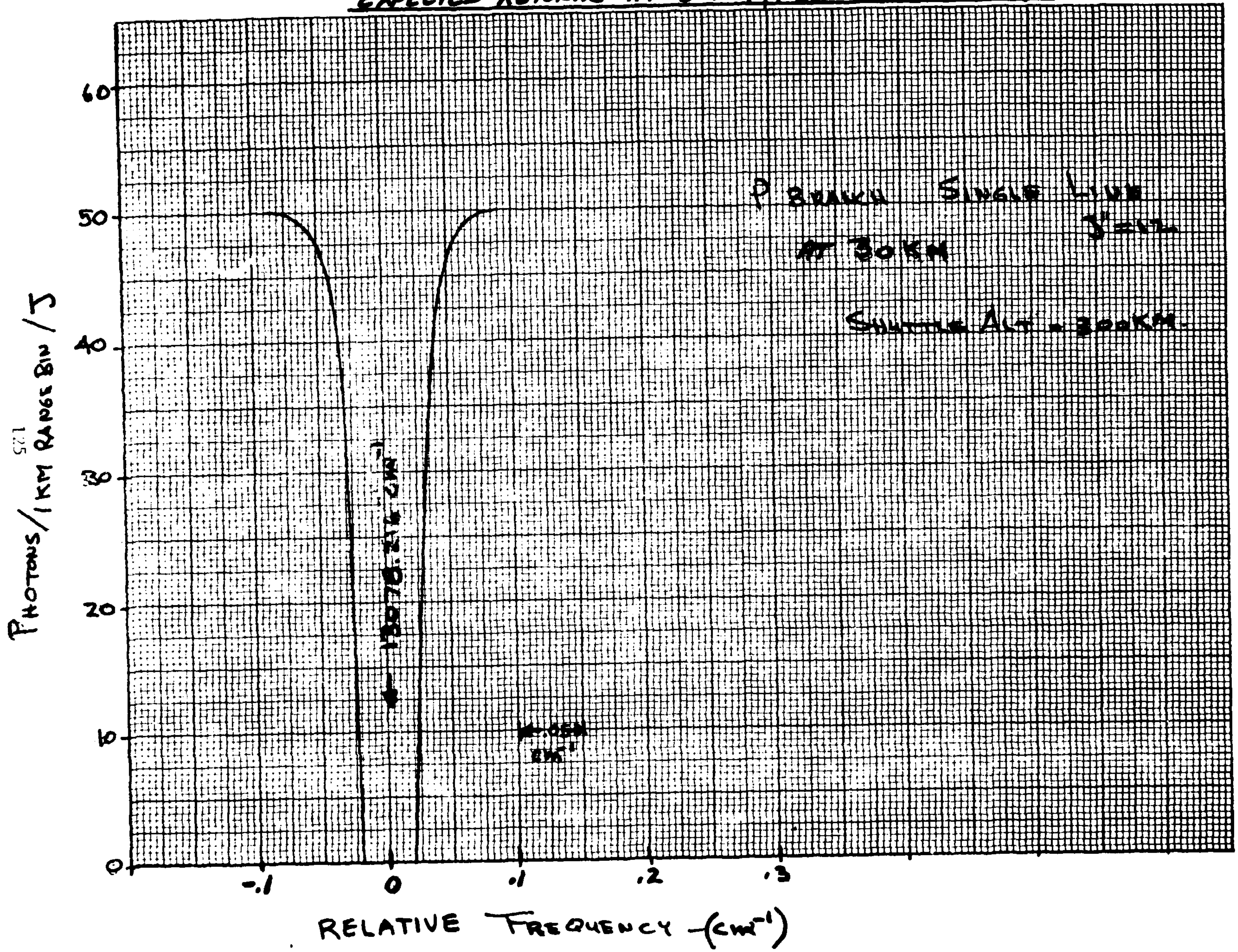

EXPECTED LIDAR RETURNS - O_2 DIAL

(ON-LINE FREQUENCY CENTERED ON SADDLE)

The O_2 DIAL experiment was simulated on our computer using the LOWTRAN 3B model atmosphere. The saddle region between the R Branch pair absorption lines (J" = 13 and J" = 15) was analyzed relative to the laser line widths shown by the curve data in the accompanying chart.

The "OFF-LINE" curve provides the nominal photon returns from broadband aerosol and molecular scattering as a function of the range bin altitude.

The three (3) "ON-LINE" curves show the effects of O_2 absorption on the photon return signals for a laser line frequency centered in the saddle region, also as a function of the range bin altitude. "ON-LINE" returns were calculated for laser line widths of 0.1, 0.5, and 0.75 cm^{-1} (rectangular line profiles were used). The reduced photon returns from broader lines are commensurate with the width of the saddle region (e.g., see figure on page 123 which shows the saddle width for the (km altitude bin).

The large attenuation of the "ON-LINE" return signals at low altitudes is naturally due to a shrinking saddle amplitude with decreasing altitude; while very little O_2 absorption is seen above 15 km, due to the combination of a shrinking O_2 absorption line width, as altitude increases, and a saddle amplitude equal to the "OFF-LINE" amplitude.

The "ON-LINE" return signals for a laser line centered on the saddle are strong enough, and sufficiently separated from the "OFF-LINE" returns, to be promising at the lower altitudes ($\leq$ 10 km), even though they are somewhat sensitive to variations in the laser line width. However, at the higher altitudes ($>$10 km), differences between "ON-LINE" and "OFF-LINE" absorption ($\Delta\sigma$) become indistinguishable, and therefore, meaningful density determination measurements are essentially unobtainable.

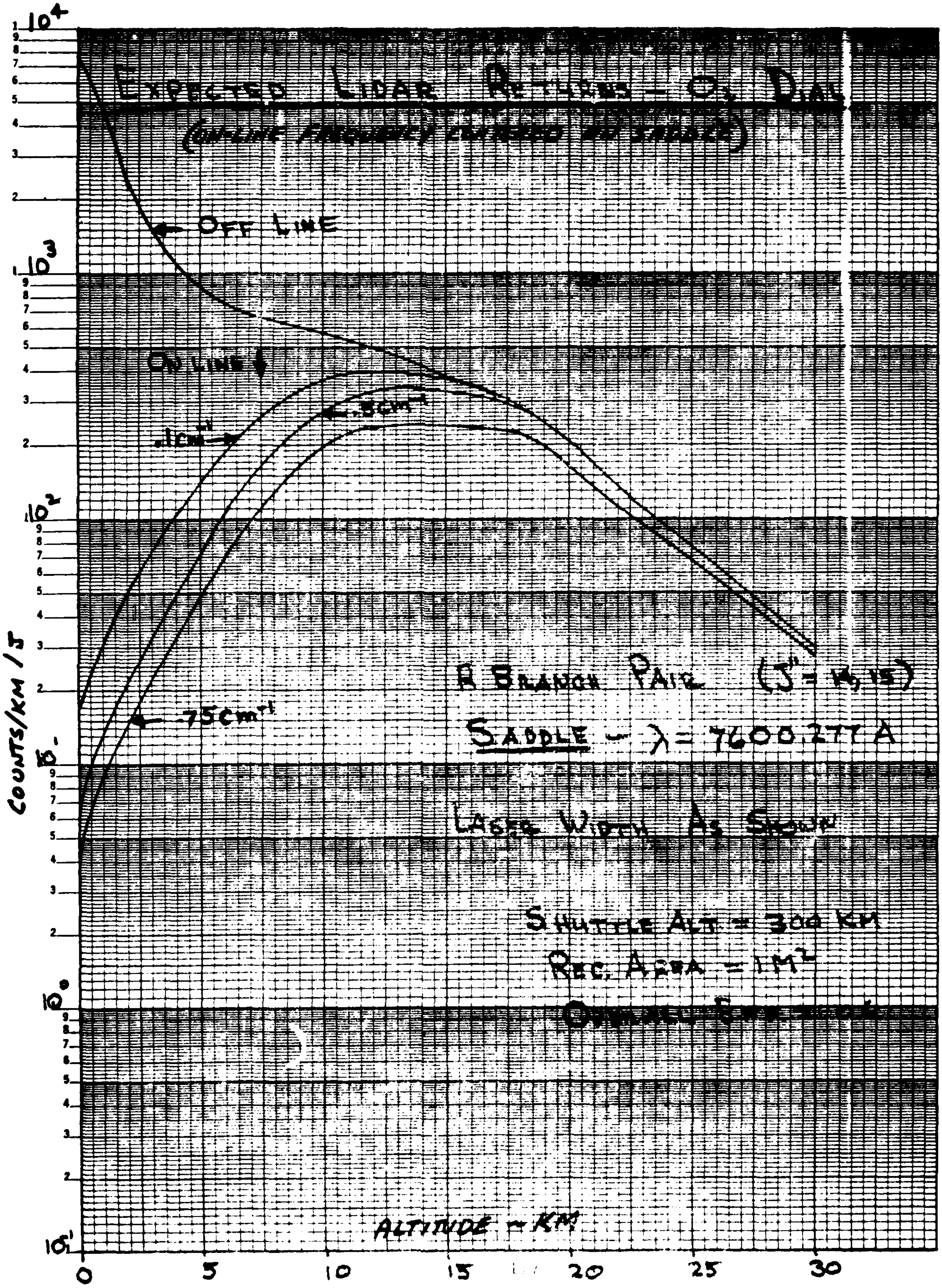

EXPECTED LIDAR RETURNS – O2 DIAL
OFF LINE
ON LINE
.1cm⁻¹
.5cm⁻¹
.75cm⁻¹
R BRANCH PAIR
SADDLE – λ = 7600.277 A
LASER WIDTH AS SHOWN
SHUTTLE ALT = 300 KM
REC. AREA = 1 M²
COUNTS/KM/J
ALTITUDE ~ KM
0
5
10
15
20
25
30

EXPECTED LIDAR RETURNS - O_2 DIAL
(ON-LINE FREQUENCY CENTERED ON PEAK ABSORPTION LINE)

Simulations were also run for returns from a laser line centered on the J" = 14 line at 7600.493A, in order to explore the possibility of working on a peak absorption line instead of in the saddle region.

The figure on the accompanying page shows the "ON-LINE" photon returns versus altitude for a range of laser line widths of 0.1, 0.15, 0.2, 0.25, 0.5, and 0.75 cm^{-1}, including the curve of the "OFF-LINE" returns, which is the same curve as shown in the preceding chart.

Since the center of the peak absorption line is totally black, even at 30 km, the "ON-LINE" curve data provides the total absorption of a line with a finite width, rather than the line-center absorption, which would have no return at all. As a result, increasing the laser line width will increase the return signal, since greater portions of the saddle and OFF-LINE" regions will be included in the returns; as a consequence, the absorption information in the measurement will be diluted. This is particularly true at high altitudes where the width of the peak absorption line is very narrow (the figure on page 125 serves as a typical example).

Although narrower "ON-LINE" laser line widths will work better in the high altitude regions, their utility rapidly diminishes in the low altitude regions. This is readily seen in the "ON-LINE" curve data where the photon returns from narrower line widths are extremely sensitive in the low altitude regions.

A predominant conclusion which can be drawn from the data is that the laser must be capable of optimizing the line width for each altitude of interest if meaningful measurements are to be obtained throughout the range of altitudes shown in the chart. The impact of laser line widths is brought out in the error analyses provided in the remainder of this section.

EXPECTED LIDAR RETURNS - O_2 DIAL

(ON-LINE FREQUENCY CENTERED ON PEAK ABSORPTION LINE)

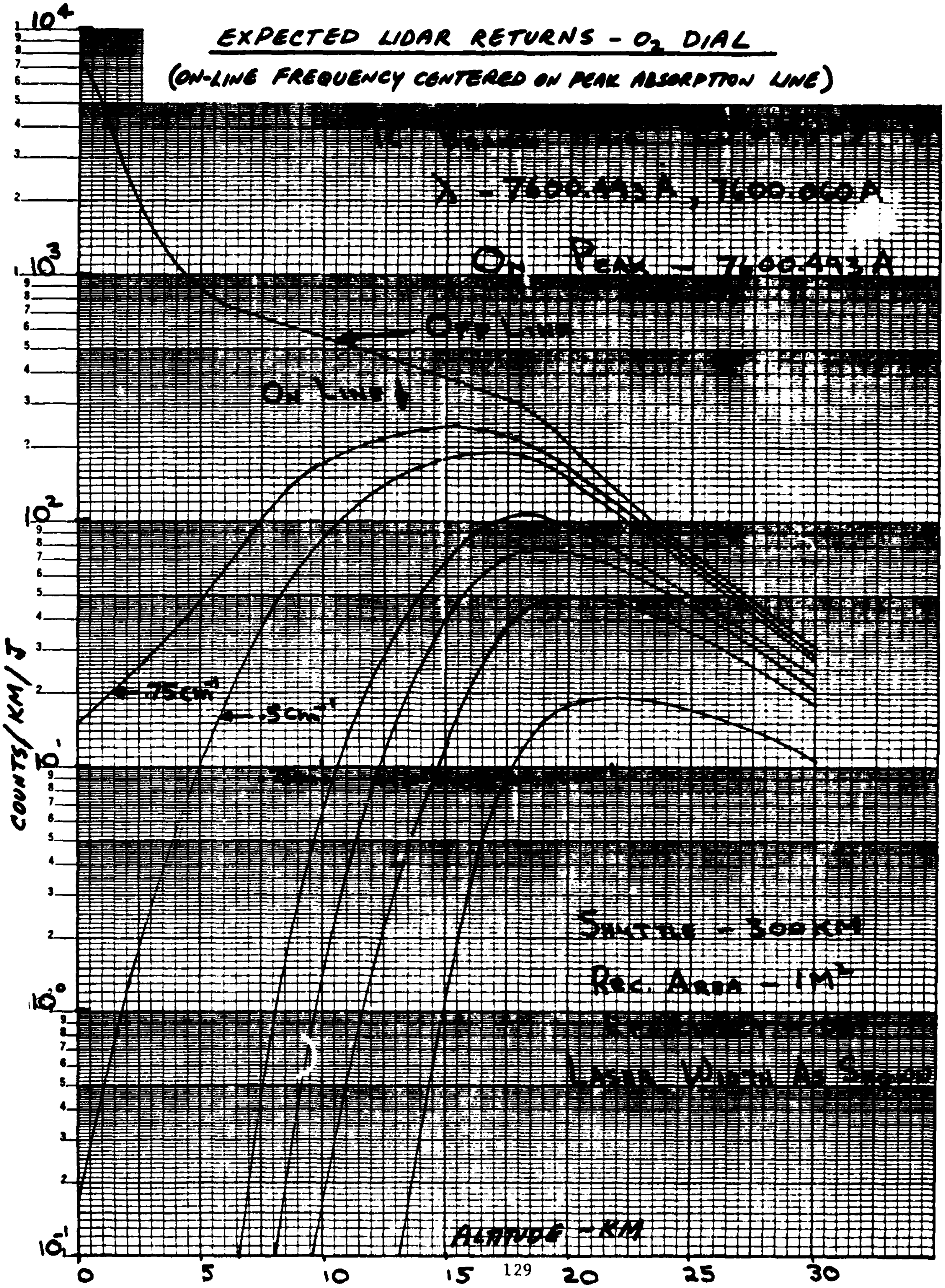

ERROR ANALYSIS

The DIAL density determination equation for closely spaced lines (see page 115) was differentiated to develop a signal-dependent error equation. This error equation, which is shown in the accompanying chart, describes the errors in density measurement generated by statistical undertainties (shot noise) in the four return signals used in the density determination equation (P_{11}, P_{12}, P_{21}, P_{22} counts per range cell).

As a first order assessment, the four factors listed in the chart were not included for the following reasons:

- No background - night operation
- No detector noise - dark counts should be negligible in each range cell
- No range jitter - range-gating electronics must be very stable
- No laser jitter - stable frequency, line width, and shape

$\Delta\sigma$ is a very complex factor involving line widths and strengths, temperature, doppler broadening, and pressure broadening. The analysis assumes that detailed theoretical analysis and ground truth calibrations can reduce uncertainties in $\Delta\sigma$ to acceptable levels.

The following interesting functional relations are apparent from the error equation:

1) Instrument efficiency calibration does not enter the equation because DIAL is a ratioing technique, not an absolute measurement. This can be a major advantage for remote space-borne instrumentation which often cannot be calibrated in orbit.

2) Each of the four return signals has an equal contribution to the error as shown by the 1/P terms; therefore, if a signal is very small, because of a very strong absorption on-line, errors can be expected to increase dramatically.

3) Although strong absorption lines, with $\Delta\sigma$ large, can reduce errors, the large absorption factors will also reduce the return signals, thereby making the 1/P terms large. Remsberg and Gordley (see reference on page 112) have shown that optical depths between 1.1 and 1.7 are optimum for balancing these effects in DIAL measurements.

GENERAL ELECTRIC

space division

ERROR ANALYSIS

$$\left(\frac{\partial \rho}{\rho}\right)^2 = \left(\frac{1}{2\Delta\sigma\Delta R}\right)^2 \left(\frac{1}{P_{11}} + \frac{1}{P_{12}} + \frac{1}{P_{21}} + \frac{1}{P_{22}}\right)$$

ERROR FROM SHOT NOISE IN RETURN SIGNALS

- o NO BACKGROUND
- o NO DETECTOR NOISE
- o NO RANGE JITTER
- o NO LASER JITTER

ERROR FROM LASER LINE-WIDTH JITTER (1, 2, 5, 10%)
ALSO RUN FOR LINE-PEAK DIAL

EXPECTED ERRORS - O_2 DIAL

(ON-LINE FREQUENCY CENTERED ON SADDLE)

Using the error equation shown on the preceding page with the curve data on page 127, errors were developed for "saddle-region" O_2 DIAL measurements from Shuttle, and are shown by the curve data in the accompanying figure. It should be noted that:

- o Single shot means one on-line pulse and one off-line pulse from a tunable dye laser, i.e., an output of 1J, in each pulse.
- o Laser line width is modelled as a rectangular line with constant total energy. The three widths bracket the probable optimum width based on the absorption profiles described previously.

The curve data portrays three general regions:

1. High altitudes ($>$ 12 km) where oxygen absorption in the saddle is so weak that the $\Delta\sigma$ term in the error equation dominates.
2. Middle altitudes (2-12 km) where absorption and return signal are optimally balanced.
3. Low altitudes ($<$ 2 km) where strong absorption reduces return signal strength to levels where 1/P shot noise begins to dominate error.

In addition, the data clearly shows that this concept (O_2 saddle-region DIAL) is extremely sensitive for obtaining accurate density measurements in the 10-30 km altitude region, which is a major goal of the Shuttle/Spacelab LIDAR experiment, i.e., even with 100 shot averaging, the expected errors would be greater than the desired measurement accuracy goal of 10%. However, this technique looks very promising for altitude regions from 10 km to ground level and, therefore, can be combined with the Rayleigh/Mie technique (see page 109) to provide measurement accuracies of better than 10% (100 shot data) for all altitudes of interest, i.e., from the ground to 30 km.

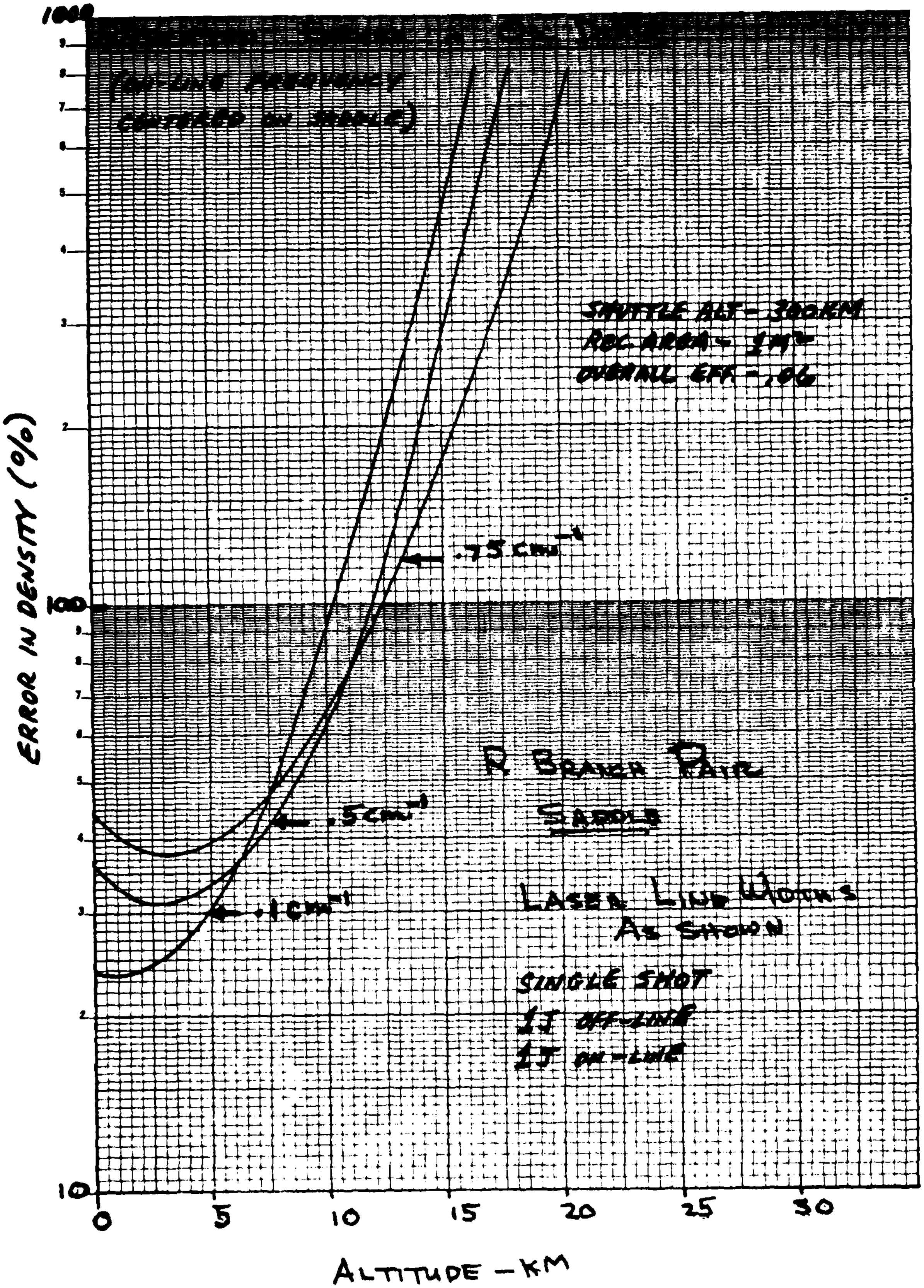

(ON-LINE FREQUENCY CENTERED ON SADDLE)
SHUTTLE ALT - 300KM
REC AREA - 1M²
OVERALL EFF. - .06
.75 CM⁻¹
.5 CM⁻¹
.1 CM⁻¹
R BRANCH PAIR
SADDLE
LASER LINE WIDTHS AS SHOWN
SINGLE SHOT
1J OFF-LINE
1J ON-LINE
ERROR IN DENSITY (%)
ALTITUDE - KM

EXPECTED ERRORS - O_2 DIAL

(ON-LINE FREQUENCY CENTERED ON PEAK ABSORPTION LINE)

In order to achieve stronger absorption at higher altitudes, and reduce the $1/\Delta\sigma$ contribution to density error, an assessment was made of the errors obtained when operating the "ON-LINE" frequency directly on the center of a peak absorption line (J" = 14) of the "saddle" pair. As shown in the figure on the accompanying page, a broad range of laser linewidths was evaluated across the altitude region of interest.

The very narrow line (0.1 cm^{-1}) is so strongly absorbed by upper atmospheric O_2 that returning signals decrease sharply with altitude (increasing optical thickness). The broadest line (0.75 cm^{-1}) loses little energy to absorption at high altitude, leading to large $1/\Delta\sigma$ errors. Intermediate linewidths (0.15 - 0.25 cm^{-1}) display error profiles optimized for the 10-20 km region, but are too strongly absorbed to provide low altitude returns.

The curve data in t is figure (and also in the preceding figure) show that the O_2 DIAL technique can provide density measurements within the 10% accuracy goal (multiple shot averging) over specific altitude regions. However, a laser system must be developed with the capability to cover a range of tunable line frequencies and linewidths in order to provide data over the total altitude region of interest. Such a system, ruggedized for an unattended space mission, is currently not available for a near-term application.

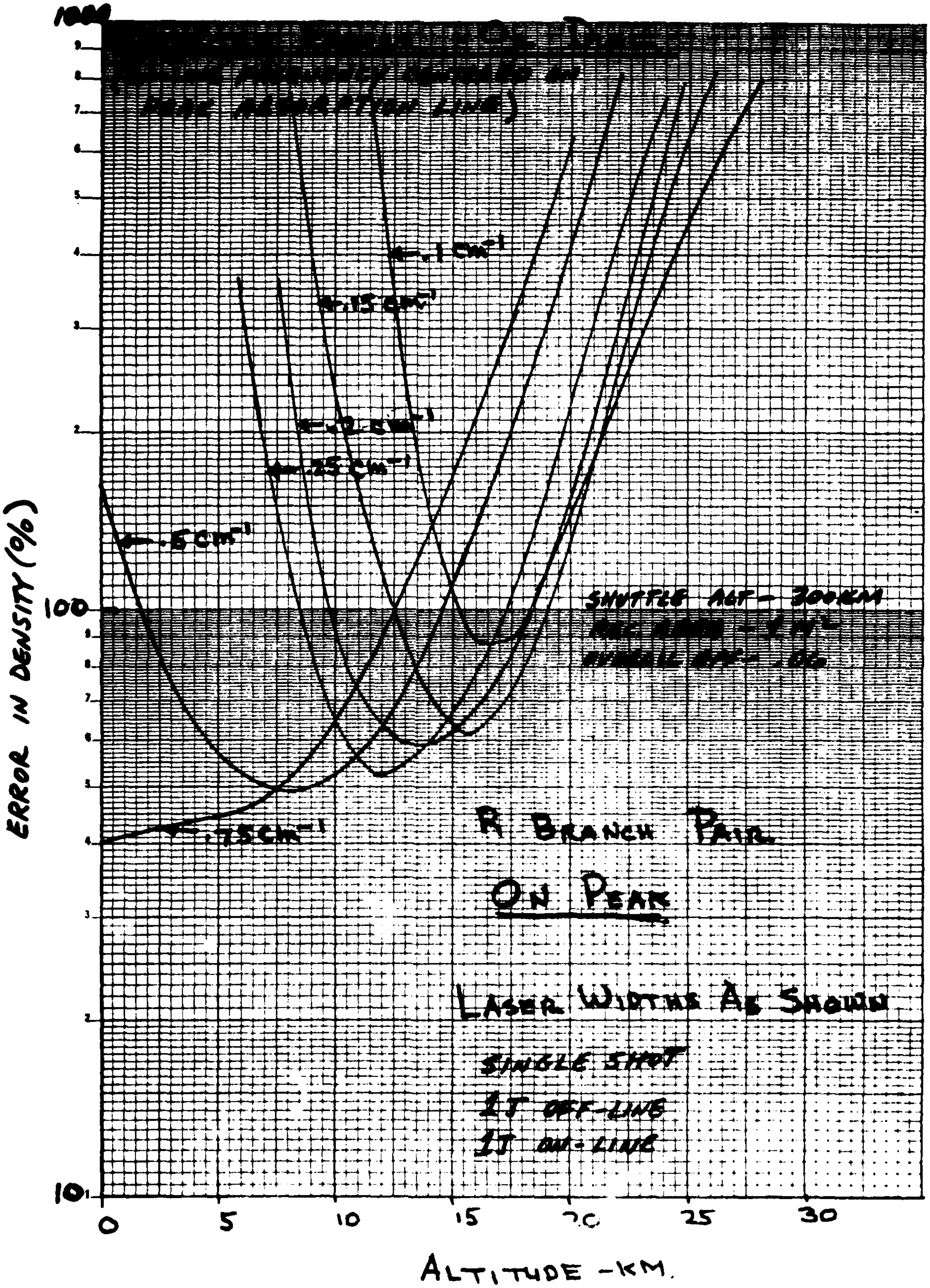

ERROR IN DENSITY (%)
ALTITUDE - KM
.1 cm⁻¹
.15 cm⁻¹
.2 cm⁻¹
.25 cm⁻¹
.5 cm⁻¹
.75 cm⁻¹
SHUTTLE ALT - 300KM
R BRANCH PAIR
ON PEAK
LASER WIDTHS AS SHOWN
SINGLE SHOT
1J OFF-LINE
1J ON-LINE

EXPECTED ERROR SENSITIVITY TO LINEWIDTH STABILITY

(ON-LINE FREQUENCY CENTERED ON PEAK ABSORPTION LINE)

The sensitivity of density error to laser linewidth stability is shown in the figure on the accompanying page. The effects of minor variations in linewidth are referenced to a nominal 0.2 cm^{-1} laser linewidth corresponding to the data shown in the preceding figure. Density errors were analyzed for 1, 2, 5 and 10% linewidth variations, assuming no 1/P shot noise (i.e. multiple shots). These errors should be RSS with those on the preceding figure if combined errors are to be obtained. For the cases considered, variations in laser linewidth enter approximately linearly as error terms. The curves indicate that very precise laser linewidth stability is required to perform accurate DIAL density measurements It is expected that it will be difficult to achieve pulse-to-pulse linewidth and/or line center frequency variations in the few percent region; as a result, the status of laser technology should be assessed in significant detail in this regard before any further commitment is made to future development of this density measurement technique.

EXPECTED ERROR SENSITIVITY TO LINEWIDTH STABILITY

(ON-LINE FREQUENCY CENTERED ON PEAK ABSORPTION LINE)

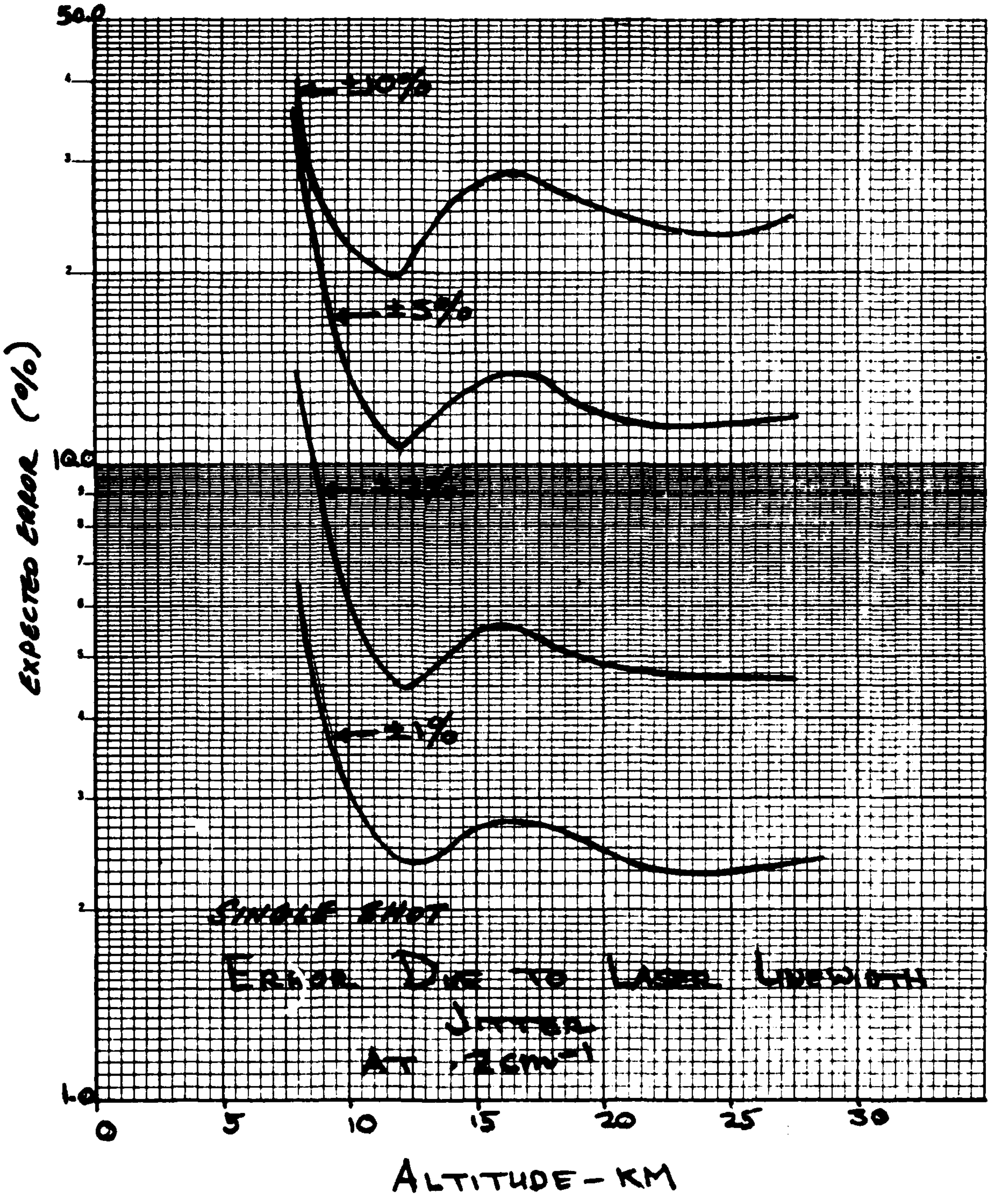

SECTION 6

BALLOON EXPERIMENT PERFORMANCE

PRECEDING PAGE BLANK-NOT FILMED

BALLOON EXPERIMENT PERFORMANCE

The series of charts in this section provide data associated with the Rayleigh/Mie Analysis of the balloon-based experiment. The first two charts on pages 141 and 143 provide selected experiment parameters for the 500 mJ and 100 mJ lasers, respectively, which are considered obtainable with existing off-the-shelf hardware. The baseline energy, i.e., the 500 mJ and 100 mJ, is the raw output energy of these 1060 nm wavelength Nd:YAG lasers prior to wavelength conversion. As a result of converting the 1060 nm wavelength to the 353 nm wavelength, the output energy is redistributed to about 54% and 9% of the baseline energy for the 1060 nm and 353 nm wavelengths, respectively. Backscattering phase functions for both molecules and aerosols at these wavelengths are provided in the computer input data shown in Appendix B on page 223.

Receiver system parameter values such as those shown for the telescope diameter, secondary mirror obscuration area, filter characteristics, and PMT (photomultiplier tube) quantum efficiency are the same for both laser configurations; however, beam divergence and FOV parameter values were varied to account for eye safe criteria under day or night operation conditions. Although not shown, the beam divergence and FOV values are the same for both configurations if the 100 mJ laser is designed to also operate at 20 km, including the corresponding background interference values (counts/km), i.e., 333 counts/km and 7174 counts/km for the 1060 nm and 353 nm wavelengths, respectively.

BALLOON LIDAR EXPERIMENT PARAMETERS

(500 mJ BASELINE)

	1060 NM	353 NM
E_L	.27J/PULSE	.045J/PULSE
PMT QUANTUM EFF.	4%	30%
TELESCOPE TRANSMISSION	65%	80%
TELESCOPE DIAMETER	0.5M	0.5M
TELESCOPE AREA OBSCURATION	15%	15%
FILTER BANDWIDTH	0.2NM	1.0NM
FILTER TRANSMISSION	10%	7%
XMTR BEAM DIVERGENCE *	.6/1.7m RAD	.6/1.7m RAD
RECEIVER FOV**	.8/1.9m RAD	.8/1.9m RAD
BACKGROUND(DAY)	333 COUNTS/KM	7174 COUNTS/KM

* DIVERGENCE TO MEET EYE SAFE CRITERIA FOR DAY/NIGHT VIEWING WITH 50 MM BINOCULARS AND 1060 NM LASER OUTPUT AT 40 KM.

** 0.2m RAD ADDED TO BEAM DIVERGENCE VALUES TO PROVIDE FOR MISALIGNMENT BETWEEN TRANSMITTER AND RECEIVER LINE OF SIGHT.

BALLOON LIDAR EXPERIMENT PARAMETERS

(100 mJ BASELINE)

	1060 NM	353 NM
E_L	.054 J/PULSE	.009 J/PULSE
PMT QUANTUM EFF.	4%	30%
TELESCOPE TRANSMISSION	65%	80%
TELESCOPE DIAMETER	0.5M	0.5M
TELESCOPE AREA OBSCURATION	15%	15%
FILTER BANDWIDTH	0.2NM	1.0NM
FILTER TRANSMISSION	10%	7%
X MTR BEAM DIVERGENCE*	.3/.8m RAD	.3/.8m RAD
RECEIVER FOV**	.5/1.0m RAD	.5/1.0m RAD
BACKGROUND (DAY)	130 COUNTS/KM	2802 COUNTS/KM

* DIVERGENCE TO MEET EYE SAFE CRITERIA FOR DAY/NIGHT VIEWING WITH 50 MM BINOCULARS AND 1060 NM LASER OUTPUT AT 40 KM.

** 0.2m RAD ADDED TO BEAM DIVERGENCE VALUES TO PROVIDE FOR MISALIGNMENT BETWEEN TRANSMITTER AND RECEIVER LINE OF SIGHT.

EXPECTED ERROR IN TWO COLOR DENSITY MEASUREMENTS
(FIRING HORIZONTALLY)

The curve data on pages 145, 146, and 147 provide expected errors in the two color density measurement technique at three separate altitudes, with the lasers firing horizontally, and no background interference. Single and multiple shot noise effects and variations in the uncertainty in the backscatter ratio are also included in the data. The curves do show that multiple shot averaging significantly improves measurement accuracy, in particular in the higher altitude regions where the $(2R\bar{\alpha}\, x^{\delta\alpha}/\alpha) \times (1 + \beta_A/\beta_R)_{353}$ contribution to the error term becomes a negligible quantity (see page 101 for the error equation which was used to determine the error in density for the analysis presented in this section).

The ordinate values of all solid curves in the vicinity of zero range are predominantly due to the errors associated with the uncertainty in the aerosol to molecular backscatter ratio $(\beta A/\beta R)$ 353. The contribution of this parameter to the error equation remains essentially constant for the ranges shown in these figures, and reaches its maximum value at about the 18 km altitude region, due to an aerosol layer within the LOWTRAN model (see page 155 for a better picture as to the impact of this parameter over the altitude regions of interest in this study). The spread in the curves on page 146 for 20 km reflect this impact.

The slopes of the curves for 1000 shots reflect the impact of the uncertainty in the optical thickness as a function of range and, as stated in the first paragraph, becomes negligible in the more rarified atmosphere of the higher altitude regions.

The remaining major error contributor to the error in density in these figures is due to shot noise which is reflected in the curve data by the angular spread between the single shot and 1000 shot curves. This angular spread increases with altitude due to a corresponding decrease in the number of returned photons at any fixed range. The slope of the total error in density at any given altitude, therefore, reflects the combined effects of diminishing returned photons with range and contributions from the previous major error terms.

EXPECTED ERROR IN TWO COLOR DENSITY MEASUREMENTS
FIRING HORIZONTALLY AT 10KM (NO BACKGROUND)

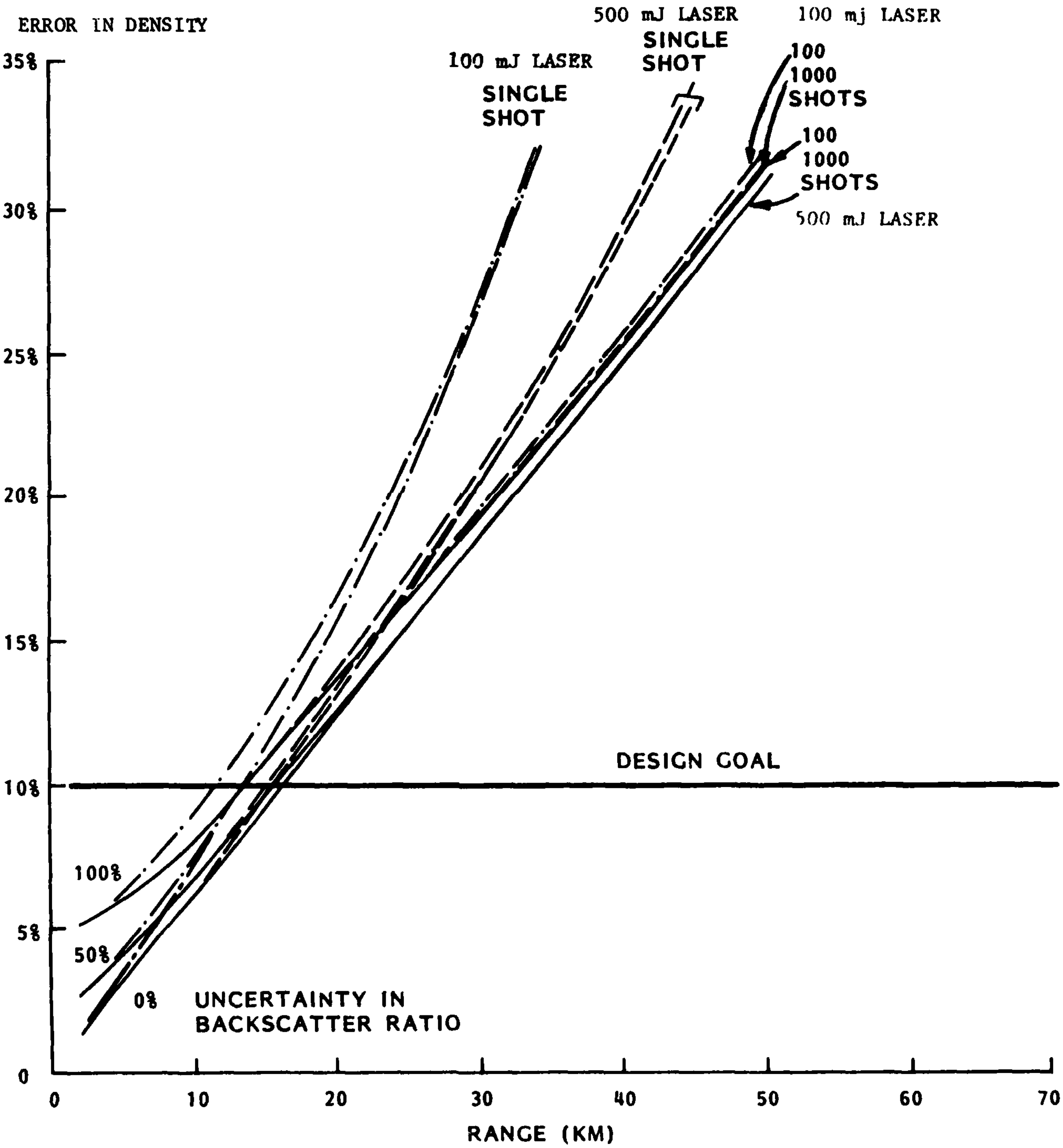

EXPECTED ERROR IN TWO COLOR DENSITY MEASUREMENTS
FIRING HORIZONTALLY AT 20KM (NO BACKGROUND)

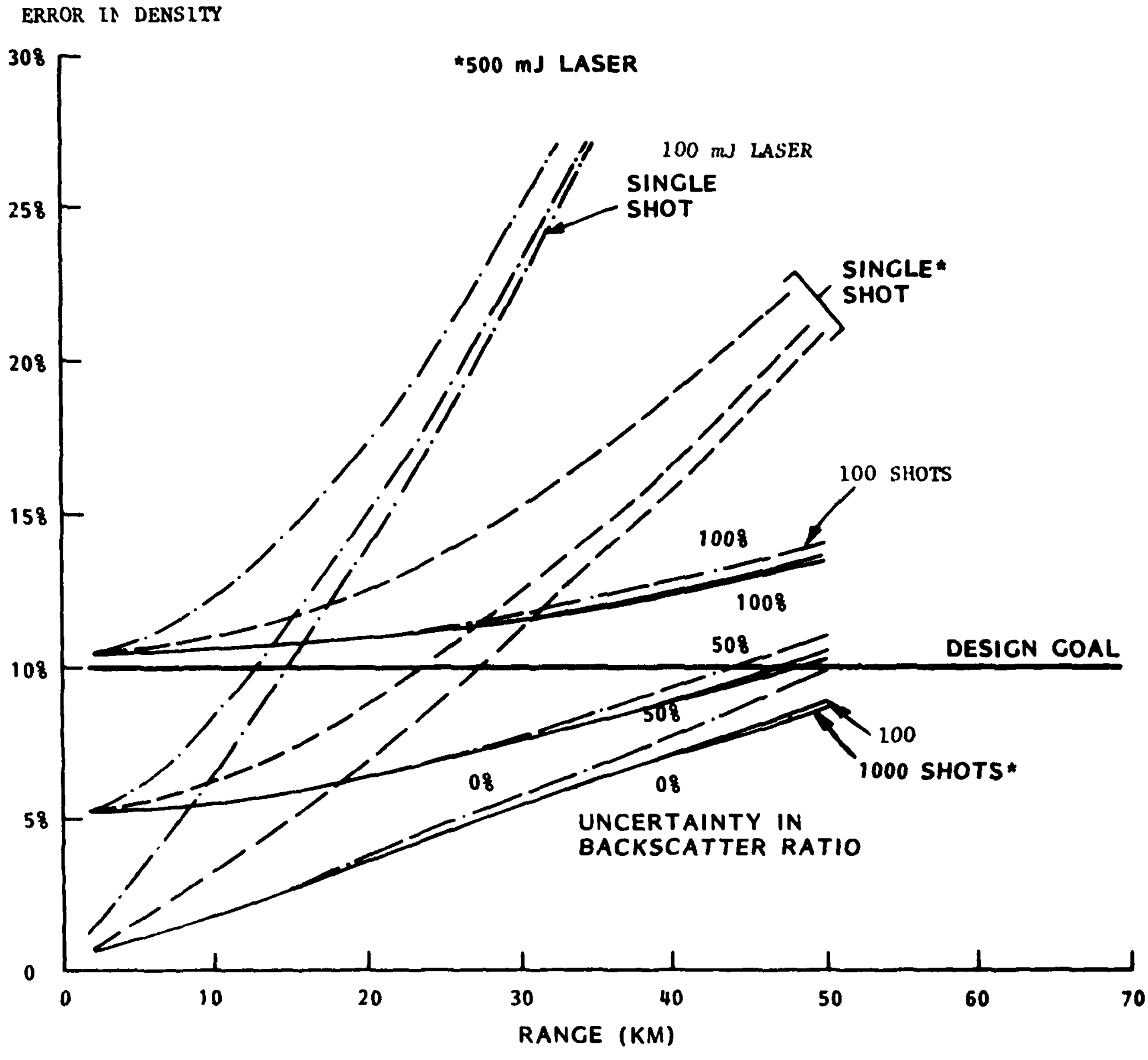

EXPECTED ERROR IN TWO COLOR DENSITY MEASUREMENTS FIRING HORIZONTALLY AT 30KM (NO BACKGROUND)

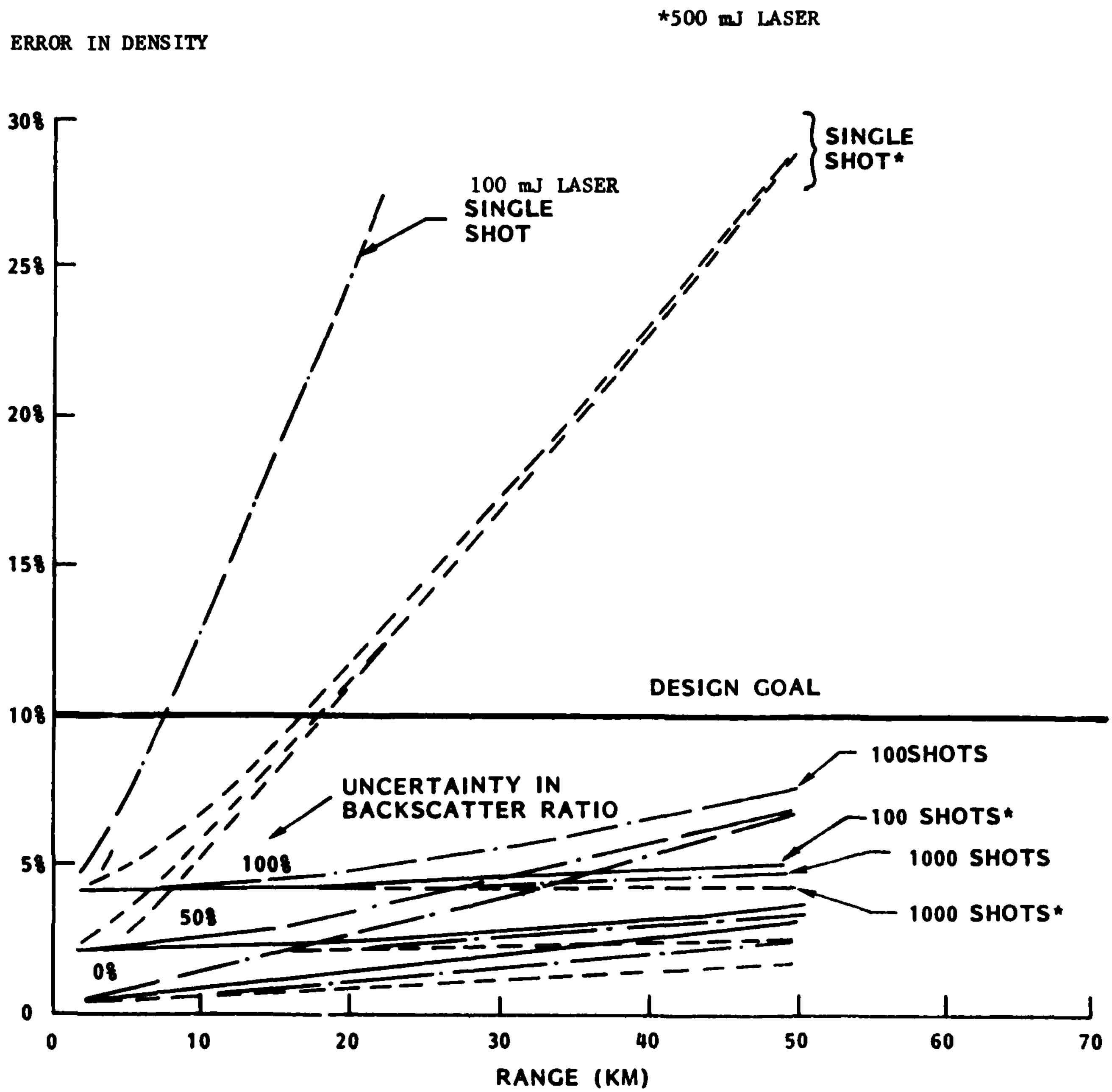

EXPECTED ERROR IN TWO COLOR DENSITY MEASUREMENTS

(FIRING UPWARD 30°, 60° AND VERTICALLY DOWNWARD)

The curve data on pages 149, 150 and 151 provide expected errors when the laser is fired upward at 30°. Page 153 provides data for a 60° upward direction. The primary advantage to firing both downward and upward is that the balloon can operate at a lower altitude and obtain very accurate data from about 5 km to high altitudes (an example of this is shown on page 150. In addition, the balloon can carry much higher payloads to the lower altitude, e.g., a 5 km reduction in altitude increases the payload capacity by a factor of about 3. On the other hand, firing upward does not duplicate the downward capability sought by an operational spacecraft instrument, although it does provide a broader scientific data base for verification of this measurement technique.

The curve data on pages 154 and 155 provide expected LIDAR returns and expected errors, respectively, in the two color density measurement techniques when the lasers are fired downward from 40 km. The data on page 154 shows the return counts also for the 20 and 30 KM altitudes. The data on page 155 shows the effects of multiple shot measurements on the error in density. The curves indicate that there is basically no difference in accuracy between the two lasers since atmospheric and backscatter uncertainties predominate the error equation under multiple shot conditions. The contribution from each term in the error equation can be seen in the curve data on page 165 for the 100 mJ laser conditions shown on page 155.

It should be pointed out that the axis labeled "Altitude" on these and subsequent charts is the actual altitude of the scattering volume center as measured from sea level.

EXPECTED ERROR IN TWO COLOR DENSITY MEASUREMENTS
FIRING UPWARD 30° AT 10KM (NO BACKGROUND)

500 mJ LASER

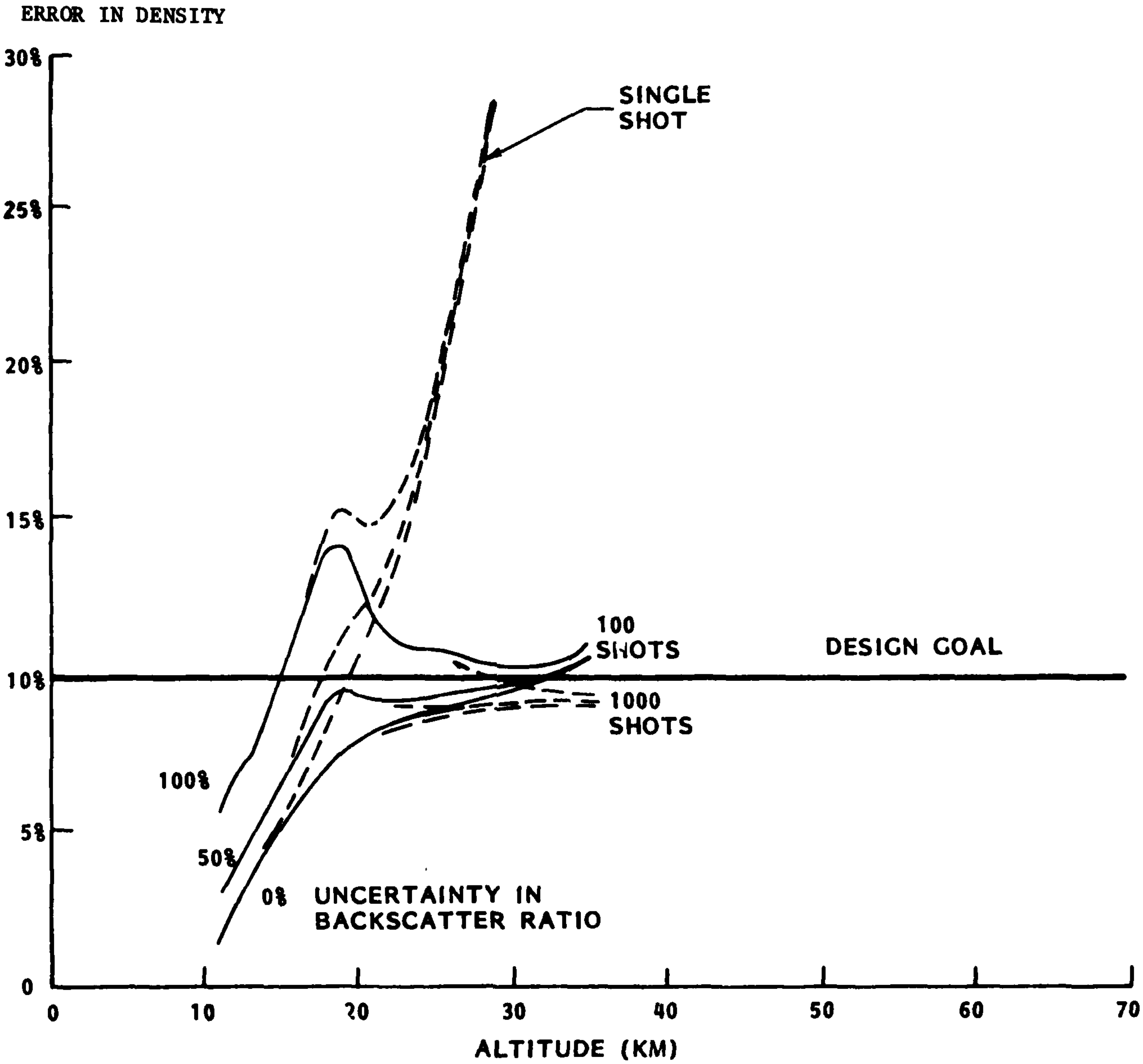

EXPECTED ERROR IN TWO COLOR DENSITY MEASUREMENTS
FIRING UPWARD 30° AT 20KM (NO BACKGROUND)

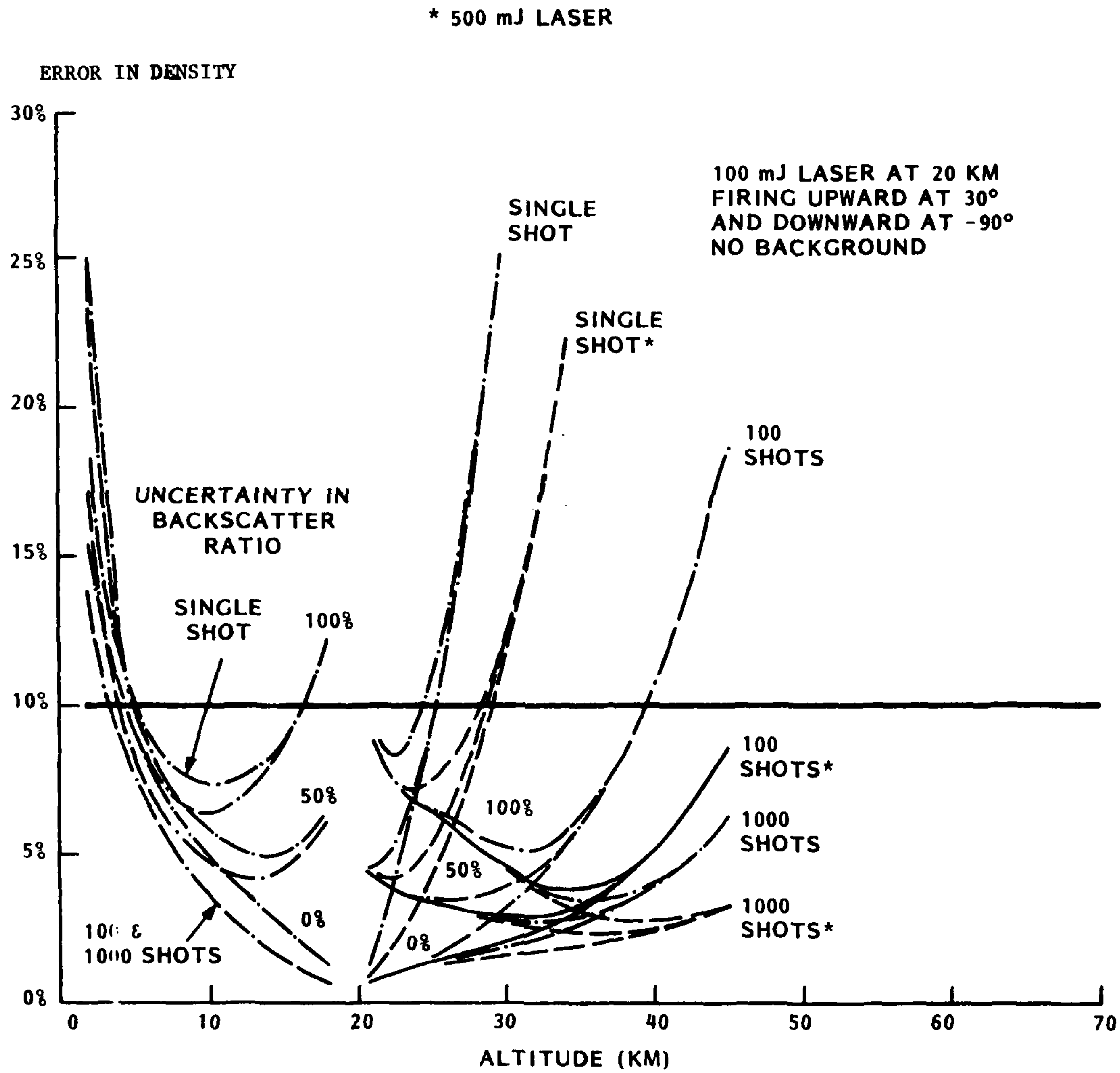

EXPECTED ERROR IN TWO COLOR DENSITY MEASUREMENTS
FIRING UPWARD 30° AT 30KM (NO BACKGROUND)

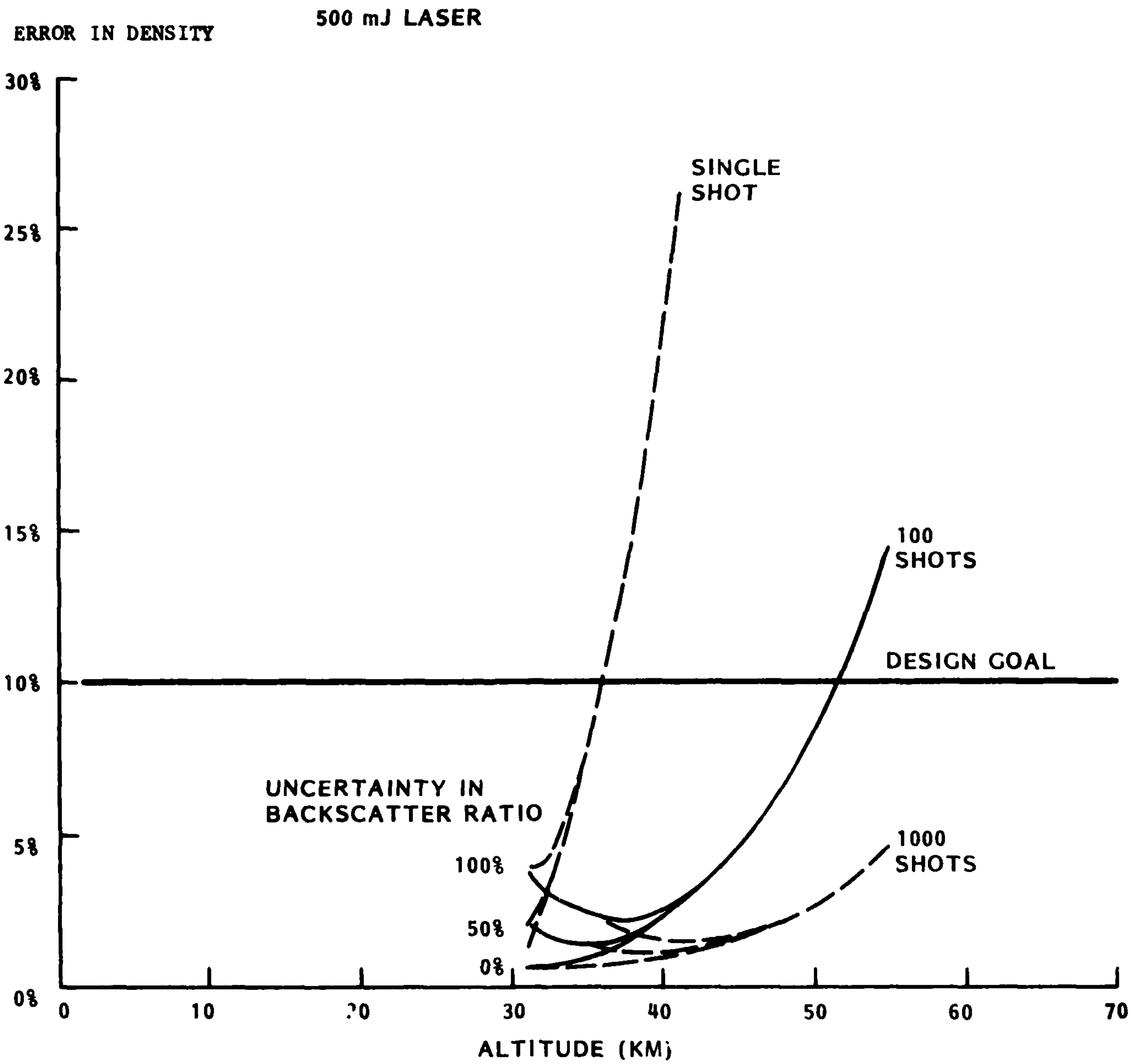

EXPECTED ERROR IN TWO COLOR DENSITY MEASUREMENTS
FIRING UPWARD 60° AT 30KM (NO BACKGROUND)

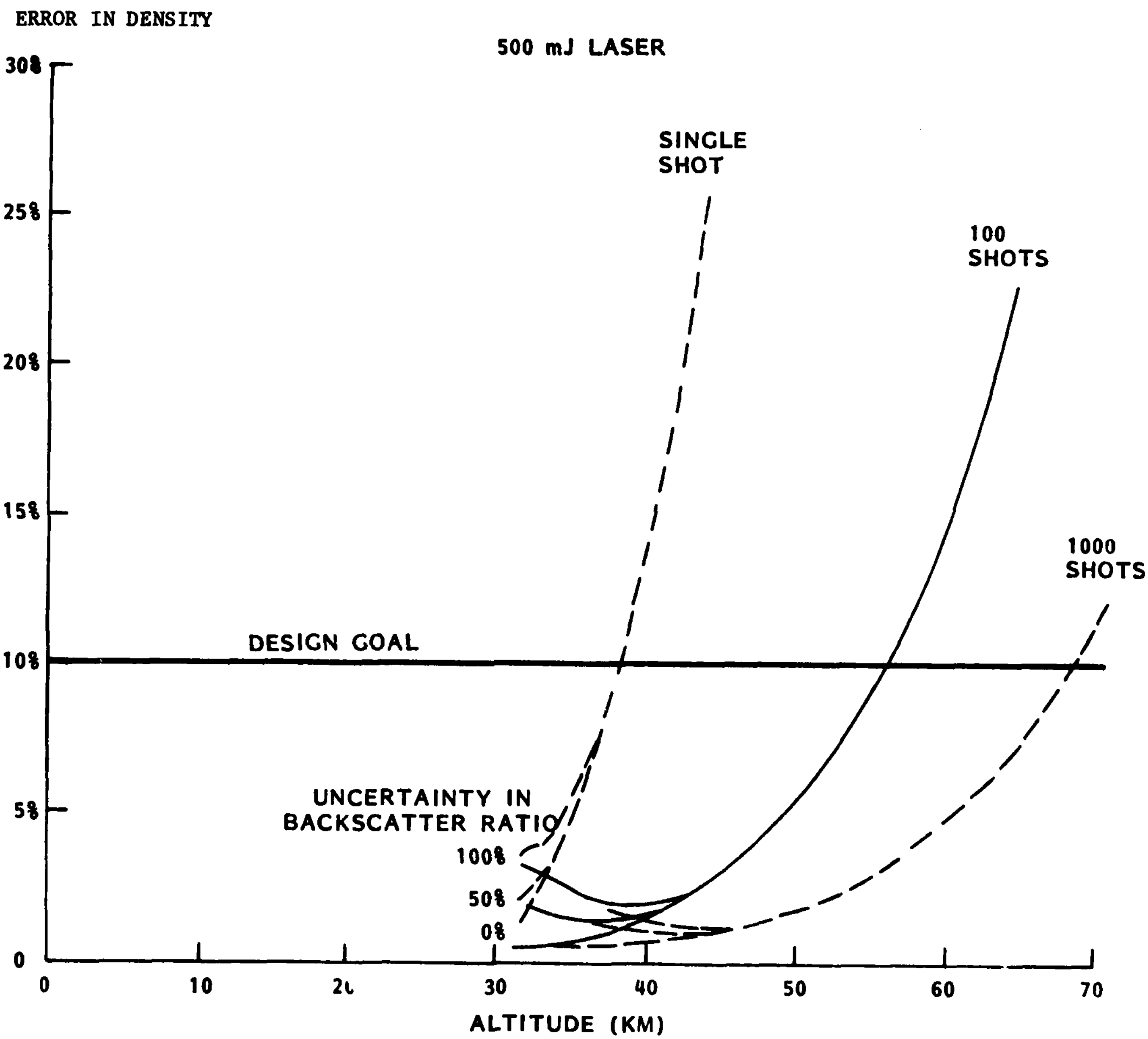

PRECEDING PAGE BLANK-NOT FILMED

EXPECTED LIDAR RETURNS FROM STANDARD
LOWTRAN 3B ATMOSPHERE
(SINGLE SHOT)

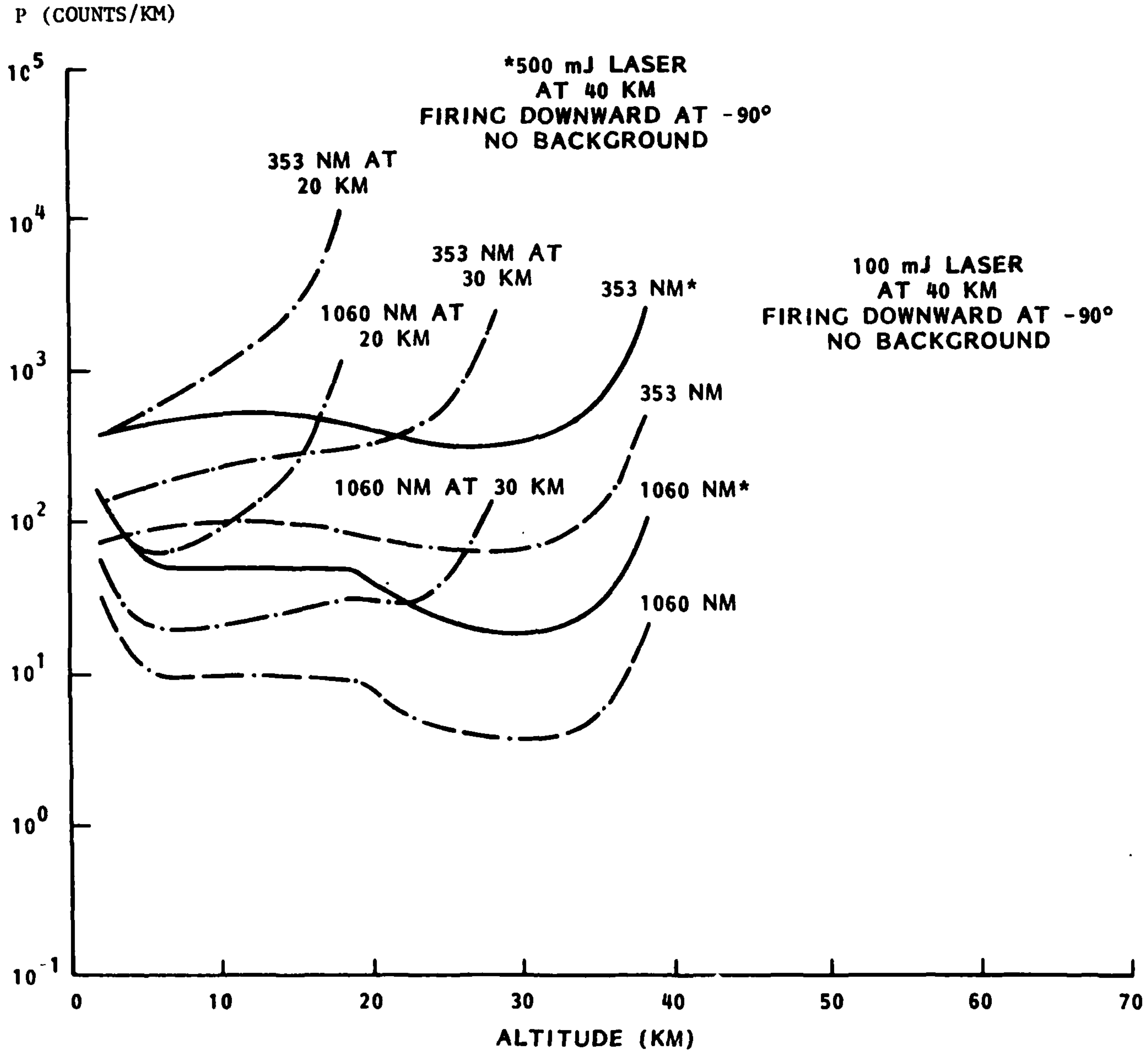

EXPECTED ERROR IN TWO COLOR DENSITY MEASUREMENTS
FIRING DOWNWARD - 90° AT 40KM (NO BACKGROUND)

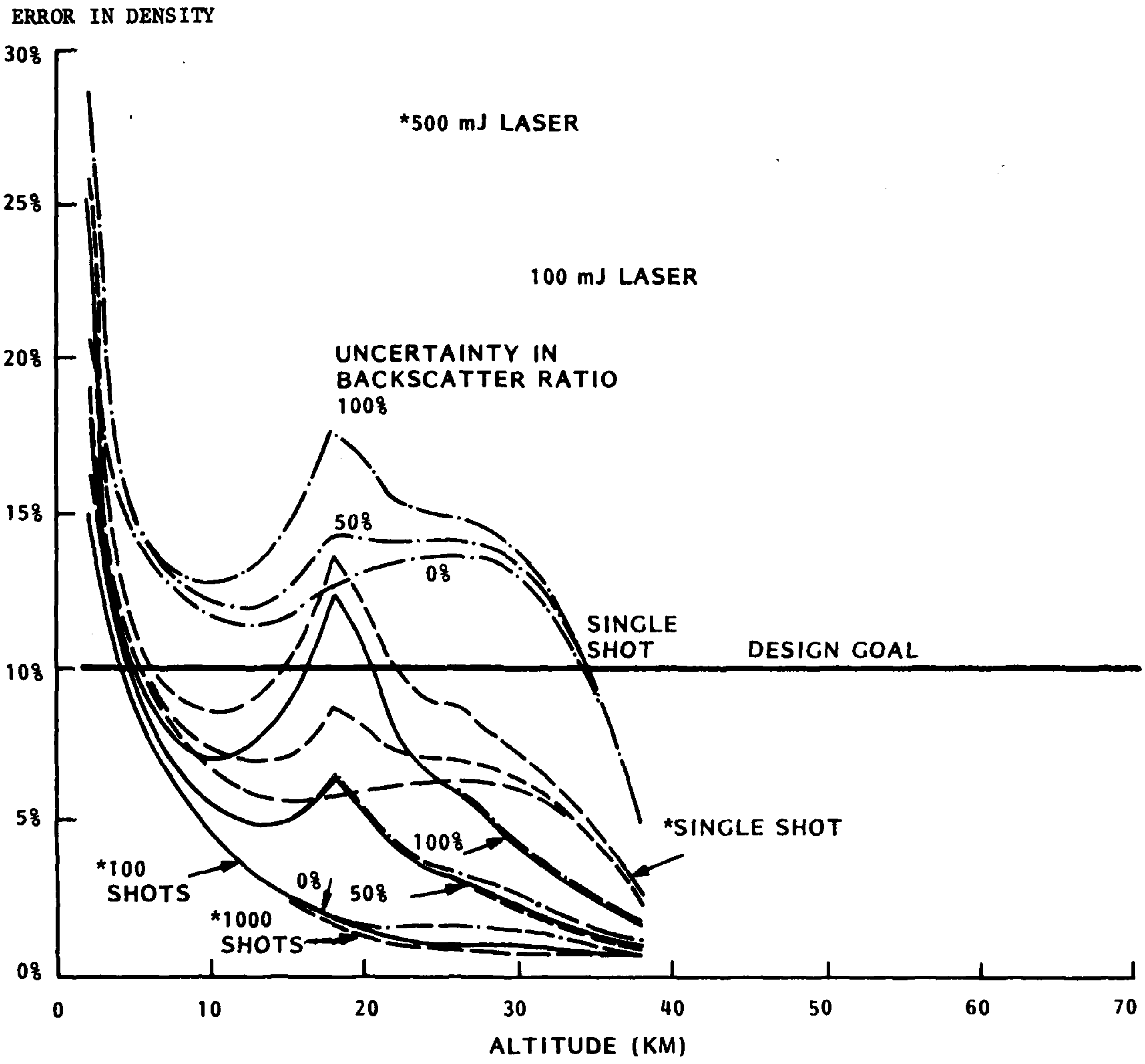

EXPECTED ERROR IN TWO COLOR DENSITY MEASUREMENT

(BACKGROUND EFFECTS)

The curve data on pages 157, 158, and 159 provide expected errors when background noise is introduced into the measurement of density. The background signal is based on the FOV's indicated in these charts. Similar comments can be made with these charts as those made with the preceding charts under multiple shot measurement conditions, i.e., accuracies are well within the 10% design goal established for this study.

The contributions from each term in the error equation which were used to develop the data on page 159 can be seen in the curve data on page 166 for the 100 mJ laser firing downward from 40 km and an 0.8 mrad FOV.

EXPECTED ERROR IN TWO COLOR DENSITY MEASUREMENTS
BACKGROUND EFFECTS ON SINGLE SHOT RETURNS

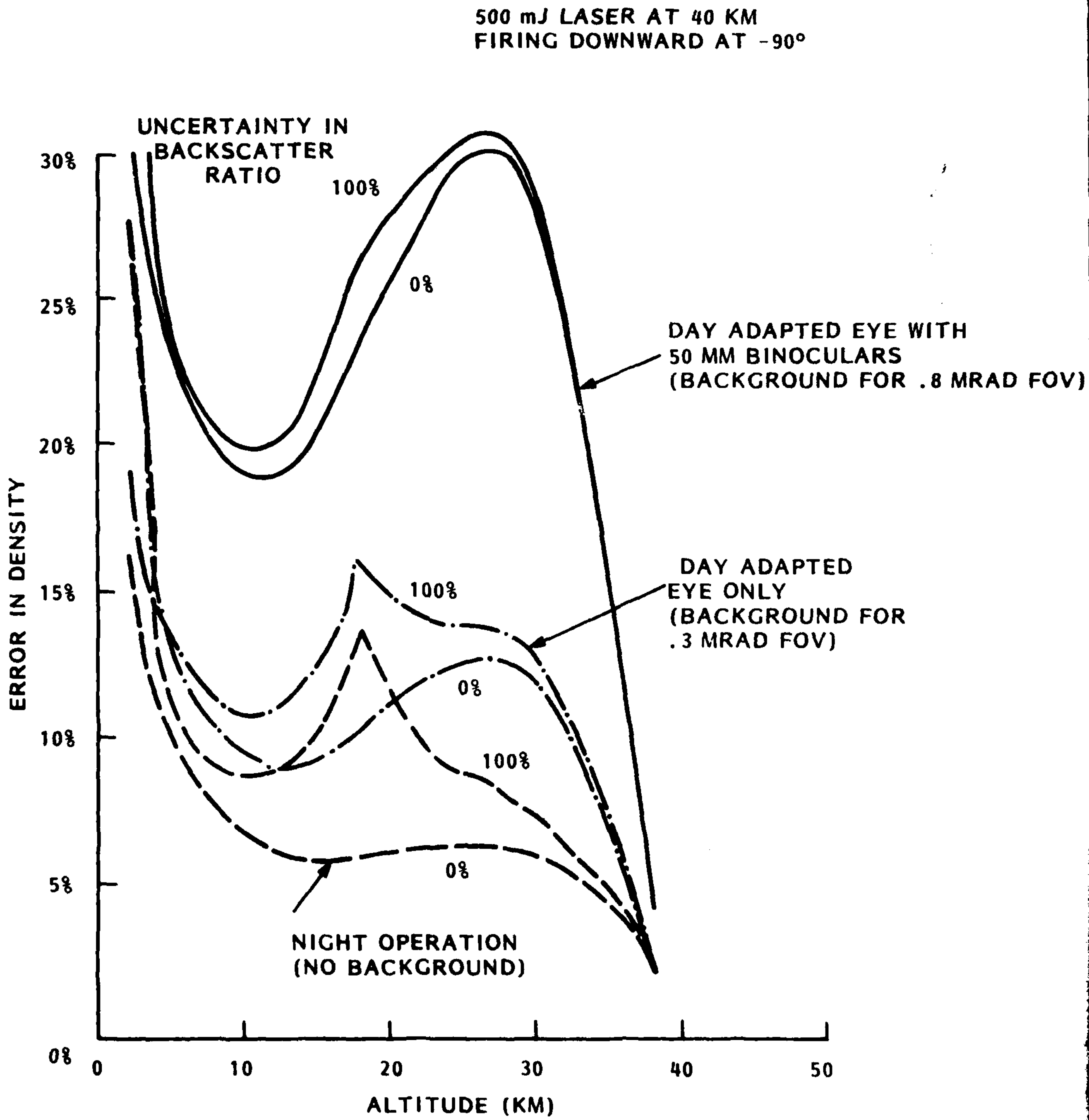

EXPECTED ERROR IN TWO COLOR DENSITY MEASUREMENTS
BACKGROUND EFFECTS ON MULTIPLE SHOT RETURNS

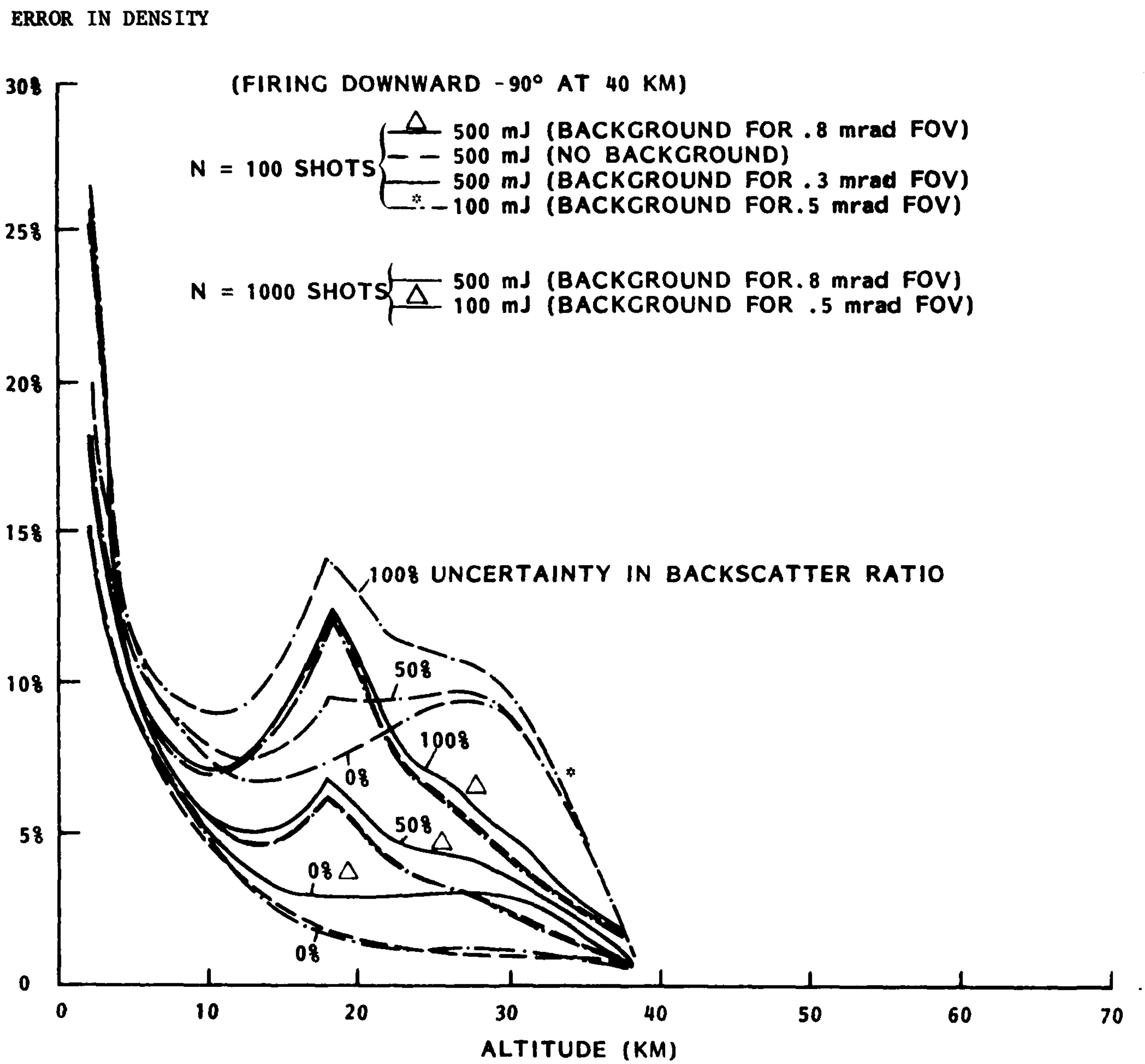

EXPECTED ERROR IN TWO COLOR DENSITY MEASUREMENTS
SAME BACKGROUND FOR TWO DIFFERENT ALTITUDES

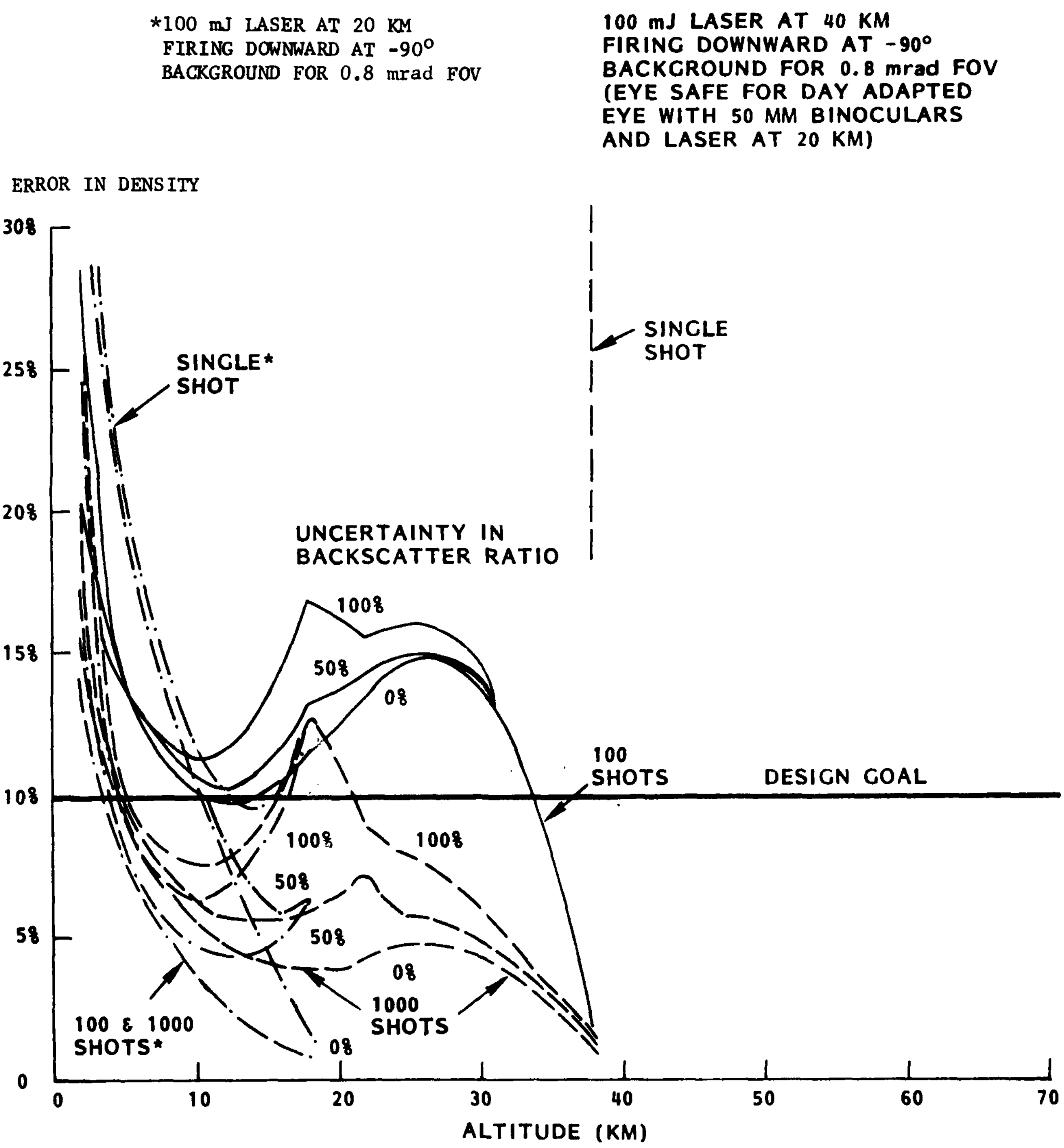

EXPECTED ERROR IN TWO COLOR DENSITY MEASUREMENTS (FIRING UPWARD FROM GROUND)

The curve data on pages 161 and 163 provide comparison data for lasers stationed on the ground and fired vertically upward. Experiment parameters used to generate the data shown on page 161 are the same as those shown on pages 141 and 143 without any background interference; however, for the data shown on page 163, a higher energy laser (2J baseline) and a larger diameter (1M) telescope primary were considered; all other parameters are the same. This includes wavelength conversion efficiencies (see page 140), overall system efficiencies (see page 223), and backscattering phase functions (see page 223) for the 1060 nm and 353 nm wavelengths. The primary reason for the poor performance for a ground based laser is the impact of the ($2R\bar{\alpha}\frac{\delta\alpha}{\alpha}$) X ($1 + \beta_\alpha/\beta_R$) term in the error equation, and which is independent of the laser energy. The contribution of this term can be seen in the curve data shown on page 167.

It should be pointed out that these curves are primarily representative of the uncertainties surrounding the density determination error equation and, therefore, do not reflect the impact of additional information which might be available to establish boundary conditions, e.g., ground based measurements of temperature and pressure can be used to determine the boundary conditions for the density measurements and, therefore, the expected error curves will shift significantly downward. Also, a possible option for the ground based instrument might be the use of a different combination of wavelengths, e.g., 1060 nm and 530 nm, which should provide greater density measurement accuracies, since the impact of uncertainty ($\delta\alpha/\alpha$) X optical thickness ($2R\bar{\alpha}$) in the error term is less at 530 nm than at 353 nm. However, the uncertainty in the backscatter ratio will still be a major contributor to the error term. More work is recommended in this area in order to reduce the uncertainties associated with this parameter.

EXPECTED ERROR IN TWO COLOR DENSITY MEASUREMENTS
FIRING UPWARED 90° FROM THE GROUND (NO BACKGROUND)

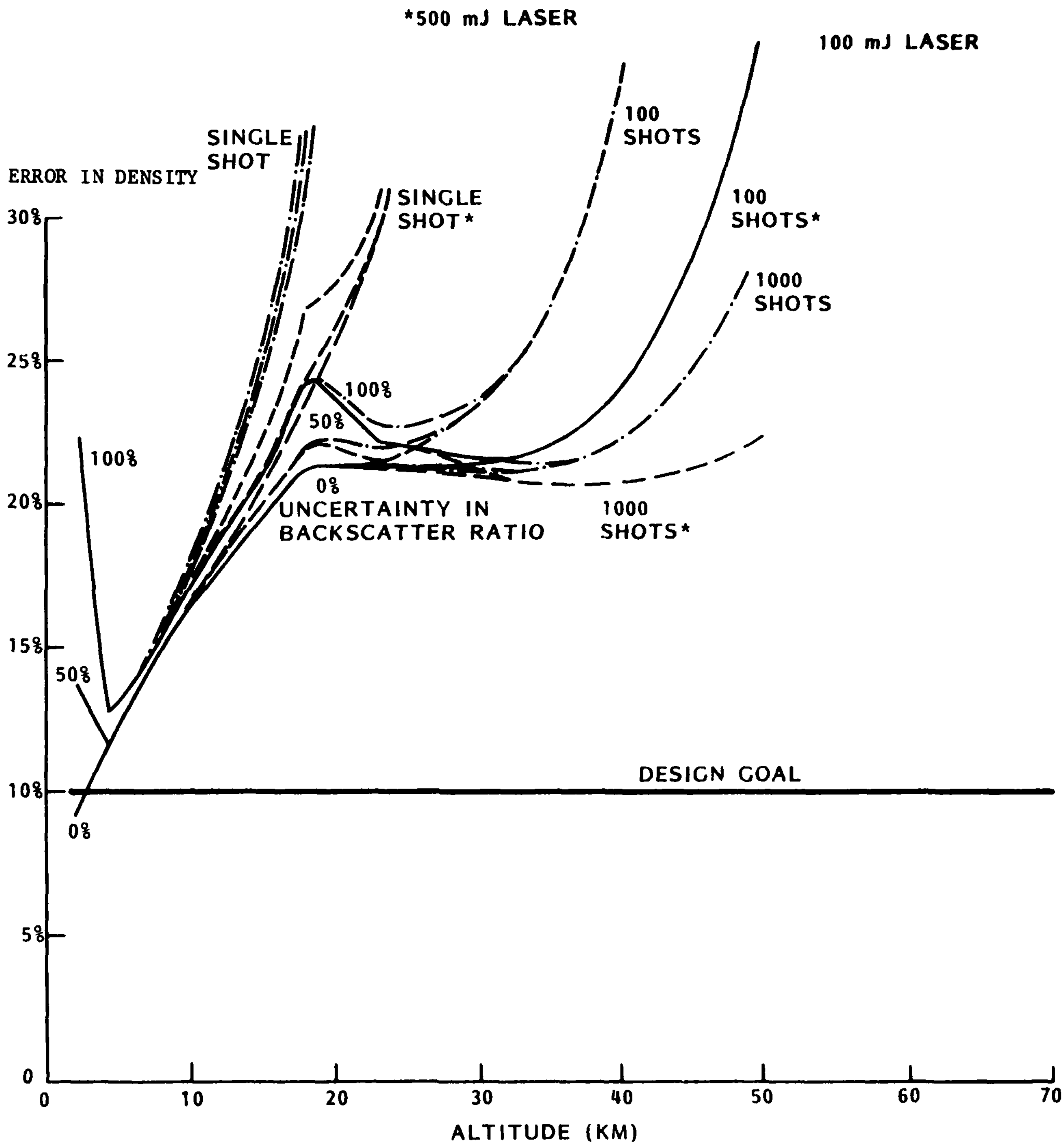

EXPECTED ERROR IN TWO COLOR DENSITY MEASUREMENTS

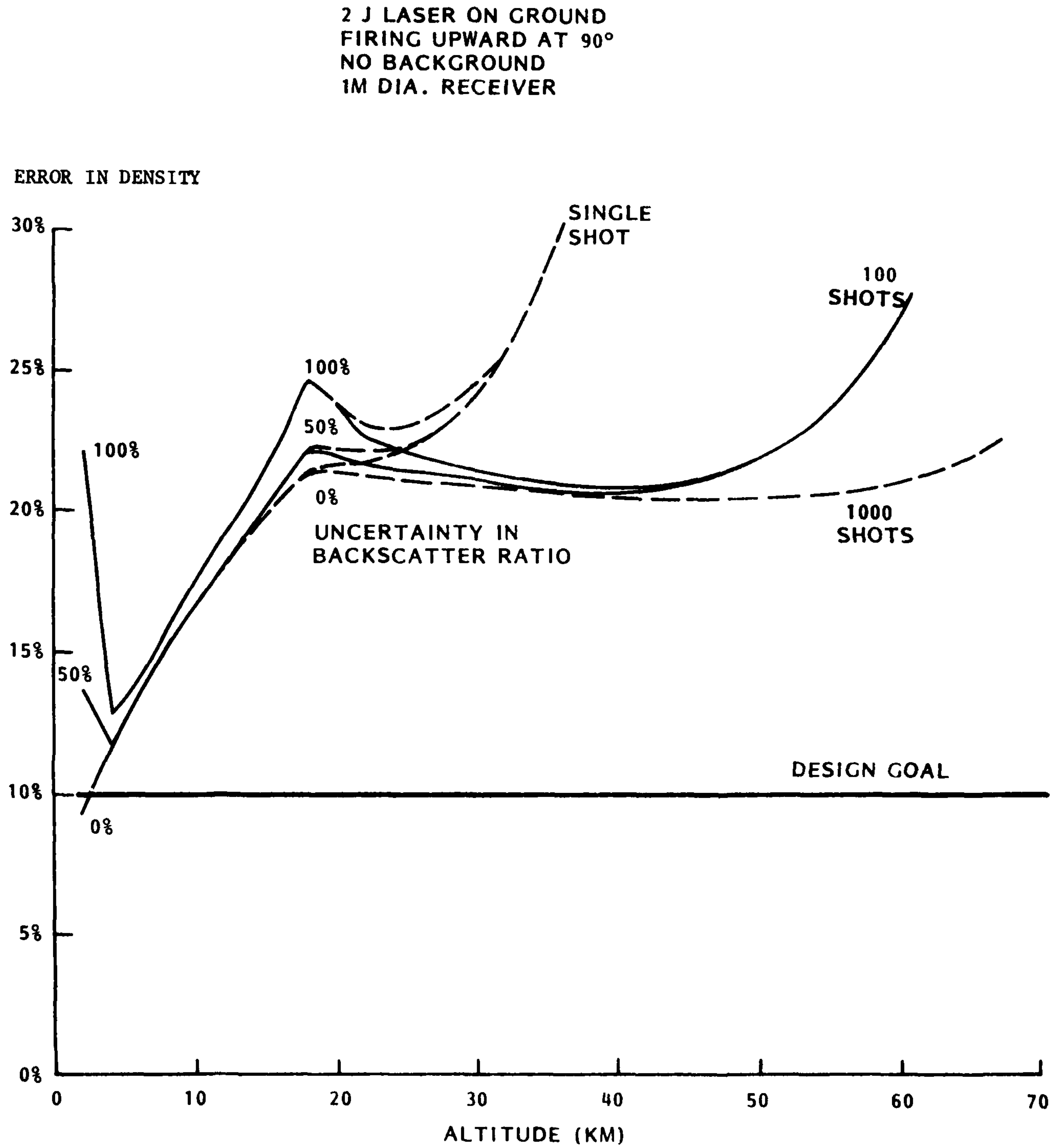

PRECEDING PAGE BLANK-NOT FILMED

ERROR PARTITIONING IN ESTIMATED ERROR OF TWO COLOR DENSITY MEASUREMENT TECHNIQUE

The following three charts provide the individual errors expected from each of the contributors to the error equation which was presented in Section 5 on page 101. These charts provide comparison of expected error data for the 100 mJ laser firing downward from 40 km, with and w/o a day background, and firing upward from the ground.

Examination of the first two charts indicates that the influence of the term containing the 50% uncertainty in the backscatter ratio has a major influence on the expected total error. Day background has, of course, a significant impact on the expected error, although averaging with a reasonable number of shots can still limit the error to less than 10%.

Examination of the final chart shows that the term containing the uncertainty in the extinction parameter and total optical thickness traversed at 353 nm is the dominant contributor to the total expected error at all altitudes below 40 km. This term can be significantly reduced by factoring in boundary conditions at the ground, i.e., ground pressure and temperature data. The anticipated result will be that the term containing shot noise at 353 nm will dominate the expected error equation at higher altitudes (also greater LIDAR ranges), and the term containing the 50% uncertainty in the backscatter ratio will dominate at the lower altitudes.

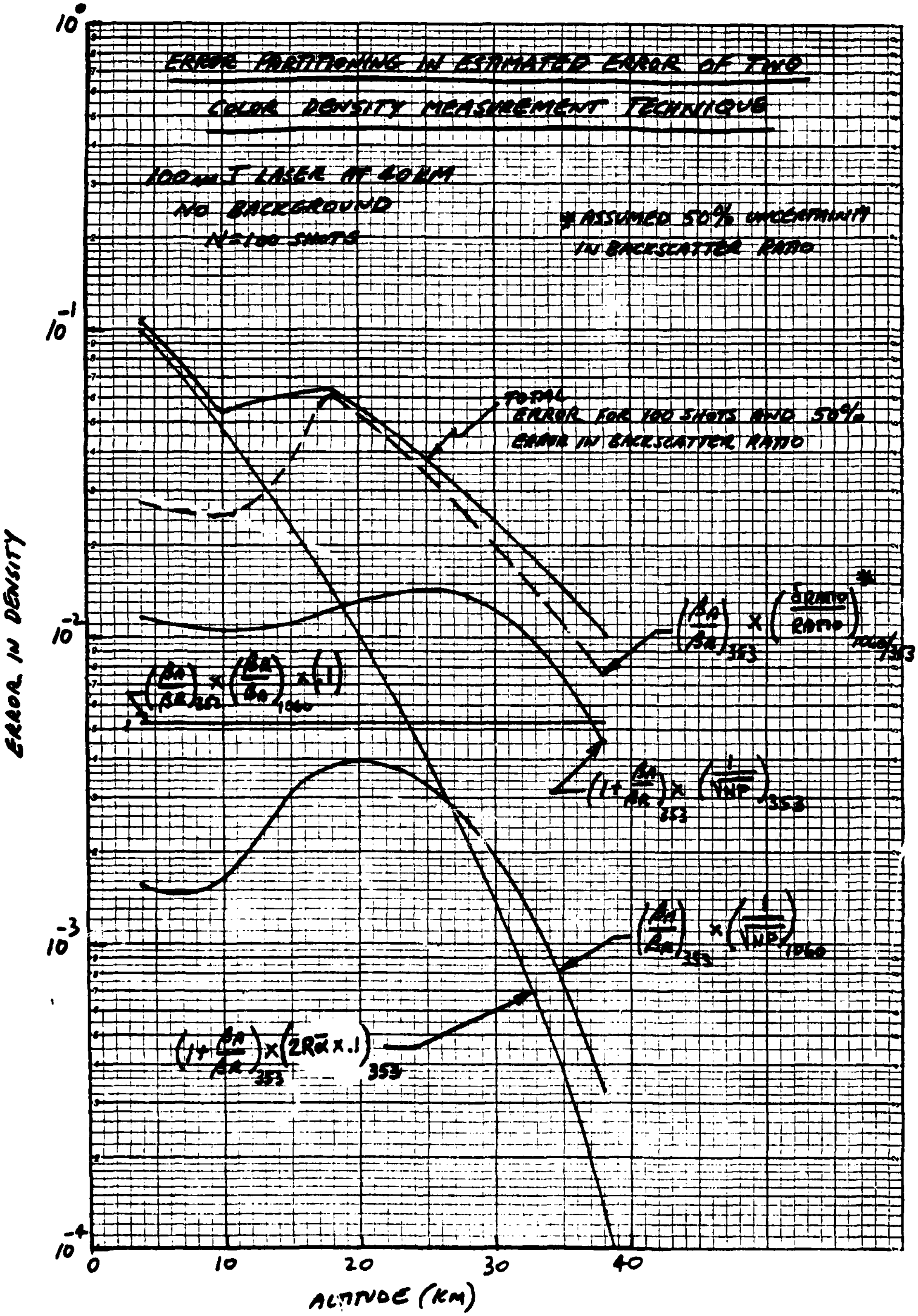

ERROR PARTITIONING IN ESTIMATED ERROR OF TWO COLOR DENSITY MEASUREMENT TECHNIQUE
100mJ LASER AT 40KM
NO BACKGROUND
N=100 SHOTS
* ASSUMED 50% UNCERTAINTY IN BACKSCATTER RATIO
TOTAL ERROR FOR 100 SHOTS AND 50% ERROR IN BACKSCATTER RATIO
ERROR IN DENSITY
ALTITUDE (KM)
10^0
10^-1
10^-2
10^-3
10^-4
0
10
20
30
40

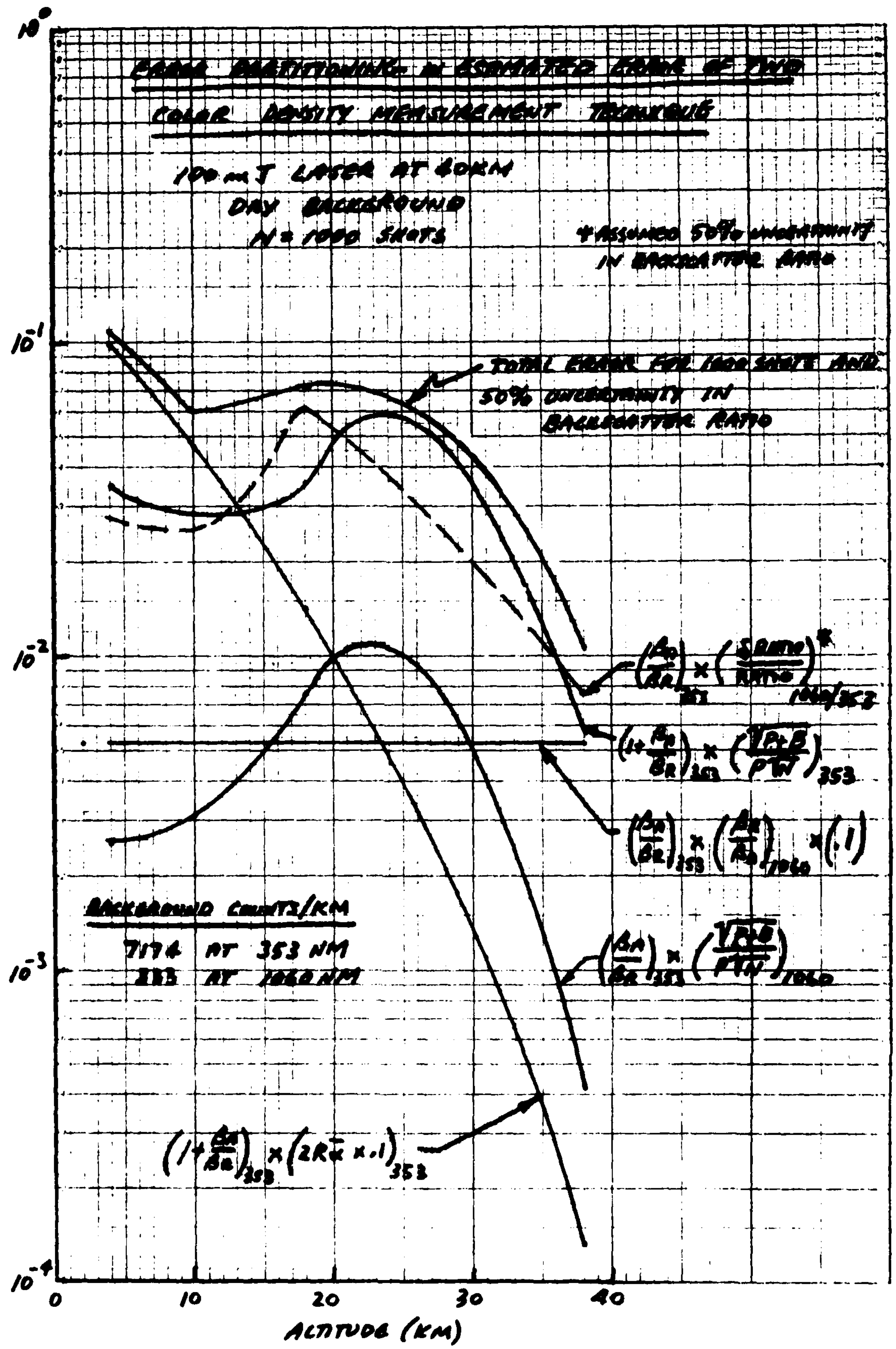
ERROR PARTITIONING IN ESTIMATED ERROR OF TWO COLOR DENSITY MEASUREMENT TECHNIQUE
100 mJ LASER AT 40KM
DAY BACKGROUND
N = 1000 SHOTS
* ASSUMED 50% UNCERTAINTY IN BACKSCATTER RATIO
TOTAL ERROR FOR 1000 SHOTS AND 50% UNCERTAINTY IN BACKSCATTER RATIO
BACKGROUND COUNTS/KM
7174 AT 353 NM
AT 1060 NM
ERROR IN DENSITY
ALTITUDE (KM)
10^0
10^-1
10^-2
10^-3
10^-4
0
10
20
30
40

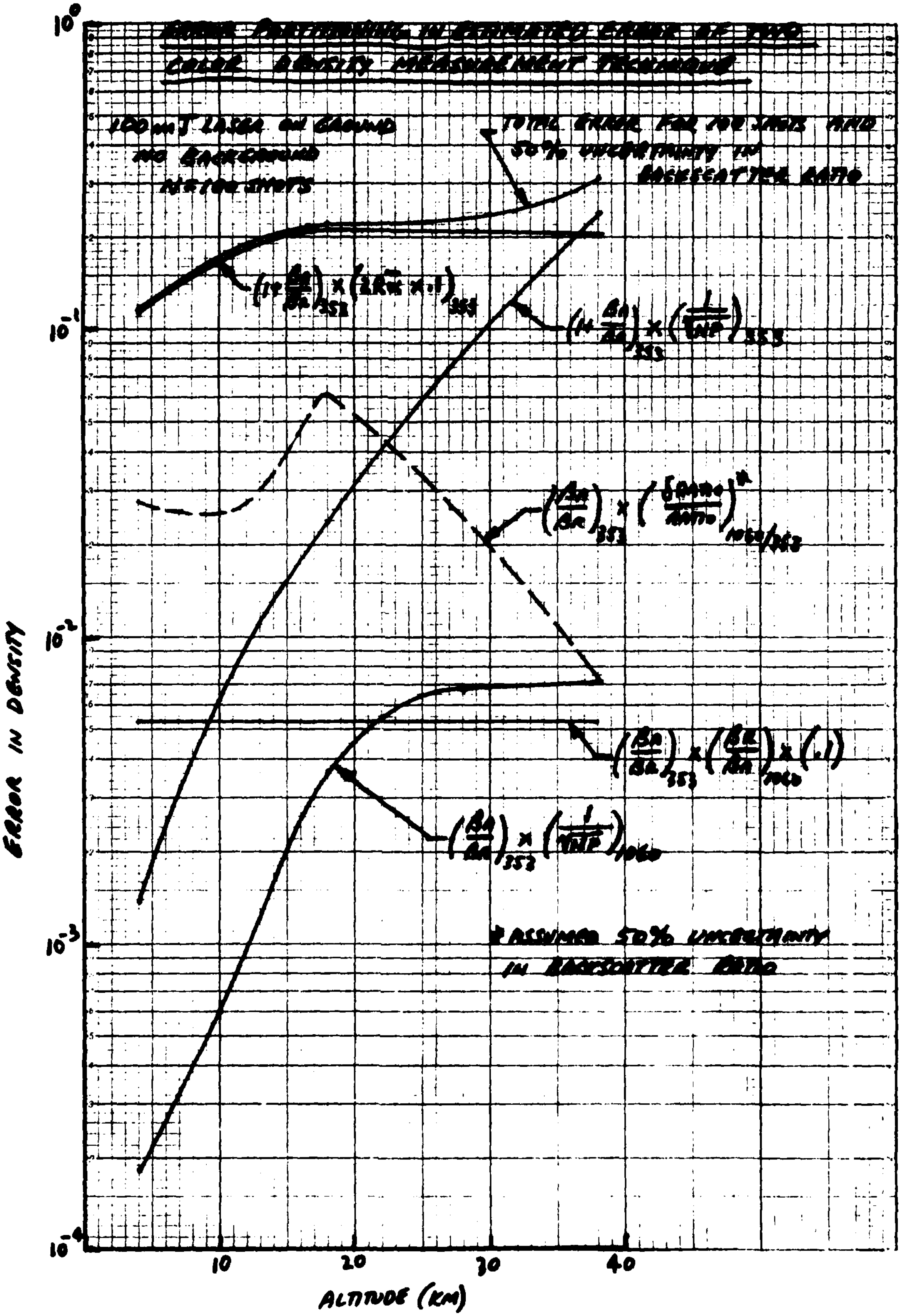

COLOR DENSITY MEASUREMENT TECHNIQUE
100 mJ LASER ON GROUND
NO BACKGROUND
N=100 SHOTS
TOTAL ERROR FOR 100 SHOTS AND
50% UNCERTAINTY IN
BACKSCATTER RATIO
*ASSUMED 50% UNCERTAINTY
IN BACKSCATTER RATIO
ERROR IN DENSITY
ALTITUDE (KM)
10
20
30
40

SECTION 7

EXPERIMENT HARDWARE DESCRIPTIONS

PRECEDING PAGE BLANK-NOT FILMED

EXPERIMENT HARDWARE DESCRIPTIONS

This section provides hardware descriptions for the implementation of the density measurement techniques under consideration in this study, particularly, for the Rayleigh/Mie and O_2-DIAL techniques. Hardware descriptions are provided for the Atmospheric Lidar Multi-User Instrument System (ALMIS), the Standard Test Rack (STR) LIDAR Experiment, as an adjunct to the WINDSAT LIDAR Experiment, and as a proof-of-concept balloon-based LIDAR experiment. Experiment hardware descriptions are discussed in the following four subsections which provide pictorial arrangements and weight, power, and volume information for each concept. The first three of these four hardware concepts were selected as viable alternatives for an operational experiment; although not intended for operational use, the balloon concept can provide a low cost approach for a feasibility demonstration experiment and, therefore, be a logical first step towards obtaining the capability to develop an experiment which can routinely provide accurate density measurements from space on a global scale.

ATMOSPHERIC LIDAR MULTI-USER

INSTRUMENT SYSTEM (ALMIS)

ATMOSPHERIC LIDAR MULTI-USER INSTRUMENT SYSTEM (ALMIS)

This figure shows the ALMIS system arrangement as mounted to a standard Spacelab pallet. The primary science objectives for this multi-user instrument are:

- To trace the global flow of H_2O and pollutants in the troposphere and lower stratosphere.
- To verify chemical, and transport, models of the stratosphere and mesosphere.
- To evaluate radiative models of the atmosphere.
- To augment the meteorological data base.
- To study excitation, propogation, and dissipation of wave motion in the upper atmosphere.
- To study chemistry and transport of thermospheric atomic species.
- To study magnetospheric aspects of sun/weather relationships.

The criteria used to ensure that these scientific objectives can be met with a viable operational hardware concept are that:

- The instrument be defined to provide maximum *life at lowest overall cost* in order to accommodate the largest number of experiments in a cost effective manner.
- A modular design be used to provide for the lowest experiment integration and reconfiguration time between flights in order that a single system be capable of performing 3 missions per year.
- The system be flexible in order to provide several types of measurements during any one mission, to accommodate principal investigator supplied lasers and detectors, and to have the capability of examining targets of opportunity.
- The system has growth capability to accept the maximum accommodation of lasers and detectors and to allow for their time phased implementation.
- The first mission have a high scientific success-potential.

The LIDAR system arrangement shown illustrates the "maximum" accommodation configuration and includes hardware components for growth options. It simultaneously offset-mounts three lasers and three detectors with a fourth laser/detector assembly mounted to the pallet and accessing the telescope along its central axis.

The telescope, lasers, and detectors are mounted to a cylindrical optical bench to assure their alignment integrity and achieve a modular, controllable optical assembly. *The entire optical assembly* as well as the associated supporting subsystems is contained within a thermal shroud to assure isolation from companion payloads.

GENERAL ELECTRIC

SYSTEM ARRANGEMENT

space division

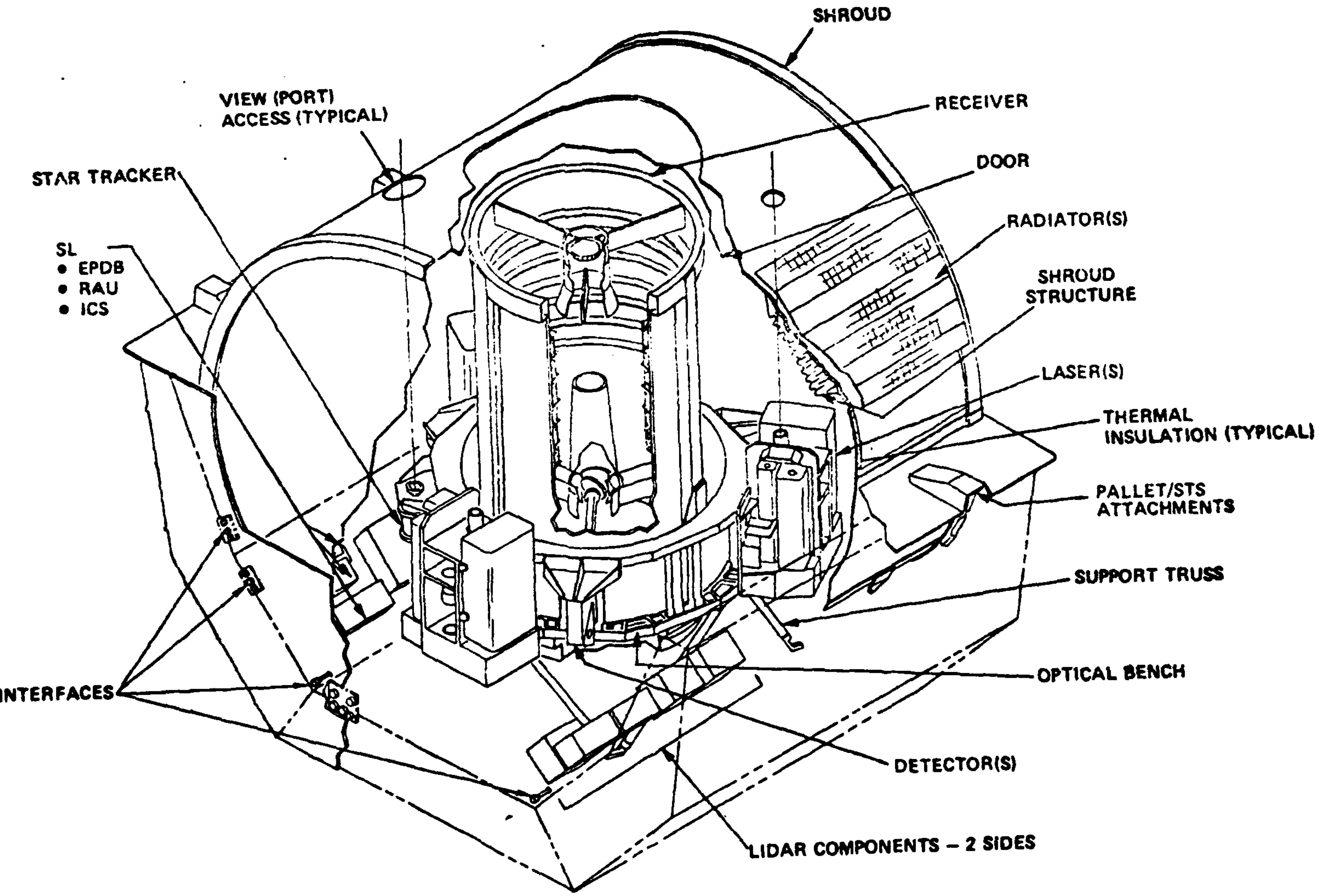

ALMIS - SYSTEM DESIGN CHARACTERISTICS SUMMARY

The following two charts provide the mass, power and volume breakdown of the major components selected for the Phase 1 and maximum accommodation ALMIS experiment. Although an instrument operating power of 2310 W is indicated in the table for the Phase 1 ALMIS experiment, duty cycling will substantially lower the orbit average power demands of this experiment; an orbit average power of about 977 W is expected, based on a 1/3 orbit duty cycle for the source and detector subsystems while the other subsystems are "on" continuously. Additional orbit average power reductions can be obtained if the source and detector subsystems are duty cycled within the 1/3 orbit duty cycle, e.g., 10 seconds of laser and detector operation per minute during the 1/3 orbit duty cycle results in an orbit average power of about 421 W.

The maximum accommodation ALMIS experiment is shown on page 176 and compared to the Phase 1 system has sizable increases in weight and power (CO_2 - **Pulse laser**) requirements. However, duty cycling of the CO_2 laser and detector subsystems will significantly lower the orbit average power requirements, e.g., 10 seconds of laser operation per minute throughout an orbit will result in an orbit average power of about 963 W. If this duty cycle is performed only during a 1/3 orbit period, the orbit average power will be about 528 W (assumes other subsystems are "on" continuously).

GENERAL ELECTRIC

PHASE 1 – SYSTEM DESIGN CHARACTERISTICS

SUMMARY

space division

SYSTEM/ SUBSYSTEM	ITEMS	EACH	TOTAL MASS KG	DC POWER WATTS	TOTAL VOLUME LITERS
SOURCE	Nd-YAG X 2 X DYE X 3 X 2 POWER SUPPLY	1 1	140 30	1870	300 60
RECEIVER	1.25M F/2	1	635	INTERMITTENT 35	4550
DETECTOR	SINGLE PMT DUAL PMT DETECTOR PROCESSOR	2 1 1	4 8 12	35 70 60	2.8 5.6 17.2
C&DH	CDH UNIT	1	17	100	17.2
ELECTRICAL POWER & DIST	POWER DIST UNIT BATTERY HARNESS SET	1 2 1	10 44 85	10	7.1 30.3
STRUCTURE	OPTICAL SUPPORT COLD PLATES SHROUD/DOOR	1 2 1	70 12 85	INTERMITTENT 60	56.0 N/A
THERMAL CONTROL	RADIATORS MULTILAYER INSULATION SET PUMP, VALVES TUBE-SET HEATERS COOLANT	2 1 1 1	60 30 60 50	200	300
CORRELATIVE SENSORS	STAR TRACKER IN. REF. UNIT	1 1	5 5	INTERMITTENT 20	10
TOTAL			1362 (3003 LBS)	2310	

GENERAL ELECTRIC

MAXIMUM ACCOMMODATION – SYSTEM DESIGN CHARACTERISTICS SUMMARY

space division

SYSTEM/ SUBSYSTEM	ITEMS	EACH	TOTAL MASS KG	DC POWER WATTS	TOTAL VOLUME LITERS
SOURCE	Nd-YAG /DYE CO_2 PULSE	3 1	510 210	1870 3750	1080 330
RECEIVER	1.25M; F/2 SWING AWAY MIRROR	1	693	INTERMITTENT 35	4550
DETECTOR	SINGLE PMT DUAL PMT TRIPLE PMT DETECTOR PROCESSOR	1 1 1 1	4 8 12 12	35 70 110 60	18
C&DH	CDH UNIT	1	17	100	18
ELECTRICAL POWER & DIST	POWER DIST UNIT BATTERY HARNESS SET	1 2 1	10 44 85	10	8 30
STRUCTURE	OPTICAL SUPPORT COLD PLATES SHROUD/DOOR	1 3 1	70 18 85	INTERMITTENT 60	160
THERMAL CONTROL	RADIATORS MULTILAYER INSULATION SET PUMP VALVES TUBE, HEATERS SET COOLANT	2 1 1 1	60 30 70 50	200	300
CORRELATIVE SENSOR	A/R	A/R	60	INTERMITTENT 100	30
TOTAL			1990 (4375 LB)	2350 -Nd:YAG 4230 -CO_2PULSE	

STANDARD TEST RACK (STR)

LIDAR EXPERIMENT

STR BASIC CONFIGURATION

The figure shows the basic configuration of the Standard Test Rack (STR) which was designed by GE to provide the capability for additional resources (e.g. thermal, C&DH, power, attitude reference) accommodations than provided by Shuttle, and by using a structural modular concept minimize integration activities associated with flight-to-flight turnaround time. The modular concept not only provides the means to shorten the turnaround time period but also minimizes the number of interfaces with the Shuttle; thereby providing a high degree of autonomy and quick response capability for flights of opportunity to Principal Investigators.

Eight interchangeable modules (six on the main structure and two on the bridge) provide space for heat capacitors (15 KWH) and cold plates, 600 W (378 KWH) /module battery packs, data recorders (3 x 10^8 bits), an inertial reference unit (IRU), and computer/ supporting electronics. Integrated variable conductance heat pipes provide uniform dissipation of heat throughout the structural elements.

Mounting of the STR to the Shuttle cargo bay is very similar to the scheme used to mount Spacelab pallets, i.e., trunnions are attached directly to the cargo bay longeron and keel fittings. The length of the STR, which is approximately 42% of a standard Spacelab pallet, is ideally suited to the 1 M class telescope under consideration for this experiment.

GENERAL ELECTRIC

space division

STR BASIC CONFIGURATION

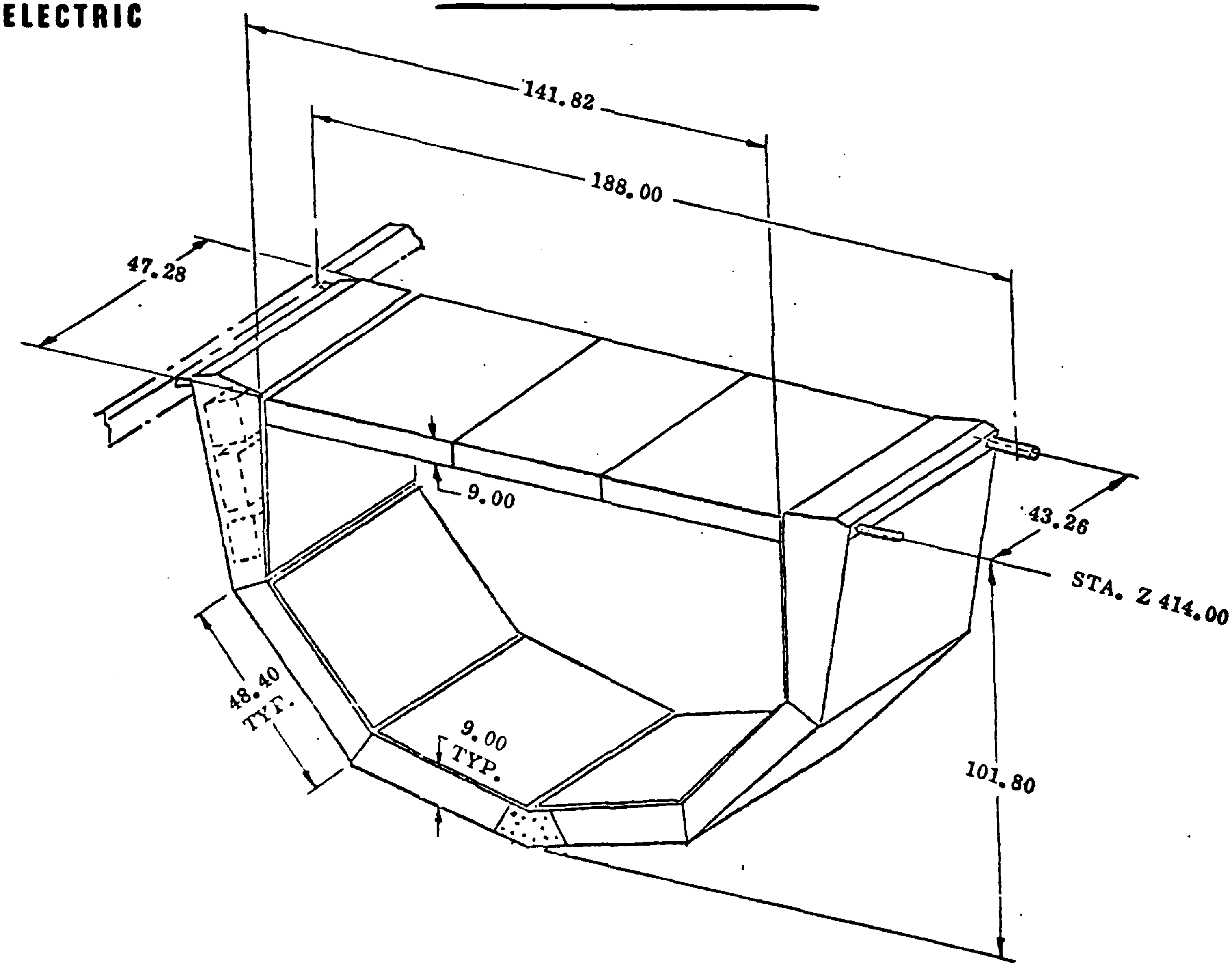

WEIGHT INCREMENTS FOR MODULAR PAYLOAD RESOURCES

This chart shows the weights associated with the various modular element options for the STR. The baseline STR weight is also shown within the tabular data. It should be pointed out that any combination of resources options, up to a maximum of 8 (with the bridge configuration), may be used on the STR. For most experiment applications 1 C&DH module and 1 attitude determination model is sufficient, if required, with the remaining 6 panels made up from the thermal and power module options, if required. For example, if all modular options are used, including 2 thermal radiators and an 8.5 KW cold plate, and assuming 5 power modules with 1 heat capacitor module, the total STR weight will equal 4077 lb. Without the movable structural bridge, only 6 modules can be accommodated with an accompanying weight reduction of 630 lbs. plus the weights associated with the loss of two module options.

GENERAL ELECTRIC

space division

WEIGHT INCREMENTS* FOR MODULAR PAYLOAD RESOURCES

• THERMAL	15 KWH / HEAT CAPACITOR	444 lb.
	0.25 KW RADIATOR (20 FT^2)	40 lb.
	8.5 KW COLD PLATE	18 lb.
• C&DH	1 Kbps COMMAND / TELEMETRY	99 lb.
	1.024 Mbps DATA HANDLING	
• POWER	38 KWH BATTERY PANEL	300 lb.
• ATTITUDE DETERMINATION	STAR TRACKERS, IRU, SUN SENSORS, COMPUTER, ETC.	106 lb.

*BASELINE STR WEIGHT

STRUCTURE (INCLUDES BRIDGE AND ALL PANELS)	1480 lb. (850 lb. w/o bridge)
POWER REGULATOR / CONTROLLER	130 lb.
THERMAL (HEAT PIPES, MLI, ETC.)	220 lb.
	1830 lb. (1200 lb. w/o bridge)

ACCOMMODATIONS

This chart provides a comparison between the STR and the Shuttle/Spacelab capabilities for experiment support accommodations. The estimated maximum accommodations required to support the LIDAR experiment are also shown. The 3 KW max. shown in the chart, for both the thermal and power support accommodations requirements, is based on an estimated peak operating power required for the LIDAR experiment. However, it is expected that both the thermal heat dissipation and battery ampere-hour requirements will be sized according to orbit average values (duty cycling of the instrument), inasmuch as continuous operation of the instrument is probably unnecessary throughout an entire orbit period.

The chart does show, however, that sufficient capability exists for either the STR or the Spacelab to support the LIDAR experiment. The primary advantage that the STR has over the Spacelab is that the required support accommodations shown do not have to be shared with other experiments, as is the case when the experiment is integrated into the Spacelab payload. The experiment data rate of 10 Kbps is based on 8 bit accuracy using 1 KM range bins over a 30 KM altitude regime and operating with a 10 PPS laser over 4 different wavelengths. The data rate will equate to 18 M bits per orbit if data is taken during a half hour period each orbit (about 1/3 duty cycle). The data rate can be further reduced by minimizing the duty cycle of the instrument if shorter periods of operation can be used without jeopardizing the scientific objectives of this experiment.

The 150 KWH is based on the total energy required over the 7 day mission and assumes about 50 hours of instrument operation during this time period. A shorter duty cycle will reduce this requirement to values appropriate with a minimum number of battery power modules (a 1/12 duty cycle, or 5 min. operation each hour, at 3 KW requires only a single power module and equates to an orbit average power of only 250 W which can easily be handled by the STR .26 KW radiator).

GENERAL ELECTRIC

space division

ACCOMMODATIONS

	REQUIREMENTS	STR	SPACELAB*
MECHANICAL (TELESCOPE)	1M CLASS	0.8M	1.2M
THERMAL	< 3 KW MAX.	15 KWH / HEAT CAPACITOR 0.26 KW RADIATOR (20 ft.^{2}) COLD PLATE →	8.5 KW AVG.
C&DH	10Kbps 18M BITS/ORBIT	1 Kbps COMMAND 1.024 Mbps DATA HANDLING (3×10^8 BITS)	2Kbps COMMAND 64 Kbps TELEMETRY DATA (WITH STS OPERATIONS DATA) UP TO 1.024 Mbps DATA HANDLING
POWER	3 KW MAX. 150 KWH	5 BATTERY PANELS @ 38 KWH / PANEL AND 600 W/PANEL	7 KW AVG. 50 KWH + 840 KWH ENERGY KIT**
POINTING ACCURACY ACCURACY		HARD MOUNT →	$0.5^0 (3\sigma)$ + CARGO BAY / STRUCTURE EFFECTS
ATTITUDE KNOWLEDGE		1 $\widehat{\text{MIN}}$	

*MUST BE SHARED WITH OTHER EXPERIMENTS

**CHARGED TO PAYLOAD (SIGNIFICANT WEIGHT AND VOLUME PENALTY - 1632 lbs/KIT)

STR/PALLET FRONTAL COMPARISONS

This chart shows frontal comparisons between the STR and a standard Shuttle Spacelab pallet. Included within the figure is an outline of the Spacelab Module tunnel around which the STR was designed to accommodate and, therefore, provided the user of the STR with the capability to be located between the Spacelab module and the front wall of the Orbiter cargo bay. This capability also provides an additional number of missions on which an experiment could potentially be accommodated for Spacelab missions. However, the tunnel prevents the use of this region for placement of an experiment on the STR, although a sufficiently large volume above the STR bridge is available for the LIDAR experiment if the receiver telescope can be limited to sizes smaller than 1 M aperture.

GENERAL ELECTRIC

STR / PALLET FRONTAL COMPARISONS

space division

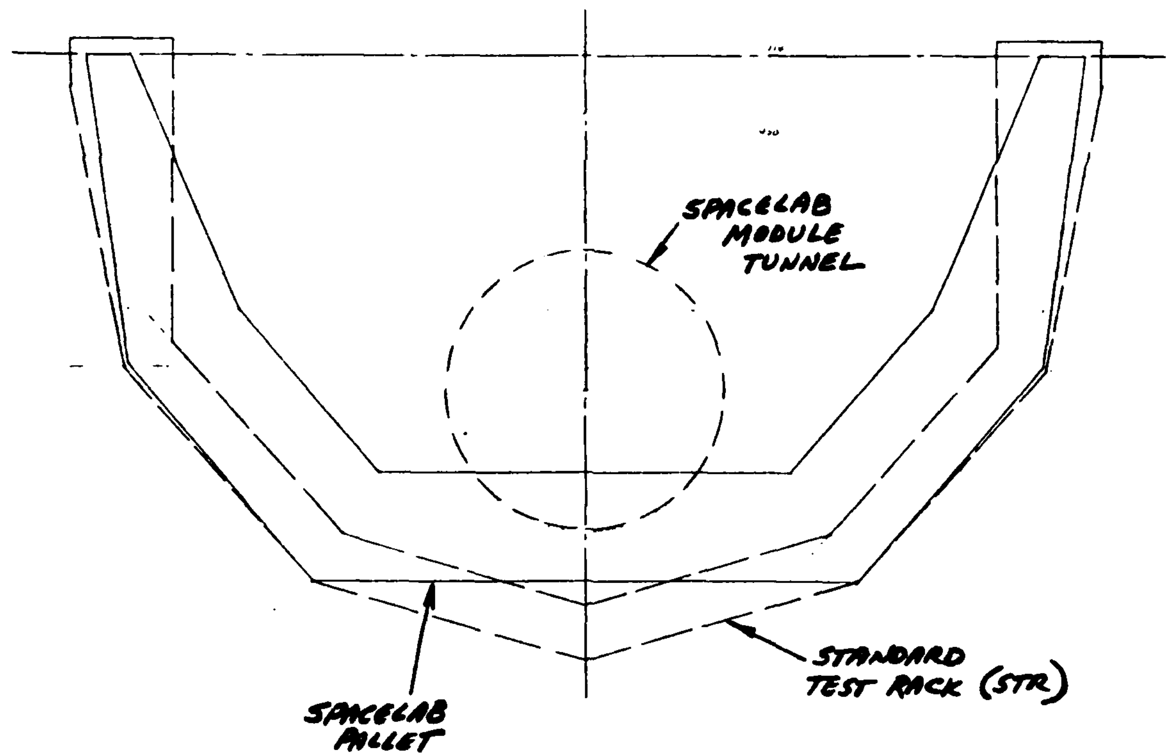

STR/LIDAR WITH BRIDGE STRUCTURE

This figure shows a possible configurational arrangement for the LIDAR experiment. The experiment is located on the STR bridge structure and provides the capability to use all 8 module options for support subsystems accommodations. The particular STR configuration shown has the bridge structure in its lowest position which would prevent placement of this concept with the Spacelab module tunnel configuration, however, use of a smaller telescope would provide complete flexibility. The natural frequency of the STR in the vertical and longitudinal directions is about 15 Hz. This frequency can be increased to higher values, if necessary, with the addition of simple truss members within the STR envelope.

GENERAL ELECTRIC

STR / LIDAR WITH BRIDGE STRUCTURE

space division

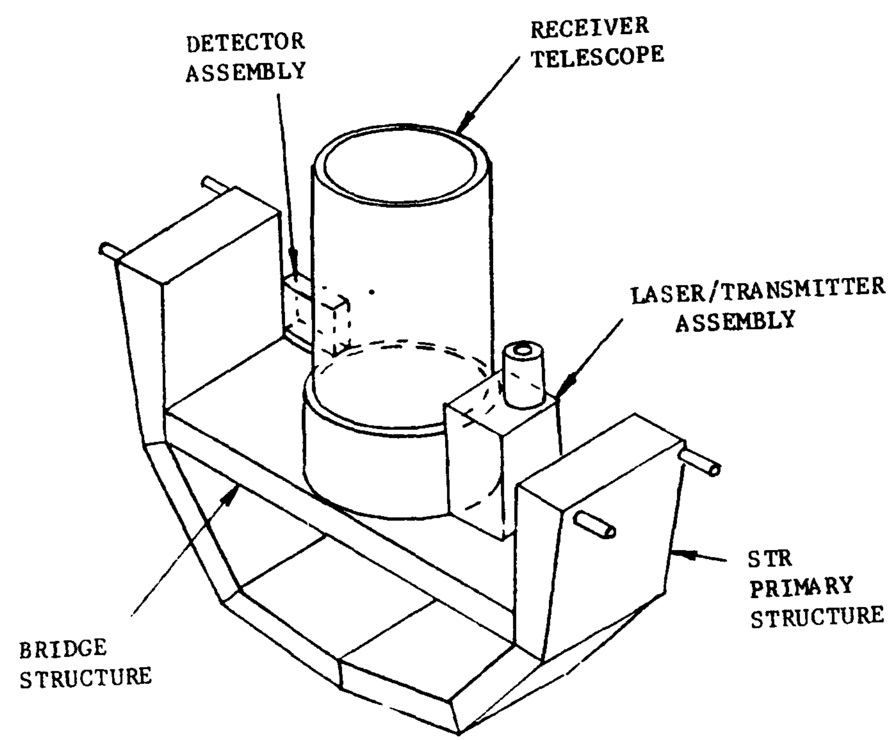

STR/LIDAR WITH STRUT STRUCTURE

This figure shows a possible STR configuration for the LIDAR experiment which uses a strut structure in place of the bridge concept shown in the preceding figure. The stiffness of this concept can also be increased with the addition of diagonally placed truss members within the STR envelope. Although not necessarily restrictive, this concept cannot be placed in the tunnel area with a Spacelab module flight. In addition, only 6 modular subsystem elements, instead of 8, can be accommodated in the STR with this LIDAR onfiguration. Current subsystem sizing estimates indicate that this configuration is a feasible concept for this LIDAR experiment.

GENERAL ELECTRIC

STR / LIDAR WITH STRUT STRUCTURE

space division

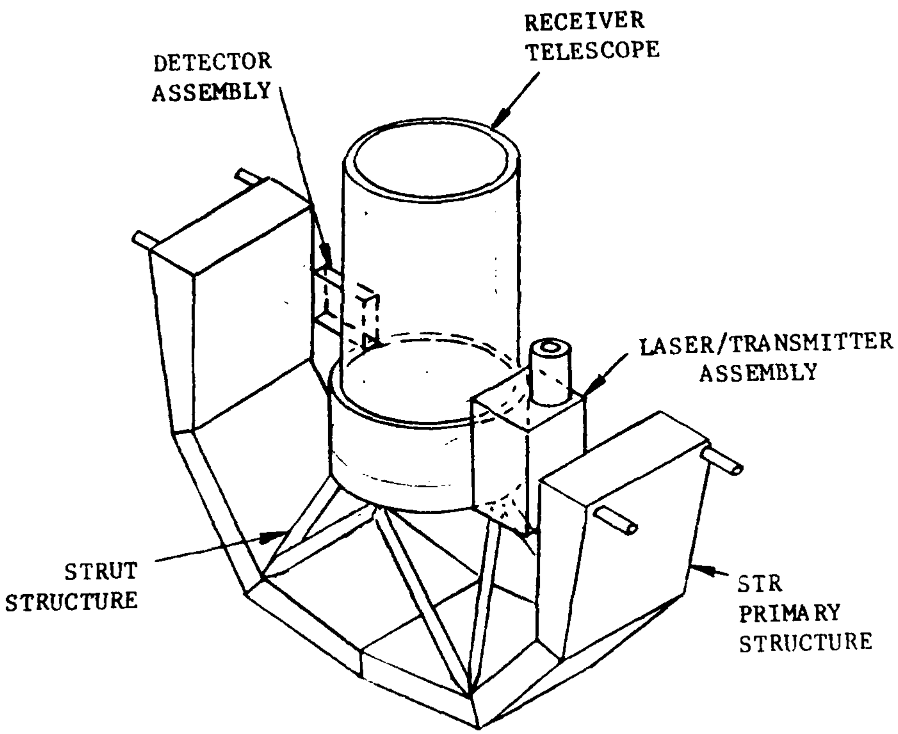

SYSTEM DESIGN CHARACTERISTICS SUMMARY

STR LIDAR EXPERIMENT

... of the estimated system design characteristics for the STR LIDAR experiment. ... aracteristics were scaled from the tabulation provided for the NASA ALMIS experi- ... data are the weights and powers associated with the STR subsystem support modules. ... for the STR are based on the strut configuration shown in the preceding figure which ... to provide the experiment with the use of 6 support modules. For example, if necessary, up ... power modules, one C&DH module, and one thermal module can be provided with this configuration.

... power modules, the STR can provide the capability for 1.8 KW of electrical power, an amount which ... considered to be more than adequate to support the requirements for this experiment, since full time (continuous) operation is not contemplated. For example, if the experiment is run on a 1/6 duty cycle, i.e., 10 seconds operation (100 shots with 10 PPS laser) out of every minute, the average power required will be 431 W (assumes only the laser and detector on 1/6 duty cycle while other components are "on" continuously). The 431W requirement can *easily be handled with* a single 600 W power module, however, three modules are still necessary if the 1/6 duty cycle is maintained over a 7 day mission, since the total energy requirement of 72.4 KWH would exceed the 38 KWH capability of a single power module (.431 KW x 168 Hours = 72.4 KWH).

It should be pointed out that this experiment, due to severe background noise for daylight measurements, is limited to only *night operation*, which, on an average basis, constitutes *only 1/3 of an orbit period* and results in an effective instrument orbit period duty cycle of 1/18; therefore, orbit average power is reduced to 216 W, and over a 7 day mission can be handled with a single power module since the total energy requirement is only 36.3 KWH (.216 KW x 168 Hours = 36.3 KWH).

A *single thermal module was* included in the STR to dissipate peak heat loads during laser operation, although an indepth thermal analysis may show that this module is unnecessary since the heat load may be handled by a single .26 KW STR radiator and heat pipe system.

Single STR C&DH and Attitude Reference modules are also included in the accompanying tabulation and provide complete autonomy for this experiment. It is conceivable that the Attitude Reference module may not be required since Shuttle pointing accuracy may be sufficient, however, the computer within this module, or a compatible dedicated experiment computer, should be included with the experiment components.

GENERAL ELECTRIC

space division

SYSTEM DESIGN CHARACTERISTICS SUMMARY

STR LIDAR EXPERIMENT

SUBSYSTEM	ITEMS	EACH	TOTAL WEIGHT (LB.)	DC POWER (WATTS)	TOTAL VOLUME (FT^3)
LASER TRANSMITTER	Nd:YAG x 3 DYE x 3 x 2 POWER SUPPLY	1	374	1870	12.7
RECEIVER	0.8 M TELESCOPE	1	284	N/A	39.2
DETECTOR	SINGLE PMT	2	9	35	0.1
	DUAL PMT	1	18	70	0.2
C&DH	C&DH MODULE (STR)	1	99	46	N/A
POWER	POWER MODULES (STR)	1	300	10	N/A
STRUCTURE	OPTICAL SUPPORT	1	63	N/A	18.1
	COLD PLATES (STR)	1	13	N/A	1.0
	COVER	1	28	N/A	N/A
	BASELINE STR (W/O BRIDGE)	1	1200	N/A	N/A
THERMAL CONTROL	THERMAL MODULES (STR)	1	444	N/A	N/A
	RADIATORS/PUMPS/VALVES	1	50	10	4.5
	COLD PLATE (STR)	1	20	N/A	N/A
ATTITUDE REFERENCE	ATTITUDE REFERENCE MODULE (STR)	1	106	42	N/A
TOTAL			3008	2048	75.8

WINDSAT LIDAR EXPERIMENT

ADJUNCT

PRECEDING PAGE BLANK-NOT FILMED

WINDSAT LIDAR EXPERIMENT

The accompanying chart shows several possible instrument configurations for the WINDSAT experiment. Since this *experiment concept* is still under study by NOAA, the configurations shown should be viewed as representative concepts only. One of the configurations shown is an F/2.4 m prime focus telescope instrument system which is mounted on the Standard Test Rack (STR) and requires elevation for FOV/ integration purposes. This configuration could also be mounted to a Spacelab pallet, if necessary. Another Shuttle configuration is a significantly more compact Cassegrain telescope with a F/1.5 m parabolic primary mounted to a rotating two axis gimbal. A single configuration is shown for the dedicated spacecraft platform, the F/2.4 m prime focus telescope mounted via a kinematic structure to the spacecraft.

The primary object of the WINDSAT experiment is to measure wind profiles, i.e., the horizontal velocity field as a function of height in the atmosphere, around the globe from operational meteorological satellites. It is expected that other information such as boundary-layer depth, aerosol concentration, sea current drift, atmospheric turbulence levels, and pollutant levels may also be obtainable with this instrument concept.

It should be pointed out that this concept, as currently envisioned, has a very wide scan line-of-sight (LOS) from NADIR (about 63^{o}) and, in addition, the LOS rotates about NADIR during a rather short period of revolution (as short as 10 sec); as a consequence, the measurements can be expected to encounter a wide range of atmospheric conditions over the extremely long ground path ($\sim$7000 km), as compared to pure NADIR viewing where the 7 km/sec satellite velocity and a 10 sec period equate to only a 70 km ground path. Therefore, unless single shot measurements can give the desired measurement accuracy, it is doubtful that this experiment will be able to provide a workable solution unless, of course, a dedicated density measurement experiment package were included along with the WINDSAT experiment as part of the satellite payload.

WINDSAT LIDAR EXPERIMENT

GENERAL ELECTRIC

space division

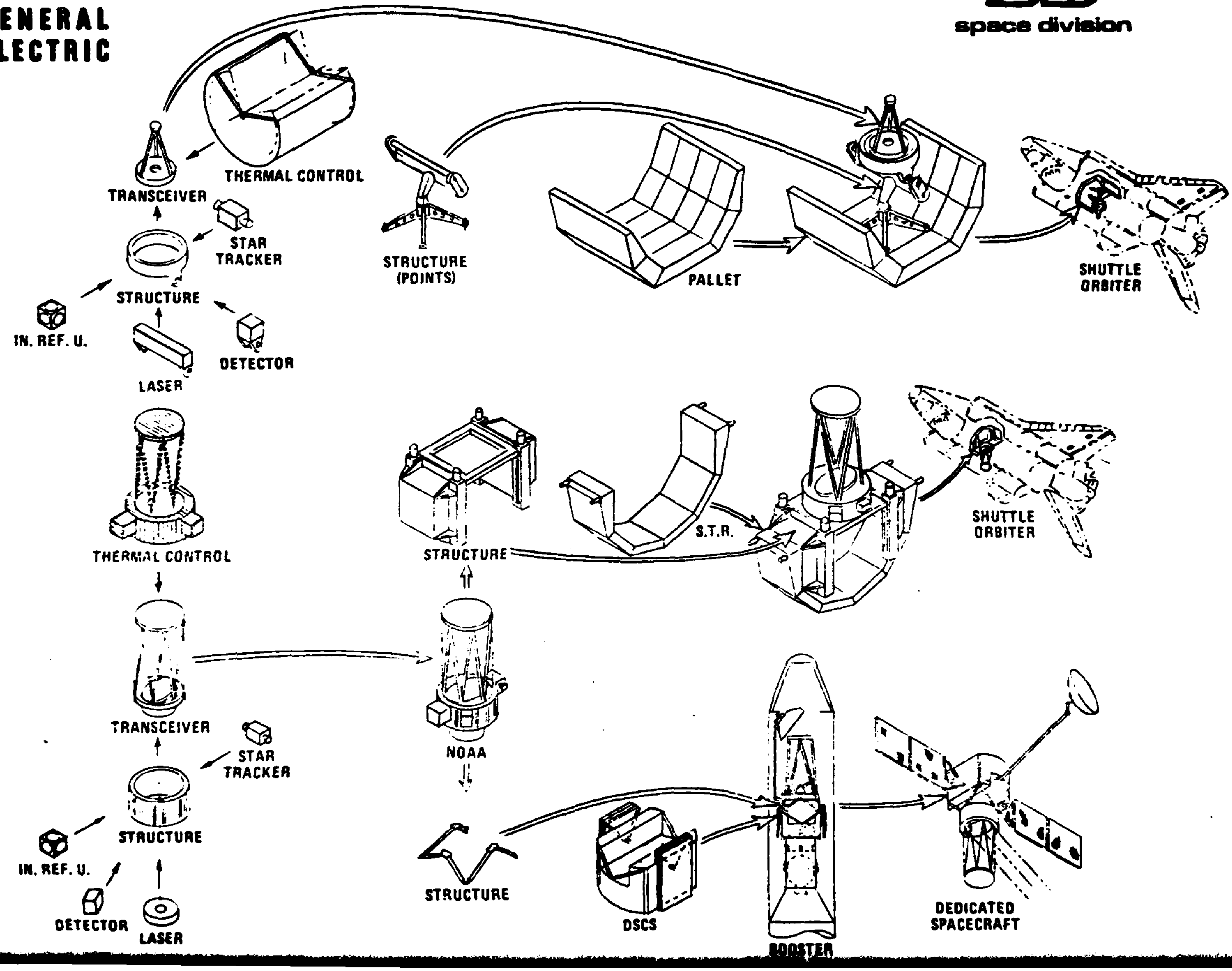

ESTIMATED POWER AND WEIGHT OF BASIC ELECTRONIC COMPONENTS FOR BASELINE WINDSAT CONFIGURATIONS

This chart provides estimated power and weight values of the basic electronic components for the three WINDSAT experiment configurations shown on the preceding page. Since this instrument is intended to be operated continuously in order to obtain full global coverage, the power values shown cannot be reduced via a duty cycling approach as applied to the two previously described experiments. On the other hand, if the components/subsystems above the horizontal separation line in the table can be duty cycled over only a 1/3 orbit period, the resulting orbit average power values would be 737 W, 720 W, and 692 W for the STR, pallet, and dedicated spacecraft configurations, respectively.

It should be pointed out that the power values shown for the laser transmitter are based on the use of E-beam technology rather than over-volted technology in the design of the CO_2 TEA laser. An additional 1100 W should be added to the power values if the over-volted technology is used (based on 15% efficiency for E-beam versus 5% for over-volted designs) and, correspondingly, the weight increased by 100 lbs. As a result, for a 1/3 orbit duty cycle, the orbit average power values using over-volted technology, would be 1104 W, 1087 W, and 959 W for the STR, pallet, and dedicated spacecraft configurations, respectively.

GENERAL ELECTRIC

space division

ESTIMATED POWER AND WEIGHT OF BASIC ELECTRONIC COMPONENTS FOR BASELINE WINDSAT CONFIGURATIONS

Electronic Component / Subsystems	Shuttle Baseline Configurations				Dedicated Spacecraft Baseline Configuration	
	STR		Pallet			
	Power (W)	Weight (lb)	Power (W)	Weight (lb)	Power (W)	Weight (lb)
Laser Transmitter	550	150	550	150	550	150
Telescope/Scanner Subsystem	50	500	150	800	50	500
Detector/Cooler	50	5	50	5	5	53
Microwave Signal Processor	250	28	250	28	250	28
Microprocessor	30	20	30	20	30*	20*
Thermal	150	30	100	20	150	30
Attitude Reference	57	77	57	77	57*	77*
Miscellaneous and Contingency	200	140	200	140	200	140
Totals	1337	950	1387	1230	1292	998

*These Components can be provided within spacecraft subsystems.

BALLOON BASED LIDAR EXPERIMENT

BALLOON LIDAR EXPERIMENT

This figure shows an artists rendering of the balloon LIDAR experiment. The size of the experiment package is estimated to occupy approximately a 3 ft. x 3 ft. x 3 ft. envelope. A standard range provided electronics package is shown attached to the upper portion of the LIDAR gondola structure. This electronics package furnishes command control, altitude, telemetry and temperature capabilities for all balloon flights.

The LIDAR experiment components are shown primarily mounted to an optical bench structure which has been configured with a rotatable mechanism to provide a downward, upward and horizontal FOV for the laser transmitter and telescope receiver. Not shown is the enclosure surrounding the experiment package which would provide environmental protection and thermal control to sensitive optical components.

GENERAL ELECTRIC

space division

BALLOON LIDAR EXPERIMENT

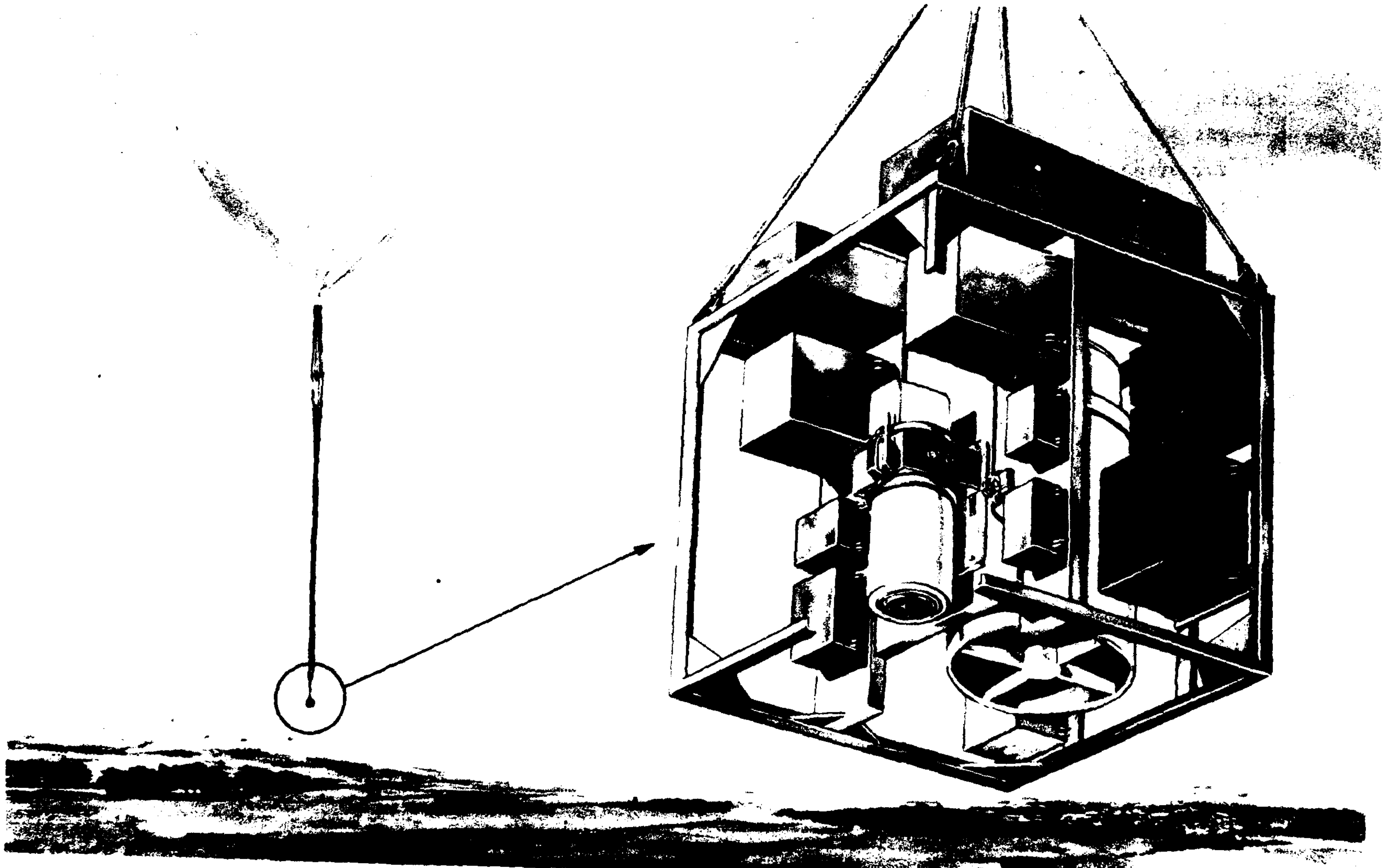

SYSTEM DESIGN CHARACTERISTICS SUMMARY

BALLOON LIDAR EXPERIMENT

System design characteristics are summarized in this chart for the balloon LIDAR experiment, and should be interpreted as representative values for an experiment of this type. The laser transmitter values are typical of currently ruggedized off-the-shelf components manufactured by ILS, i.e., their 100 mJ and 500 mJ lasers. Examination of the performance analyses data documented in Section 6 indicates that for night operation with multiple pulse measurements (100 shots) the 100 mJ laser is essentially equal in performance to that of the 500 mJ laser; however, day operation requires a much greater number of shots for the 100 mJ laser (about 1000 shots vs. 100 shots) if equal measurement accuracy is to be achieved.

Values shown for the other components have been either obtained or scaled from similar components shown previously in this section for the ALMIS experiment package. Included also are typical operating temperature limits for these components; however, variation in temperature between these limits during operation of sensitive optical components will probably be constrained to $\pm 5^{\circ}C$, in order to maintain reasonable alignment stability between the transmitter and receiver line-of-sight (LOS).

A single pair of 12 volt batteries are indicated in the table, since it is felt that duty cycling of this experiment would provide an adequate amount of data, e.g., 10 seconds of operation per minute provides the accuracy associated with 100 shots (10 PPS laser) and equates to a 1/6 duty cycle for the instrument. This 1/6 duty cycle will, for a single battery pair, ensure at least 10 hours and 6 hours of experiment operation for the 100 mJ and 500 mJ lasers, respectively. An additional battery pair, if desired, would double the operating times or be capable of providing a 1/3 duty cycle (10 seconds operation every 30 seconds) without having any significant weight impact on balloon operating altitude, i.e., the peak operating altitude would be lowered by about 0.3 km with an additonal 100 lb. battery pair and associated support structure weight.

GENERAL ELECTRIC

space division

SYSTEM DESIGN CHARACTERISTICS SUMMARY

BALLOON LIDAR EXPERIMENT

SUBSYSTEM	ITEMS	EACH	TOTAL WEIGHT (LB)	DC POWER (WATTS)	TOTAL VOLUME (FT^3)	OPER. TEMP. LIMITS (°C)
LASER TRANSMITTER	Nd:YAG X 3 POWER SUPPLY	1	82/53*	960/384*	2.0	50/0***
RECEIVER	0.5M TELESCOPE	1	150	N/A	5.5	AR
DETECTOR	SINGLE PMT	2	9	35	0.1	-20/-70
C&DH	C&DH UNIT	1	8	50	8.6	50/0
POWER	BATTERY PAIR	1	100	N/A	2.0	50/0
STRUCTURE	OPTICAL SUPPORT	1	28	N/A	1.5	AR
THERMAL CONTROL	RADIATOR/PUMP/ VALVE	1	25	10	1.0	50/0
CORRELATIVE SENSORS	TEMPERATURE PRESSURE	1	8	5	0.1	AR
TOTAL			410/381*	1060/484**	20.8	

* 500 mJ/100 mJ LASER
** 260 w/164 W AVERAGE POWER FOR 500 mJ/100 mJ LASER, RESPECTIVELY (OPERATED ON 1/6 DUTY CYCLE)
*** MAX/MIN

APPENDIX A

ATMOSPHERIC DENSITIES FROM SHUTTLE-BASED

RAMAN LIDAR MEASUREMENTS

ATMOSPHERIC DENSITIES FROM SHUTTLE-BASED RAMAN LIDAR * MEASUREMENTS

SUMMARY:

Of the various potential methods for measuring atmospheric density from space Shuttle-based lidar systems, this analysis considers only the use of both vibrational and rotational Raman-scattered return signals.

Briefly, neither vibrational nor rotational Raman lidar return signals from a reasonable lidar system appear to be capable of good enough single shot S/N to provide the desired 10% accuracy at any altitude. However, if data integration could be satisfactory for 70 shots, then the calculated best night-time rotational Raman system (with height resolution of 1 km) yields S/N $\gtrsim$ 20 for altitude (Z) $\leq$ 5km, decreasing to S/N = 15 at Z = 10km, S/N = 7.6 at Z = 20 km, and S/N = 3.6 at Z = 30km. Equivalent optimum vibrational Raman S/N values are 2 to 3 times smaller. An accuracy of 10% would require S/N $\geq$ 10.

Daytime measurements are not practical due to high background levels yielding very low S/N values ($<$ 1). Eye safety considerations have not been incorporated into these calculated results.

* General Electric PIR U-1255-IR5-260, Bethke, G.W., 10 November 1978

AD-A082 332 GENERAL ELECTRIC CO PHILADELPHIA PA SPACE DIV F/G 4/1
DESIGN STUDY OF A LASER RADAR SYSTEM FOR SPACELIGHT APPLICATION--ETC(U)
DEC 79 W F BREHM, J L BUCKLEY F19628-78-C-0204
UNCLASSIFIED AFGL-TR-79-0264 NL

3 of 3
AD
A082332

END
DATE
FILMED
4 80
DTIC

EQUATIONS

Lidar Equations

The expression which relates the lidar receiver output to the lidar system parameters and atmospheric conditions is called the range equation. When expressed as number of backscattered photons detected/sec(N_s), the range equation is

$$N_s = [\pi/(8h)] \cdot k(180) \cdot \lambda_s E_L (d/r)^2 ET_i T_s \quad (1)$$

where

$$E = E_o \cdot E_{pm} \quad (2)$$

$$r = ct/2. \quad (3)$$

For same-wavelength (Mie plus Rayleigh) scattering ($\lambda_s = \lambda_i$)

$$k(180) = k_r (180) + k_m (180) = N \cdot Q_r(180) + M \cdot Q_m(180) \quad (4)$$

$$T_s = T_i = \exp [-\int_0^r (k_{ei} + k_{ai}) dr] \quad (5)$$

$$k_{ei} = k_{ri} + k_{mi} = NQ_{ri} + MQ_{mi} \quad (6)$$

Here, h is the Planck constant, k(180) is the atmospheric backscatter coefficient, λ_s is the wavelength of scattered light, E_L is laser transmitter output energy, d is the receiver objective diameter, r is the range from receiver objective to the propagating laser output energy, E is the lidar receiver efficiency, T is the one-way atmospheric transmittance, E_o is the lidar receiver optical efficiency, E_{pm} is the detector quantum efficiency, c is the velocity of light, t is the time since lidar time zero, N is the atmospheric number density of all gas molecules, $Q_r(180)$ is the Rayleigh backscatter cross section for air, M is the mass concentration of aerosols, $Q_m(180)$ is the mass-normalized (Mie) backscatter cross section for aerosols, k_e, k_r, and k_m are extinction coefficients, Q_r is the Rayleigh total scatter cross section for aerosols, k_a is the atmospheric absorption coefficient, sub-r and sub-m refer to Rayleigh and Mie scattering, respectively, and sub-i and sub-s refer to incident (laser) and scattered (detected) wavelengths, respectively.

For wavelength-shifted (Raman) scattering ($\lambda_s \neq \lambda_i$),

$$k(180) = k_g(180) = \dot{N}_g \cdot Q_g(180) \tag{7}$$

$$T_i = \text{same as above (eq. 5)} \tag{8}$$

$$T_s = \exp\left[-\int_0^r (k_{es} + k_{as})\, dr\right] \tag{9}$$

$$k_{ei} = \text{same as above (eq. 6)} \tag{10}$$

$$k_{es} = k_{rs} + k_{ms} = NQ_{rs} + MQ_{ms} \tag{11}$$

Here, $k_g(180)$ is the Raman power backscatter coefficient for gas component g, N_g is the number density of atmospheric gas component g, and $Q_g(180)$ is the Raman power backscatter cross section for gas g.

Daytime Background Signal

Depending on the lidar pointing direction, the cw background signal will normally be due to diffuse reflection of light by the earth local background. The number of background photons detected per second (N_b) are

$$N_b(\text{target}) = [10^7\, \pi/(16\, hc)] \cdot F_s R_s T_s \lambda_s\, B\, d^2\, \alpha^2\, E \tag{12}$$

for diffuse reflection of light incident on the earth background. Here F_s is the light flux (W $cm^{-2}A^{-1}$) incident on the background at λs, B is the receiver spectral bandpass (FWHH), α is the full angle field of view of the lidar receiver, and R_s is the background total reflectivity or local albedo at λs. In the infrared at 3 microns wavelength, another significant source of cw background radiation which must be considered is thermal emission from the earth's surface, air and clouds. If F_s is the solar flux (actually irradiance) outside the earth's atmosphere and R_s is the earth albedo from space, then $T_s = 1$.

Signal :o Noise (S/N) Ratio

Lidar systems operating in the visble and ultraviolet spectral regions usually use photomultiplier tube detectors due to their relatively high quantum efficiencies and relatively noise-free high gain. As a result, high sensitivity photomultiplier tubes can detect individual photons when illuminated by low light levels. In this case, the primary noise is due to the statistical flunctuations in arrival of the individual photons(yielding shot noise). Thus assuming Poisson statistics, the standard deviation variation or noise count, N_n, in a specific time (lidar range) interval is

$$N_n = \sqrt{N\ (avg)} \tag{13}$$

If the signal (S) contains no background photons and the detector dark current is negligible or discriminated against, then

$$S/N = N_s / \sqrt{N_s} = \sqrt{N_s} \tag{14}$$

If the background count level is not negligible, then

$$S/N = N_s / \sqrt{N_s + N_b} \ . \tag{15}$$

CALCULATIONS

Using the above equations plus the additional relations and assumptions discussed below and summarized in Tables I, II, and III, Raman lidar signals (N_s) and signal to noise ratios (S/N) have been calculated for a variety of potentially useful laser wavelengths. Tables II and III present optimum ground level (Z=0) signal returns from both vibrational Raman and rotational Raman shuttle - mounted lidar systems, respectively. In both cases, the single shot N_s is tabulated in units of photons detected/micro-second and in photons detected (counts)/km of range resolution (6.67 micro-seconds). A night-time S/N is also tabulated for each case.

Table IV lists the assumptions and calculated results for the best-wavelength vibrational and rotational Raman lidar systems (based on Table II and III results) as a function of scatterer altitude Z. Thus the vibrational Raman lidar calculation is for a near UV system (about 3500A laser) while the rotational Raman lidar calculation is for a mid-visible system (5300A laser). Here, the results are tabulated as single shot N_s/km of range resolution, plus night (and day) S/N for both single shot use and also for 70 shots integrated.

Raman Scattering Cross Sections

Although Raman cross sections of gases have been measured at only a very few wavelengths, the values can be converted to other wavelengths as follows:

The $Q_g(180, \lambda_i)$ value for desire incident wavelength λ_i can be calculated from a measured value at wavelength λ_i' from the relation

$$Q_g(180, \lambda_i) = Qg(180, \lambda_i') \cdot (\nu_s/\nu_s')^4$$

$$= Q_g(180, \lambda_i') \cdot \left[\frac{(1/\lambda_i) - \Delta\nu_s}{(1/\lambda_i') - \Delta\nu_s}\right]^4 \qquad (16)$$

where $\Delta\nu_s$ $(= \nu_i - \nu_s)$ is Raman-scattered frequency shift in cm^{-1}, and λ_i and λ_i' values are in cm.

In this way, both the vibrational [1] and the rotational [2] Raman literature values for $Q_g(180)$ of nitrogen and oxygen have been converted from measurements at about 5000A (see Table I) to the wavelengths of interest for these calculations (see Tables II and III). Table I also lists other important information about the nitrogen and oxygen Raman bands. Finally, since the rotational Raman spectra of atmospheric nitrogen and oxygen (as well as most other gases) occupy the same wavelength interval, the total rotational $Q_g(180)$ for air is calculated as indicated below Table I.

Assumptions

Tables II, III, and IV are calculated from equations 1-16 and the information in Table I plus the following assumptions and literature values: The shuttle altitude is 300 km, the laser transmitter output E_L is 1 joule/pulse, and the lidar receiver is a compound telescope (2 reflections plus 1 collimating lens) of 1 meter^2 area (d = 1.128 m. diam.) with an optical efficiency of 0.7. This value of 0.7 does not include filter efficiency E_f and any Raman band selection efficiency. For all three tables, the filtering is assumed to consist of two narrow band pass filters in series (each 2 or 3 cavity type) so as to reject the relatively much stronger Rayleigh/Mie signal. Thus

$$E_f = E_{f\,1} \cdot E_{f\,2}$$

The detectors are all assumed to be photomultiplier tubes with quantum efficiency E_{pm} and negligible dark current (<<.1 count/microsecond). Finally, the laser wavelengths for λ_i were chosen on the basis of existing or anticipated availability of reliable short-pulsed high output laser systems.

Tables II and III were calculated for only ground level (Z=0) scattering and at night, so as to allow selection of the best wavelengths for further consideration. The one-way $Z=0 \rightarrow \infty$ atmospheric transmittance values T_i and T_s are all based on the very clear atmospheric conditions of Allen(3).

Since nitrogen is the major (and a well mixed) atmospheric constituent, the vibrational Raman lidar calculations of Table II are based on the nitrogen Raman band which has $\Delta\nu = 2331\ cm^{-1}$. Implicit in selecting realistic E_f values, is the assumption that the spectral filter bandwidth B (FWHM) is wide enough to include the entire nitrogen vibrational band. Thus

$$B \approx 300\ cm^{-1} \approx (\lambda_s - \lambda_i)/7$$

The rotational Raman lidar calculations of Table III are based on the assumption that the spectral filtering passes only the longest wavelength half of the Stokes

branch, with that branch having 60% of the total rotational $Q_g(180$. Thus $E_o = 0.7E_f' = 0.21E_f$, where $E_f' = 0.6 \times 0.5\ E_f$. Implicit in selecting E_f values is the assumption that (FWHM)

$$B \approx 2\ (\lambda_s(\text{Stokes max}) - \lambda_i)$$

As indicated earlier, since the rotational Raman spectra of all major atmospheric gases fall in the same wavelength interval, the rotational Raman calculations are based on the total atmospheric density for N_g, and the effective average rotational $Q_g(180)$ (see beneath Table I).

The "best case" Raman lidar calculations of Table IV have the same vibrational Raman assumptions as Table II and the same rotational Raman assumptions as Table III, except that the atmospheric density (N(air)) values are here from the U.S. Standard Atmosphere(1962). Also for Table IV, the range equation factor r is a function of scatterer altitude Z.

$$r = Z(\text{shuttle}) - Z \qquad (17)$$

Since the scattering is now calculated for various altitudes, T_i and T_s are functions of Z which approach $T_i = T_s = 1$ at Z = infinity. We assume that

$$k = (k_e + k_a) = C \cdot N \qquad (18)$$

where here, $N \equiv N(\text{air})$.

Thus $$T(Z - \infty) = \exp\left(- \int_Z^\infty k\, dZ\right) = \exp\left(- C \int_Z^\infty N\, dZ\right) \qquad (19)$$

where $$C = -\ln T\ (0-\infty)/\left(\int_0^\infty N\, dZ\right). \qquad (20)$$

Combining (18) and (19) for both $T_i\ (Z - \infty)$ and $T_s\ (Z - \infty)$, we have

$$T_i \cdot T_s = \exp\left\{\left[\int_Z^\infty N\, dZ/\left(\int_0^\infty N\, dZ\right)\right] \cdot \left[\ln T_i\ (0-\infty) + \ln T_s(0-\infty)\right]\right\} \qquad (21)$$

For Table IV, the $T_i \cdot T_s$ values of equation (1) are calculated as a function of Z via equation (21).

The daytime background N_b and S/N numbers of Table IV are based on a receiver field of view (α) of .001 radian full angle. Since the target irradiance F_s' value used[4] is the solar irradiance outside the earth's atmosphere, and the target reflectivity R_s

value used [5] is the earth albedo, we set $T_s = 1$ for the calculation of N_b via equation (12).

CONCLUSIONS

A comparison of the results from Tables II and III leads us to conclude that rotational Raman lidar has the potential for significantly better performance than vibrational Raman lidar. Also, rotational Raman lidar appears to perform best for laser wavelengths (λ_ℓ) in the green and probably blue regions of the visible spectrum. The best rotational Raman lidar performance would be found for the near UV (as with vibrational Raman systems), except that use of the rotational Raman signal requires relatively narrow very sharp cut-off filters (or other spectral isolation) especially in the UV, while band pass filter technology is less advanced in the UV as compared with the visible.

Table IV shows us that for the size lidar system and laser energy (1 joule/pulse) assumed, the "best case" green laser rotational Raman lidar can yield the necessary accuracy of 10% (and thus $S/N > 10$) during night time only if the 1 km range-resolved night time signals are integrated over at least 16 shots, and preferably more (50-100-shots). During the day time, the earth background signal and noise dominate, making the Raman method not useable during daytime.

It should be noted that while the vibrational Raman spectral requirements are relatively easy to meet and thus the assumptions are reliable, the rotational Raman spectral requirements are more difficult to meet resulting in lower reliability for the assumed spectral purity and receiver efficiency (E_o). Thus depending on the exact technique used for rotational Raman spectral isolation and the "state of the art" at the time of system design, a rotational Raman system could perform significantly better (it has good potential in the near UV) or worse than calculated. Finally, eye safety considerations have not been incorporated into these results, and may limit laser output to less than 1 joule/shot and/or require larger fields of

view which result in poorer filter performance. Also, note that the results were based on the atmospheric transmittance for extremely clear air. With less than very clearest weather, the results for $Z < 5$ km will be degraded, especially at short wavelengths.

REFERENCES

1. C. Penney, L. Goldman, & M. Lapp, Nature 235, 110 (1972).
2. C. Penny, R. St. Peters, & M. Lapp, JOSA 64, 712 (1974).
3. C.W. Allen, "Astrophysical Quantities" Second Edition, The Athlone Press, London, 1963, page 122.
4. "Solar Electromagnetic Radiation", National Aeronautics and Space Administration document number NASA SP-8005, May 1971.
5. Monte Ross, "Laser Receivers", John Wiley and Sons, Inc., New York, 1966, page 270.

TABLE I

RAMAN BACKSCATTER CROSS SECTIONS
and related information

GAS	NITROGEN	OXYGEN
Vol. % in air	78.03%	20.99%
Stokes Vibrational Band:		
$Q_g(180, \lambda_i)$ $(cm^{-2} sr^{-1})$	4.40×10^{-31}	5.40×10^{-31}
at λ_i (A)	5145	5145
Band $\Delta\nu = \nu_i - \nu_s$ (cm^{-1})	2331	1557
Rotational Bands:		
Stokes + Anti Stokes total		
$Q_g(180, \lambda_i)$ $(cm^{2}\ sr^{-1})$	1.64×10^{-29}	4.28×10^{-29}
at λ_i (A)	4880	4880
Rot Band Widths* (FWHM) (cm^{-1})		
Stokes Band	~95	~82
Anti Stokes Band	~91	~82
Band Max $\Delta\nu$* (cm^{-1})		
Stokes Band	+58	+52
Anti Stokes Band	-56	-45

NOTES:

* Gas at 23°C.

For Air $Q_g(180) = (0.78 \times 1.64 + 0.21 \times 4.28) \times 10^{-29}$

$= 2.18 \times 10^{-29}\ cm^{2}\ sr^{-1}$ at 4880A

TABLE II. Vibrational Raman Single Shot Lidar Returns from ground level (Z = 0) at night.

LASER SOURCE	Nd	Ruby	Nd/2	Nd/3	Ruby/2
λ_i (A)	10600	6943	5300	3533	3472
λ_s (A)	14079	8284	6047	3850	3778
$Q_g(180, N_2)$ ($cm^2\ sr^{-1}$)	1.31(-32)	1.09(-31)	3.84(-31)	2.34(-30)	2.52(-30)
T_i	0.96	0.91	0.81	0.47	0.47
T_s	0.98	0.94	0.85	0.58	0.58
E_f	0.15	0.25	0.25	0.1	0.1
E_{pm}	___*	0.10	0.15	0.3	0.3
N_s (counts/μ sec)	___	0.0221	0.0686	0.0843	0.0891
N_s (cts/1 km Δr)	___	0.148	0.458	0.562	0.594
S/N (Δr = 1 km)	___	0.38	0.68	0.75	0.77

* No photomultiplier tube or Si photodiode available for this λ_s.

Assumed:

Night-time (no background)

E_L = 1 joule/pulse $E_o = 0.7\ E_f$

d = 1.128 m. diam E_f is for two filters in series.

r = 300 km

The vibrational Raman signal used, is that from atmospheric nitrogen, where:

$\Delta\nu = \nu_i - \nu_s = 2331\ cm^{-1}$

$N_g = 1.951 \times 10^{19}\ cm^{-3}$ at 20°C. and 1 atm (Z=0).

TABLE III. Rotational Raman Single Shot Lidar Returns from ground level (Z = 0) at night

LASER SOURCE	Nd	Ruby	Nd/2	Nd/3	Ruby/2
λ_i (A)	10600	6943	5300	3533	3472
$Q_g(180, \text{air})$ ($cm^2\ sr^{-1}$)	5.79(-31)	5.32(-30)	1.57(-29)	7.94(-29)	8.51(-29)
$T_i = T_s$	0.96	0.91	0.81	0.47	0.47
λ_s(Stokes max)$-\lambda_i$ (A)	63.	27.	15.8	7.0	6.8
E'_f	.075	.075	.06	.007	.007
E_{pm}	.02	.12	.20	.30	.30
N_s(counts/μ sec)	.0124	.407	.961	.191	.201
N_s(cts/1 km Δr)	.083	2.71	6.41	1.27	1.34
S/N (Δr=1 km)	.28	1.65	2.53	1.13	1.16

Assumed:

Night time (no background)

E_L = 1 joule/pulse

$E'_f = 0.3\ E_f$

d = 1.128 m. diam.

E_f is for two filters in series

r = 300 km

$E_o = 0.7E'_f = 0.21E_f$

$\lambda_s \approx \lambda_i$

The rotational Raman signal is from both atmospheric nitrogen and oxygen, where for Stokes plus anti Stokes values,

$Q_g(\text{air}) = 0.78 \cdot Q_g(N_2) + 0.21 \cdot Q_g(O_2)$

$N_g = 2.50 \times 10^{19}\ cm^{-3}$ at $20^{\circ}C$ and 1 atm (Z=0)

TABLE IV. **Best Case Raman Lidar Returns and S/N**

Z (km)	N(air) (cm^{-3})	$\int_z^\infty NdZ \,/\, \int_0^\infty NdZ$	VIBRATIONAL RAMAN N_s (cts/km) 1 shot	VIBRATIONAL RAMAN S/N (night) 1 shot	VIBRATIONAL RAMAN S/N (night) 70 shots	ROTATIONAL RAMAN N_s (cts/km) 1 shot	ROTATIONAL RAMAN S/N (night) 1 shot	ROTATIONAL RAMAN S/N (night) 70 shots
0	2.55 (19)	1.	.590	.768	6.4	6.56	2.56	21.4
5	1.53 (19)	.534	.671	.819	6.8	4.95	2.23	18.6
10	8.60 (18)	.263	.555	.745	6.2	3.23	1.80	15.0
15	4.05 (18)	.121	.325	.570	4.8	1.67	1.29	10.8
20	1.85 (18)	.0558	.168	.409	3.4	.813	.902	7.6
25	8.33 (17)	.0251	.081	.285	2.4	.385	.620	5.2
30	3.83 (17)	.0117	.040	.199	1.7	.184	.430	3.6
40	8.31 (16)	.0032	.009	.097	0.8	.043	.208	1.7
Day earth N_b (cts/6.7 μs)			1.88 (5)	—	—	4.42 (4)	—	—
Day S/N (best Z)			—	.0016	.013	—	.0312	.26

ASSUMPTIONS:

	Vibrational Raman	Rotational Raman
λ_i (A)	3472 to 3533 (avg. used)	5300
λ_s (A)	3778 to 3850 (avg. used)	~5320
$Q_g(180)$ ($cm^2 sr^{-1}$)	2.43 (-30)	1.57 (-29)
N_g	0.78 · N(air)	N(air)
B (A)	50	16
E_f (2 filters in series)	0.1	0.2
E_o	0.7 E_f	0.21 E_f
E_{pm}	0.[illegible]	0.2
T_i ($Z = 0 \to \infty$)	0.47	0.81
T_s ($Z = 0 \to \infty$)	0.58	0.81
R_s	0.5	0.4
F_s ($W\ cm^{-2} A^{-1}$)	1.1[illegible] (-5)	1.84 (-5)

More Assumptions:

Z (shuttle) = 300 km

r = Z(shuttle) - Z

E_L = 1 joule/pulse

d = 1.128 m. diam.

Δt = 6.67 μs for Δr = 1 km

α = .001 radian full angle

Detector dark current(counts) are negligible.

APPENDIX B

SAMPLE OUTPUT FROM COMPUTER SIMULATION PROGRAM FOR RAYLEIGH/MIE ANALYSIS

SAMPLE OUTPUT FROM COMPUTER SIMULATION PROGRAM FOR RAYLEIGH/MIE ANALYSIS

The sample output provides data for the 100 mJ laser firing downward from 40 KM, 30 KM, and 20 KM altitudes with no background interference, and also with a worse case day background for a receiver with an 0.8 mrad FOV. Input parameters are shown on the accompanying page. The laser lines correspond to the 353 NM and 1060 NM wavelengths for line 1 and line 2, respectively. Program "times" are provided as a means of correlating the graphical curve plots with the analytical program output data for each case investigated. The curve plots provide, as a function of altitude, the $\log_{10}$ of the detected scattering at the receiver in terms of counts/km, and the estimated error in the two color density measurement technique as calculated by the error equation presented in Section 5 (page 101) of this report.

BALLOON BORN LIDAR INPUT INFORMATION 22-OCT-79 00:02:13

ATMOSPHERIC SCATTERING PROPERTIES

PHASE FUNCTION AEROSOLS LINE 1	0.30000E-01	
PHASE FUNCTION AEROSOLS LINE 2	0.24000E-01	
PHASE FUNCTION MOLECULES LINE 1	0.12000E+00	
PHASE FUNCTION MOLECULES LINE 2	0.12000E+00	
GROUND VISIBILITY	0.23000E+02	KM.

LASER LINE 1 (λ_1 = 353 NM)

LASER INTENSITY	0.9000000E-02	JOULES
LASER WAVENUMBER	0.2832900E+05	CM-1
EFFICIENCY	0.1600000E-01	
MIRROR AREA	0.1660000E+04	CM**2
LASER INTENSITY	0.1598227E+17	PHOTONS PER PULSE
BACKGROUND	0.7174000E+04	COUNTS/KM

LASER LINE 2 (λ_2 = 1060 NM)

LASER INTENSITY	0.5400000E-01	JOULES
LASER WAVENUMBER	0.9434000E+04	CM-1
EFFICIENCY	0.2600000E-02	
MIRROR AREA	0.1668000E+04	CM**2
LASER INTENSITY	0.2079554E+18	PHOTONS PER PULSE
BACKGROUND	0.3330000E+03	COUNTS/KM

SENSOR PARAMETERS

SENSOR ALTITUDE	0.40000E+02	KM.
SENSOR ANGLE	-0.90000E+02	DEGREES
TIME	00:02:30	

PROPERTIES OF FIRST LINE
WAVENUMBER = 0.2833E+05

THIS PAGE IS BEST QUALITY PRACTICABLE FROM COPY FURNISHED TO DDC

SLANT RANGE KM	ALTITUDE KM	DENSITY CM-3	SCATTERING TO SENSOR PHOT/KM-STR	DETECTED SCATTERING COUNTS/KM	OPTICAL THICKNESS	TRANSMISSION	MOLECULAR SCATTERING CM-1	AEROSOL SCATTERING CM-1	AEROSOL ABSORPTION CM-1	TOTAL EXTINCTION CM-1
2.0000E+00	3.8000E+01	1.2465E+17	1.7288E+01	4.8446E+02	6.5417E-04	9.9935E-01	4.2675E-10	6.5037E-12	1.1467E-11	3.7045E-09
4.0000E+00	3.6000E+01	1.6655E+17	5.7916E+00	1.6229E+02	1.5397E-03	9.9846E-01	5.7022E-10	1.1362E-11	2.0033E-11	5.1506E-09
6.0000E+00	3.4000E+01	2.[illegible]567E+17	3.4562E+00	9.7131E+01	2.7522E-03	9.9725E-01	7.6577E-10	1.9293E-11	3.4018E-11	7.0586E-09
8.0000E+00	3.2000E+01	3.0172E+17	2.6370E+00	7.3994E+01	4.4155E-03	9.9559E-01	1.0330E-09	3.2319E-11	5.6985E-11	9.7426E-09
1.0000E+01	3.0000E+01	4.[illegible]63E+17	2.2935E+00	6.4410E+01	6.7344E-03	9.9329E-01	1.3990E-09	5.8614E-11	1.0335E-10	1.3716E-08
1.2000E+01	2.8000E+01	5.[illegible]05E+17	2.1919E+00	6.1423E+01	1.0004E-02	9.9005E-01	1.9202E-09	9.4653E-11	1.6689E-10	1.9324E-08
1.4000E+01	2.6000E+01	7.[illegible]E+17	2.2024E+00	6.1717E+01	1.4525E-02	9.8540E-01	2.6254E-09	1.5574E-10	2.7461E-10	2.7344E-08
1.6000E+01	2.4000E+01	1.[illegible]60E+18	2.2816E+00	6.3937E+01	2.1120E-02	9.7910E-01	3.5812E-09	2.3118E-10	4.0763E-10	3.7957E-08
1.3000E+01	2.2000E+01	1.[illegible]E+18	2.4545E+00	6.9062E+01	3.0231E-02	9.7022E-01	4.9264E-09	3.8116E-10	6.7207E-10	5.4431E-08
2.6000E+01	2.0000E+01	1.[illegible]71E+18	2.7351E+00	7.6643E+01	4.3570E-02	9.5740E-01	6.7691E-09	6.9871E-10	1.2320E-09	8.0932E-08
2.2000E+01	1.8000E+01	2.7[illegible]32E+18	3.0407E+00	8.5207E+01	6.3419E-02	9.3855E-01	9.3234E-09	1.1301E-09	1.9927E-09	1.1736E-07
2.4000E+01	1.6000E+01	3.[illegible]6E+18	3.2288E+00	9.0470E+01	8.9037E-02	9.1408E-01	1.2745E-08	1.1817E-09	2.0836E-09	1.4768E-07
2.6000E+01	1.4000E+01	[illegible].1312E+18	3.4980E+00	9.7743E+01	1.2359E-01	8.8375E-01	1.7568E-08	1.3226E-09	2.3319E-09	1.9281E-07
2.8000E+01	1.2000E+01	6.[illegible]E+18	3.6192E+00	1.0142E+02	1.6737E-01	8.4599E-01	2.3349E-08	1.4631E-09	2.5790E-09	2.4593E-07
3.0000E+01	[illegible]	[illegible]E+18	3.5525E+00	9.9550E+01	2.2130E-01	8.0140E-01	2.9656E-08	1.4867E-09	2.6214E-09	2.9931E-07
3.2000E+01	8.0000E+00	1.[illegible]E+19	3.4069E+00	9.5470E+01	2.8749E-01	7.5014E-01	3.7202E-08	1.5890E-09	2.0032E-09	3.6581E-07
3.4000E+01	6.0000E+00	1.[illegible]517E+19	3.1764E+00	8.9910E+01	3.6774E-01	6.9230E-01	4.6277E-08	1.6600E-09	2.9269E-09	4.4390E-07
3.6000E+01	[illegible]	[illegible]604E+19	2.8374E+00	8.1193E+01	4.7023E-01	6.2406E-01	5.7052E-08	3.1231E-09	5.5068E-09	5.8504E-07
3.8000E+01	[illegible]	2.[illegible]E+19	2.6682E+00	7.4769E+01	6.2333E-01	5.3616E-01	6.9792E-08	1.4069E-08	2.4806E-09	1.0754E-06

PROPERTIES OF SECOND LINE
WAVENUMBER = 0.9434E+04

SLANT RANGE KM	ALTITUDE KM	DENSITY	SCATTERING TO SENSOR PHOT/KM-STR	DETECTED SCATTERING COUNTS/KM	OPTICAL THICKNESS	TRANSMISSION	MOLECULAR SCATTERING CM-1	AEROSOL SCATTERING CM-1	AEROSOL ABSORPTION CM-1	TOTAL EXTINCTION CM-1
2.0000E+00	3.8000E+01	1.2465E+17	4.8033E+00	2.0831E+01	1.0828E-05	9.9990E-01	5.1813E-12	1.4912E-12	9.3931E-12	1.1471E-10
4.0000E+00	3.6000E+01	1.6[illegible]E+17	1.7147E+00	7.4363E+00	4.7868E-05	9.9995E-01	6.9234E-12	2.6051E-12	1.6409E-11	1.8265E-10
6.0000E+00	3.4000E+01	2.2[illegible]E+17	1.0973E+00	4.7509E+00	9.5137E-05	9.9990E-01	9.2976E-12	4.4237E-12	2.7064E-11	2.8966E-10
8.0000E+00	3.2000E+01	[illegible]E+17	0.9742E-01	3.8919E+00	1.6032E-04	9.9903E-01	1.2542E-11	7.4104E-12	4.6677E-11	4.5996E-10
1.0000E+01	3.0000E+01	4.0[illegible]63E+17	8.7563E-01	3.7974E+00	2.8937E-04	9.9971E-01	1.6986E-11	1.3440E-11	8.4655E-11	7.8620E-10
1.2000E+01	2.8000E+01	5.6005E+17	8.9932E-01	3.9002E+00	4.8740E-04	9.9951E-01	2.3314E-11	2.1703E-11	1.3670E-10	1.2353E-09
1.4000E+01	2.6000E+01	7.6602E+17	9.9136E-01	4.2993E+00	8.0334E-04	9.9920E-01	3.1876E-11	3.5710E-11	2.2493E-10	1.9785E-09
1.6000E+01	2.4000E+01	1.04[illegible]0E+18	1.0825E+00	4.6947E+00	1.2929E-03	9.9871E-01	4.3481E-11	5.3009E-11	3.3389E-10	2.9049E-09
1.8000E+01	2.2000E+01	1.4309E+18	1.3030E+00	5.6510E+00	2.0303E-03	9.9797E-01	5.9814E-11	8.7397E-11	5.5050E-10	4.6985E-09
2.0000E+01	2.0000E+01	1.9771E+18	1.7335E+00	7.5181E+00	3.2862E-03	9.9672E-01	8.2187E-11	1.6021E-10	1.0091E-09	8.3694E-09
2.2000E+01	1.8000E+01	2.7232E+18	2.1909E+00	9.5014E+00	5.5140E-03	9.9450E-01	1.1320E-10	2.5913E-10	1.6322E-09	1.3373E-08
2.4090E+01	1.6000E+01	3.7226E+18	2.0932E+00	9.0776E+00	8.2953E-03	9.9174E-01	1.5474E-10	2.7096E-10	1.7067E-09	1.4286E-08
2.6000E+01	1.4000E+01	[illegible]E+18	2.1510E+00	9.3284E+00	1.1339E-02	9.8872E-01	2.1330E-10	3.0325E-10	1.9101E-09	1.6323E-08

2.8000E+01	1.2000E+01	6.8198E+18	2.2073E+00	9.5727E+00	1.4756E-02	9.8535E-01	2.8349E-10	3.3548E-10	2.1132E-09	1.8454E-08
3.0000E+01	1.0000E+01	8.6620E+18	2.1616E+00	9.3745E+00	1.8413E-02	9.0170E-01	3.6007E-10	3.4089E-10	2.1472E-09	1.9351E-08
3.2000E+01	8.0000E+00	1.0066E+19	2.1945E+00	9.5171E+00	2.2449E-02	9.7780E-01	4.5109E-10	3.6454E-10	2.2962E-09	2.1249E-08
3.4000E+01	6.0000E+00	1.3517E+19	2.2254E+00	9.6513E+00	2.6743E-02	9.7361E-01	5.6187E-10	3.8062E-10	2.3975E-09	2.2939E-08
3.6000E+01	4.0000E+00	1.6664E+19	2.9303E+00	1.2708E+01	3.2991E-02	9.6755E-01	6.9269E-10	7.1611E-10	4.5106E-09	4.0121E-08
3.8000E+01	2.0000E+00	2.0305E+19	7.3609E+00	3.1923E+01	4.9230E-02	9.5190E-01	8.4737E-10	3.2258E-09	2.0319E-08	1.6179E-07

ERROR ANALYSIS FOR 1.100.1000 SHOTS BACKSCATTER UNCERTAINTY = 0.50.100%

RANGE KM	1.0%	100.0%	1000.0%	1.50%	100.50%	1000.50%	1.100%	100.100%	1000.100%
2.0000E+00	1.8399E-01	1.9138E-02	7.8663E-03	1.8414E-01	2.0600E-02	1.0952E-02	1.8462E-01	2.4465E-02	1.7151E-02
4.0000E+00	5.4057E-01	5.4314E-02	1.7898E-02	5.4066E-01	5.5220E-02	2.0484E-02	5.4094E-01	5.7853E-02	2.6783E-02
6.0000E+00	9.0527E-01	9.0682E-02	2.9118E-02	9.0536E-01	9.1553E-02	3.1726E-02	9.0562E-01	9.4117E-02	3.8504E-02
8.0000E+00	1.1973E+00	1.1985E-01	3.8241E-02	1.1974E+00	1.2087E-01	4.1317E-02	1.1977E+00	1.2387E-01	4.9408E-02
1.0000E+01	1.3911E+00	1.3921E-01	4.4329E-02	1.3912E+00	1.4078E-01	4.9029E-02	1.3917E+00	1.4538E-01	6.0994E-02
1.2000E+01	1.4715E+00	1.4726E-01	4.6880E-02	1.4717E+00	1.4931E-01	5.2965E-02	1.4723E+00	1.5529E-01	6.8027E-02
1.4000E+01	1.4819E+00	1.4831E-01	4.7261E-02	1.4822E+00	1.5125E-01	5.5797E-02	1.4831E+00	1.5974E-01	7.5846E-02
1.6000E+01	1.4389E+00	1.4406E-01	4.6029E-02	1.4393E+00	1.4763E-01	5.6218E-02	1.4403E+00	1.5786E-01	7.9285E-02
1.8000E+01	1.3514E+00	1.3548E-01	4.3550E-02	1.3519E+00	1.4081E-01	5.8251E-02	1.3536E+00	1.5594E-01	8.8786E-02
2.0000E+01	1.2516E+00	1.2564E-01	4.1070E-02	1.2527E+00	1.3583E-01	6.5957E-02	1.2559E+00	1.6260E-01	1.1109E-01
2.2000E+01	1.1458E+00	1.1557E-01	3.9281E-02	1.1474E+00	1.3050E-01	7.2223E-02	1.1522E+00	1.6748E-01	1.2742E-01
2.4000E+01	1.0468E+00	1.0661E-01	3.8843E-02	1.0478E+00	1.1626E-01	6.0401E-02	1.0509E+00	1.4129E-01	1.0053E-01
2.6000E+01	9.5031E-01	9.8703E-02	4.0457E-02	9.5106E-01	1.0571E-01	5.5260E-02	9.5329E-01	1.2420E-01	8.5466E-02
2.8000E+01	9.0262E-01	9.7096E-02	4.5399E-02	9.0317E-01	1.0203E-01	5.5574E-02	9.0480E-01	1.1556E-01	7.7676E-02
3.0000E+01	9.0629E-01	1.0180E-01	5.4840E-02	9.0664E-01	1.0492E-01	6.0297E-02	9.0767E-01	1.1355E-01	7.4301E-02
3.2000E+01	9.3687E-01	1.1119E-01	6.7059E-02	9.3711E-01	1.1323E-01	7.0301E-02	9.3784E-01	1.1912E-01	7.9518E-02
3.4000E+01	9.9711E-01	1.2536E-01	8.2588E-02	9.9727E-01	1.2664E-01	8.4513E-02	9.9775E-01	1.3040E-01	9.0041E-02
3.6000E+01	1.1138E+00	1.4891E-01	1.0535E-01	1.1142E+00	1.5141E-01	1.0085E-01	1.1152E+00	1.5866E-01	1.1072E-01
3.0000E+01	1.3817E+00	2.0331E-01	1.5606E-01	1.3854E+00	2.2692E-01	1.8577E-01	1.3963E+00	2.8630E-01	2.5493E-01

SENSOR PARAMETERS

SENSOR ALTITUDE	0.30000E+02	KM.
SENSOR ANGLE	-0.90000E+02	DEGREES
TIME	08:02:47	

PROPERTIES OF FIRST LINE
WAVENUMBER = 0.2833E+05

SLANT	ALTITUDE	DENSITY	SCATTERING	DETECTED	OPTICAL	TRANSMISSION	MOLECULAR	AEROSOL	AEROSOL	TOTAL

RANGE KM	KM	CM-3	TO SENSOR PHOT/KM-STR	SCATTERING COUNTS/KM	THICKNESS		SCATTERING CM-1	SCATTERING CM-1	ABSORPTION CM-1	EXTINCTION CM-1
2.0000E+00	2.8000E+01	5.6085E+17	7.9900E+01	2.2412E+0[illegible]	3.2098E-03	9.96[illegible]E-01	1.9202E-09	9.46[illegible]-11	1.6609E-10	1.9324E-08
4.0000E+00	2.6000E+01	7.6682E+17	2.7345E+01	7.6629E+02	7.0905E-03	9.921[illegible]E-01	2.6254E-09	1.55[illegible]-10	2.7451E-10	2.7344E-08
6.0000E+00	2.4000E+01	1.0460E+18	1.6445E+01	4.6083E+02	1.4305E-02	9.857[illegible]E-01	3.5012E-09	2.3110E-10	4.0763E-10	3.7957E-08
8.0000E+00	2.2000E+01	1.4389E+18	1.2046E+01	3.5487E+02	2.3497E-02	9.7678E-01	4.9264E-09	3.8110E-10	6.7207E-10	5.4431E-08
1.0000E+01	2.0000E+01	1.9771E+18	1.1089E+01	3.1073E+02	3.6795E-02	9.6387E-01	6.7691E-09	6.9071E-10	1.2320E-09	8.0932E-08
1.2000E+01	1.8000E+01	2.7232E+18	1.0359E+01	2.9020E+02	5.6685E-02	9.4489E-01	9.3234E-09	1.1301E-09	1.9927E-09	1.1736E-07
1.4000E+01	1.6000E+01	3.7226E+18	9.6173E+00	2.6950E+02	8.3103E-02	9.2020E-01	1.2745E-08	1.1017E-09	2.0036E-09	1.4768E-07
1.6000E+01	1.4000E+01	5.1312E+18	9.3355E+00	2.6160E+02	1.1605E-01	8.8972E-01	1.7560E-08	1.3220E-09	2.3319E-09	1.9281E-07
1.8000E+01	1.2000E+01	6.8198E+18	8.8763E+00	2.4874E+02	1.6063E-01	8.5161E-01	2.3349E-08	1.4631E-09	2.5798E-09	2.4593E-07
2.0000E+01	1.0000E+01	8.6620E+18	8.1015E+00	2.2702E+02	2.1456E-01	8.0689E-01	2.9656E-08	1.4867E-09	2.6214E-09	2.9931E-07
2.2000E+01	8.0000E+00	1.0966E+19	7.3050E+00	2.0473E+02	2.8076E-01	7.5521E-01	3.7202E-08	1.5890E-09	2.8032E-09	3.6581E-07
2.4000E+01	6.0000E+00	1.3517E+19	6.4513E+00	1.8105E+02	3.6100E-01	6.9690E-01	4.6277E-08	1.66[illegible]-09	2.92[illegible]-09	4.4390E-07
2.6000E+01	4.0000E+00	1.6664E+19	5.6302E+00	1.5777E+02	4.6349E-01	6.2900E-01	5.7052E-08	3.1[illegible]-09	5.5000E-09	5.8504E-07
2.8000E+01	2.0000E+00	2.0385E+19	4.9810E+00	1.3958E+02	6.1659E-01	5.3978E-01	6.5792E-08	1.40[illegible]-08	2.[illegible]00E-08	1.0754E-06

PROPERTIES OF SECOND LINE
WAVENUMBER = 0.9434E+04

SLANT RANGE KM	ALTITUDE KM	DENSITY	SCATTERING TO SENSOR PHOT/KM-STR	DETECTED SCATTERING COUNTS/KM	OPTICAL THICKNESS	TRANSMISSION	MOLECULAR SCATTERING CM-1	AEROSOL SCATTERING CM-1	AEROSOL ABSORPTION CM-1	TOTAL EXTINCTION CM-1
2.0000E+00	2.8000E+01	5.6085E+17	3.2394E+01	1.4049E+02	1.9803E-04	9.9980E-01	2.3314E-11	2.1703E-11	1.3670E-10	1.2353E-09
4.0000E+00	2.6000E+01	7.6682E+17	1.2151E+01	5.2697E+01	5.1397E-04	9.9949E-01	3.1076E-11	3.5710E-11	2.2493E-10	1.9785E-09
6.0000E+00	2.4000E+01	1.0460E+18	7.7025E+00	3.3494E+01	1.0035E-03	9.9900E-01	4.3481E-11	5.3009E-11	3.3309E-10	2.9049E-09
8.0000E+00	2.2000E+01	1.4389E+18	6.6005E+00	2.8625E+01	1.7409E-03	9.9826E-01	5.9814E-11	8.7397E-11	5.5050E-10	4.6985E-09
1.0000E+01	2.0000E+01	1.9771E+18	6.9302E+00	3.0090E+01	2.9960E-03	9.9701E-01	8.2107E-11	1.6021E-10	1.0091E-09	8.3694E-09
1.2000E+01	1.8000E+01	2.7232E+18	7.3681E+00	3.1954E+01	5.2240E-03	9.9479E-01	1.1320E-10	2.5913E-10	1.6322E-09	1.3373E-08
1.4000E+01	1.6000E+01	3.7226E+18	6.1549E+00	2.6692E+01	8.0059E-03	9.9203E-01	1.5474E-10	2.7090E-10	1.7067E-09	1.4286E-08
1.6000E+01	1.4000E+01	5.1312E+18	5.6832E+00	2.4647E+01	1.1050E-02	9.8901E-01	2.1330E-10	3.0325E-10	1.9101E-09	1.6323E-08
1.8000E+01	1.2000E+01	6.8198E+18	5.3442E+00	2.3177E+01	1.4467E-02	9.8564E-01	2.8349E-10	3.3540E-10	2.1132E-09	1.8454E-08
2.0000E+01	1.0000E+01	8.6620E+18	4.8664E+00	2.1105E+01	1.8124E-02	9.8204E-01	3.6007E-10	3.4089E-10	2.1472E-09	1.9351E-08
2.2000E+01	8.0000E+00	1.0966E+19	4.6456E+00	2.0147E+01	2.2160E-02	9.7808E-01	4.5169E-10	3.6454E-10	2.2962E-09	2.1249E-08
2.4000E+01	6.0000E+00	1.3517E+19	4.4689E+00	1.9381E+01	2.6454E-02	9.7389E-01	5.6187E-10	3.8062E-10	2.3975E-09	2.2939E-08
2.6000E+01	4.0000E+00	1.6664E+19	5.6211E+00	2.4378E+01	3.2702E-02	9.6783E-01	6.9269E-10	7.1611E-10	4.5106E-09	4.0121E-08
2.8000E+01	2.0000E+00	2.0385E+19	1.3565E+01	5.8030E+01	4.8940E-02	9.5224E-01	8.4737E-10	3.2258E-09	2.0319E-08	1.6179E-07

ERROR ANALYSIS FOR 1,100,1000 SHOTS BACKSCATTER UNCERTAINTY = 0,50,100%

RANGE KM	1,0%	100,0%	1000,0%	1,50%	100,50%	1000,50%	1,100%	100,100%	1000,100%
2.0000E+00	4.6374E-02	7.0520E-03	5.5346E-03	5.2517E-02	2.5636E-02	2.5261E-02	6.7679E-02	4.9796E-02	4.9603E-02

4.0000E+00	1.2528E-01	1.3692E-02	6.0189E-03	1.2874E-01	3.2669E-02	3.0455E-02	1.3861E-01	6.0002E-02	5.9713E-02
6.0000E+00	2.0530E-01	2.1414E-02	8.9181E-03	2.0782E-01	3.8735E-02	3.3407E-02	2.1521E-01	6.0015E-02	6.5169E-02
8.0000E+00	2.6885E-01	2.7856E-02	1.1221E-02	2.7162E-01	4.7671E-02	4.0200E-02	2.7977E-01	8.2233E-02	7.0180E-02
1.0000E+01	3.1419E-01	3.2866E-02	1.3877E-02	3.1840E-01	6.1186E-02	5.3415E-02	3.3071E-01	1.0073E-01	1.0415E-01
1.2000E+01	3.4177E-01	3.6821E-02	1.7499E-02	3.4710E-01	7.0916E-02	6.3003E-02	3.6263E-01	1.2600E-01	1.2247E-01
1.4000E+01	3.5647E-01	4.0311E-02	2.2013E-02	3.5947E-01	6.1434E-02	5.1320E-02	3.6033E-01	1.0110E-01	9.5296E-02
1.6000E+01	3.6003E-01	4.4149E-02	2.8080E-02	3.6199E-01	5.8018E-02	4.6962E-02	3.6782E-01	8.7274E-02	8.0350E-02
1.8000E+01	3.7320E-01	5.0738E-02	3.6492E-02	3.7451E-01	5.9633E-02	4.8097E-02	3.7842E-01	8.0630E-02	7.2515E-02
2.0000E+01	4.0300E-01	6.0517E-02	4.7108E-02	4.0378E-01	6.5503E-02	5.3361E-02	4.0611E-01	7.0504E-02	6.0792E-02
2.2000E+01	4.4324E-01	7.3392E-02	6.0410E-02	4.4376E-01	7.6439E-02	6.4077E-02	4.4530E-01	8.4930E-02	7.3998E-02
2.4000E+01	4.9756E-01	8.9672E-02	7.6574E-02	4.9788E-01	9.1448E-02	7.0647E-02	4.9885E-01	9.6581E-02	8.4560E-02
2.6000E+01	5.8229E-01	1.1350E-01	9.9585E-02	5.8294E-01	1.1675E-01	1.0320E-01	5.8486E-01	1.2001E-01	1.1364E-01
2.8000E+01	7.5404E-01	1.6568E-01	1.5010E-01	7.6075E-01	1.9393E-01	1.0080E-01	7.8052E-01	2.6093E-01	2.5133E-01

SENSOR PARAMETERS

SENSOR ALTITUDE	0.20000E+02	KM.
SENSOR ANGLE	-0.90000E+02	DEGREES
TIME	08:02:58	

PROPERTIES OF FIRST LINE
WAVENUMBER = 0.2833E+05

SLANT RANGE KM	ALTITUDE KM	DENSITY CM-3	SCATTERING TO SENSOR PHOT/KM-STR	DETECTED SCATTERING COUNTS/KM	OPTICAL THICKNESS	TRANSMISSION	MOLECULAR SCATTERING CM-1	AEROSOL SCATTERING CM-1	AEROSOL ADSORPTION CM-1	TOTAL EXTINCTION CM-1
2.0000E+00	1.8000E+01	2.7232E+18	4.0139E+02	1.1248E+04	1.9890E-02	9.8031E-01	9.3234E-09	1.1301E-09	1.9927E-09	1.1736E-07
4.0000E+00	1.6000E+01	3.7226E+18	1.2681E+02	3.5535E+03	4.6307E-02	9.5475E-01	1.2745E-08	1.1017E-09	2.0036E-09	1.4760E-07
6.0000E+00	1.4000E+01	5.1312E+18	7.1455E+01	2.0023E+03	8.0056E-02	9.2306E-01	1.7568E-08	1.3220E-09	2.3319E-09	1.9281E-07
8.0000E+00	1.2000E+01	6.8198E+18	4.0368E+01	1.3554E+03	1.2384E-01	8.8352E-01	2.3349E-08	1.4631E-09	2.5798E-09	2.4593E-07
1.0000E+01	1.0000E+01	8.6620E+18	3.4081E+01	9.7745E+02	1.7777E-01	8.3714E-01	2.9656E-08	1.4867E-09	2.6214E-09	2.9931E-07
1.2000E+01	8.0000E+00	1.0866E+19	2.6431E+01	7.4066E+02	2.4396E-01	7.8352E-01	3.7202E-08	1.5090E-09	2.8032E-09	3.6581E-07
1.4000E+01	6.0000E+00	1.3517E+19	2.0438E+01	5.7273E+02	3.2421E-01	7.2310E-01	4.6277E-08	1.6000E-09	2.9269E-09	4.4390E-07
1.6000E+01	4.0000E+00	1.6664E+19	1.6003E+01	4.4843E+02	4.2670E-01	6.5266E-01	5.7052E-08	3.1231E-09	5.5069E-09	5.8504E-07
1.8000E+01	2.0000E+00	2.0305E+19	1.2973E+01	3.6354E+02	5.7980E-0	5.6601E-01	6.9792E-08	1.4060E-08	2.4606E-08	1.0754E-06

PROPERTIES OF SECOND LINE
WAVENUMBER = 0.9434E+04

SLANT RANGE KM	ALTITUDE KM	DENSITY	SCATTERING TO SENSOR PHOT/KM-STR	DETECTED SCATTERING COUNTS/KM	OPTICAL THICKNESS	TRANSMISSION	MOLECULAR SCATTERING CM-1	AEROSOL SCATTERING CM-1	AEROSOL ABSORPTION CM-1	TOTAL EXTINCTION CM-1
2.0000E+00	1.8000E+01	2.7232E+18	2.6685E+02	1.1573E+03	2.2270E-03	9.9777E-01	1.1320E-10	2.5913E-10	1.6322E-09	1.3373E-06
4.0000E+00	1.6000E+01	3.7226E+18	7.5050E+01	3.2895E+02	5.0091E-03	9.9500E-01	1.5474E-10	2.7094E-10	1.7067E-09	1.4286E-08
6.0000E+00	1.4000E+01	5.1312E+18	4.0657E+01	1.7632E+02	8.6530E-03	9.9150E-01	2.1330E-10	3.0329E-10	1.9101E-09	1.6323E-08
8.0000E+00	1.2000E+01	6.8193E+18	2.7210E+01	1.1004E+02	1.1470E-02	9.8860E-01	2.8349E-10	3.3540E-10	2.1132E-09	1.8454E-08
1.0000E+01	1.0000E+01	8.6620E+18	1.9503E+01	8.4927E+01	1.5127E-02	9.8499E-01	3.6007E-10	3.4005E-10	2.1472E-09	1.9351E-08
1.2000E+01	8.0000E+00	1.0066E+19	1.5708E+01	6.8123E+01	1.9163E-02	9.8102E-01	4.5169E-10	3.6454E-10	2.2962E-09	2.1249E-08
1.4000E+01	6.0000E+00	1.3517E+19	1.3212E+01	5.7298E+01	2.3457E-02	9.7682E-01	5.6187E-10	3.8062E-10	2.3975E-09	2.2939E-08
1.6000E+01	4.0000E+00	1.6664E+19	1.4933E+01	6.4759E+01	2.9705E-02	9.7073E-01	6.9269E-10	7.1611E-10	4.5106E-09	4.0121E-08
1.8000E+01	2.0000E+00	2.0385E+19	3.3022E+01	1.4321E+02	4.5943E-02	9.5510E-01	8.4737E-10	3.2250E-09	2.0319E-08	1.6179E-07

ERROR ANALYSIS FOR 1.100.1000 SHOTS BACKSCATTER UNCERTAINTY = 0.50.100%

RANGE KM	1.0%	100.0%	1000.0%	1.50%	100.50%	1000.50%	1.100%	100.100%	1000.100%
2.0000E+00	1.5727E-02	7.0658E-03	6.9377E-03	6.2615E-02	6.1018E-02	6.1003E-02	1.2223E-01	1.2142E-01	1.2141E-01
4.0000E+00	3.4604E-02	1.1880E-02	1.1468E-02	5.7850E-02	4.7857E-02	4.7757E-02	9.8966E-02	9.3477E-02	9.3425E-02
6.0000E+00	5.5350E-02	1.8757E-02	1.8088E-02	6.6937E-02	4.2057E-02	4.1762E-02	9.3441E-02	7.7585E-02	7.7426E-02
8.0000E+00	7.8044E-02	2.7829E-02	2.6947E-02	8.4099E-02	4.1906E-02	4.1326E-02	1.0009E-01	6.8565E-02	6.8212E-02
1.0000E+01	1.0477E-01	3.8956E-02	3.7836E-02	1.0773E-01	4.6323E-02	4.5386E-02	1.1614E-01	6.3488E-02	6.2087E-02
1.2000E+01	1.3507E-01	5.2679E-02	5.1307E-02	1.3754E-01	5.6847E-02	5.5579E-02	1.4244E-01	6.7833E-02	6.6774E-02
1.4000E+01	1.7330E-01	6.9242E-02	6.7565E-02	1.7423E-01	7.1527E-02	6.9905E-02	1.7698E-01	7.7982E-02	7.6497E-02
1.6000E+01	2.2491E-01	9.2491E-02	9.0402E-02	2.2657E-01	9.6456E-02	9.4455E-02	2.3147E-01	1.0748E-01	1.0566E-01
1.0000E+01	3.2051E-01	1.4239E-01	1.3973E-01	3.3599E-01	1.7445E-01	1.7229E-01	3.7063E-01	2.4680E-01	2.4527E-01

BALLOON BORN LIDAR INPUT INFORMATION 22-OCT-79 08:04:24

ATMOSPHERIC SCATTERING PROPERTIES

PHASE FUNCTION AEROSOLS LINE 1	0.30000E-01	
PHASE FUNCTION AEROSOLS LINE 2	0.24000E-01	
PHASE FUNCTION MOLECULES LINE 1	0.12000E+00	
PHASE FUNCTION MOLECULES LINE 2	0.12000E+00	
GROUND VISIBILITY	0.23000E+02	KM.

LASER LINE 1 (λ_1 = 353 NM)

LASER INTENSITY	0.9000000E-02	JOULES
LASER WAVENUMBER	0.2832900E+05	CM-1
EFFICIENCY	0.1600000E-01	
MIRROR AREA	0.1668000E+04	CM**2
LASER INTENSITY	0.1598227E+17	PHOTONS PER PULSE
BACKGROUND	0.0000000E+00	COUNTS/KM

LASER LINE 2 (λ_2 = 1060NM)

LASER INTENSITY	0.5400000E-01	JOULES
LASER WAVENUMBER	0.9434000E+04	CM-1
EFFICIENCY	0.2600000E-02	
MIRROR AREA	0.1668000E+04	CM**2
LASER INTENSITY	0.2879554E+18	PHOTONS PER PULSE
BACKGROUND	0.0000000E+00	COUNTS/KM

SENSOR PARAMETERS

SENSOR ALTITUDE	0.40000E+02	KM.
SENSOR ANGLE	-0.90000E+02	DEGREES
TIME	08:04:45	

PROPERTIES OF FIRST LINE
WAVENUMBER = 0.2033E+05

SLANT RANGE KM	ALTITUDE KM	DENSITY CM-3	SCATTERING TO SENSOR PHOT/KM-STR	DETECTED SCATTERING COUNTS/KM	OPTICAL THICKNESS	TRANSMISSION	MOLECULAR SCATTERING CM-1	AEROSOL SCATTERING CM-1	AEROSOL ABSORPTION CM-1	TOTAL EXTINCTION CM-1
2.0000E+00	3.8000E+01	1.2465E+17	1.7288E+01	4.8446E+02	6.5417E-04	9.9935E-01	4.2675E-10	6.5037E-12	1.1467E-11	3.7845E-09
4.0000E+00	3.6000E+01	1.6655E+17	5.7916E+00	1.6229E+02	1.5397E-03	9.9846E-01	5.7022E-10	1.1362E-11	2.0033E-11	5.1506E-09
6.0000E+00	3.4000E+01	2.2367E+17	3.4662E+00	9.7131E+01	2.7522E-03	9.9725E-01	7.6577E-10	1.9293E-11	3.4018E-11	7.0586E-09
8.0000E+00	3.2000E+01	3.0172E+17	2.6370E+00	7.3894E+01	4.4155E-03	9.9559E-01	1.0330E-09	3.2319E-11	5.6985E-11	9.7426E-09
1.0000E+01	3.0000E+01	4.0863E+17	2.2985E+00	6.4410E+01	6.7344E-03	9.9329E-01	1.3990E-09	5.8614E-11	1.0335E-10	1.3716E-08
1.2000E+01	2.8000E+01	5.6085E+17	2.1919E+00	6.1423E+01	1.0004E-02	9.9005E-01	1.9202E-09	9.4653E-11	1.6609E-10	1.9324E-08
1.4000E+01	2.6000E+01	7.6682E+17	2.2024E+00	6.1717E+01	1.4625E-02	9.8540E-01	2.6254E-09	1.5574E-10	2.7461E-10	2.7344E-08
1.6000E+01	2.4000E+01	1.0460E+18	2.2816E+00	6.3937E+01	2.1120E-02	9.7910E-01	3.5812E-09	2.3110E-10	4.0763E-10	3.7957E-08
1.8000E+01	2.2000E+01	1.4389E+18	2.4645E+00	6.9062E+01	3.0231E-02	9.7022E-01	4.9264E-09	3.8110E-10	6.7207E-10	5.4431E-08
2.0000E+01	2.0000E+01	1.9771E+18	2.7351E+00	7.6643E+01	4.3530E-02	9.5740E-01	6.7691E-09	6.9071E-10	1.2320E-09	8.0932E-08
2.2000E+01	1.8000E+01	2.7232E+18	3.0407E+00	8.5207E+01	6.3419E-02	9.3855E-01	9.3234E-09	1.1301E-09	1.9927E-09	1.1736E-07
2.4000E+01	1.6000E+01	3.7226E+18	3.2288E+00	9.0470E+01	8.9837E-02	9.1400E-01	1.2745E-08	1.1817E-09	2.0836E-09	1.4768E-07
2.6000E+01	1.4000E+01	5.1312E+18	3.4880E+00	9.7743E+01	1.2359E-01	8.8375E-01	1.7568E-08	1.3220E-09	2.3319E-09	1.9201E-07
2.8000E+01	1.2000E+01	6.8198E+18	3.6192E+00	1.0142E+02	1.6737E-01	8.4589E-01	2.3349E-08	1.4631E-09	2.5798E-09	2.4593E-07
3.0000E+01	1.0000E+01	8.6620E+18	3.5525E+00	9.9550E+01	2.2130E-01	8.0148E-01	2.9656E-08	1.4867E-09	2.6214E-09	2.9931E-07
3.2000E+01	8.0000E+00	1.0866E+19	3.4069E+00	9.5470E+01	2.8749E-01	7.5014E-01	3.7202E-08	1.5890E-09	2.8032E-09	3.6581E-07
3.4000E+01	6.0000E+00	1.3517E+19	3.1764E+00	8.9010E+01	3.6774E-01	6.9230E-01	4.6277E-08	1.6600E-09	2.9269E-09	4.4390E-07
3.6000E+01	4.0000E+00	1.6664E+19	2.8974E+00	8.1193E+01	4.7023E-01	6.2496E-01	5.7052E-08	3.1231E-09	5.5068E-09	5.0504E-07
3.8000E+01	2.0000E+00	2.0385E+19	2.6602E+00	7.4769E+01	6.2333E-01	5.3616E-01	6.9792E-08	1.4069E-08	2.4806E-08	1.0754E-06

PROPERTIES OF SECOND LINE
WAVENUMBER = 0.9434E+04

SLANT RANGE KM	ALTITUDE KM	DENSITY	SCATTERING TO SENSOR PHOT/KM-STR	DETECTED SCATTERING COUNTS/KM	OPTICAL THICKNESS	TRANSMISSION	MOLECULAR SCATTERING CM-1	AEROSOL SCATTERING CM-1	AEROSOL ABSORPTION CM-1	TOTAL EXTINCTION CM-1
2.0000E+00	3.8000E+01	1.2465E+17	4.8033E+00	2.0031E+01	1.0828E-05	9.9998E-01	5.1813E-12	1.4912E-12	9.3931E-12	1.1471E-10
4.0000E+00	3.6000E+01	1.6655E+17	1.7147E+00	7.4363E+00	4.7866E-05	9.9995E-01	6.9234E-12	2.6051E-12	1.6409E-11	1.8265E-10
6.0000E+00	3.4000E+01	2.2367E+17	1.0973E+00	4.7589E+00	9.5137E-05	9.9990E-01	9.2976E-12	4.4237E-12	2.7864E-11	2.8966E-10
8.0000E+00	3.2000E+01	3.0172E+17	8.9742E-01	3.8919E+00	1.6032E-04	9.9983E-01	1.2542E-11	7.4101E-12	4.6677E-11	4.5996E-10
1.0000E+01	3.0000E+01	4.0863E+17	8.7563E-01	3.7974E+00	2.8937E-04	9.9971E-01	1.6986E-11	1.3440E-11	8.4655E-11	7.8620E-10
1.2000E+01	2.8000E+01	5.6085E+17	8.9932E-01	3.9002E+00	4.8740E-04	9.9951E-01	2.3314E-11	2.1703E-11	1.3670E-10	1.2353E-09
1.4000E+01	2.6000E+01	7.6682E+17	9.9136E-01	4.2993E+00	8.0334E-04	9.9920E-01	3.1876E-11	3.5710E-11	2.2493E-10	1.9785E-09
1.6000E+01	2.4000E+01	1.0460E+18	1.0825E+00	4.6947E+00	1.2929E-03	9.9871E-01	4.3481E-11	5.3000E-11	3.3389E-10	2.9049E-09
1.8000E+01	2.2000E+01	1.4309E+18	1.3030E+00	5.6510E+00	2.0303E-03	9.9797E-01	5.9814E-11	8.7397E-11	5.5050E-10	4.6905E-09
2.0000E+01	2.0000E+01	1.9771E+18	1.7335E+00	7.5181E+00	3.2062E-03	9.9672E-01	8.2107E-11	1.6021E-10	1.0091E-09	8.3694E-09
2.2000E+01	1.8000E+01	2.7232E+18	2.1909E+00	9.5014E+00	5.5140E-03	9.9450E-01	1.1320E-10	2.5913E-10	1.6322E-09	1.3373E-08
2.4000E+01	1.6000E+01	3.7226E+18	2.0932E+00	9.0776E+00	8.2953E-03	9.9174E-01	1.5474E-10	2.7090E-10	1.7067E-09	1.4286E-08
2.6000E+01	1.4000E+01	5.1312E+18	2.1510E+00	9.3284E+00	1.1339E-02	9.8872E-01	2.1330E-10	3.0325E-10	1.9101E-09	1.6323E-08

2.8000E+01	1.2000E+01	6.8193E+18	2.2073E+00	9.5727E+00	1.4756E-02	9.0535E-01	2.0349E-10	3.3446E-10	2.1133E-09	1.8454E-08
3.0000E+01	1.0000E+01	8.6620E+18	2.1616E+00	9.3745E+00	1.8413E-02	9.8176E-01	3.6007E-10	3.4009E-10	2.1472E-09	1.9351E-08
3.2000E+01	8.0000E+00	1.0866E+19	2.1945E+00	9.5171E+00	2.2449E-02	9.7780E-01	4.5169E-10	3.6454E-10	2.2962E-09	2.1249E-08
3.4000E+01	6.0000E+00	1.3517E+19	2.2254E+00	9.6513E+00	2.6743E-02	9.7501E-01	5.6187E-10	3.0002E-10	2.3975E-09	2.2939E-08
3.6000E+01	4.0000E+00	1.6664E+19	2.9303E+00	1.2700E+01	3.2991E-02	9.6755E-01	6.9269E-10	7.1611E-10	4.5106E-09	4.0121E-08
3.8000E+01	2.0000E+00	2.0385E+19	7.3609E+00	3.1923E+01	4.9230E-02	9.5190E-01	8.4737E-10	3.2256E-09	2.0319E-08	1.6179E-0[illegible]

ERROR ANALYSIS FOR 1,100,1000 SHOTS BACKSCATTER UNCERTAINTY = 0.50,100%

RANGE KM	1.0%	100.0%	1000.0%	1.50%	100.50%	1000.50%	1,100%	100,100%	1000,100%
2.0000E+00	4.6549E-02	7.0316E-03	5.4951E-03	4.7168E-02	1.0369E-02	9.3940E-03	4.0900E-02	1.6704E-02	1.6201E-02
4.0000E+00	8.0560E-02	9.6316E-03	5.8823E-03	8.1182E-02	1.3057E-02	1.1569E-02	8.2995E-02	2.2131E-02	2.0775E-02
6.0000E+00	1.0480E-01	1.1743E-02	6.2699E-03	1.0555E-01	1.7222E-02	1.4071E-02	1.0778E-01	2.7796E-02	2.5962E-02
8.0000E+00	1.2113E-01	1.3241E-02	6.5964E-03	1.2214E-01	2.0494E-02	1.6977E-02	1.2511E-01	3.3970E-02	3.1974E-02
1.0000E+01	1.3170E-01	1.4254E-02	6.8793E-03	1.3336E-01	2.5337E-02	2.2049E-02	1.3821E-01	4.4254E-02	4.2457E-02
1.2000E+01	1.3631E-01	1.4762E-02	7.1411E-03	1.3852E-01	2.8730E-02	2.5661E-02	1.4495E-01	5.1457E-02	4.9808E-02
1.4000E+01	1.3798E-01	1.5088E-02	7.5260E-03	1.4113E-01	3.3278E-02	3.0601E-02	1.5019E-01	6.1211E-02	5.9798E-02
1.6000E+01	1.3660E-01	1.5310E-02	8.1775E-03	1.4037E-01	3.5725E-02	3.3298E-02	1.5109E-01	6.6340E-02	6.5072E-02
1.8000E+01	1.3393E-01	1.5784E-02	9.3988E-03	1.3940E-01	4.1782E-02	3.9011E-02	1.5467E-01	7.8900E-02	7.7940E-02
2.0000E+01	1.3198E-01	1.7125E-02	1.1730E-02	1.4171E-01	5.4377E-02	5.2926E-02	1.6755E-01	1.0453E-01	1.0388E-01
2.2000E+01	1.2857E-01	1.9831E-02	1.5703E-02	1.4214E-01	6.3769E-02	6.2609E-02	1.7670E-01	1.2283E-01	1.2223E-01
2.4000E+01	1.2065E-01	2.3557E-02	2.0680E-02	1.2925E-01	5.2001E-02	5.0763E-02	1.5217E-01	9.5605E-02	9.4997E-02
2.6000E+01	1.1477E-01	2.9305E-02	2.7329E-02	1.2078E-01	4.7704E-02	4.6516E-02	1.3726E-01	8.0706E-02	8.0091E-02
2.0000E+01	1.1331E-01	3.7534E-02	3.6123E-02	1.1756E-01	4.8892E-02	4.7818E-02	1.2948E-01	7.3045E-02	7.2330E-02
3.0000E+01	1.1634E-01	4.7976E-02	4.6900E-02	1.1901E-01	5.4130E-02	5.3178E-02	1.2668E-01	6.9309E-02	6.8650E-02
3.2000E+01	1.2330E-01	6.1144E-02	6.0265E-02	1.2514E-01	6.4770E-02	6.3960E-02	1.3050E-01	7.4590E-02	7.3896E-02
3.4000E+01	1.3424E-01	7.7163E-02	7.6449E-02	1.3543E-01	7.9220E-02	7.8525E-02	1.3895E-01	8.5094E-02	8.4447E-02
3.6000E+01	1.5429E-01	1.0003E-01	9.9405E-02	1.5670E-01	1.0371E-01	1.0310E-01	1.6371E-01	1.1400E-01	1.1348E-01
3.0000E+01	2.0740E-01	1.5057E-01	1.4996E-01	2.3067E-01	1.8119E-01	1.8060E-01	2.8928E-01	2.5161E-01	2.5124E-01

SENSOR PARAMETERS

SENSOR ALTITUDE	0.30000E+02	KM.
SENSOR ANGLE	-0.90000E+02	DEGREES
TIME	08:04:59	

PROPERTIES OF FIRST LINE
WAVENUMBER = 0.2833E+05

SLANT	ALTITUDE	DENSITY	SCATTERING	DETECTED	OPTICAL	TRANSMISSION	MOLECULAR	AEROSOL	AEROSOL	TOTAL

RANGE KM	KM	CM-3	TO SENSOR PHOT/KM-STR	SCATTERING COUNTS/KM	THICKNESS		SCATTERING CM-1	SCATTERING CM-1	ABSORPTION CM-1	EXTINCTION CM-1
2.0000E+00	2.8000E+01	5.6085E+17	7.9980E+01	2.2412E+03	3.2620E-03	9.9674E-01	1.0202E-09	9.4653E-11	1.6609E-10	1.9324E-08
4.0000E+00	2.6000E+01	7.6682E+17	2.7345E+01	7.6629E+02	7.0905E-03	9.921[illegible]E-01	2.6254E-09	1.5574E-10	2.7431E-10	2.7344E-08
6.0000E+00	2.4000E+01	1.0460E+18	1.6445E+01	4.6083E+02	1.4300E-02	9.857[illegible]E-01	5.5812E-09	2.3110E-10	4.0763E-10	3.7957E-08
8.0000E+00	2.2000E+01	1.4389E+18	1.2646E+01	3.5437E+02	2.3497E-02	9.7678E-01	4.9264E-09	3.0116E-10	6.7207E-10	5.4431E-08
1.0000E+01	2.0000E+01	1.9771E+18	1.1009E+01	3.1073E+02	3.6795E-02	9.6387E-01	6.7691E-09	6.9071E-10	1.2320E-09	8.0932E-08
1.2000E+01	1.8000E+01	2.7232E+18	1.0359E+01	2.9028E+02	5.6685E-02	9.4409E-01	9.3234E-09	1.1301E-09	1.9927E-09	1.1736E-07
1.4000E+01	1.6000E+01	3.7226E+18	9.6173E+00	2.6950E+02	8.3103E-02	9.2030E-01	1.2745E-08	1.1817E-09	2.0036E-09	1.4768E-07
1.6000E+01	1.4000E+01	5.1312E+18	9.3355E+00	2.6160E+02	1.1685E-01	8.8972E-01	1.7568E-08	1.3220E-09	2.3319E-09	1.9281E-07
1.8000E+01	1.2000E+01	6.8198E+18	8.8763E+00	2.4874E+02	1.6063E-01	8.5161E-01	2.3349E-08	1.4631E-09	2.5798E-09	2.4593E-07
2.0000E+01	1.0000E+01	8.6620E+18	8.1015E+00	2.2702E+02	2.1456E-01	8.0689E-01	2.9656E-08	1.4867E-09	2.6214E-09	2.9931E-07
2.2000E+01	8.0000E+00	1.0866E+19	7.3050E+00	2.0473E+02	2.8076E-01	7.5521E-01	3.7202E-08	1.5890E-09	2.6032E-09	3.6581E-07
2.4000E+01	6.0000E+00	1.3517E+19	6.4613E+00	1.8106E+02	3.6100E-01	6.9690E-01	4.6277E-08	1.6600E-09	2.9269E-09	4.4396E-07
2.6000E+01	4.0000E+00	1.6664E+19	5.6302E+00	1.5777E+02	4.6349E-01	6.2900E-01	5.7052E-08	3.1231E-09	5.5030E-09	5.8504E-07
2.8000E+01	2.0000E+00	2.0385E+19	4.9810E+00	1.3958E+02	6.1659E-01	5.3970E-01	6.9792E-08	1.4060E-08	2.4006E-08	1.0754E-06

PROPERTIES OF SECOND LINE
WAVENUMBER = 0.9434E+04

SLANT RANGE KM	ALTITUDE KM	DENSITY	SCATTERING TO SENSOR PHOT/KM-STR	DETECTED SCATTERING COUNTS/KM	OPTICAL THICKNESS	TRANSMISSION	MOLECULAR SCATTERING CM-1	AEROSOL SCATTERING CM-1	AEROSOL ABSORPTION CM-1	TOTAL EXTINCTION CM-1
2.0000E+00	2.8000E+01	5.6085E+17	3.2394E+01	1.4049E+02	1.9003E-04	9.9900E-01	2.3314E-11	2.1703E-11	1.3670E-10	1.2353E-09
4.0000E+00	2.6000E+01	7.6682E+17	1.2151E+01	5.2697E+01	5.1397E-04	9.9949E-01	3.1876E-11	3.5710E-11	2.2493E-10	1.9785E-09
6.0000E+00	2.4000E+01	1.0460E+18	7.7025E+00	3.3404E+01	1.0035E-03	9.9900E-01	4.3481E-11	5.3009E-11	3.3309E-10	2.9049E-09
8.0000E+00	2.2000E+01	1.4389E+18	6.6005E+00	2.8625E+01	1.7409E-03	9.9826E-01	5.9814E-11	8.7397E-11	5.5050E-10	4.6905E-09
1.0000E+01	2.0000E+01	1.9771E+18	6.9382E+00	3.0090E+01	2.9968E-03	9.9701E-01	8.2187E-11	1.6021E-10	1.0091E-09	8.3694E-09
1.2000E+01	1.8000E+01	2.7232E+18	7.3601E+00	3.1954E+01	5.2246E-03	9.9479E-01	1.1320E-10	2.5913E-10	1.6322E-09	1.3373E-08
1.4000E+01	1.6000E+01	3.7226E+18	6.1549E+00	2.6692E+01	8.0059E-03	9.9203E-01	1.5474E-10	2.7090E-10	1.7067E-09	1.4286E-08
1.6000E+01	1.4000E+01	5.1312E+18	5.6832E+00	2.4647E+01	1.1050E-02	9.8901E-01	2.1330E-10	3.0325E-10	1.9101E-09	1.6327E-08
1.8000E+01	1.2000E+01	6.8198E+18	5.3442E+00	2.3177E+01	1.4457E-02	9.8564E-01	2.8349E-10	3.3540E-10	2.1132E-09	1.8454E-08
2.0000E+01	1.0000E+01	8.6620E+18	4.8664E+00	2.1105E+01	1.8124E-02	9.8204E-01	3.6007E-10	3.4080E-10	2.1472E-09	1.9351E-08
2.2000E+01	8.0000E+00	1.0866E+19	4.6456E+00	2.0147E+01	2.2160E-02	9.7808E-01	4.5169E-10	3.6454E-10	2.2962E-09	2.1249E-08
2.4000E+01	6.0000E+00	1.3517E+19	4.4609E+00	1.9301E+01	2.6454E-02	9.7389E-01	5.6187E-10	3.8066E-10	2.3975E-09	2.2939E-08
2.6000E+01	4.0000E+00	1.6664E+19	5.6211E+00	2.4370E+01	3.2702E-02	9.6783E-01	6.9269E-10	7.1611E-10	4.5106E-09	4.0121E-08
2.8000E+01	2.0000E+00	2.0385E+19	1.3565E+01	5.8830E+01	4.8940E-02	9.5224E-01	8.4737E-10	3.2250E-09	2.0319E-08	1.6179E-07

ERROR ANALYSIS FOR 1,100,1000 SHOTS BACKSCATTER UNCERTAINTY = 0,50,100%

RANGE KM	1,0%	100,0%	1000,0%	1,50%	100,50%	1000,50%	1,100%	100,100%	1000,100%
2.0000E+00	2.3175E-02	5.7962E-03	5.3869E-03	3.3831E-02	2.5319E-02	2.5290E-02	5.4470E-02	4.9623E-02	4.9587E-02

4.0000E+00	3.9523E-02	6.7931E-03	5.6090E-03	4.9415E-02	3.0429E-02	3.0[illegible]-02	7.1202E-02	5.9710[illegible]-02	5.9594E-02
6.0000E+00	5.1200E-02	7.9536E-03	6.3249E-03	6.0525E-02	3.3243E-02	3.2[illegible]-02	8.2394E-02	6.50[illegible]-02	6.4065E-02
8.0000E+00	5.9434E-02	9.4004E-03	7.5802E-03	7.0957E-02	3.9013E-02	3.94[illegible]-02	9.7594E-02	7.7941E-02	7.7740E-02
1.0000E+01	6.6060E-02	1.1690E-02	9.9100E-03	8.3036E-02	5.2917E-02	5.2[illegible]-02	1.2255E-01	1.0[illegible]-01	1.0369E-01
1.2000E+01	7.0571E-02	1.5412E-02	1.3943E-02	9.3024E-02	6.2536E-02	6.2191E-02	1.4026E-01	1.2[illegible]-01	1.2201E-01
1.4000E+01	7.1480E-02	2.0135E-02	1.9043E-02	8.5204E-02	5.0543E-02	5.0116E-02	1.1708E-01	9.4[illegible]-02	9.4654E-02
1.6000E+01	7.2865E-02	2.6571E-02	2.5772E-02	8.2014E-02	4.6075E-02	4.5619E-02	1.0477E-01	7.96[illegible]-02	7.9573E-02
1.8000E+01	7.6031E-02	3.5223E-02	3.4616E-02	8.2974E-02	4.7142E-02	4.6[illegible]-02	9.9145E-02	7.1[illegible]-02	7.1589E-02
2.0000E+01	8.3877E-02	4.5919E-02	4.5429E-02	8.7542E-02	5.2315E-02	5.1865E-02	9.7717E-02	6.7[illegible]-02	6.7653E-02
2.2000E+01	9.4117E-02	5.9240E-02	5.6836E-02	9.6512E-02	6.2983E-02	6.2590E-02	1.0336E-01	7.30[illegible]-02	7.2719E-02
2.4000E+01	1.0777E-01	7.5376E-02	7.5118E-02	1.0925E-01	7.7481E-02	7.7132E-02	1.1558E-01	8.34[illegible]-02	8.3153E-02
2.6000E+01	1.2947E-01	9.0282E-02	9.7953E-02	1.3333E-01	1.0202E-01	1.0171E-01	1.4056E-01	1.12[illegible]-01	1.1221E-01
2.8000E+01	1.8171E-01	1.4854E-01	1.4831E-01	2.0779E-01	1.7959E-01	1.7931E-01	2.7139E-01	2.50[illegible]-01	2.5026E-01

SENSOR PARAMETERS

SENSOR ALTITUDE	0.20000E+02	KM.
SENSOR ANGLE	-0.90000E+02	DEGREES
TIME	08:05:17	

PROPERTIES OF FIRST LINE
WAVENUMBER = 0.2833E+05

SLANT RANGE KM	ALTITUDE KM	DENSITY CM-3	SCATTERING TO SENSOR PHOT/KM-STR	DETECTED SCATTERING COUNTS/KM	OPTICAL THICKNESS	TRANSMISSION	MOLECULAR SCATTERING CM-1	AEROSOL SCATTERING CM-1	AEROSOL ADSORPTION CM-1	TOTAL EXTINCTION CM-1
2.0000E+00	1.0000E+01	2.7232E+18	4.0139E+02	1.1240E+04	1.9390E-02	9.8031E-01	9.3234E-09	1.1301E-09	1.9927E-09	1.1736E-07
4.0000E+00	1.6000E+01	3.7226E+18	1.2631E+02	3.5535E+03	4.6307E-02	9.5475E-01	1.2745E-08	1.1017E-09	2.0[illegible]-09	1.4768E-07
6.0000E+00	1.4000E+01	5.1312E+18	7.1455E+01	2.0023E+03	8.0056E-02	9.2306E-01	1.7560E-08	1.3[illegible]-09	2.3319E-09	1.9281E-07
8.0000E+00	1.2000E+01	6.0190E+18	4.8360E+01	1.3554E+03	1.2304E-01	8.8352E-01	2.3349E-08	1.4551E-09	2.5798E-09	2.4593E-07
1.0000E+01	1.0000E+01	8.6620E+18	3.4801E+01	9.7745E+02	1.7777E-01	8.3714E-01	2.9656E-08	1.4307E-09	2.6214E-09	2.9931E-07
1.2000E+01	8.0000E+00	1.0066E+19	2.6431E+01	7.4066E+02	2.4396E-01	7.0352E-01	3.7202E-08	1.580[illegible]-09	2.[illegible]E-09	3.6581E-07
1.4000E+01	6.0000E+00	1.3517E+19	2.0438E+01	5.7273E+02	3.2421E-01	7.2310E-01	4.6277E-08	1.6[illegible]-09	2.9[illegible]E-09	4.4390E-07
1.6000E+01	4.0000E+00	1.6664E+19	1.6002E+01	4.4043E+02	4.2670E-01	6.5200E-01	5.7052E-08	3.1251E-09	5.50[illegible]E-09	5.8504E-07
1.8000E+01	2.0000E+00	2.0305E+19	1.2973E+01	3.6354E+02	5.7000E-01	5.0001E-01	6.9792E-08	1.4[illegible]	[illegible]E-09	1.0754E-06

PROPERTIES OF SECOND LINE
WAVENUMBER = 0.9434E+04

SLANT RANGE KM	ALTITUDE KM	DENSITY	SCATTERING TO SENSOR PHOT/KM-STR	DETECTED SCATTERING COUNTS/KM	OPTICAL THICKNESS	TRANSMISSION	MOLECULAR SCATTERING CM-1	AEROSOL SCATTERING CM-1	AEROSOL ABSORPTION CM-1	TOTAL EXTINCTION CM-1
2.0000E+00	1.8000E+01	2.7232E+18	2.6685E+02	1.1573E+03	2.2270E-03	9.9777E-01	1.1320E-10	2.591[illegible]E-10	1.6322E-09	1.3373E-08
4.0000E+00	1.6000E+01	3.7226E+18	7.5050E+01	3.2095E+02	5.0091E-03	9.9500E-01	1.5474E-10	2.709[illegible]E-10	1.7067E-09	1.4286E-08
6.0000E+00	1.4000E+01	5.1312E+18	4.0657E+01	1.7632E+02	8.0530E-03	9.9198E-01	2.1330E-10	3.0325E-10	1.9101E-09	1.6323E-08
8.0000E+00	1.2000E+01	6.0190E+18	2.7218E+01	1.1004E+02	1.1470E-02	9.8860E-01	2.0349E-10	3.354[illegible]E-10	2.1132E-09	1.8454E-08
1.0000E+01	1.0000E+01	8.6620E+18	1.9503E+01	8.4927E+01	1.5127E-02	9.8499E-01	3.6007E-10	3.40[illegible]E-10	2.1472E-09	1.9351E-08
1.2000E+01	8.0000E+00	1.0866E+19	1.5708E+01	6.0123E+01	1.9163E-02	9.8102E-01	4.5169E-10	3.645[illegible]E-10	2.2962E-09	2.1249E-08
1.4000E+01	6.0000E+00	1.3517E+19	1.3212E+01	5.7290E+01	2.3457E-02	9.7682E-01	5.6187E-10	3.806[illegible]E-10	2.3975E-09	2.2939E-08
1.6000E+01	4.0060E+00	1.6664E+19	1.4933E+01	6.4759E+01	2.9705E-02	9.7073E-01	6.9269E-10	7.1611E-10	4.5106E-09	4.0121E-08
1.8000E+01	2.0000E+00	2.0385E+19	3.3022E+01	1.4321E+02	4.5943E-02	9.5510E-01	8.4737E-10	3.2258E-09	2.0319E-08	1.6179E-07

ERROR ANALYSIS FOR 1.100.1000 SHOTS BACKSCATTER UNCERTAINTY - 0.50.100%

RANGE KM	1.0%	100.0%	1000.0%	1.50%	100.50%	1000.50%	1.100%	100.100%	1000.100%
2.0000E+00	1.3130E-02	7.0126E-03	6.9323E-03	6.2013E-02	6.1012E-02	6.1003E-02	1.2192E-01	1.2142E-01	1.2141E-01
4.0000E+00	2.2195E-02	1.1579E-02	1.1438E-02	5.1398E-02	4.7784E-02	4.7749E-02	9.5338E-02	9.3439E-02	9.3422E-02
6.0000E+00	3.0562E-02	1.8181E-02	1.8029E-02	4.8487E-02	4.1803E-02	4.1737E-02	8.1251E-02	7.7448E-02	7.7413E-02
8.0000E+00	3.9839E-02	2.7008E-02	2.6863E-02	5.0634E-02	4.1365E-02	4.1271E-02	7.4256E-02	6.8236E-02	6.8179E-02
1.0000E+01	5.0792E-02	3.7863E-02	3.7725E-02	5.6640E-02	4.5408E-02	4.5293E-02	7.1365E-02	6.2823E-02	6.2740E-02
1.2000E+01	6.4120E-02	5.1299E-02	5.1167E-02	6.7587E-02	5.5571E-02	5.5450E-02	7.7057E-02	6.6767E-02	6.6666E-02
1.4000E+01	8.0222E-02	6.7516E-02	6.7390E-02	8.2202E-02	6.9058E-02	6.9736E-02	8.7876E-02	7.6454E-02	7.6342E-02
1.6000E+01	1.0323E-01	9.0307E-02	9.0181E-02	1.0680E-01	9.4364E-02	9.4243E-02	1.1685E-01	1.0560E-01	1.0550E-01
1.8000E+01	1.5394E-01	1.3959E-01	1.3945E-01	1.8400E-01	1.7217E-01	1.7206E-01	2.5364E-01	2.4519E-01	2.4511E-01

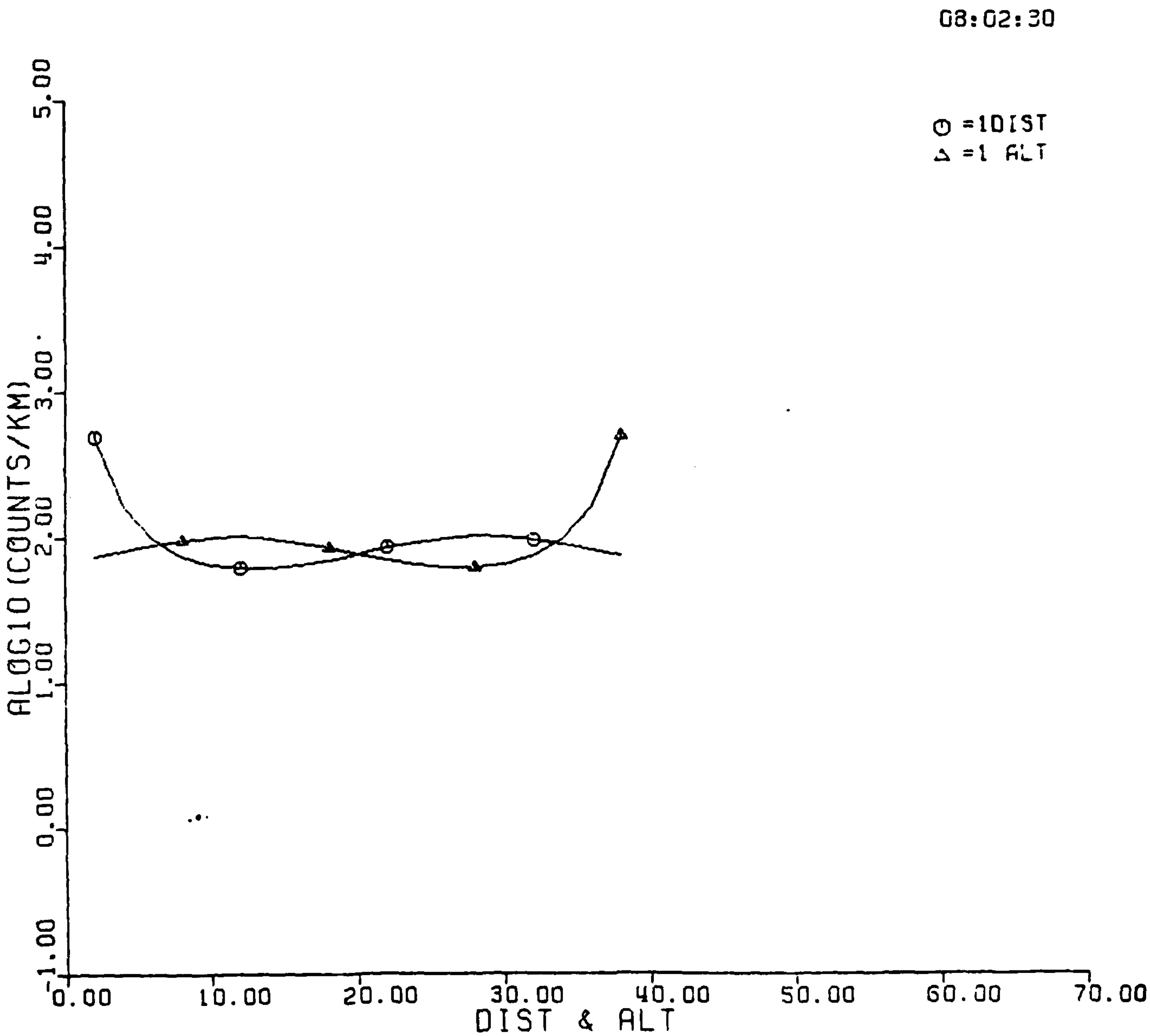
08:02:30
⊙ =1DIST
Δ =1 ALT
5.00
4.00
3.00
2.00
1.00
0.00
-1.00
ALOG10(COUNTS/KM)
0.00
10.00
20.00
30.00
40.00
50.00
60.00
70.00
DIST & ALT

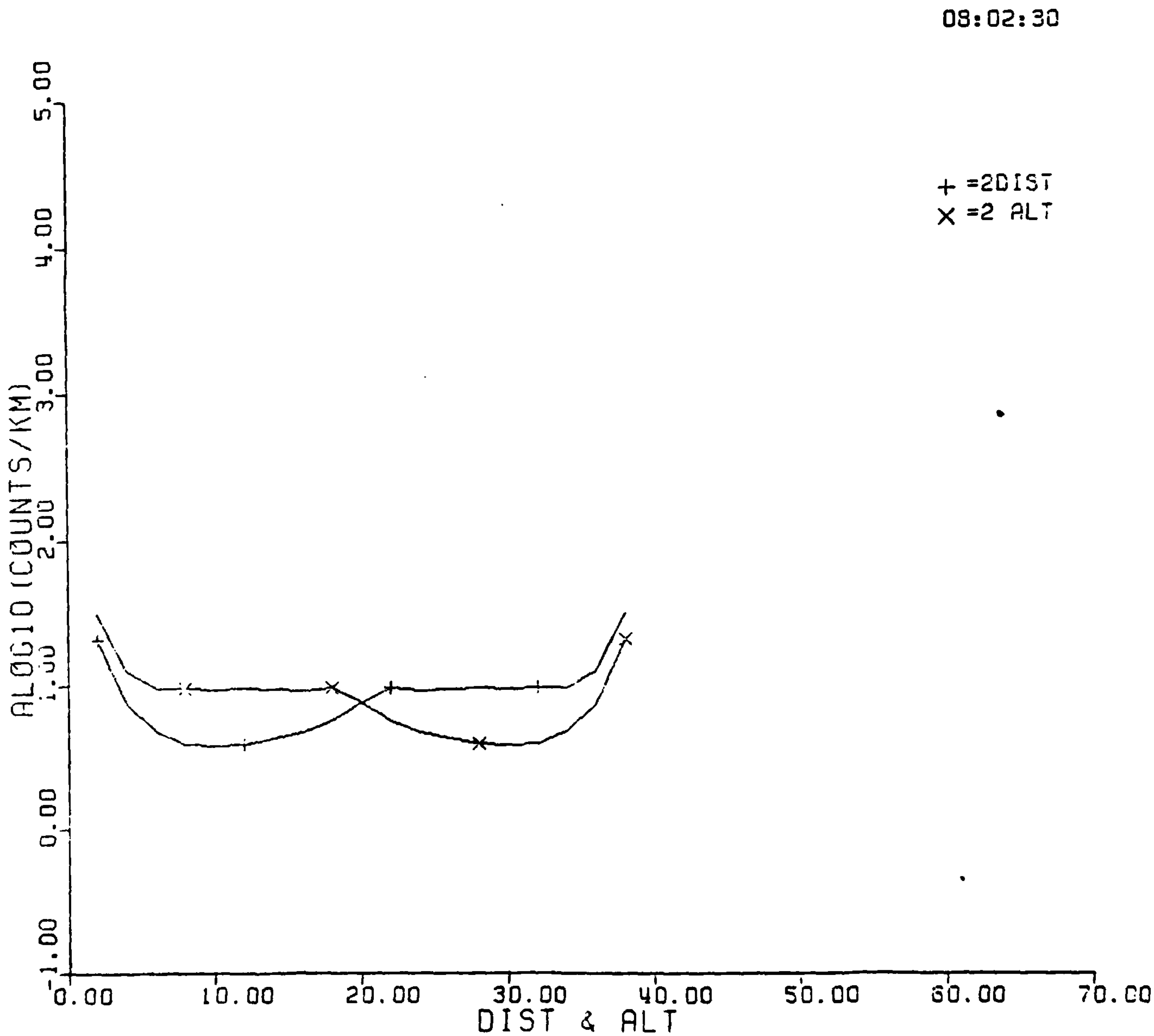

08:02:30
+ =2DIST
× =2 ALT
ALOG10(COUNTS/KM)
5.00
4.00
3.00
2.00
1.00
0.00
-1.00
0.00
10.00
20.00
30.00
40.00
50.00
60.00
70.00
DIST & ALT

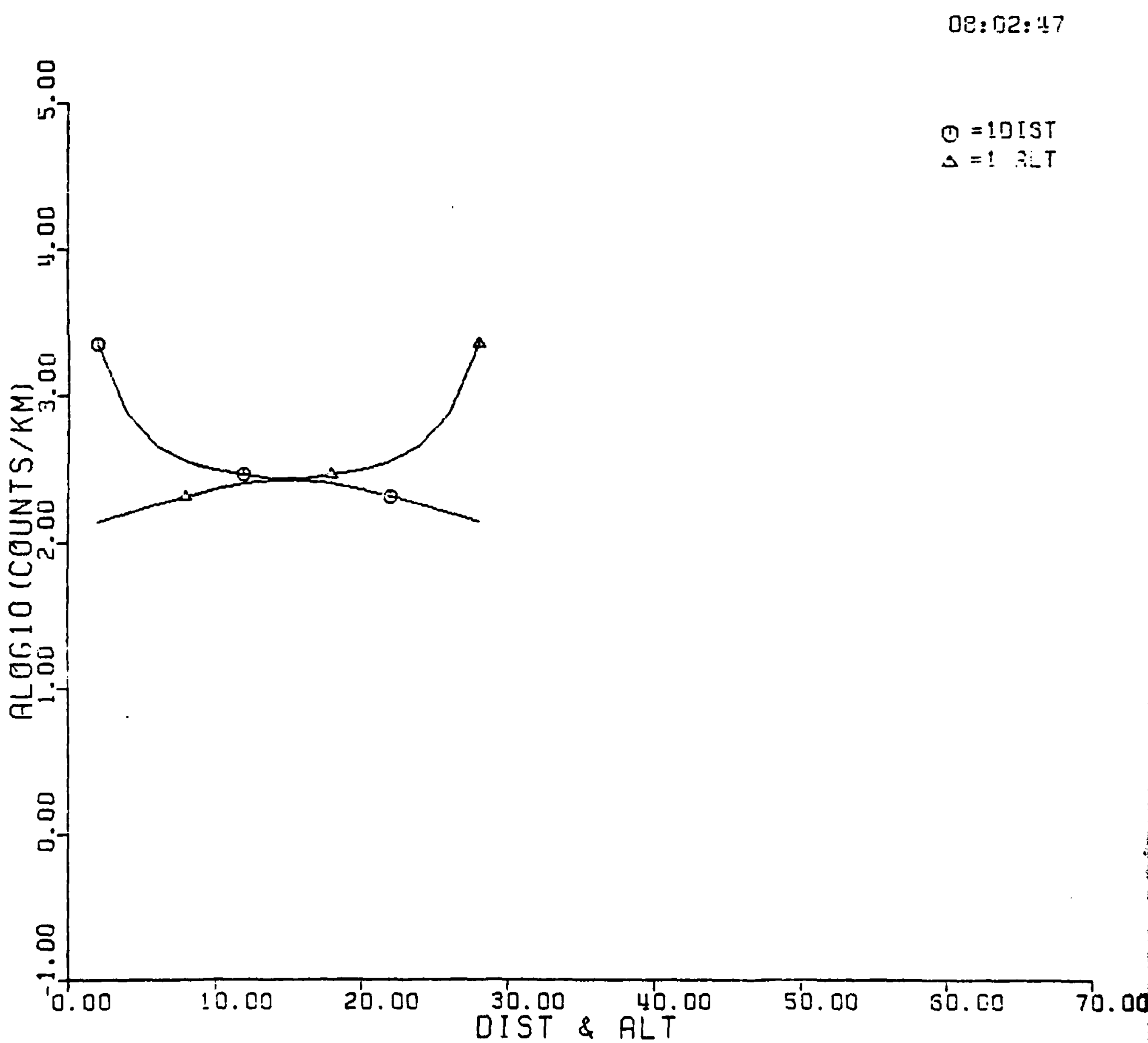

08:02:47
ʘ =1DIST
△ =1 ALT
5.00
4.00
3.00
2.00
1.00
0.00
-1.00
ALOG10(COUNTS/KM)
0.00
10.00
20.00
30.00
40.00
50.00
60.00
70.00
DIST & ALT

08:02:47

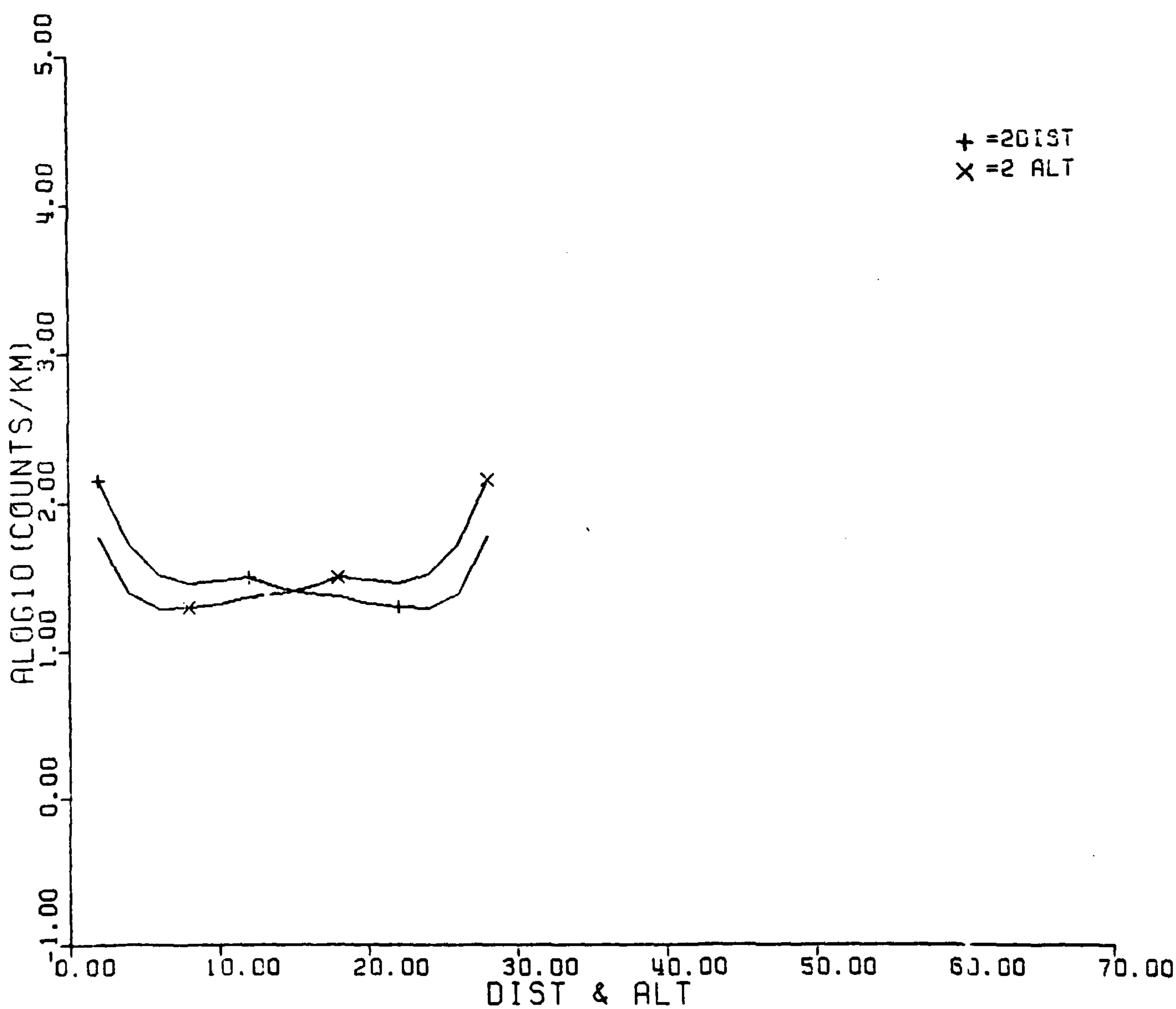

+ =2DIST
× =2 ALT
ALOG10(COUNTS/KM)
5.00
4.00
3.00
2.00
1.00
0.00
-1.00
0.00
10.00
20.00
30.00
40.00
50.00
60.00
70.00
DIST & ALT

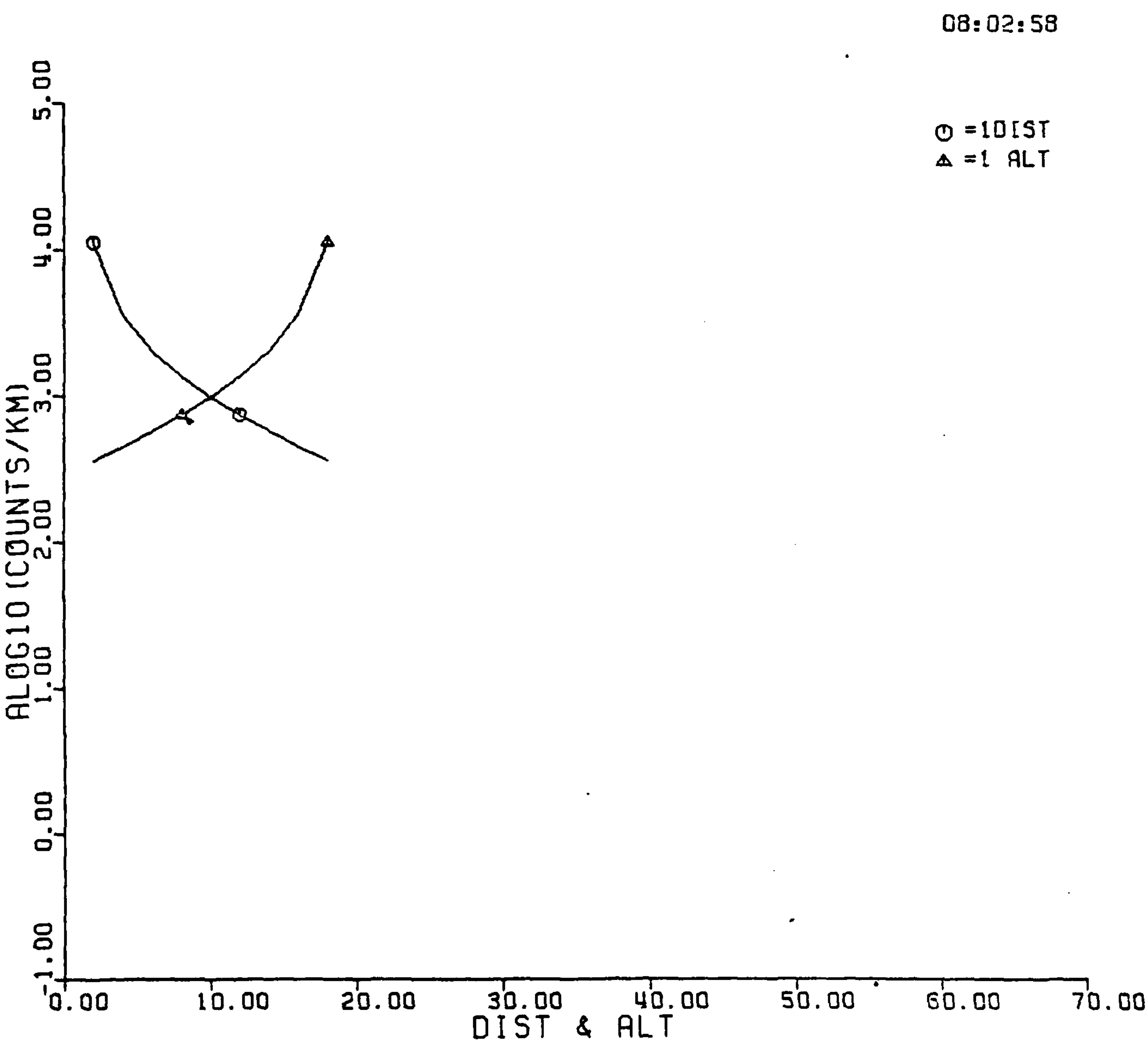

08:02:58
⊙ =1DIST
△ =1 ALT
ALOG10(COUNTS/KM)
5.00
4.00
3.00
2.00
1.00
0.00
-1.00
0.00
10.00
20.00
30.00
40.00
50.00
60.00
70.00
DIST & ALT

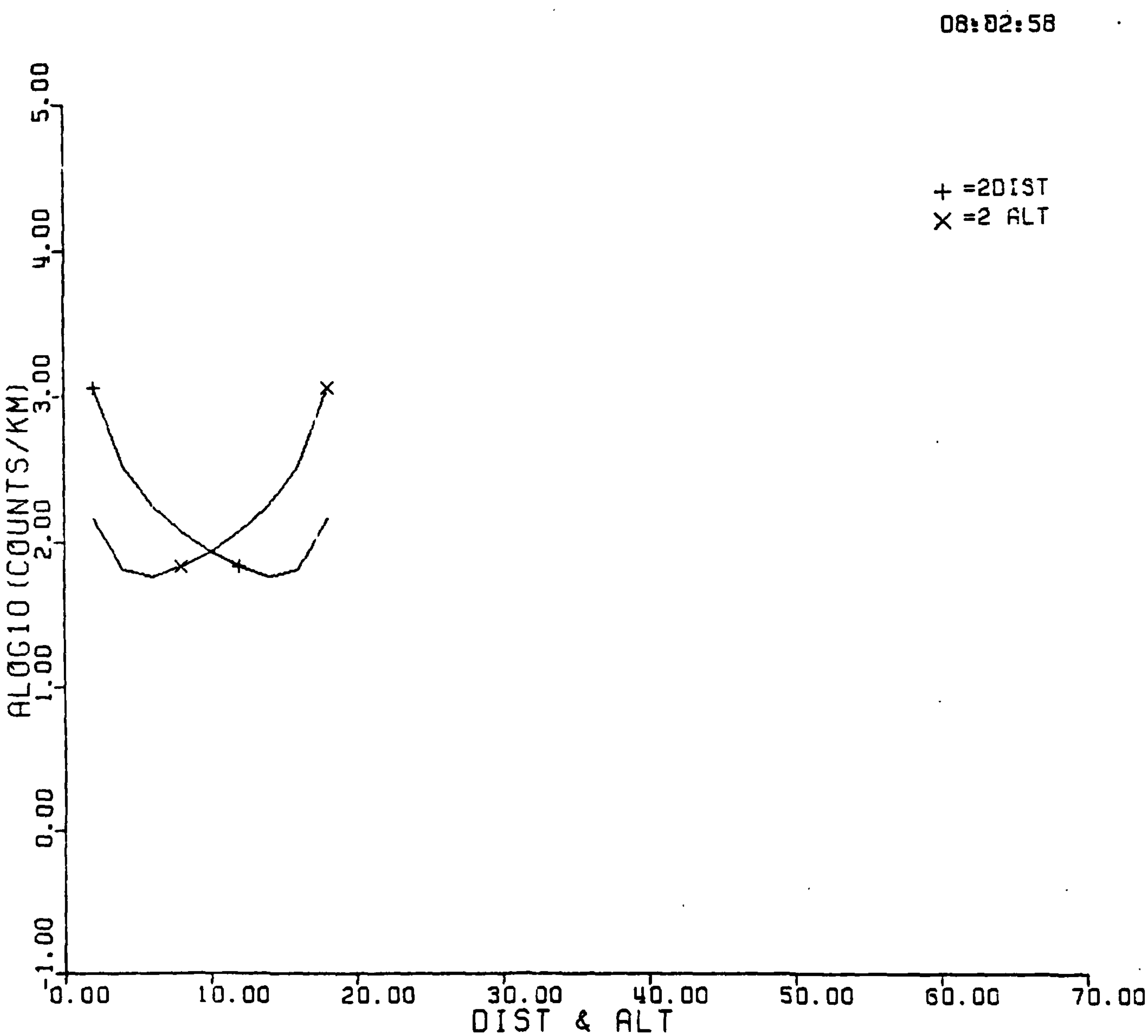
08:02:58
+ =2DIST
X =2 ALT
ALOG10(COUNTS/KM)
5.00
4.00
3.00
2.00
1.00
0.00
-1.00
0.00
10.00
20.00
30.00
40.00
50.00
60.00
70.00
DIST & ALT

08:04:45

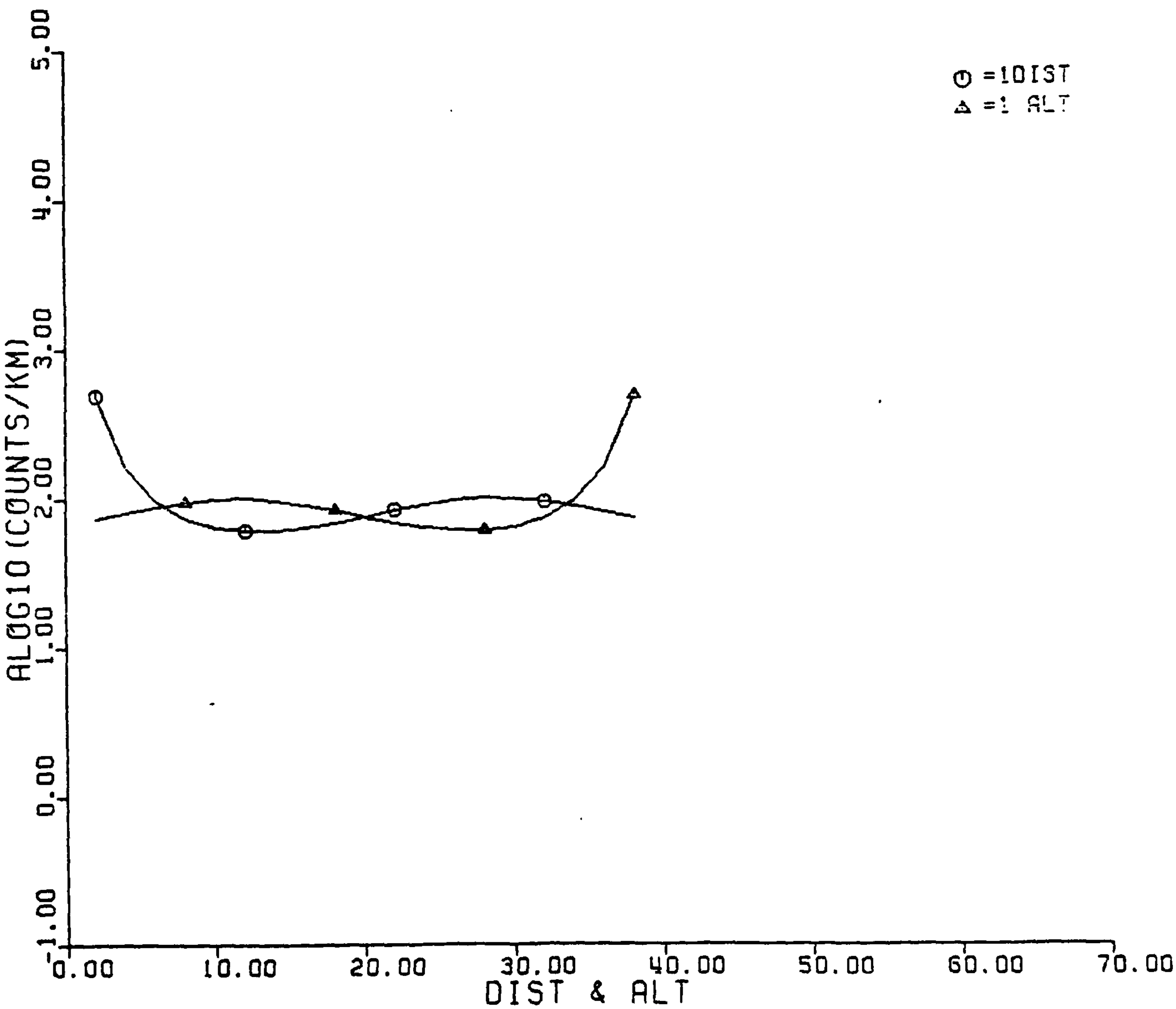

⊙ =1DIST
△ =1 ALT
5.00
4.00
3.00
2.00
1.00
0.00
-1.00
ALOG10(COUNTS/KM)
0.00
10.00
20.00
30.00
40.00
50.00
60.00
70.00
DIST & ALT

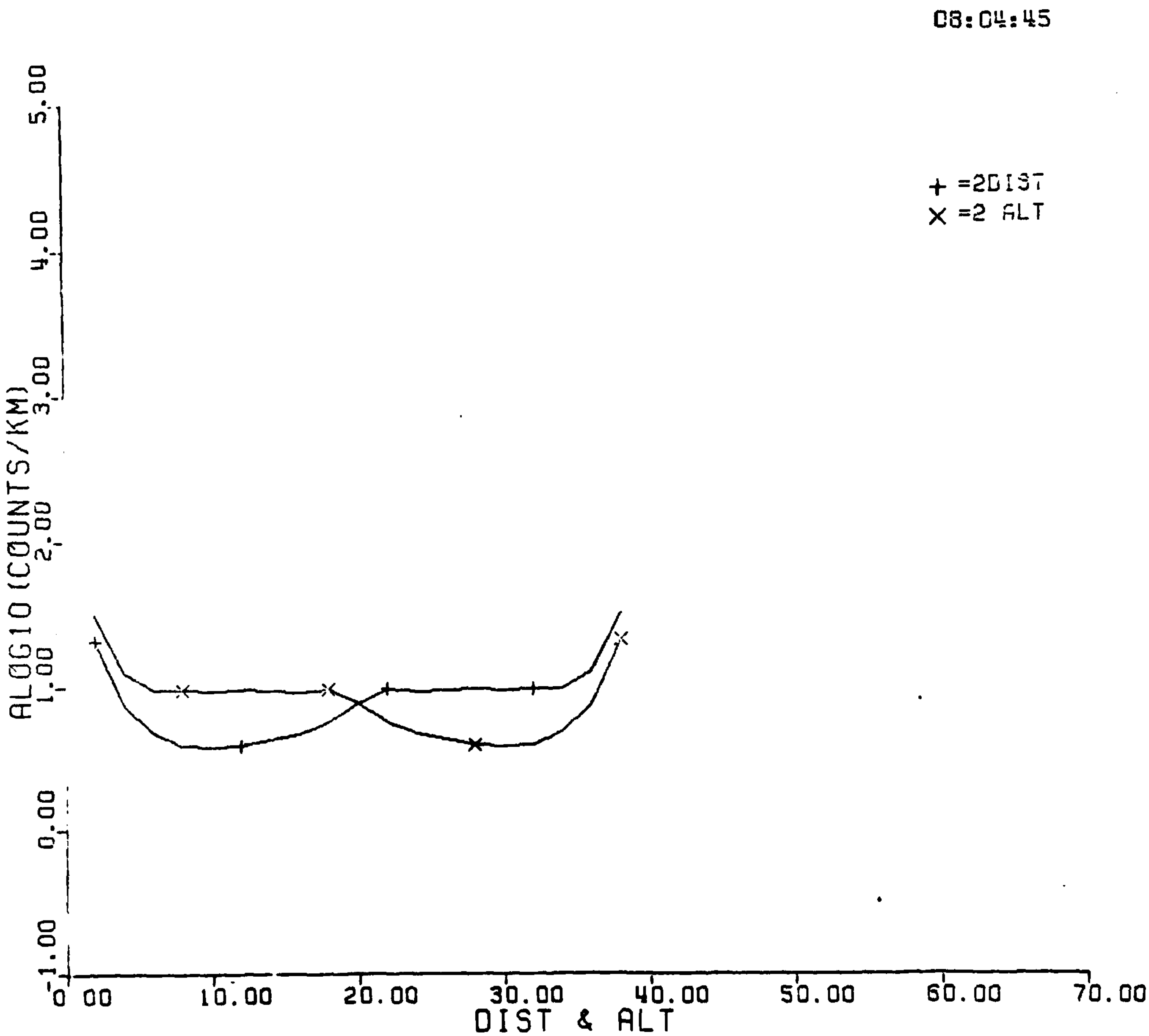

08:04:45
+ =2DIST
× =2 ALT
ALOG10(COUNTS/KM)
5.00
4.00
3.00
2.00
1.00
0.00
-1.00
0.00
10.00
20.00
30.00
40.00
50.00
60.00
70.00
DIST & ALT

08:04:59

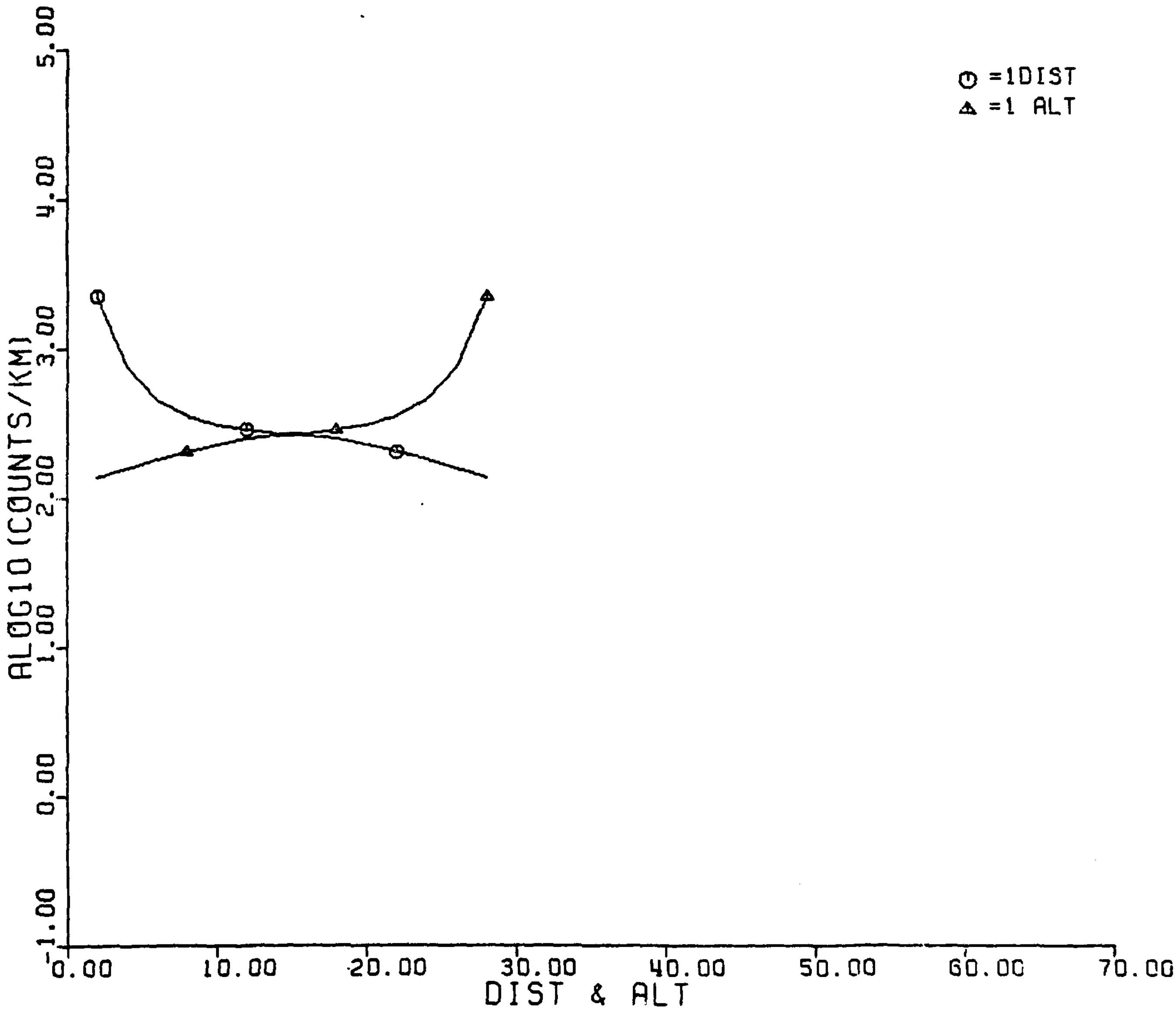

ALOG10 (COUNTS/KM)
5.00
4.00
3.00
2.00
1.00
0.00
-1.00
0.00
10.00
20.00
30.00
40.00
50.00
60.00
70.00
DIST & ALT
⊙ =1DIST
△ =1 ALT

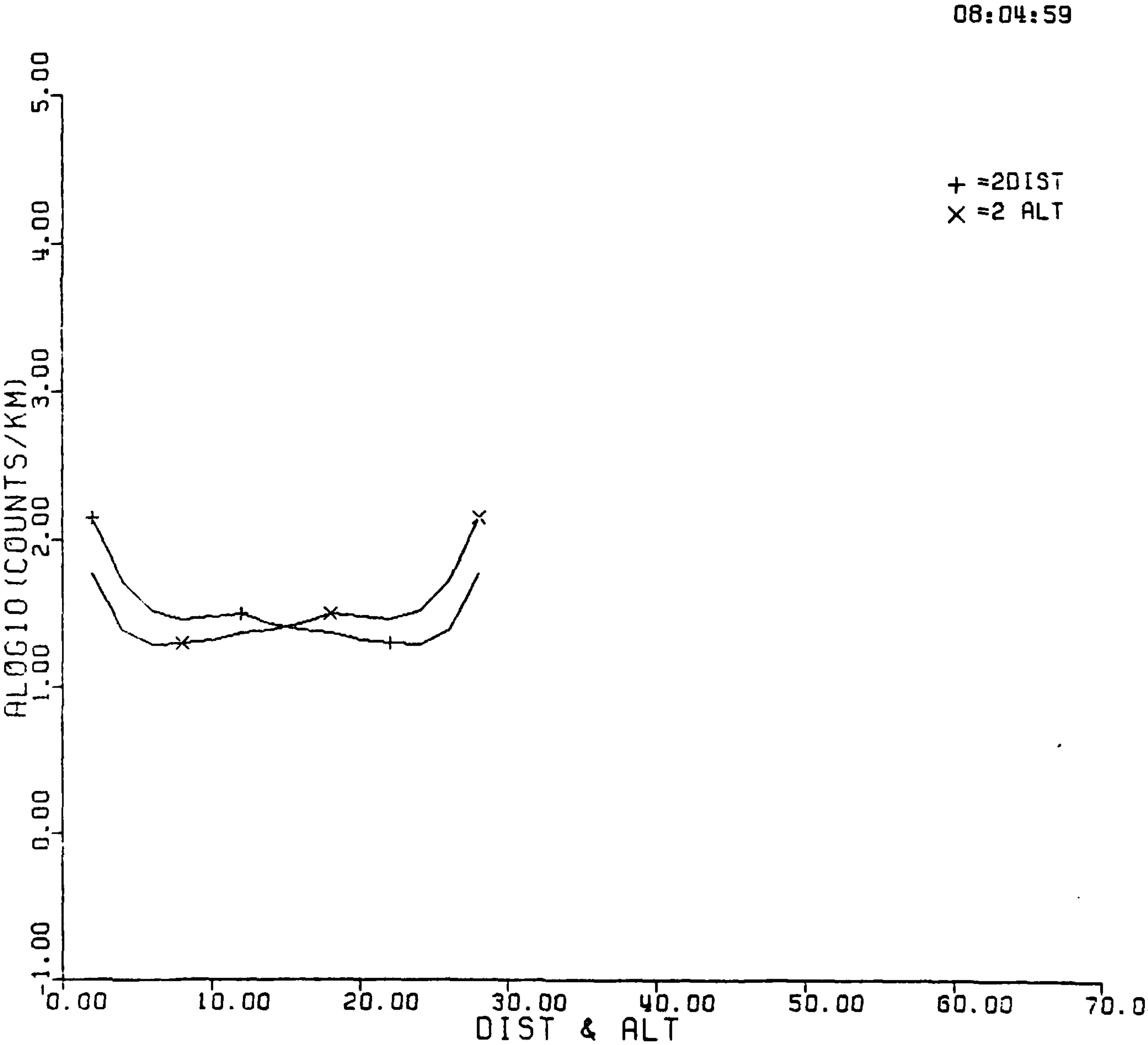

08:04:59
+ =2DIST
X =2 ALT
ALOG10(COUNTS/KM)
5.00
4.00
3.00
2.00
1.00
0.00
-1.00
0.00
10.00
20.00
30.00
40.00
50.00
60.00
70.00
DIST & ALT

08:05:17

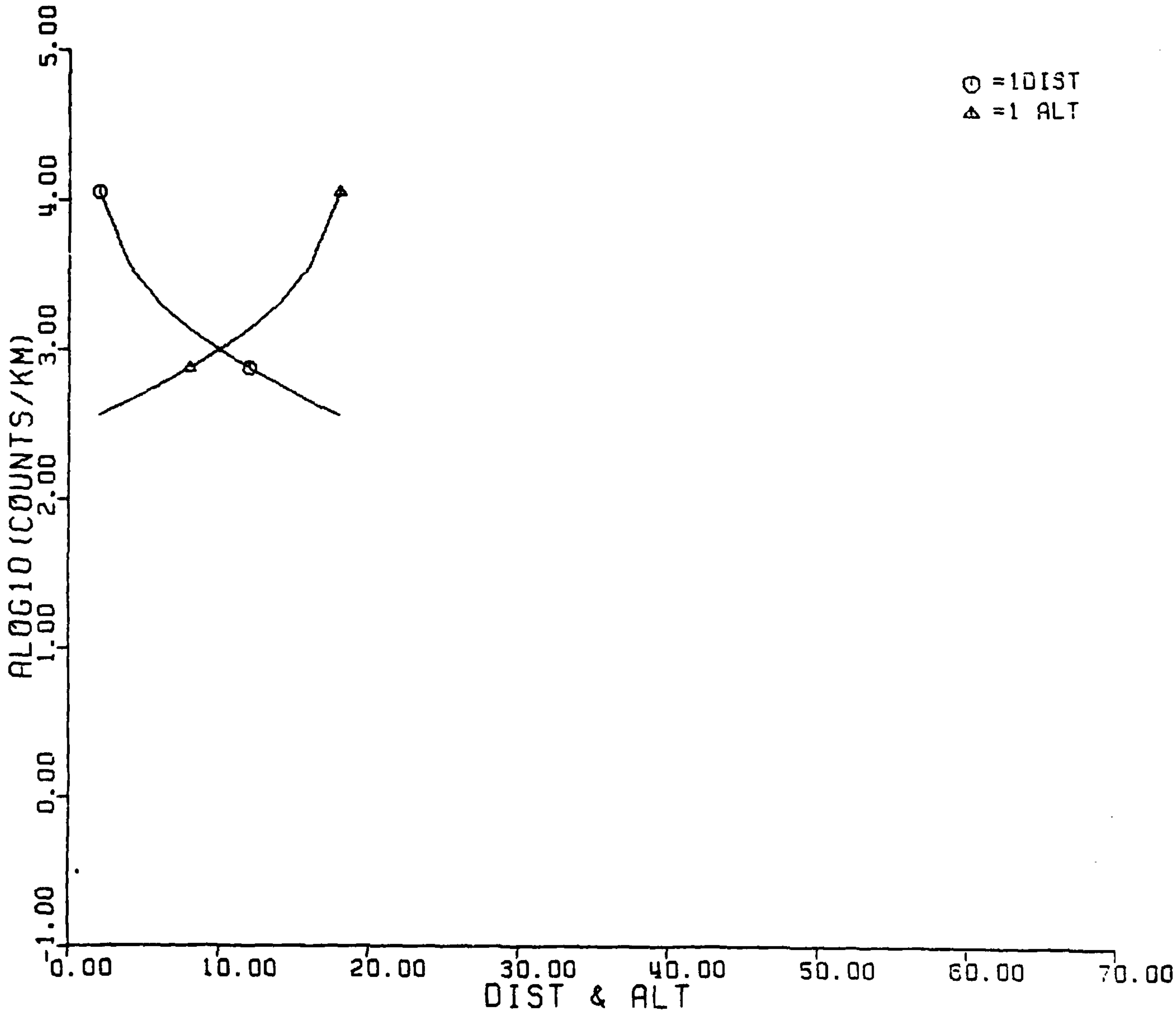

ALOG10(COUNTS/KM)
5.00
4.00
3.00
2.00
1.00
0.00
-1.00
0.00
10.00
20.00
30.00
40.00
50.00
60.00
70.00
DIST & ALT
⊙ =1DIST
△ =1 ALT

08:05:17

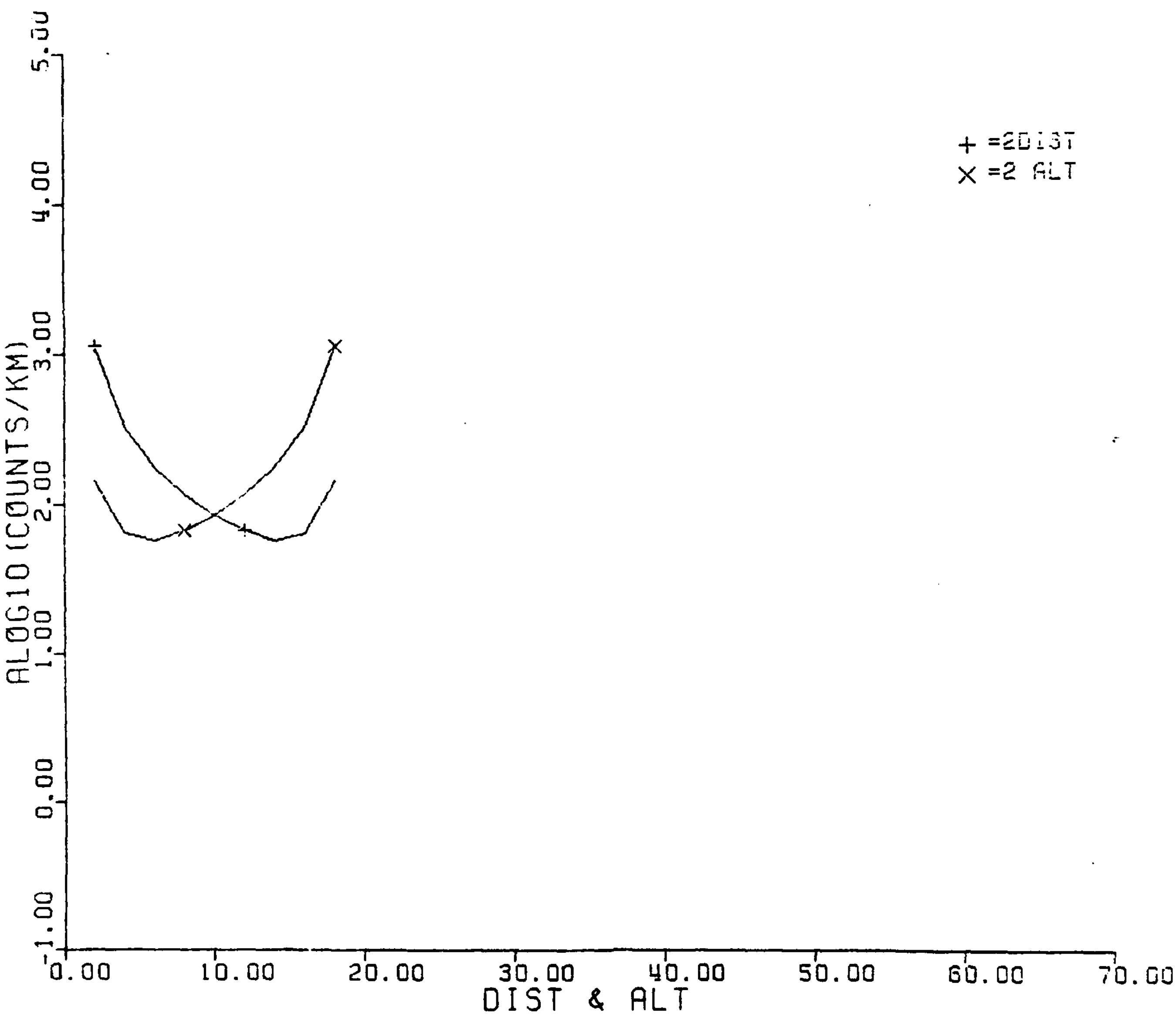

+ =2DIST
× =2 ALT
ALOG10(COUNTS/KM)
5.00
4.00
3.00
2.00
1.00
0.00
-1.00
0.00
10.00
20.00
30.00
40.00
50.00
60.00
70.00
DIST & ALT

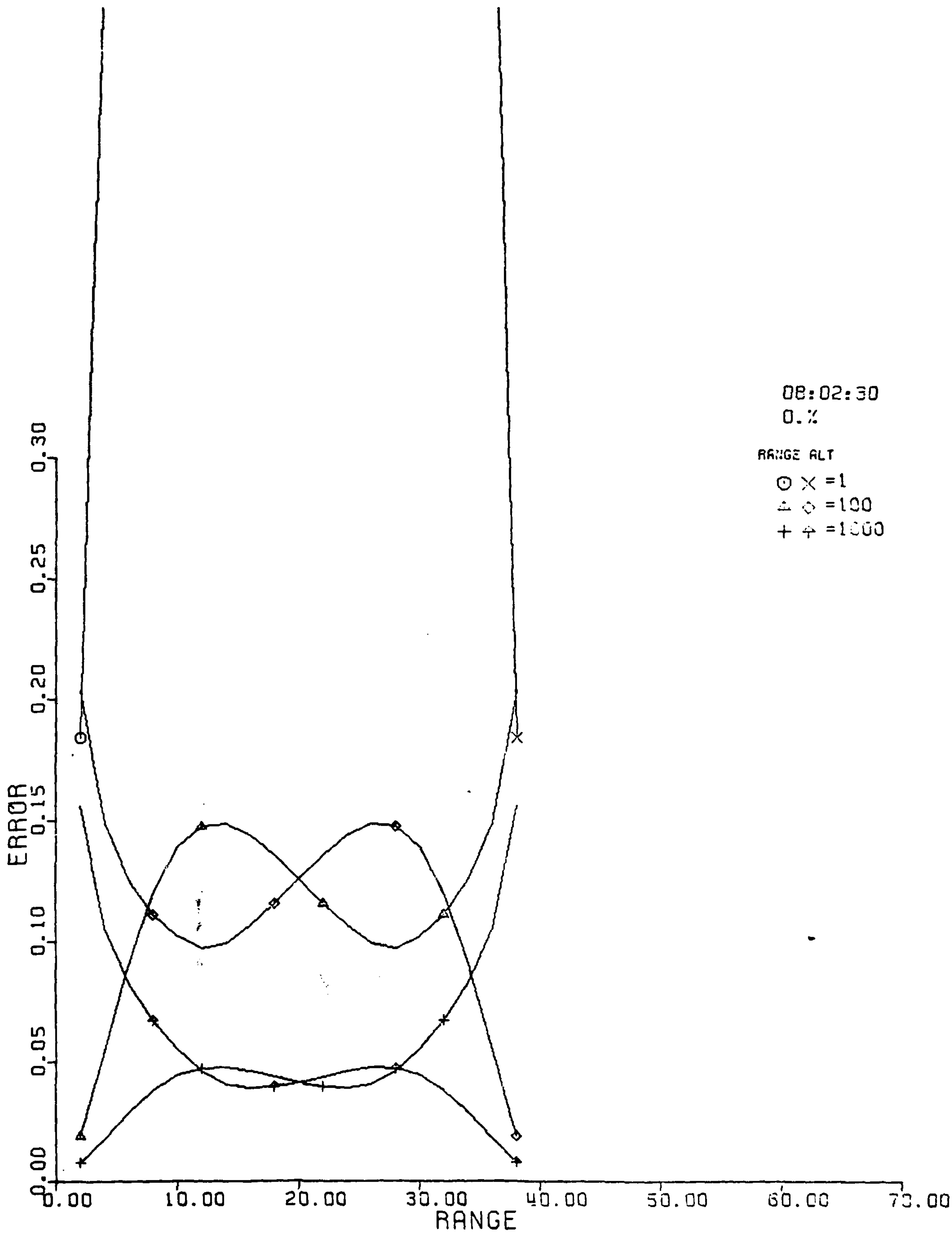
08:02:30
0.%
RANGE ALT
=1
=100
=1000
ERROR
0.00
0.05
0.10
0.15
0.20
0.25
0.30
0.00
10.00
20.00
30.00
40.00
50.00
60.00
70.00
RANGE

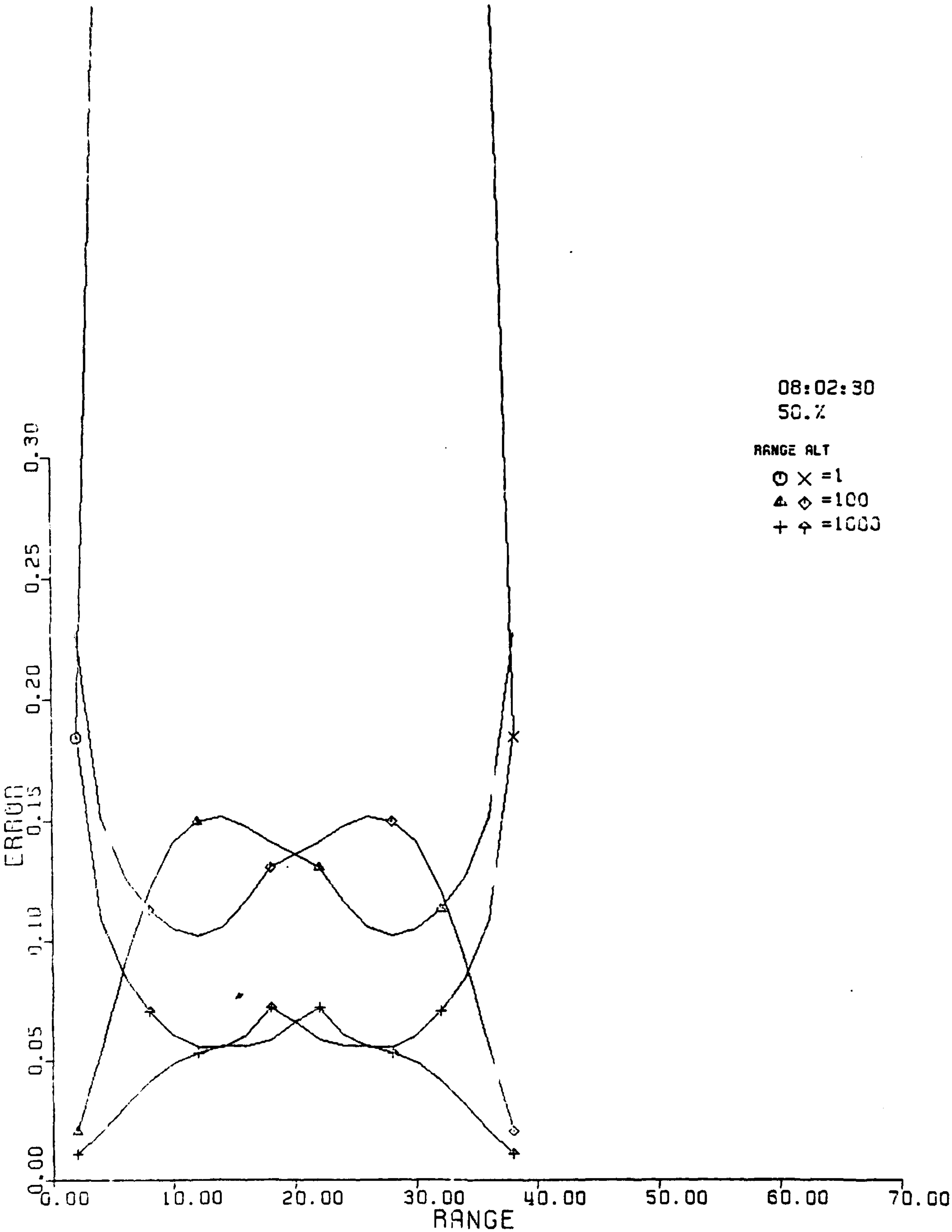
08:02:30
50.%
RANGE ALT
=1
=100
=1000
ERROR
0.00
0.05
0.10
0.15
0.20
0.25
0.30
0.00
10.00
20.00
30.00
40.00
50.00
60.00
70.00
RANGE

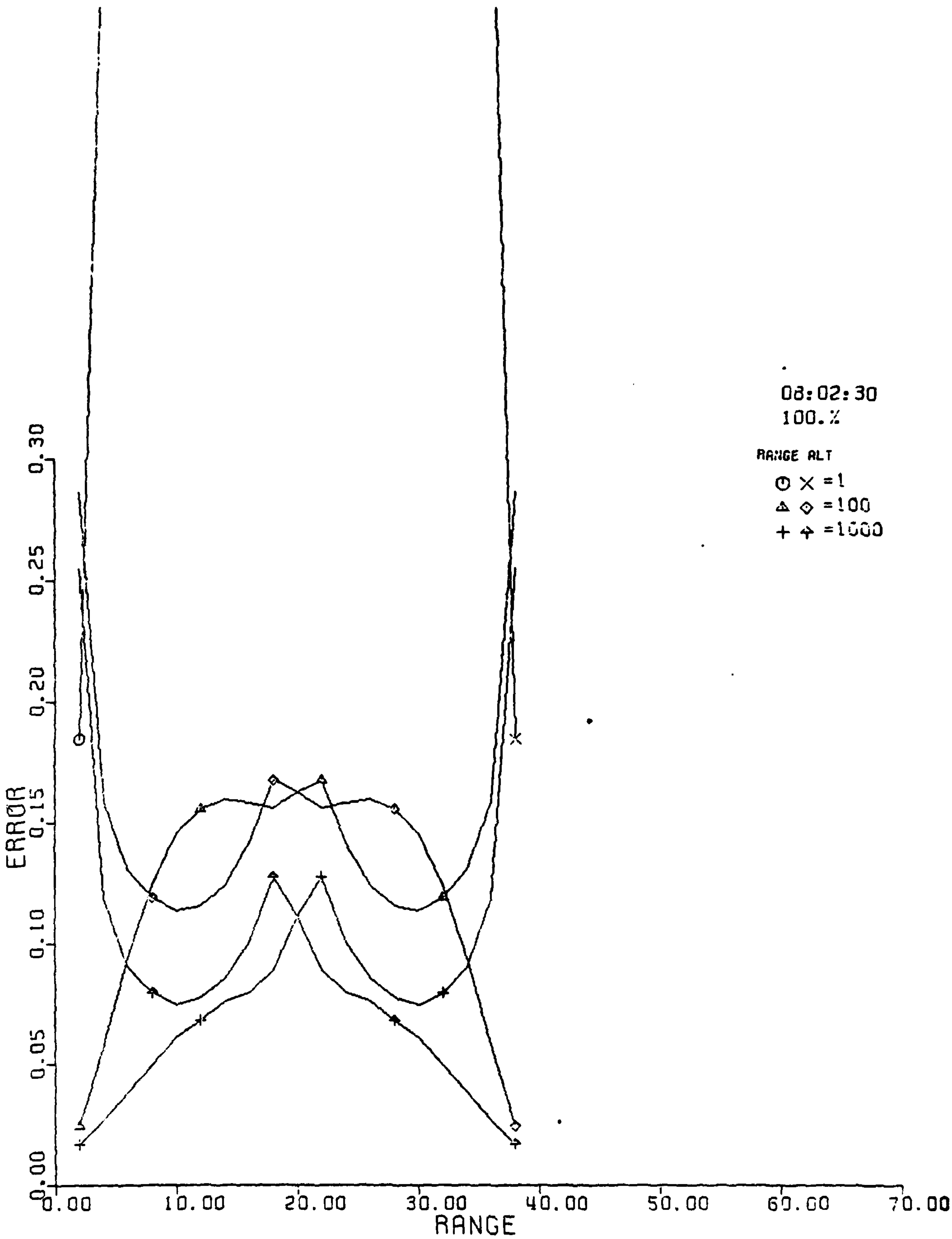
08:02:30
100.%
RANGE ALT
= 1
= 100
= 1000
ERROR
0.00
0.05
0.10
0.15
0.20
0.25
0.30
RANGE
0.00
10.00
20.00
30.00
40.00
50.00
60.00
70.00

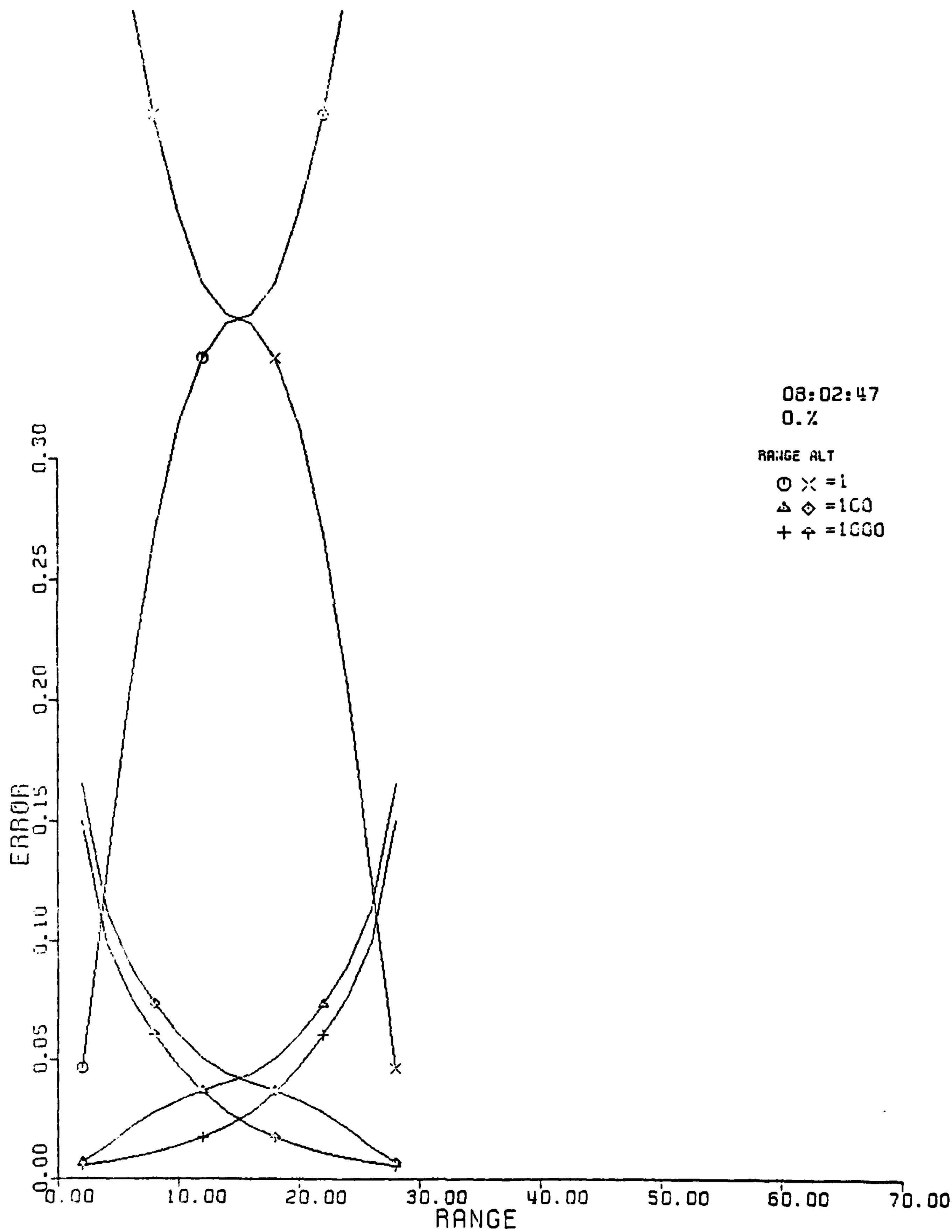
08:02:47
0.%
RANGE ALT
=1
=100
=1000
ERROR
0.00
0.05
0.10
0.15
0.20
0.25
0.30
0.00
10.00
20.00
30.00
40.00
50.00
60.00
70.00
RANGE

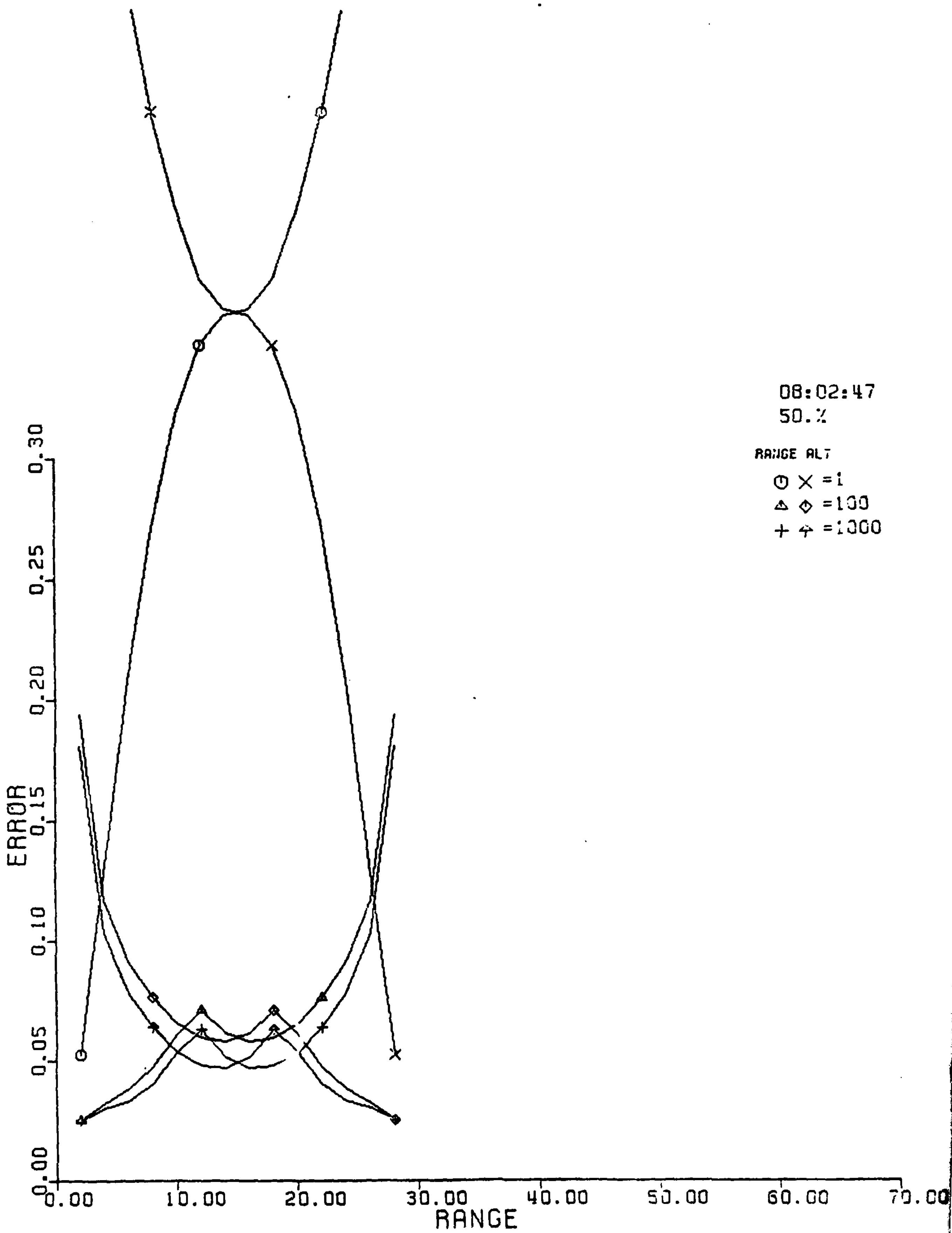
08:02:47
50.%
RANGE ALT
=1
=100
=1000
ERROR
0.00
0.05
0.10
0.15
0.20
0.25
0.30
0.00
10.00
20.00
30.00
40.00
50.00
60.00
70.00
RANGE

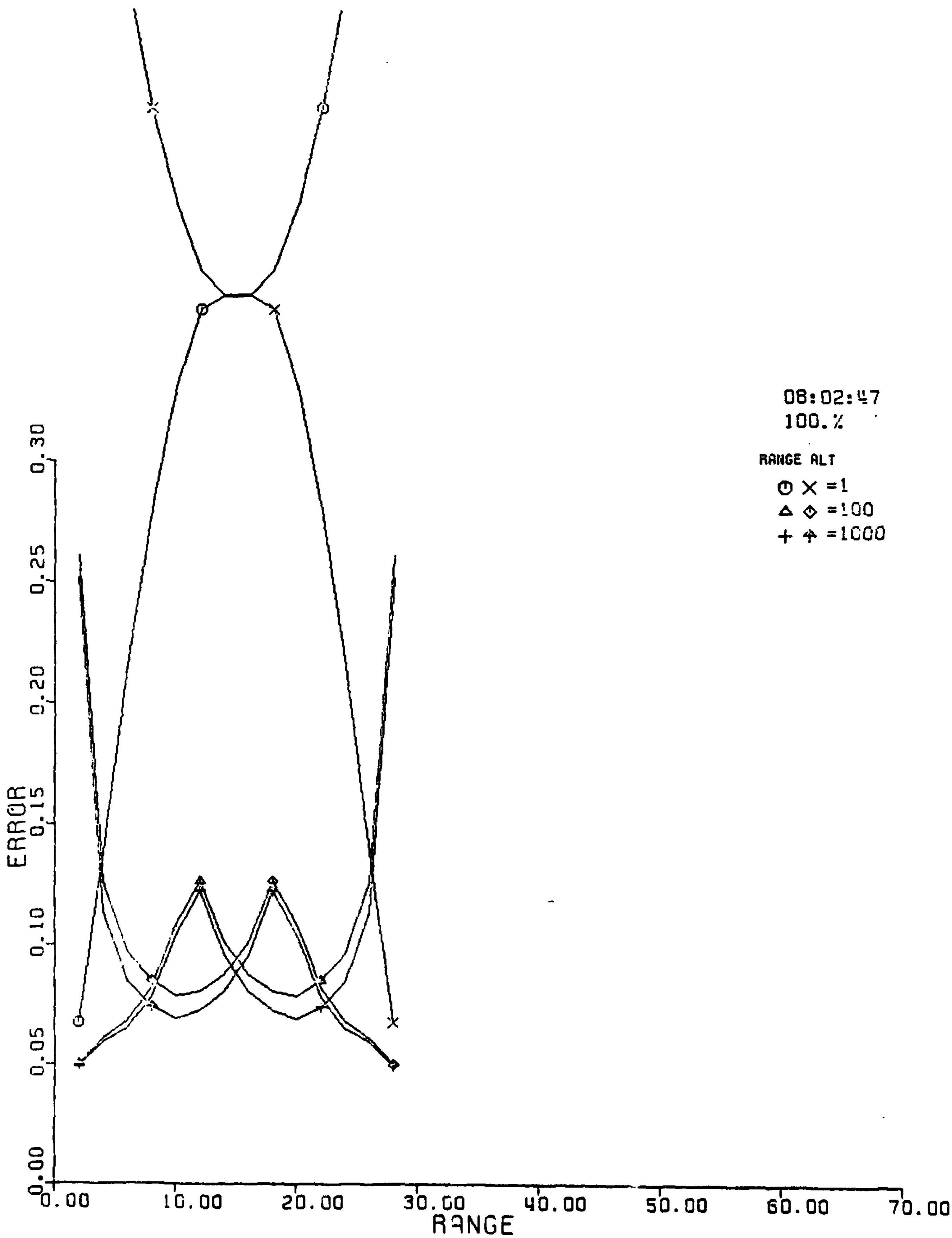
08:02:47
100.%
RANGE ALT
=1
=100
=1000
ERROR
0.00
0.05
0.10
0.15
0.20
0.25
0.30
0.00
10.00
20.00
30.00
40.00
50.00
60.00
70.00
RANGE

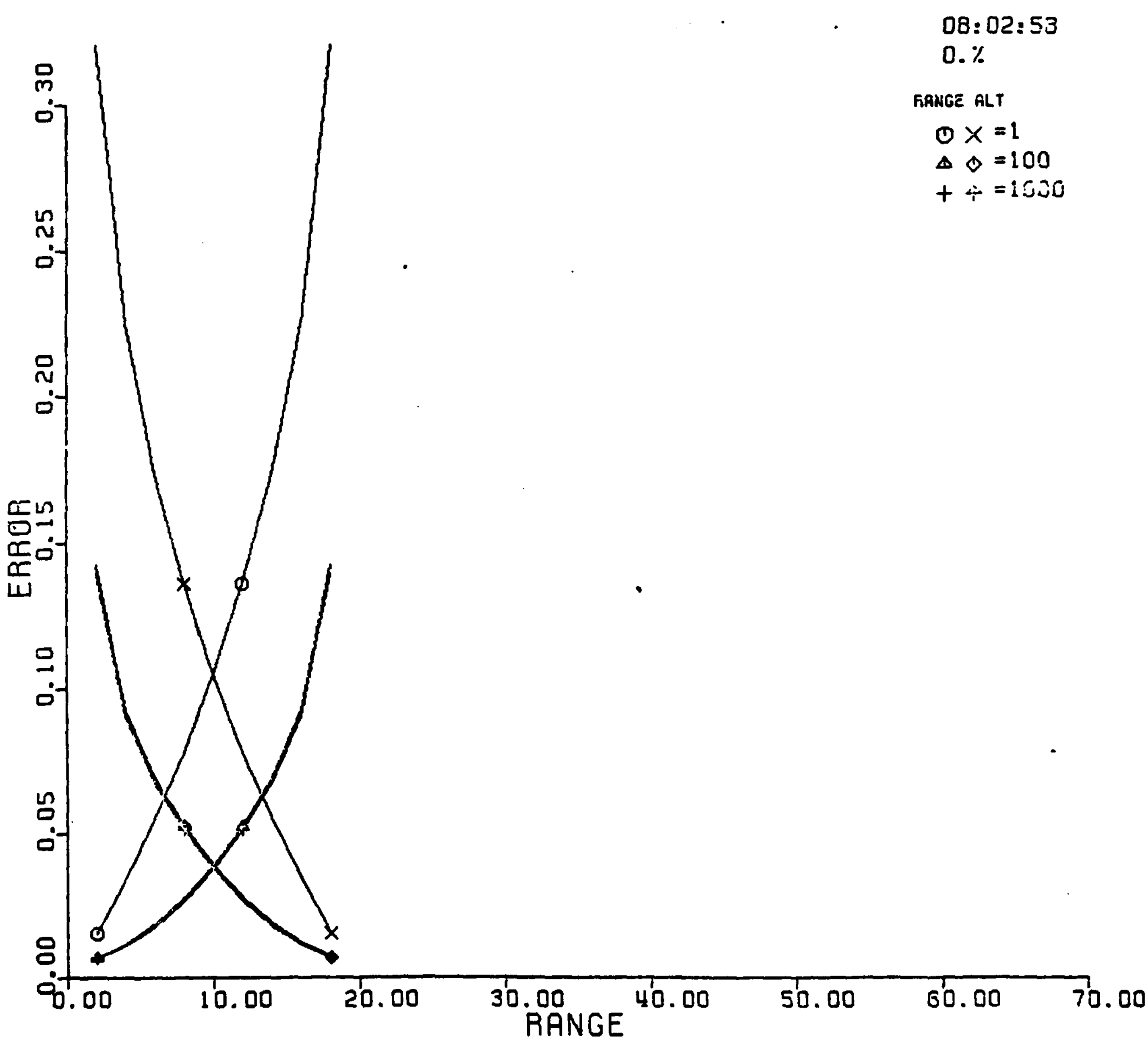
08:02:53
0.%
RANGE ALT
=1
=100
=1000
ERROR
0.00
0.05
0.10
0.15
0.20
0.25
0.30
0.00
10.00
20.00
30.00
40.00
50.00
60.00
70.00
RANGE

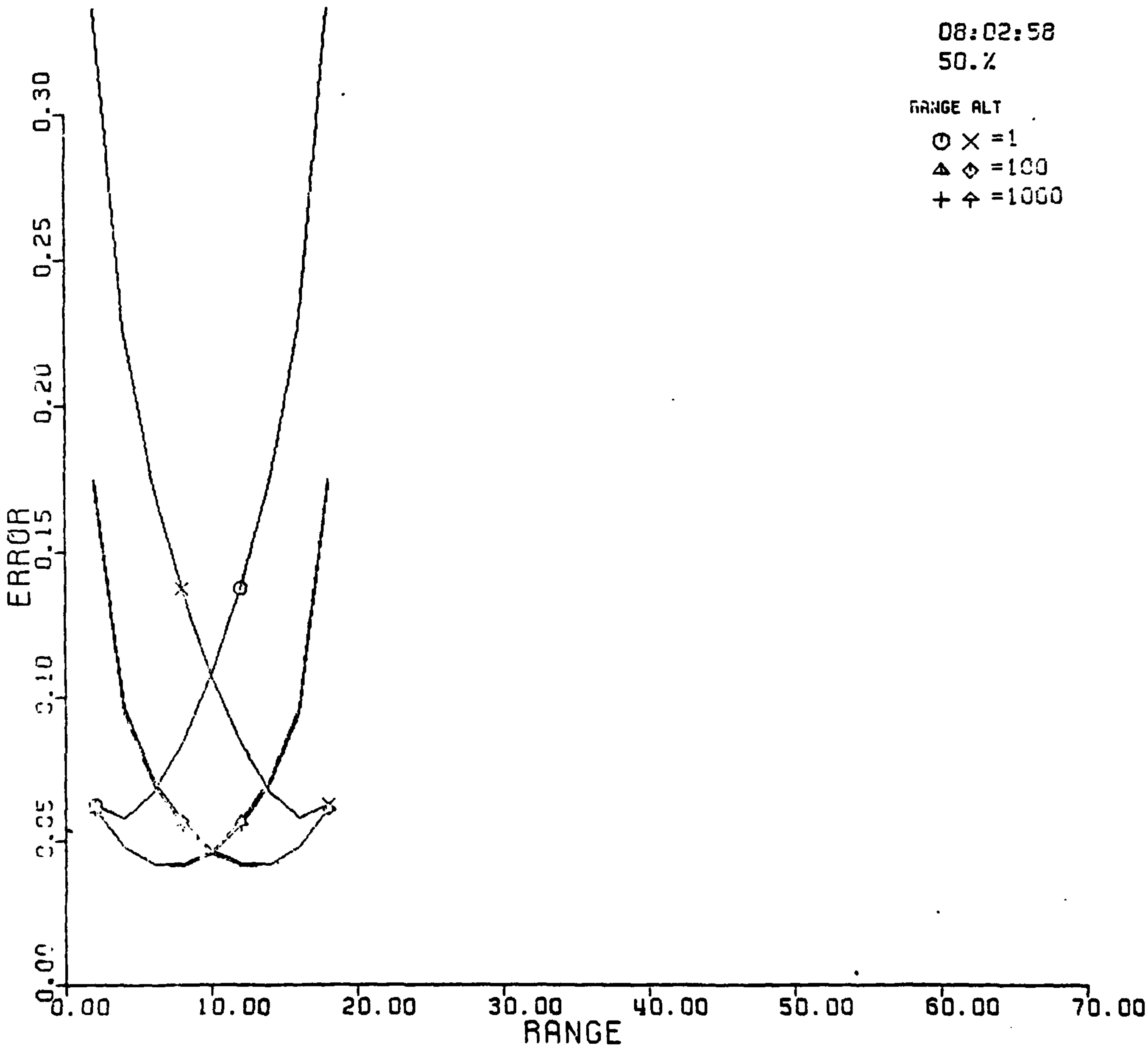
08:02:58
50.%
RANGE ALT
=1
=100
=1000
ERROR
0.00
0.05
0.10
0.15
0.20
0.25
0.30
0.00
10.00
20.00
30.00
40.00
50.00
60.00
70.00
RANGE

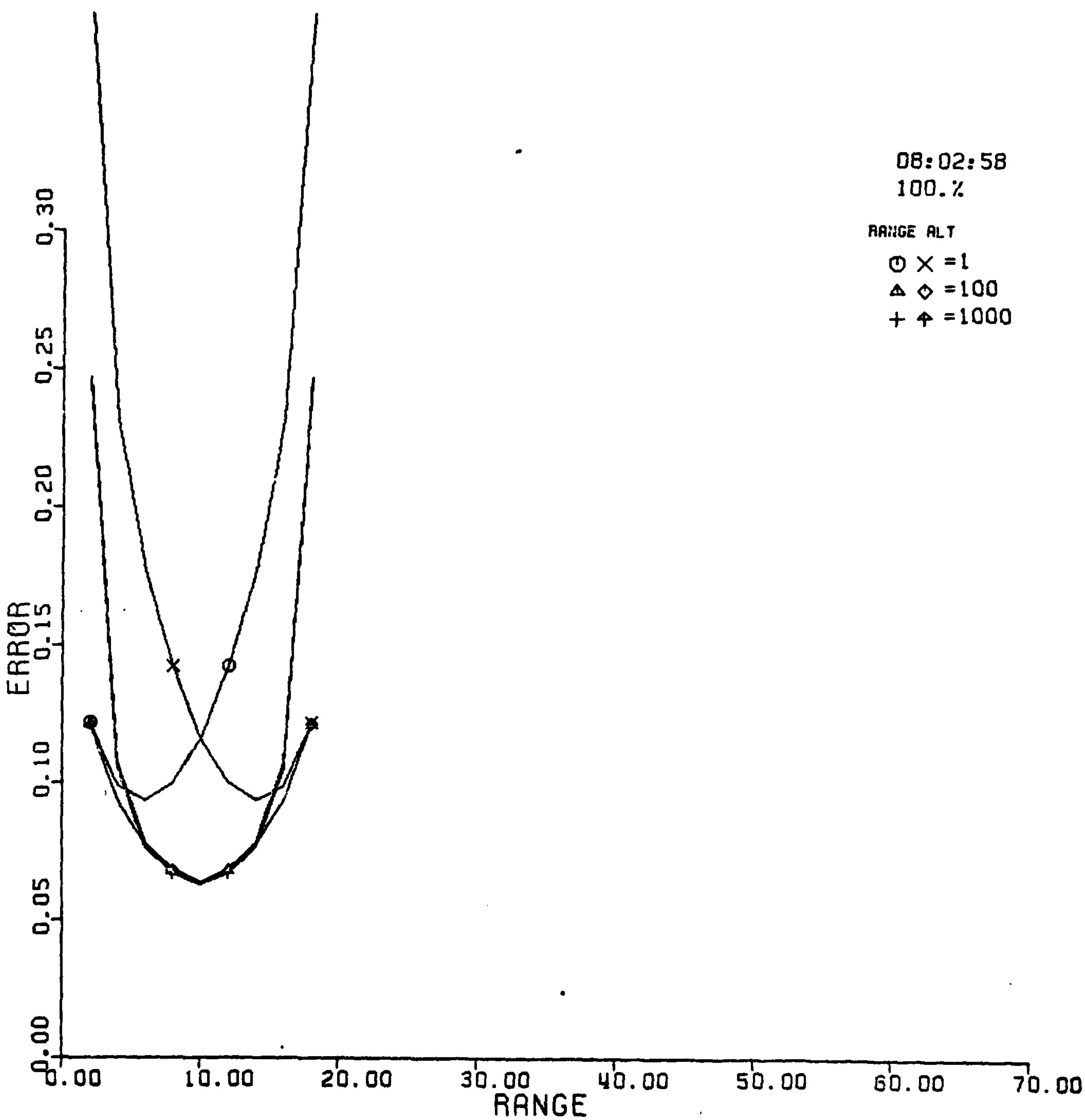
08:02:58
100.%
RANGE ALT
=1
=100
=1000
ERROR
0.00
0.05
0.10
0.15
0.20
0.25
0.30
0.00
10.00
20.00
30.00
40.00
50.00
60.00
70.00
RANGE

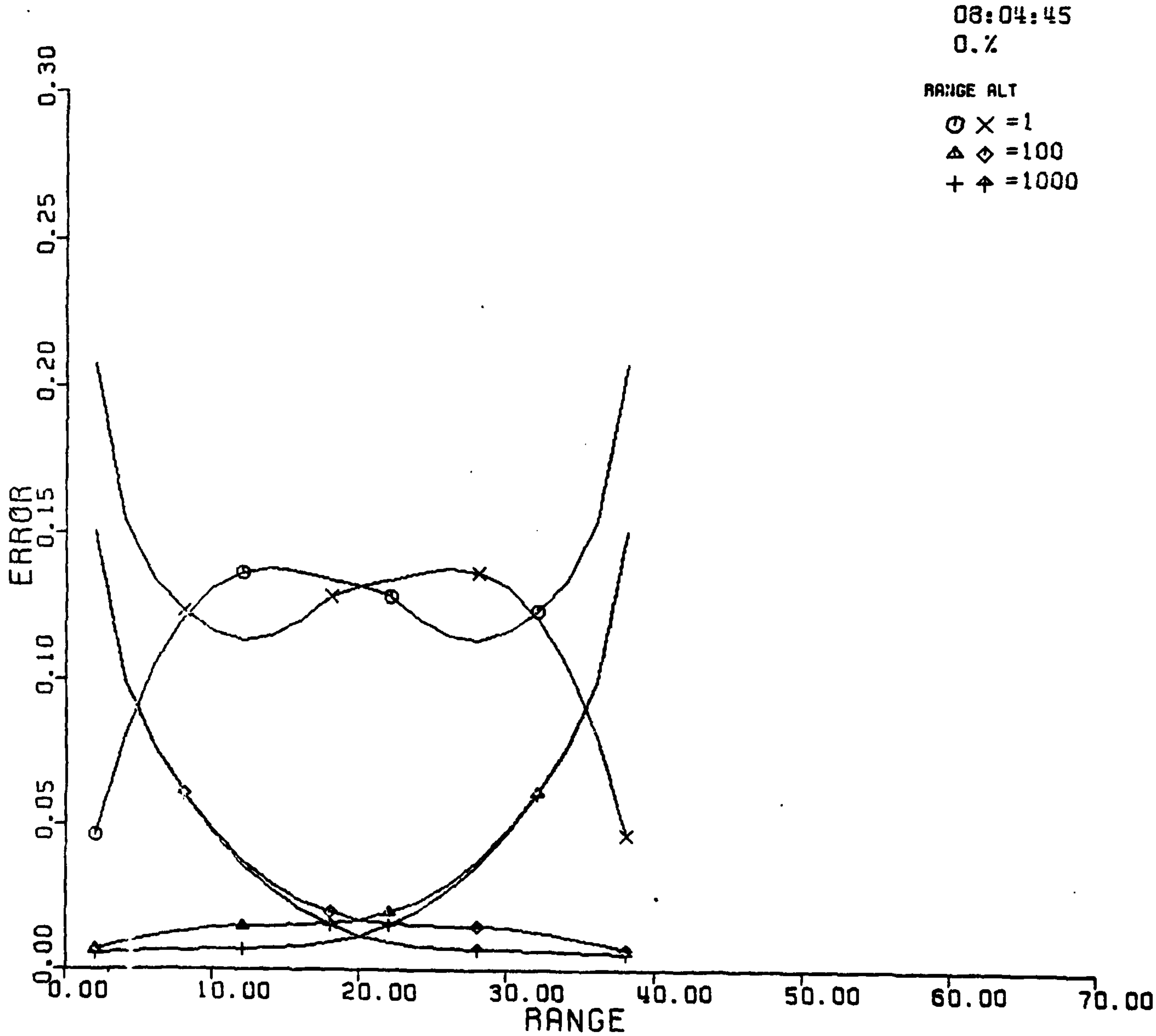
08:04:45
0.%
RANGE ALT
=1
=100
=1000
ERROR
0.00
0.05
0.10
0.15
0.20
0.25
0.30
0.00
10.00
20.00
30.00
40.00
50.00
60.00
70.00
RANGE

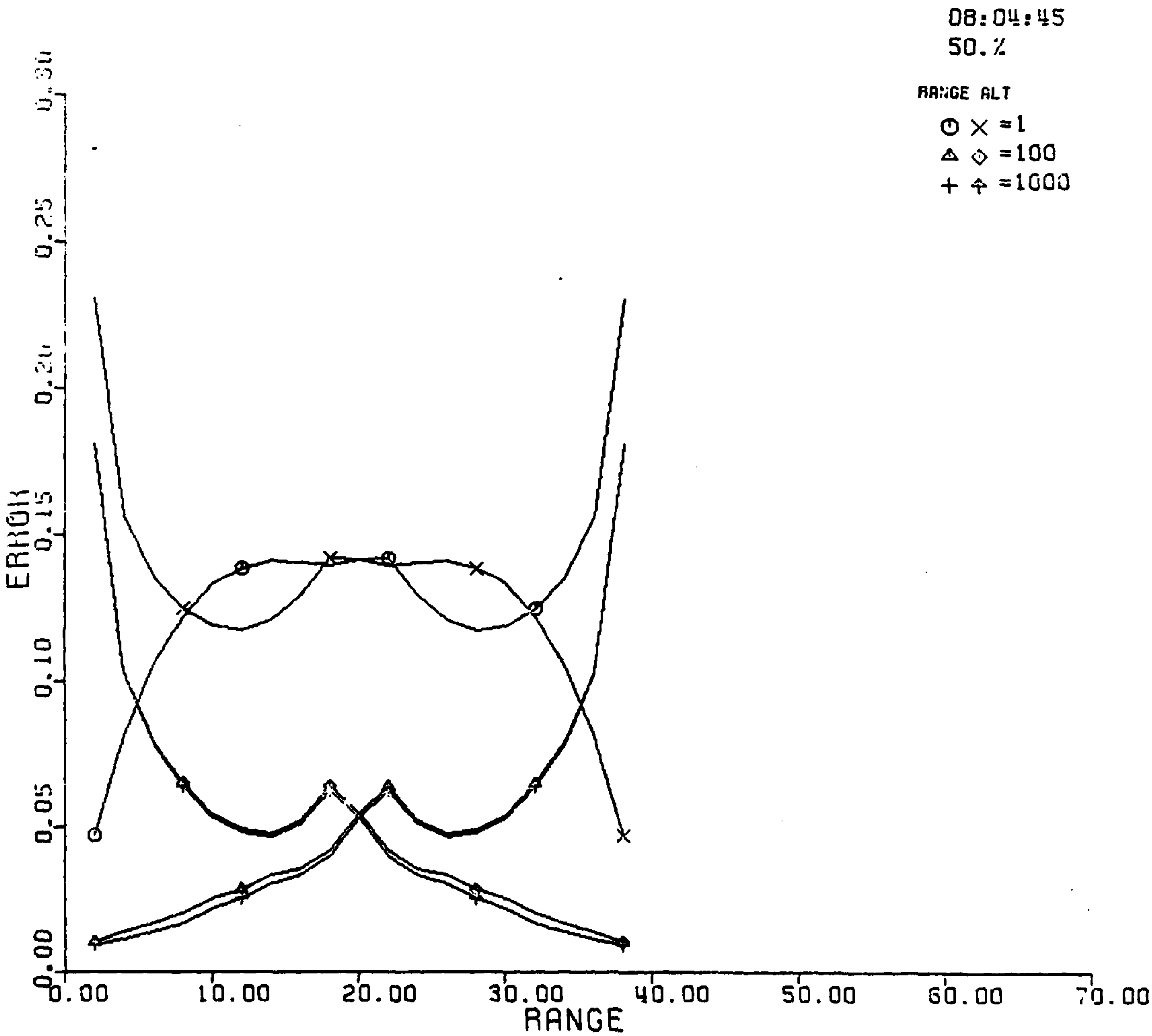

08:04:45
50.%
RANGE ALT
=1
=100
=1000
ERROR
0.00
0.05
0.10
0.15
0.20
0.25
0.30
0.00
10.00
20.00
30.00
40.00
50.00
60.00
70.00
RANGE

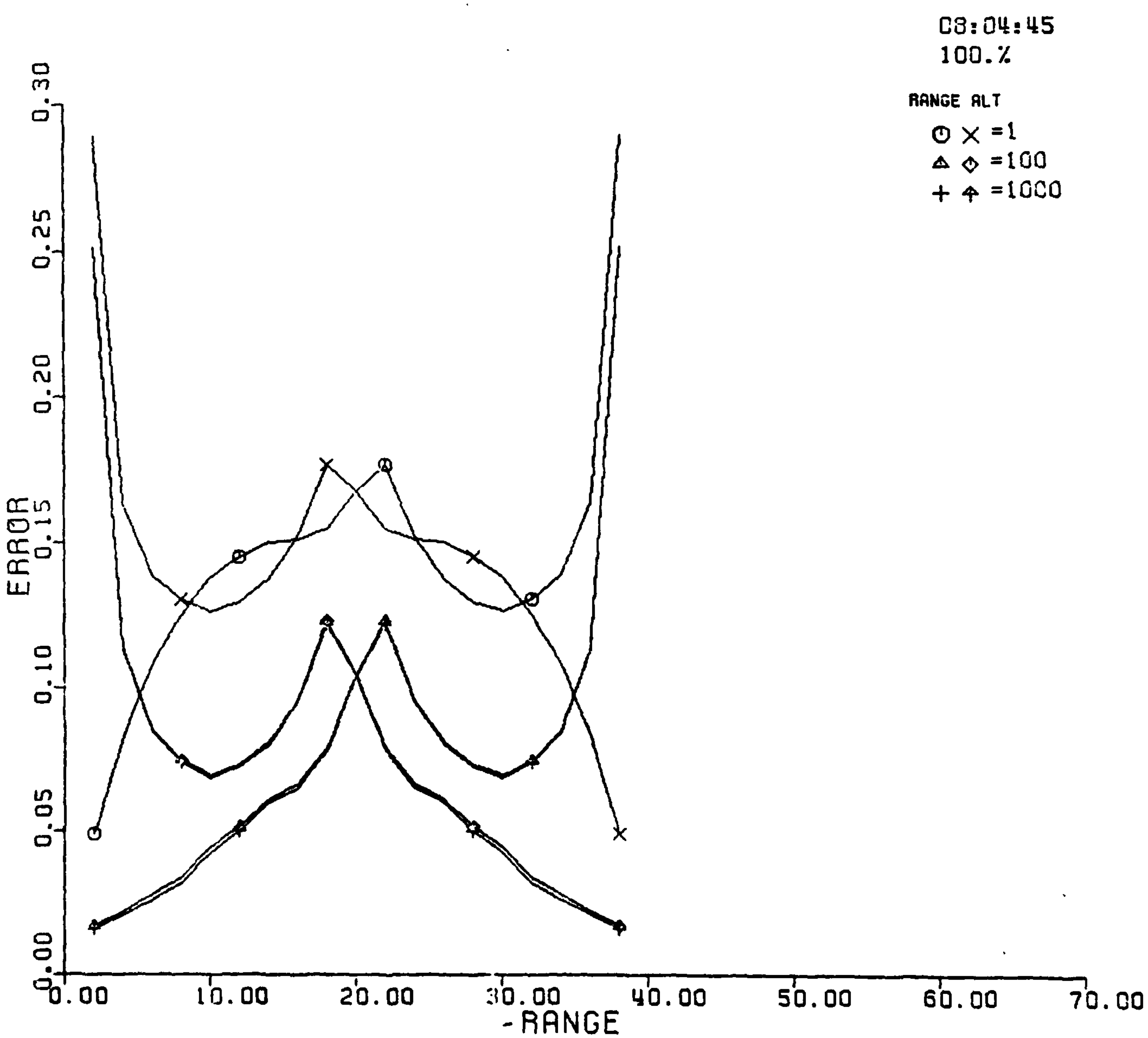
08:04:45
100.%
RANGE ALT
=1
=100
=1000
ERROR
0.00
0.05
0.10
0.15
0.20
0.25
0.30
0.00
10.00
20.00
30.00
40.00
50.00
60.00
70.00
-RANGE

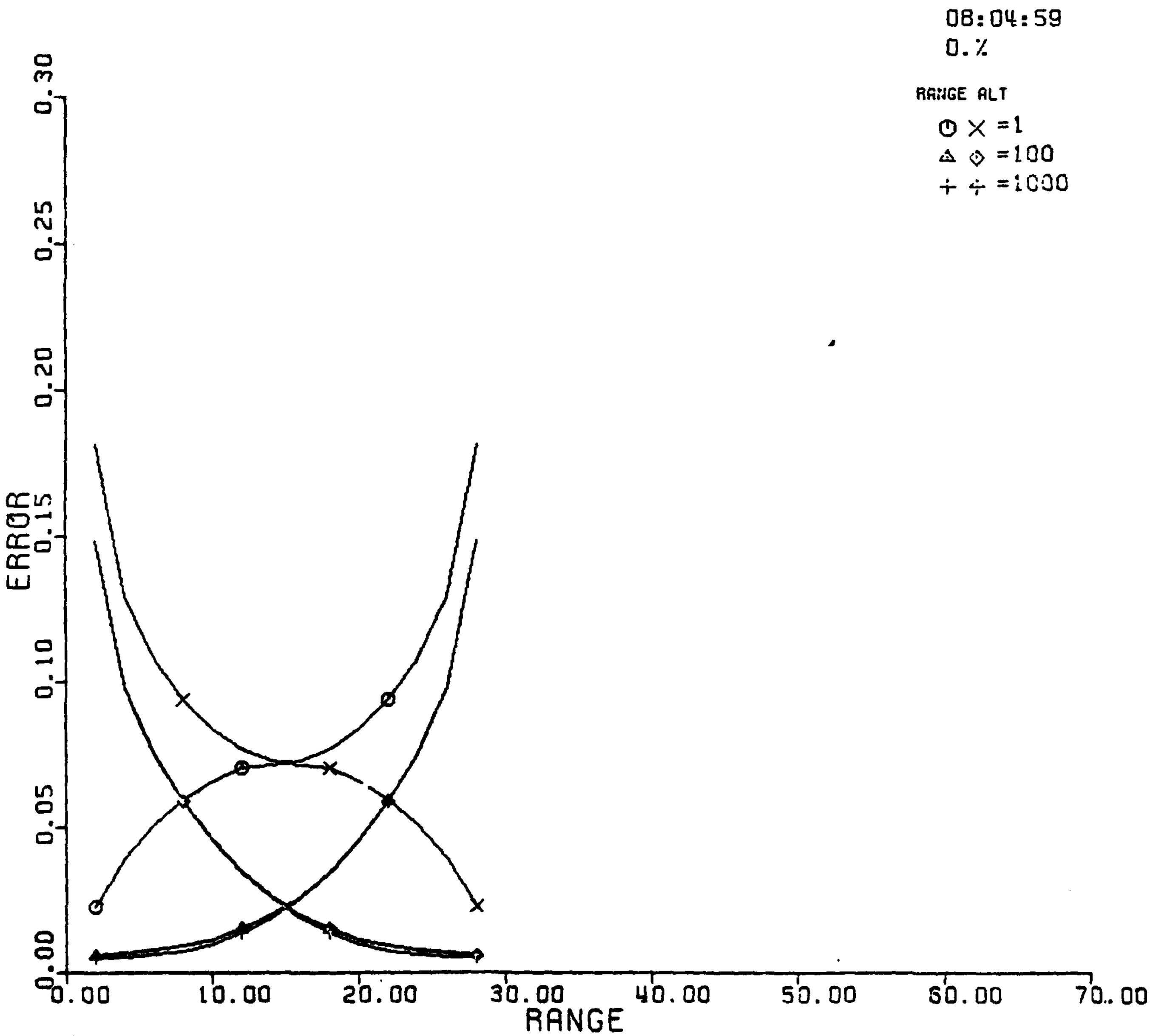
08:04:59
0.%
RANGE ALT
=1
=100
=1000
ERROR
0.00
0.05
0.10
0.15
0.20
0.25
0.30
0.00
10.00
20.00
30.00
40.00
50.00
60.00
70.00
RANGE

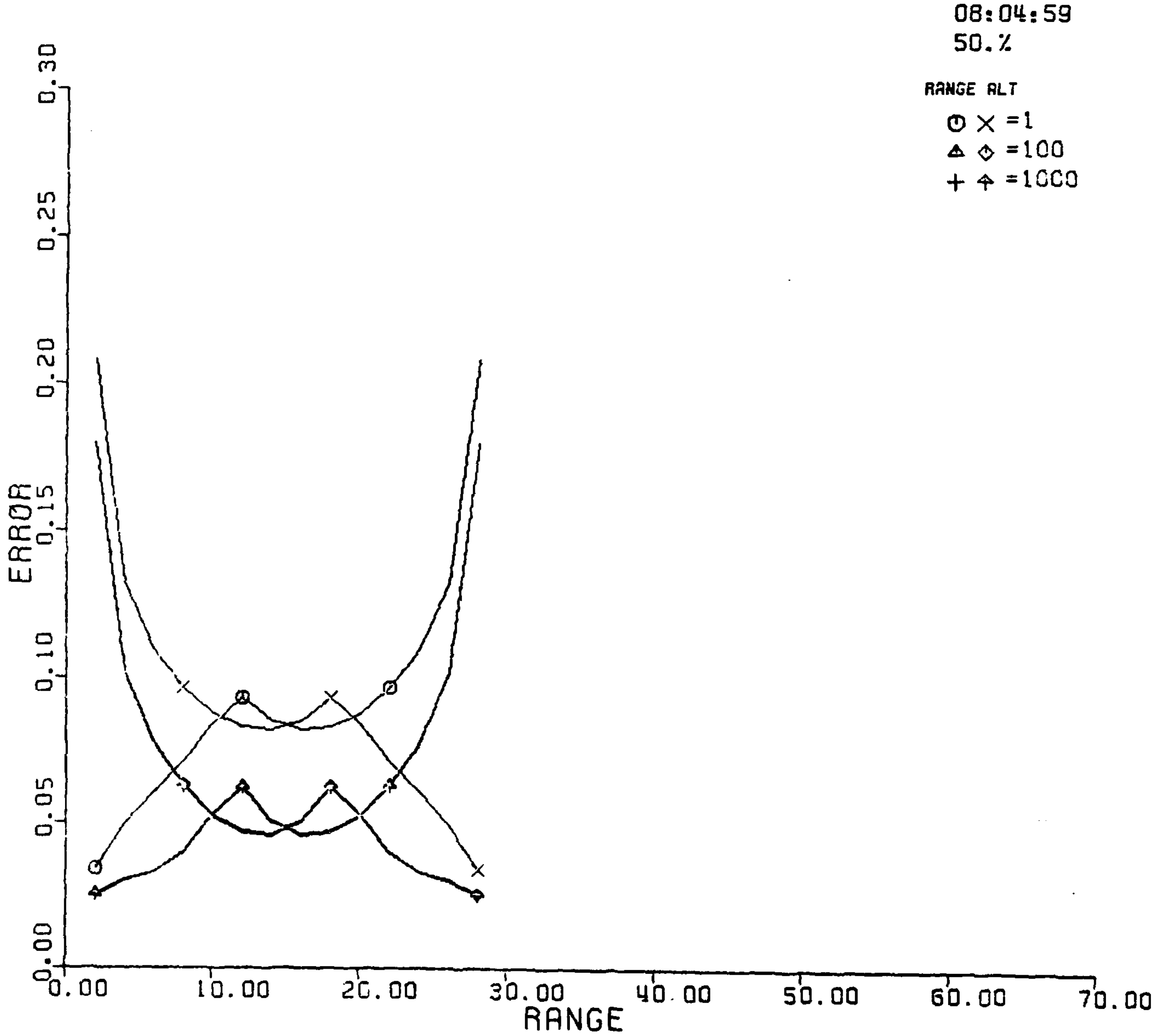
08:04:59
50.%
RANGE ALT
=1
=100
=1000
ERROR
0.00
0.05
0.10
0.15
0.20
0.25
0.30
0.00
10.00
20.00
30.00
40.00
50.00
60.00
70.00
RANGE

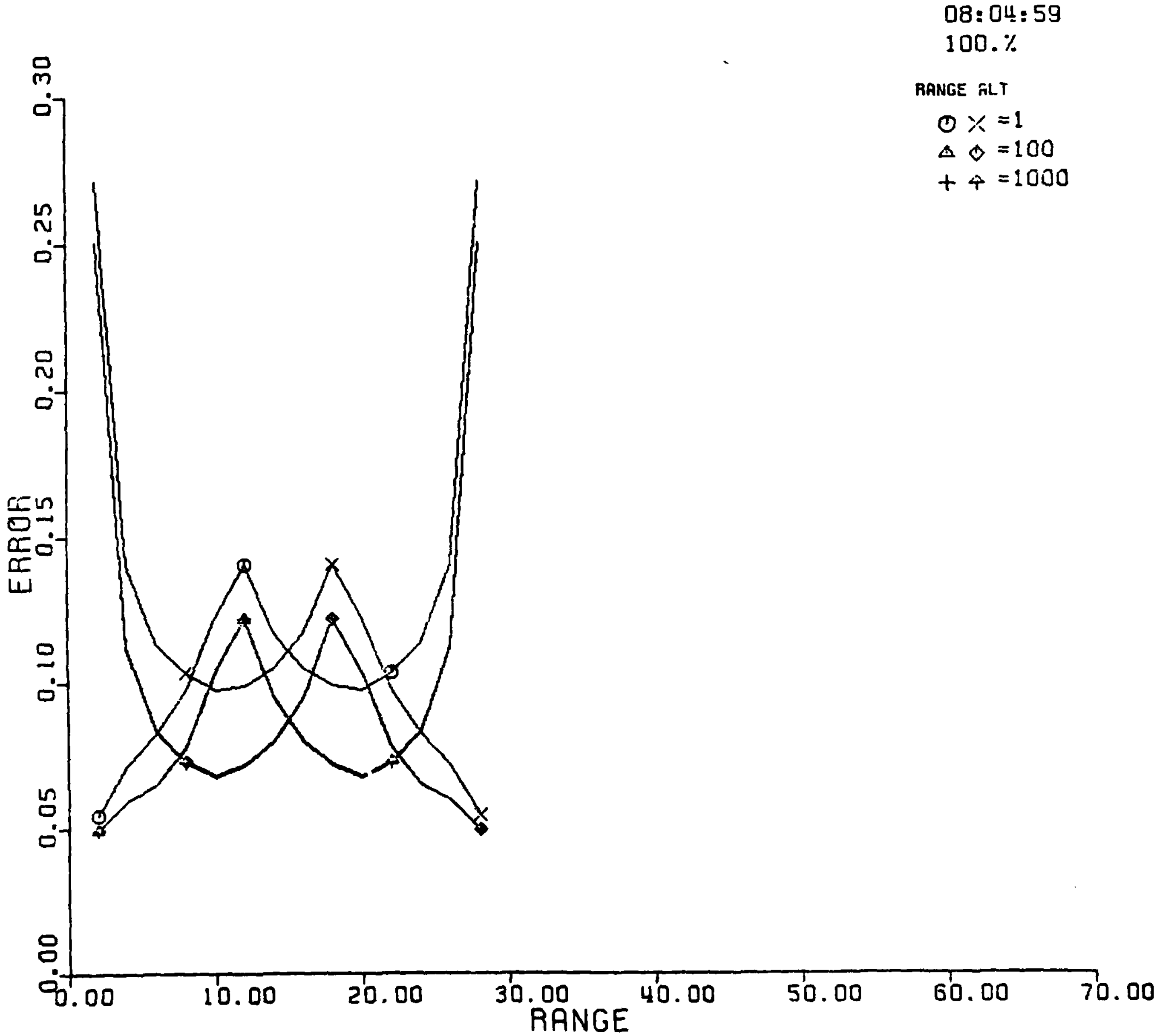
08:04:59
100.%
RANGE ALT
=1
=100
=1000
ERROR
0.00
0.05
0.10
0.15
0.20
0.25
0.30
0.00
10.00
20.00
30.00
40.00
50.00
60.00
70.00
RANGE

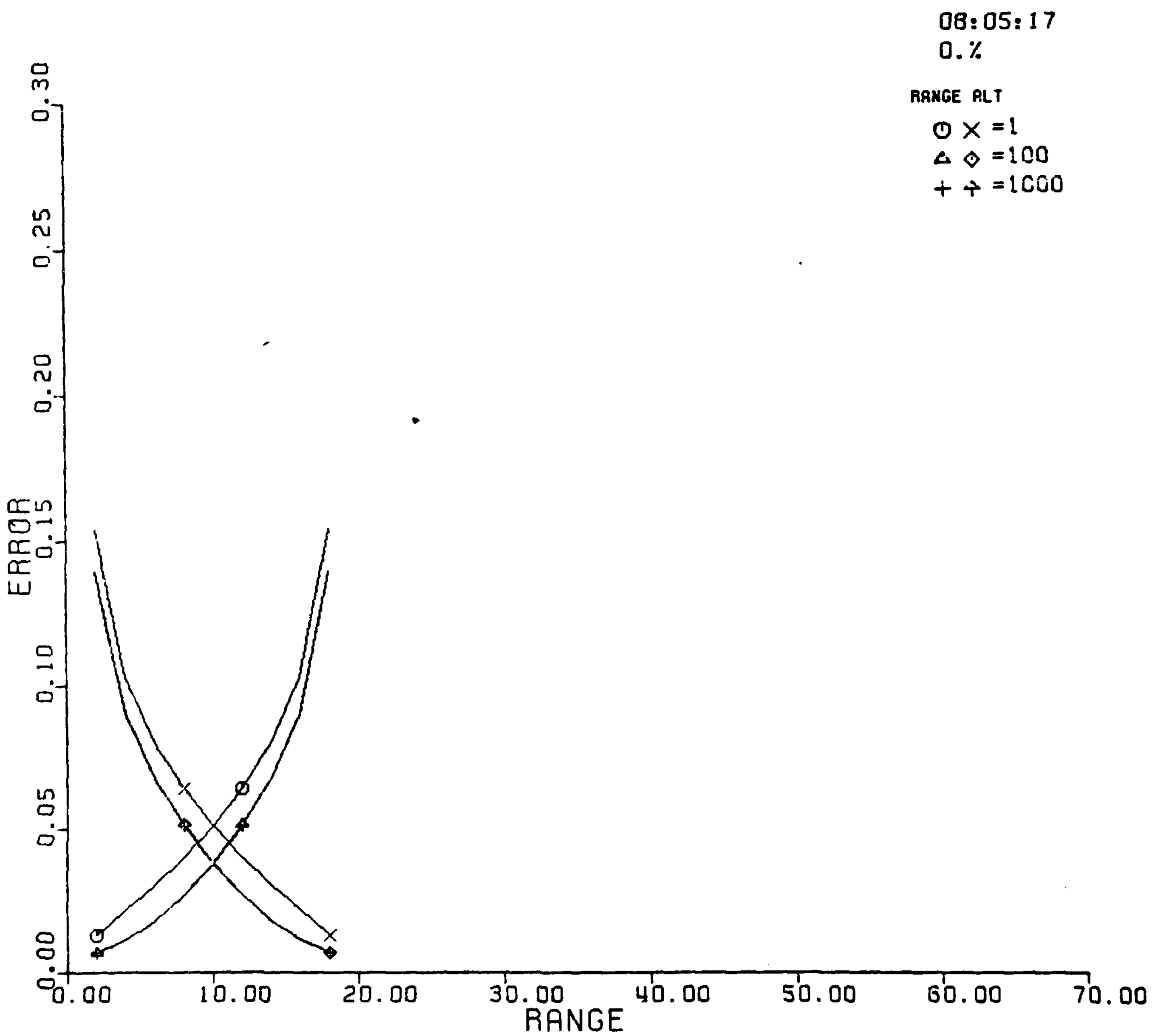
08:05:17
0.%
RANGE ALT
=1
=100
=1000
ERROR
0.00
0.05
0.10
0.15
0.20
0.25
0.30
0.00
10.00
20.00
30.00
40.00
50.00
60.00
70.00
RANGE

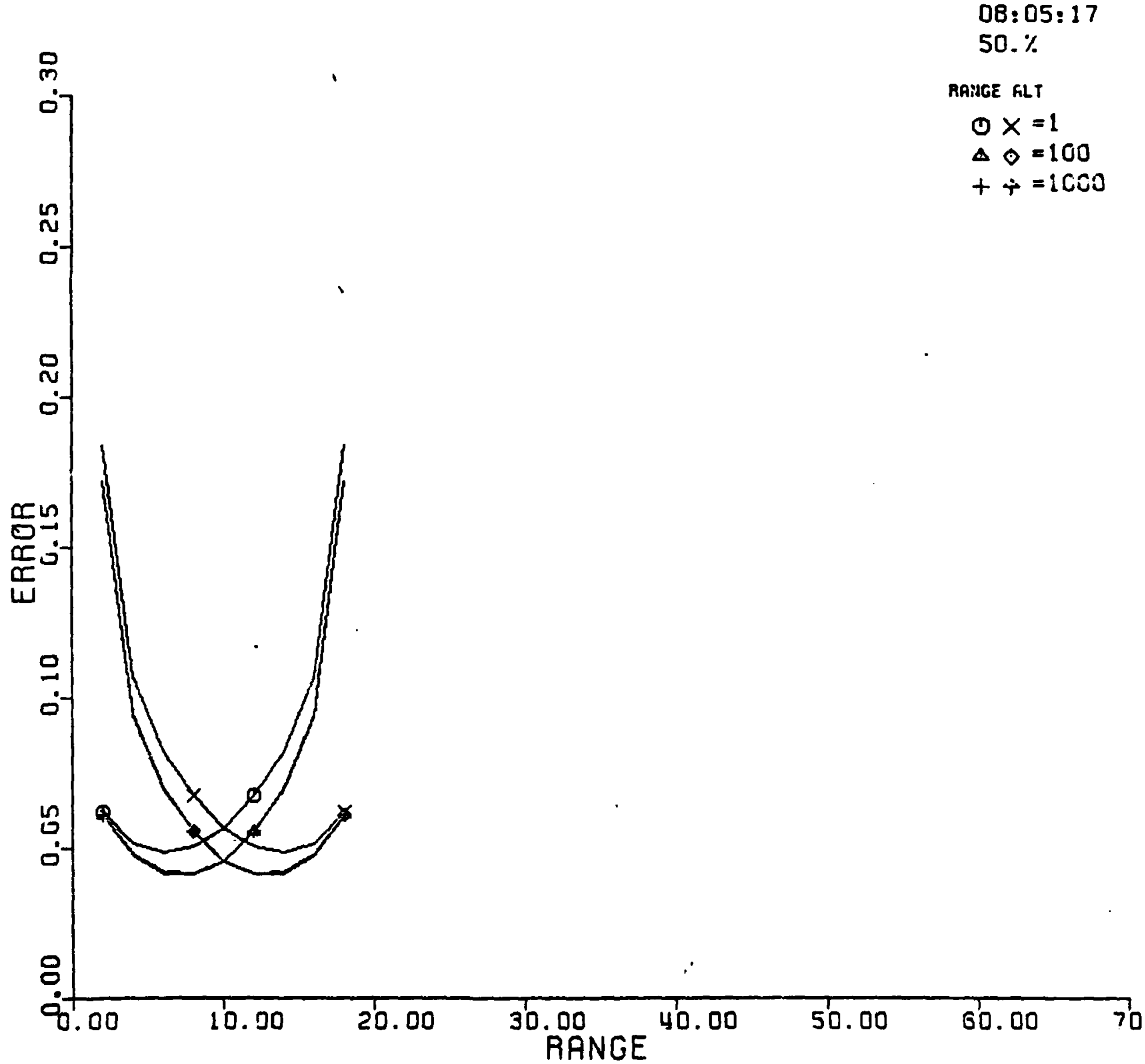
08:05:17
50.%
RANGE ALT
=1
=100
=1000
ERROR
0.00
0.05
0.10
0.15
0.20
0.25
0.30
RANGE
0.00
10.00
20.00
30.00
40.00
50.00
60.00
70.00

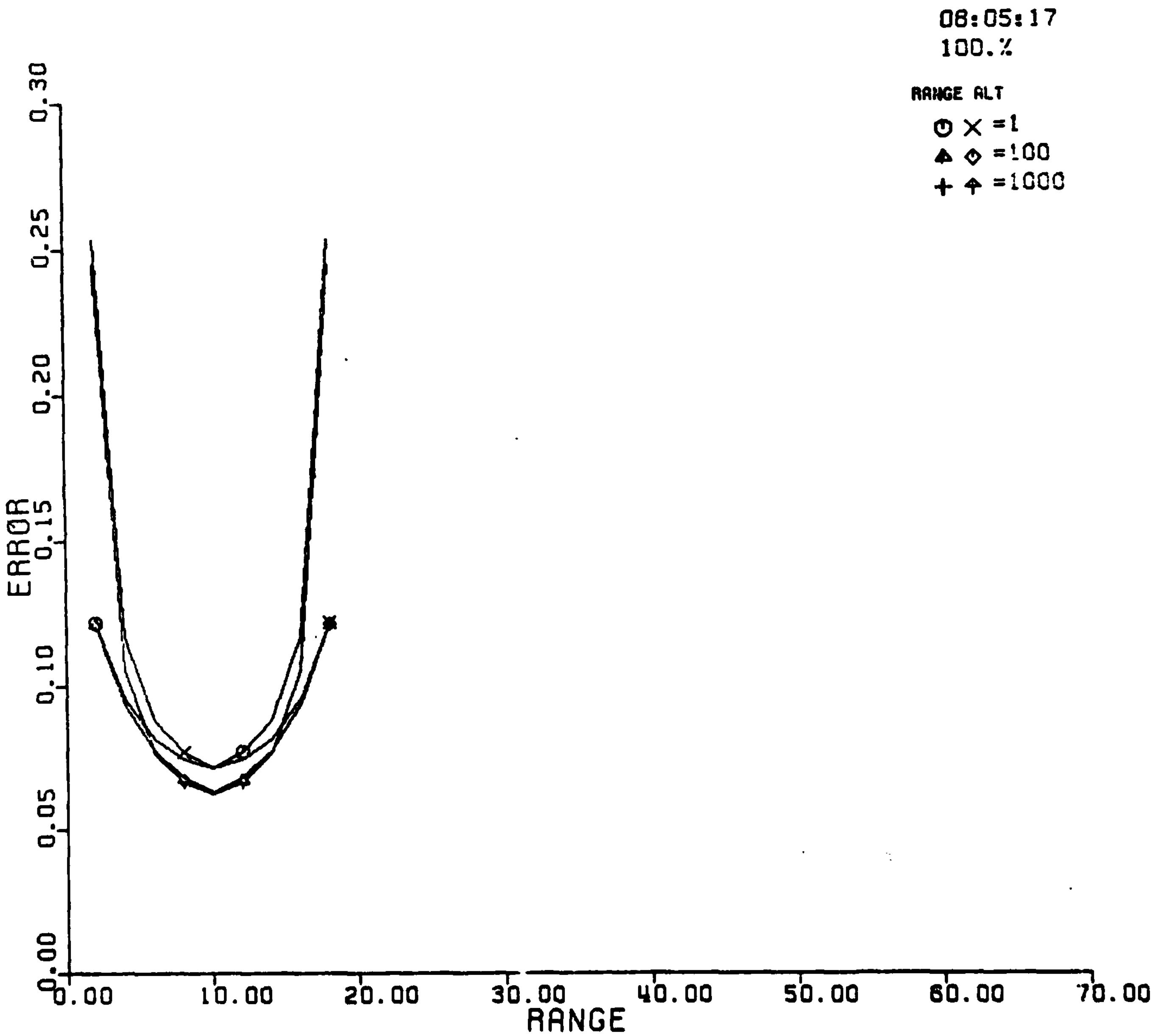
08:05:17
100.%
RANGE ALT
=1
=100
=1000
ERROR
0.00
0.05
0.10
0.15
0.20
0.25
0.30
0.00
10.00
20.00
30.00
40.00
50.00
60.00
70.00
RANGE